

2022-07

Canarium schweinfurthii resin as an organic binder for carbonized briquettes

Kivumbi, Bernard

NM-AIST

<https://doi.org/10.58694/20.500.12479/1656>

Provided with love from The Nelson Mandela African Institution of Science and Technology

**CANARIUM SCHWEINFURTHII RESIN AS AN ORGANIC BINDER FOR
CARBONIZED BRIQUETTES**

Kivumbi Bernard

**A Dissertation Submitted in Partial Fulfilment of the Requirements for the Degree of
Doctor of Philosophy in Sustainable Energy Science and Engineering of the Nelson
Mandela African Institution of Science and Technology**

Arusha, Tanzania

July, 2022

ABSTRACT

Charcoal is the predominant fuel used in many developing countries for domestic and commercial purposes. Transport and handling of charcoal produces fines amounting to 10-20% by weight. The fines can be turned into lumps of charcoal by briquetting using suitable binders. This study investigated the use of *Canarium Schweinfurthii* resin as a binder for production of carbonized briquettes from charcoal fines. The binder and charcoal fines were characterized through proximate analysis, ultimate analysis, higher heating value (HHV), and SEM. Four briquette samples (B25, B30, B35, and B40) with a ratio of charcoal fines: binder of 3:1, 7:3, 13:7, and 3:2, respectively were produced at a compaction pressure of 5.92-7.96 MPa. The physical properties of briquettes determined were bulk density, impact resistance index (IRI), compressive strength (CS), splitting tensile strength (STS), water resistance index (WRI), and morphology. The chemical properties of briquettes determined were proximate analysis, ultimate analysis, HHV, and energy density. The physical properties of briquettes were analysed using Design Expert. One-way ANOVA and Fisher's LSD were used to analyse the chemical properties of briquettes. The phases of the Water Boiling Test (WBT) considered were Cold Start High Power, Hot Start High Power and Simmer phases. Ignition properties, combustion properties, gas temperature, water temperature, ambient temperature, emissions, and WBT performance metrics were investigated using the Laboratory Emission Monitoring System. The ignition properties included ignition time, flame and incandescence. The combustion properties included smoke, flame, soot, and ash. The emissions measured were $PM_{2.5}$, SO_2 , NO_x , C_xH_y , CO , and CO_2 . The WBT performance metrics evaluated were time to boil, burning rate, thermal efficiency, specific fuel consumption, firepower, total emissions, specific emissions, emissions per MJ, and emissions rate. The ash from charcoal fines was analysed using x-ray diffraction. The briquettes had a bulk density of 0.770-1.036 g/cm³, IRI of 2.90-73.33, CS of 2.25-10.94 MPa, STS of 0.09-0.42 MPa, WRI of 99.26-99.29, and an HHV of 29.7-31.3 MJ/kg. The ignition time was 6.47-7.01 min, time to boil was 14.7-41.9 min, burning rate was 1.1-8.2 g/min, thermal efficiency was 21.79-54.61%, specific fuel consumption was 21.7-70.1 g/L, and firepower of 535.9-4123.2 W. The ash was found to contain $CaCO_3$ (76.6 wt%), CaO (13.1 wt%) and amorphous compounds (10.3 wt%). Design Expert predicted briquette B40 with the optimum physical properties. The produced briquettes can be used as an alternative source of fuel to wood fuel since they exhibit similar combustion properties.

DECLARATION

I, Kivumbi Bernard do hereby declare to the senate of Nelson Mandela African Institution of Science and Technology that this dissertation is my own original work and that it has neither been submitted nor being concurrently submitted for degree award in any other institution.

Kivumbi Bernard

Name and Signature of the Candidate

Date

The above declaration is confirmed by:

Dr. Thomas T. Kivevele

Name and signature of Supervisor 1

Date

Dr. Yusufu A. C. Jande

Name and Signature of Supervisor 2

Date

Prof. John B. Kirabira



Name and Signature of Supervisor 3

Date

COPYRIGHT

This dissertation is copyright material protected under the Berne Convention, the Copyright Act of 1999 and other international and national enactments, in that behalf, on intellectual property. It must not be reproduced by any means, in full or in part, except for short extracts in fair dealing; for researcher private study, critical scholarly review or discourse with an acknowledgement, without a written permission of the Deputy Vice Chancellor for Academic, Research and innovation, on behalf of both the author and the Nelson Mandela African Institution of Science and Technology.

CERTIFICATION

The undersigned certify that they have read and hereby recommend for acceptance by the Nelson Mandela African Institution of Science and Technology a dissertation titled “*Canarium Schweinfurthii Resin as an Organic Binder for Carbonized Briquettes*” in Partial Fulfillment of the Requirements for the Degree of Doctor of Philosophy in Sustainable Energy Science and Engineering of the Nelson Mandela African Institution of Science and Technology.

Dr. Thomas T. Kivevele

Name and signature of Supervisor 1 Date

Dr. Yusufu A. C. Jande

Name and Signature of Supervisor 2 Date

Prof. John B. Kirabira



Name and Signature of Supervisor 3 Date

ACKNOWLEDGEMENTS

I am indebted to Wise-Futures centre for giving me the scholarship opportunity to pursue PhD studies in Sustainable Energy Science and Engineering at the Nelson Mandela African Institution of Science and Technology, NM-AIST, Arusha Tanzania. I am grateful to Gulu University for granting me the study-leave to pursue PhD studies.

I wish to extend my heartfelt thanks to my supervisors Dr. Thomas T. Kivevele, Dr. Yusufu Abeid Chande Jande, and Prof. John Baptist Kirabira for their generous guidance and support towards the success of this research. Their intellectual positive criticism of the research contributed to its enormous improvement throughout its course.

I extend my sincere gratitude to all the technicians at the laboratories of NM-AIST, Arusha Technical College (Arusha, Tanzania), College of Engineering, Design, Art and Technology, Makerere University (Kampala, Uganda) and Centre for Research in Energy and Energy Conservation (CREEC), Makerere University for the technical support towards the success of this research.

I am indebted to my father, Mr. Paul Ssonko (RIP) and my ailing mother, Miss Teddy Nalubega for nurturing me to become who I am today. May his soul rest in eternal peace and may the Almighty continue to protect her. Also, special thanks to my dear wife, Jackline Auma for the moral support and looking after the family diligently during the times I was busy with studies in Arusha, Tanzania.

I also appreciate the academic staff at NM-AIST for the knowledge they imparted unto me and nonteaching staff at NM-AIST that made the smooth running of the research possible. I am grateful to my masters and PhD colleagues, workmates, relatives and friends for the moral support and sharing of ideas that led to the success of the research.

May the Almighty reward you abundantly.

DEDICATION

To my father, Mr. Paul Ssonko (RIP) and my ailing mother, Miss Teddy Nalubega. Also to my dear wife, Jackline Auma , and my two children: Andrea Maria Nakirijja and Adonai Paul Ssonko.

TABLE OF CONTENTS

| | |
|---|------|
| ABSTRACT..... | i |
| DECLARATION | ii |
| COPYRIGHT | iii |
| CERTIFICATION | iv |
| ACKNOWLEDGEMENTS | v |
| DEDICATION | vi |
| TABLE OF CONTENTS..... | vii |
| LIST OF TABLES | xi |
| LIST OF FIGURES | xii |
| LIST OF APPENDICES..... | xv |
| LIST OF ABBREVIATION AND SYMBOLS | xvii |
| CHAPTER ONE | 1 |
| INTRODUCTION | 1 |
| 1.1 Background of the Problem | 1 |
| 1.2 Statement of the Problem..... | 2 |
| 1.3 Rationale of the Study..... | 3 |
| 1.4 Research Objectives | 3 |
| 1.4.1 General Objective..... | 3 |
| 1.4.2 Specific Objectives..... | 3 |
| 1.5 Research Questions..... | 4 |
| 1.6 Significance of the Study | 4 |
| 1.7 Delineation of the Study..... | 4 |
| CHAPTER TWO | 5 |
| LITERATURE REVIEW | 5 |
| 2.1 Biomass, Biofuels and Bioenergy | 5 |

| | | |
|----------------------------|--|----|
| 2.2 | Fundamental Aspects of Briquetting..... | 9 |
| 2.2.1 | Overview | 9 |
| 2.2.2 | Properties of Solids Important to Densification | 9 |
| 2.2.3 | Compaction Characteristics of Biomass and their Significance | 10 |
| 2.2.4 | Types of Binders | 11 |
| 2.2.5 | Binding Mechanisms of Densification..... | 12 |
| 2.2.6 | Briquetting Technology..... | 18 |
| 2.3 | Ignition of Carbonized Briquettes..... | 24 |
| 2.4 | Combustion Products and Pollutants | 25 |
| 2.5 | Water Boiling Test (WBT)..... | 26 |
| 2.5.1 | Cold Start High Power (CSHP) Phase | 26 |
| 2.5.2 | Hot Start High Power (HSHP) Phase | 26 |
| 2.5.3 | Simmer Phase..... | 26 |
| 2.5.4 | Emissions Testing | 27 |
| 2.5.5 | Water Boil Test Performance Metrics..... | 27 |
| 2.6 | Conclusion..... | 47 |
| CHAPTER THREE | | 49 |
| MATERIALS AND METHODS..... | | 49 |
| 3.1 | Conceptual Framework..... | 49 |
| 3.2 | Purification of the <i>Canarium schweinfurthii</i> Resin (Binder)..... | 49 |
| 3.3 | Preparation of the Charcoal Fines | 50 |
| 3.4 | Characterization of Charcoal Fines a <i>Canarium schweinfurthii</i> Resin (Binder) | 51 |
| 3.5 | Physical and Chemical Properties of Carbonized Briquettes..... | 52 |
| 3.5.1 | Production of Carbonized Briquettes | 52 |
| 3.5.2 | Physical and Chemical Properties of the Carbonized Briquettes | 53 |
| 3.5.3 | Statistics of Proximate Analysis, Ultimate Analysis and HHV of Briquettes..... | 55 |

| | | |
|------------------------------|---|----|
| 3.5.4 | Effect of Binder Concentration and Compaction Pressure on Physical Properties of Briquettes | 55 |
| 3.6 | Water Boiling Test of the Carbonized Briquettes | 56 |
| 3.6.1 | Experimental Setup | 56 |
| 3.6.2 | Ignition of Briquettes | 56 |
| 3.6.3 | Combustion | 57 |
| 3.6.4 | Gaseous Emissions and Particulate Matter During the Water Boiling Test..... | 58 |
| CHAPTER FOUR..... | | 59 |
| RESULTS AND DISCUSSION | | 59 |
| 4.1 | Characterization of the <i>Canarium Schweinfurthii</i> Resin (Binder) and Charcoal Fines | 59 |
| 4.1.1 | Thermogravimetric and Differential Thermogravimetric Thermograms from Proximate Analysis | 59 |
| 4.1.2 | Proximate Analysis of Binder and Charcoal Fines | 60 |
| 4.1.3 | Ultimate Analysis, and Higher Heating Value of Binder and Charcoal Fines | 60 |
| 4.1.4 | Morphology of Binder and Charcoal Fines | 61 |
| 4.2 | Physical Properties of the Carbonized Briquettes | 63 |
| 4.2.1 | Bulk density..... | 63 |
| 4.2.2 | Impact Resistance Index (IRI)..... | 64 |
| 4.2.3 | Compressive and Splitting Tensile Strength | 65 |
| 4.2.4 | Water Resistance Index (WRI)..... | 66 |
| 4.2.5 | Morphology of Briquettes | 67 |
| 4.3 | Chemical Properties of the Carbonized Briquettes | 71 |
| 4.3.1 | Thermogravimetric and Differential Thermogravimetric Thermograms from Proximate Analysis | 71 |
| 4.3.2 | Proximate Analysis of Briquettes..... | 72 |
| 4.3.3 | Ultimate Analysis, Higher Heating Value, and Energy Density of Briquettes | 73 |

| | | |
|--------------------------------------|---|-----|
| 4.4 | Effect of Binder Concentration and Compaction Pressure on Physical Properties of Briquettes | 76 |
| 4.4.1 | Development of Model..... | 76 |
| 4.4.2 | Diagnostics | 78 |
| 4.4.3 | Response Surface Plots | 82 |
| 4.5 | Water Boiling Test of the Carbonized Briquettes | 84 |
| 4.5.1 | Ignition | 84 |
| 4.5.2 | Combustion | 86 |
| 4.5.3 | Temperature Profiles and Gaseous Emissions | 87 |
| 4.5.4 | WBT Performance Metrics | 91 |
| 4.6 | Ash | 100 |
| CHAPTER FIVE | | 103 |
| CONCLUSION AND RECOMMENDATIONS | | 103 |
| 5.1 | Conclusion..... | 103 |
| 5.2 | Recommendations | 103 |
| REFERENCES | | 105 |
| APPENDICES | | 116 |
| RESEARCH OUTPUTS..... | | 184 |

LIST OF TABLES

| | | |
|-----------|---|-----|
| Table 1: | Proximate analysis of selected feedstock and briquettes; FS-UC (feedstock-uncarbonized), FS-C (feedstock-carbonized), B-C (briquettes-carbonized) | 6 |
| Table 2: | Ultimate analysis and higher heating value (HHV) of selected feedstock and briquettes; FS-UC (feedstock- uncarbonized), FS-C (feedstock-carbonized), B-C (briquettes-carbonized)..... | 8 |
| Table 3: | Feedstock, binder, binder concentration (BC), compaction pressure (CP), compressive strength (CS), splitting tensile strength (STS), bulk density (ρ), impact resistance index (IRI), and water resistance index (WRI) of selected carbonized briquettes | 20 |
| Table 4: | Proximate analysis, ultimate analysis, and HHV of binder and charcoal fines | 61 |
| Table 5: | Fishers LSD test for proximate analysis, ultimate analysis, and HHV of briquettes. | 74 |
| Table 6: | One-way ANOVA for proximate analysis, ultimate analysis, and HHV of briquettes | 74 |
| Table 7: | Data for factors and responses analysed in Design Expert | 76 |
| Table 8: | ANOVA for the models of the experimental design..... | 79 |
| Table 9: | Peak concentration (ppm) of the gaseous emissions..... | 88 |
| Table 10: | Specific emissions and emissions rate of PM _{2.5} , CO, and CO ₂ | 100 |

LIST OF FIGURES

| | | |
|------------|---|----|
| Figure 1: | (a) Carbonized briquettes with a hole at the centre (Suhartini <i>et al.</i> , 2011), (b) carbonized honey comb briquette with multiple holes (Ferguson, 2012), (c) carbonized briquette without a hole (Carnaje <i>et al.</i> , 2018), (d) uncarbonized straw briquette with a hole at the centre (Ferguson, 2012) | 9 |
| Figure 2: | The bonding mechanism of sodium silicate (Zhang <i>et al.</i> , 2018) | 15 |
| Figure 3: | The bonding mechanism of sodium silicate (Zhang <i>et al.</i> , 2018) | 15 |
| Figure 4: | The hydroxyl groups on the surface of kaolin (Zhang <i>et al.</i> , 2018) | 16 |
| Figure 5: | The chemical bond between binder and coal particles (Zhang <i>et al.</i> , 2018) | 17 |
| Figure 6: | The bonding mechanism of corn starch (Zhang <i>et al.</i> , 2018)..... | 17 |
| Figure 7: | Screw extruder (Kpalo <i>et al.</i> , 2020a)..... | 19 |
| Figure 8: | Piston press (Kpalo <i>et al.</i> , 2020a)..... | 22 |
| Figure 9: | Roller press (Kpalo <i>et al.</i> , 2020a)..... | 23 |
| Figure 10: | Manual press (WU-presser) (Kpalo <i>et al.</i> , 2020a)..... | 24 |
| Figure 11: | Temperature profile during the WBT (Clean cooking alliance, 2014)..... | 26 |
| Figure 12: | Conceptual framework..... | 49 |
| Figure 13: | Binder preparation: (a) as-received, (b) melting/boiling, (c) sieving, (d) liquid binder (e) solid binder..... | 50 |
| Figure 14: | Preparation of charcoal fines: (a) lumps of charcoal, (b) Sealing Type Swinging Pulveriser (c) loading the lumps of charcoal in the pulveriser, (d) Electromagnetic sieve shaker, (e) charcoal fines..... | 51 |
| Figure 15: | Production of briquettes: (a) melting binder, (b) mixing binder/charcoal fines, (c) compaction, (d) sample briquettes..... | 52 |
| Figure 16: | (a) compressive strength (b) splitting tensile strength (Bazargan <i>et al.</i> , 2014)..... | 54 |
| Figure 17: | Water resistance index; briquettes immersed in water contained in a beaker | 54 |
| Figure 18: | Schematic diagram of the Laboratory Emission Monitoring System..... | 56 |

| | | |
|------------|--|----|
| Figure 19: | (a) Cookstove (Burn), (b) Weighing water, (c) gas analyser (PEMS, 2000) , (d) gas analyser (Ametek Land, lancom 4), (e) Filter holder, (f) Drying the filter paper, (g) furnace, (h) XRD/XRF analyser | 57 |
| Figure 20: | (a) & (b); TG and DTG thermograms for charcoal fines and binder, respectively, (c) temperature profile during TG and DTG analysis | 60 |
| Figure 21: | SEM micrographs; (a) Binder, (b) charcoal fines..... | 63 |
| Figure 22: | Bulk density versus binder concentration..... | 64 |
| Figure 23: | Impact resistance index (IRI) versus binder concentration (wt%) | 65 |
| Figure 24: | (a) Compressive strength, (b) splitting tensile strength | 66 |
| Figure 25: | Water resistance index versus binder concentration..... | 67 |
| Figure 26: | SEM micrographs of briquettes; (a) B25, (b) B30, (c) B35, (d) B40 | 71 |
| Figure 27: | TG and DTG thermograms for briquettes; (a) B25, (b) B30, (c) B35, (d) B40 | 72 |
| Figure 28: | Normal % probability vs Externally studentized residuals;(a) Bulk density, (b) Impact resistance index, (c) Compressive strength, (d) Splitting tensile strength, (e) Water resistance index | 80 |
| Figure 29: | Externally studentized residuals vs predicted;(a) Bulk density, (b) Impact resistance index, (c) Compressive strength, (d) Splitting tensile strength, (e) Water resistance index | 81 |
| Figure 30: | Predicted vs actual;(a) Bulk density, (b) Impact resistance index, (c) Compressive strength, (d) Splitting tensile strength, (e) Water resistance index | 82 |
| Figure 31: | Response surface plots; (a) bulk density, (b) impact resistance index, (c) compressive strength, (d) splitting tensile strength, and (e) water resistance index | 84 |
| Figure 32: | Ignition images; (a) Weighing bioethanol gel, (b) Briquettes loaded on the cookstove, (c) Bioethanol gel burning with a blue flame (d) Briquettes burning with a yellow flame, (e) ignited briquette with a red glow | 85 |
| Figure 33: | Combustion images; (a) Briquette B25 burning with white smoke, (b) Briquettes B25, B30, B35, and B40 burning with a yellow flame and soot (d) Briquettes burning without soot and yellow flame (e) Ash formation around the briquettes | 86 |

| | | |
|------------|---|-----|
| Figure 34: | Briquette B25 during ignition, CSHP, HSHP, and Simmer phases; (a) Temperature profiles, (b) Gaseous emissions | 89 |
| Figure 35: | Briquette B30 during ignition, CSHP, HSHP, and Simmer phases; (a) Temperature profiles, (b) Gaseous emissions | 89 |
| Figure 36: | Briquette B35 during ignition, CSHP, HSHP, and Simmer phases; (a) Temperature profiles, (b) Gaseous emissions | 90 |
| Figure 37: | Briquette B40 during ignition, CSHP, HSHP, and Simmer phases; (a) Temperature profiles, (b) Gaseous emissions | 91 |
| Figure 38: | Time to boil | 92 |
| Figure 39: | Burning rate | 93 |
| Figure 40: | (a) Thermal efficiency, (b) Dry fuel used, (c) Effective mass of water boiled, (d) Specific fuel consumption | 95 |
| Figure 41: | Firepower | 96 |
| Figure 42: | Total Emissions; (a) PM _{2.5} , (b) CO, (c) CO ₂ | 97 |
| Figure 43: | Emissions per MJ; (a) PM _{2.5} , (b) CO and (c) CO ₂ | 99 |
| Figure 44: | XRD analysis of ash and charcoal fines; A-Calcite (CaCO ₃), B- lime (CaO) | 102 |

LIST OF APPENDICES

| | | |
|--------------|--|-----|
| Appendix 1: | Boiling point of the binder..... | 116 |
| Appendix 2: | Equipment used for characterization: (a)Elemental (CHNSO) analyser, (b)Thermogravimetric analyser (c)Bomb Calorimeter, (d) SEM..... | 117 |
| Appendix 3: | Pouring temperature of the mixture (charcoal fines and binder)..... | 118 |
| Appendix 4: | Compaction pressure of the briquettes | 119 |
| Appendix 5: | LEMS hood, ducting and gravimetric assembly (Aprovecho Research Centre, 2018)..... | 120 |
| Appendix 6: | WBT 4.2.3 Data Calculation Sheet | 121 |
| Appendix 7: | TG and DTG results for the charcoal fines..... | 128 |
| Appendix 8: | TG and DTG results for the binder..... | 130 |
| Appendix 9: | Proximate analysis of charcoal fines (C), and binder (B)..... | 132 |
| Appendix 10: | Ultimate analysis of charcoal fines (C), and binder (B)..... | 133 |
| Appendix 11: | Higher heating value of charcoal fines (C), and binder (B) | 134 |
| Appendix 12: | Outside diameter (d_1), inside diameter (d_2), height (h), mass (m), volume (V), and density (ρ) of the briquettes | 135 |
| Appendix 13: | Impact resistance index (IRI) of the briquettes | 136 |
| Appendix 14: | Testing compressive strength of briquettes; (a)flat surface of briquette placed between horizontal metal plates, (b)beginning of experiment, (c) end of experiment | 137 |
| Appendix 15: | Testing splitting tensile strength of briquettes; (a) &(b) curved surface of briquette placed between horizontal metal plates..... | 138 |
| Appendix 16: | Compressive strength of briquettes | 139 |
| Appendix 17: | Splitting tensile strength of briquettes | 140 |
| Appendix 18: | Sample results from the materials testing machine (Testometric, FS300AT) | 141 |
| Appendix 19: | Sample results from the materials testing machine (Testometric, M500-25). | 145 |
| Appendix 20: | Water resistance index (WRI) of the briquettes | 146 |

| | | |
|--------------|---|-----|
| Appendix 21: | TG and DTG results for briquette B25 | 147 |
| Appendix 22: | TG and DTG results for briquette B30..... | 149 |
| Appendix 23: | TG and DTG results for briquette B35 | 151 |
| Appendix 24: | TG and DTG results for briquette B40..... | 153 |
| Appendix 25: | Proximate analysis of briquettes..... | 155 |
| Appendix 26: | Ultimate analysis of briquettes | 156 |
| Appendix 27: | Higher heating value of briquettes..... | 157 |
| Appendix 28: | Higher heating value (HHV), density and energy density of briquettes | 158 |
| Appendix 29: | Statistical analysis- ANOVA | 159 |
| Appendix 30: | Statistical analysis-Fisher's LSD..... | 161 |
| Appendix 31: | Experimental (Exp), predicted (pred) and deviation (dev) values of the responses | 163 |
| Appendix 32: | Ignition time of the briquettes | 164 |
| Appendix 33: | Temperature profiles and gaseous emissions during the WBT (B25)..... | 165 |
| Appendix 34: | Temperature profiles and gaseous emissions during the WBT (B30) | 169 |
| Appendix 35: | Temperature profiles and gaseous emissions during the WBT (B35)..... | 172 |
| Appendix 36: | Temperature profiles and gaseous emissions during the WBT (B40)..... | 175 |
| Appendix 37: | Water Boiling Test performance metrics..... | 178 |
| Appendix 38: | Images of the filter paper for briquettes B25, B30, B35, B40; (a) CSHP phase (b) HSHP phase, (c) Simmer phase | 183 |

LIST OF ABBREVIATION AND SYMBOLS

| | |
|----------------|---|
| Δt_c | Time to Boil |
| Δt_c^T | Temperature Corrected Time to Boil |
| Δt_h^T | Temperature Corrected Time to Boil |
| CB_c | Hood Carbon Balance |
| CB_h | Hood Carbon Balance |
| CB_s | Hood Carbon Balance |
| C_c | Mass of Char With Dish After Test |
| CE_c | Total Carbon in Exhaust |
| CC_c | Exhaust Carbon Concentration |
| CC_h | Exhaust Carbon Concentration |
| CC_s | Exhaust Carbon Concentration |
| C_h | Mass of Char With Dish After Test |
| CE_h | Total Carbon in Exhaust |
| C_s | Mass of Charcoal and Container After Test |
| CE_s | Time at Start of Simmer Phase |
| C_s | Total Carbon in Exhaust |
| $E_{CO_{2c}}$ | CO ₂ Emission Per Water Boiled |
| $E_{CO_{2h}}$ | CO ₂ Emission Per Water Boiled |
| $E_{CO_{2s}}$ | CO ₂ Emission Per Water Simmered |
| E_{CO_c} | CO Emission Per Water Boiled |
| E_{CO_h} | CO Emission Per Water Boiled |
| E_{CO_s} | CO Emission Per Water Simmered |
| $EF_{CO_{2c}}$ | CO ₂ Emission Factor |
| $EF_{CO_{2h}}$ | CO ₂ Emission Factor |
| $EF_{CO_{2s}}$ | CO ₂ Emission Factor |
| EF_{CO_c} | CO Emission Factor |
| EF_{CO_h} | CO Emission Factor |
| EF_{CO_s} | CO Emission Factor |
| EF_{PM_c} | PM Emission Factor |
| EF_{PM_h} | PM Emission Factor |

| | |
|---------------|--|
| EF_{PM_s} | PM Emission Factor |
| EF_{PM_s} | PM Emission Factor |
| E_{PM_c} | PM Emission Per Water Boiled |
| E_{PM_s} | PM Emission Per Water Simmered |
| f_{cd} | Equivalent Dry Wood Consumed |
| f_{ce} | Dry Fuel Consumed Estimated From Emissions |
| f_{cf} | Mass of Fuel After Test |
| f_{ci} | Mass of Fuel Before Test |
| f_{cm} | Fuel Consumed, Moist |
| f_{hd} | Equivalent Dry Wood Consumed |
| f_{he} | Dry Fuel Consumed Estimated From Emissions |
| f_{hf} | Mass of Fuel After Test |
| f_{hi} | Mass of Fuel Before Test |
| f_{hm} | Fuel Consumed, Moist |
| FP_c | Firepower |
| FP_h | Firepower |
| FP_s | Firepower |
| f_{sd} | Equivalent Dry Wood Consumed |
| f_{se} | Dry Fuel Consumed Estimated from Emissions |
| $T1_{si}$ | Starting Water Temperature ($T1_{si} = T1_{hf}$) |
| t_{si} | Time at End of Simmer Phase |
| f_{sf} | Mass of Unburned Fuel Remaining After Test |
| f_{sm} | Fuel Consumed, Moist |
| h_c | Thermal Efficiency |
| h_h | Thermal Efficiency |
| h_s | Thermal Efficiency |
| $m_{CO_{2c}}$ | CO ₂ Mass Produced |
| $m_{CO_{2h}}$ | CO ₂ Mass Produced |
| $m_{CO_{2s}}$ | CO ₂ Mass Produced |
| m_{CO_c} | Co Mass Produced |
| m_{CO_h} | CO Mass Produced |
| m_{CO_s} | CO Mass Produced |

| | |
|------------|---|
| m_{PM_c} | PM Mass Produced |
| m_{PM_h} | PM Mass Produced |
| m_{PM_s} | PM Mass Produced |
| N_2O | Dinitrogen Oxide |
| $P1_{cf}$ | Mass of Pot with Water After Test |
| $P1_{ci}$ | Mass of Pot with Water Before Test |
| $P1_{hf}$ | Mass of Pot with Water After Test |
| $P1_{hi}$ | Mass of Pot with Water Before Test |
| $P1_{sf}$ | Mass of Pot with Water After Test |
| $P1_{sf}$ | Mass of Charcoal and Container After Test |
| $P1_{si}$ | Starting Mass of Pot with Water before Test |
| P_{atm} | Atmospheric Pressure |
| r_{cb} | Burning Rate |
| r_{hb} | Burning Rate |
| r_{sb} | Burning Rate |
| SC_c | Specific Fuel Consumption |
| SC_c^T | Temperature-Corrected Specific Fuel Consumption |
| SC_h | Specific Fuel Consumption |
| SC_h^T | Temperature-Corrected Specific Fuel Consumption |
| SC_s | Specific Fuel Consumption |
| SE_c^T | Temperature-Corrected Specific Energy Consumption |
| SE_h^T | Temperature-Corrected Specific Energy Consumption |
| SE_s | Specific Energy Consumption |
| $T1_{cf}$ | Water Temperature at End of Test |
| $T1_{ci}$ | Water Temperature at Start of Test |
| $T1_{hf}$ | Water Temperature at End of Test |
| $T1_{hi}$ | Water Temperature at Start of Test |
| $T1_{sf}$ | Water Temperature at End of Test |
| $T1_{si}$ | Water Temperature at Start of Test |
| $T1_{si}$ | Water Temperature at End of Test |
| T_a | Ambient Temperature |
| T_b | Local Boiling Point of Water |

| | |
|------------------|--|
| T_{cd} | Average duct temperature |
| t_{cf} | Time at End of Test |
| t_{ci} | Time at Start of Test |
| T_{hd} | Average Duct Temperature |
| t_{hf} | Time at End of Test |
| t_{hi} | Time at Start of Test |
| T_{sd} | Average Duct Temperature |
| t_{si} | Mass of Unburned Fuel Remaining After Test |
| V_c | Total Exhaust Flow |
| V_h | Total Exhaust Flow |
| V_s | Total Exhaust Flow |
| w_{cr} | Effective Mass of Water Boiled |
| w_{cv} | Water Vaporized |
| w_{hr} | Effective Mass of Water Boiled |
| w_{hv} | Water Vaporized |
| w_{sr} | Effective Mass of Water Simmered |
| w_{sv} | Water Vaporized |
| ΔC_c | Change in Char During Test |
| ΔC_h | Change in Char During Test |
| ΔC_s | Change in Char During Test |
| Δt_c | Time to Boil |
| Δt_h | Time to Boil |
| Δt_s | Time to Boil |
| ANOVA | Analysis of Variance |
| ASTM | American Society for Testing and Materials |
| AVG | Average |
| C | Carbon |
| CO ₂ | Carbon Dioxide |
| CO _{2b} | Background CO ₂ Concentration |
| CO _{2c} | Average CO ₂ concentration |
| CO _{2h} | Average CO ₂ Concentration |
| CO _{2s} | Average CO ₂ Concentration |

| | |
|---------------------|---|
| CO _b | Background CO Concentration |
| CO _c | Average CO concentration |
| CO _h | Average CO concentration |
| CO _s | Average CO Concentration |
| CharFracC | Char Carbon Fraction |
| CO | Carbon Monoxide |
| CREEC | Centre for Research in Energy and Energy Conservation |
| CSHP | Cold Start High Power |
| Diff | Difference |
| DTG | Differential Thermogravimetric |
| EHV | Effective Calorific Value |
| FC | Fixed Carbon |
| FuelFracC | Fuel Carbon Fraction |
| GHGs | Greenhouse Gases |
| H | Hydrogen |
| HHV | higher heating value |
| HSHP | Hot Start High Power |
| Int | Intensity |
| IRI | Impact Resistance Index |
| IWA | International Workshop Agreement |
| k | Mass of Charcoal Container |
| LCL | Lower Critical Limit |
| LEMS | Laboratory Emission Monitoring System |
| LHV _{char} | Lower Heating Value of char |
| LHV | Lower Heating Value |
| LHV | Lower heating value |
| LSD | Least Significance Difference |
| MC _{wet} | Moisture Content (wet basis) |
| MC | Moisture Content |
| Mtoe | Mega Tonnes of Oil Equivalent |
| N | Nitrogen |
| NO ₂ | Nitrogen Dioxide |
| NO _x | Nitrogen oxides |

| | |
|-----------------|---|
| NO | Nitrogen monoxide |
| O | Oxygen |
| PM _b | Background particulate matter concentration |
| PM _c | Average Particulate Matter Concentration |
| PM _h | Average PM concentration |
| PM _s | Average PM Concentration |
| P1 | Dry mass of empty pot |
| PEMS | Portable Emission Monitoring System |
| PM | Particulate Matter |
| Prob | Probability |
| PVA | polyvinyl acetate |
| Q | Hood flow rate |
| S | Sulphur |
| SO ₂ | Sulphur Dioxide |
| SO ₃ | Sulphur Trioxide |
| SE | Square Error |
| SEM | Scanning Electron Microscopy |
| STD | Standard Deviation |
| TDR | Turn Down Ratio |
| TG | Thermogravimetric |
| UCL | Upper Critical Limit |
| VM | Volatile Matter |
| WBT | Water Boiling Test |
| WHO | World Health Organization |
| WRI | Water Resistance Index |
| XRD/XRF | X-Ray Diffraction/X-Ray Fluorescence |

CHAPTER ONE

INTRODUCTION

1.1 Background of the Problem

Biomass follows coal and oil as the world's third largest energy source. Biomass continues to meet a major fraction of the energy demand in rural areas of most developing countries and its potential is estimated at 1250 Mtoe of primary energy. This is about 14% of the world's annual energy consumption (Sugumaran & Seshadri, 2010). A number of countries in the world are implementing policies towards decreasing greenhouse gas emissions, to secure and diversify the supply of energy (Heinimö & Junginger, 2009).

Charcoal is the predominant fuel used in many developing countries for domestic and commercial purposes. Transport and handling of charcoal produces fines about to 10-20% by weight (Rousset *et al.*, 2011). Charcoal fines are also obtained from the production of charcoal from sustainably managed planted eucalyptus forests or from the steel industry, a major consumer of charcoal (Rousset *et al.*, 2011). The fines can be turned into lumps of charcoal by briquetting using suitable binders. Biochar from pyrolysis of biomass waste can also be used in production of briquettes (Fadhil, 2020). For transport, handling, and storage, briquettes with high density and mechanical strength are preferred. High density reduces transport and storage costs while high compressive strength, i.e. >2.56 MPa prevents breakages (Okot *et al.*, 2018).

Oleoresins are complex mixtures of acidic and neutral diterpenes together with a more or less important fraction of volatile compounds (monoterpenes and sesquiterpenes). Industrial processing by steam distillation converts the crude oleoresin into gum turpentine (volatile compounds) and gum rosin (diterpenes). Both gums in turn are further processed into chemical industrial products such as food gums, coatings, adhesives, cleaners, printing inks, disinfectants, pharmaceuticals, fragrances and flavouring (Rezzi *et al.*, 2005). Diterpene (C₂₀) resin acids are the major components of rosin (da Silva Rodrigues-Correia *et al.*, 2013). Yadav *et al.* (2014) reported that diterpenoids and triterpenoids are not steam volatile and they are obtained from plants, tree gums and resins. Bhattacharya *et al.* (1989) classified resin under organic binders.

Natural and synthetic resins (e.g. acrylic, phenolic, formaldehyde) (Drobíková *et al.*, 2015) have been used in several studies for production of briquettes. Thoms *et al.* (1999) studied physical characteristics of cold cured anthracite/coke breeze briquettes prepared from a coal tar acid resin. Briquettes with excellent properties such as mechanical strength, thermal degradation, and water-proofing characteristics were produced. Benk (2010) studied briquette binders using air blown coal

tar pitch and phenolic resins as raw materials. The optimum amount of air blown coal tar pitch was 50% w/w in the blended binder. Briquettes cured at 200°C for 2 h had a tensile strength of 50.45 MN/m². When the cured briquettes were carbonized at temperatures of 470°C, 670°C and 950°C, their strength increased with temperature up to 71.85 MPa. Sotannde *et al.* (2010) produced charcoal briquettes from neem wood residues using starch and gum arabic (gum extract from *Acacia senegal L.*) as binders. The briquettes were analysed for fixed carbon, volatile matter, ash content and heating value. The results showed that gum arabic bonded briquettes with a blending ratio of charcoal: binder of 10:3 had better physical and combustion qualities than starch bonded briquettes with a blending ratio of charcoal: binder of 5:1.

The *Canarium Schweinfurthii* tree is found throughout tropical Africa in rainforest, gallery forest, and transitional forest from Senegal to Cameroon and extending to Ethiopia, Tanzania and Angola (Kuate, 2017). The essential oil of African Elemi resin from Uganda contains monoterpenes mainly α -phellandrene, α -terpineol, β -linalool, γ -terpinene, *p*-cymene, sabinene, carvenone and 6-camphenone (Nagawa *et al.*, 2015). The terpenoids α -phellandrene, *p*-cymene, and γ -terpinene are classified under monoterpenoid hydrocarbons while α -terpineol, β -linalool, carvenone, and 6-camphenone are classified under oxygenated monoterpenoids (Šiler & Mišić, 2016). Yousuf *et al.* (2011) isolated 3 α -Hydroxytirucalla-8,24-dien-21-oic (epielemadienolic) acid, a triterpene derivative from *Canarium Schweinfurthii* Engl. resin. The GC-MS of *Canarium Schweinfurthii* gum obtained by Ameh (2018) revealed the following phytoconstituents; Stearic acid, 1-penta-decanecarboxylic acid, 2-(hydroxymethyl)-2-nitropropane-1,3-diol, Nonacosane, 1-piperoylpiperidine, dihex-5-en-2-yl phthalate, Stigmasta-5,22-dien-3-ol, 9-octadecenoic acid, methyl ester, and Oleic acid. Thus, this study characterized the charcoal fines, *Canarium Schweinfurthii* resin as an alternative binder and also determined the physical and chemical properties of carbonized briquettes produced from charcoal fines using the resin as binder. The carbonized briquettes were tested on an improved cookstove using the Laboratory Emission Monitoring System (LEMS) to assess their suitability for cooking as well as the resulting emissions.

1.2 Statement of the Problem

Charcoal fines are a byproduct of transport and utilization of charcoal. The charcoal fines can be recycled through production of briquettes using binders. Binders are classified into three groups namely; organic, inorganic, and compound binders. Starch and molasses are the most common organic binders used for briquette production. Starch is used as food while the molasses are used as animal feed and as fermentation sources for ethyl alcohol and other chemicals. The inorganic

binders mainly used for production of briquettes are lime and clay. The inorganic binders have high ash content.

Natural resins e.g., gum arabica and synthetic resins e.g., coal tar pitch, coal tar acid, and phenolic have been used as binders for production of briquettes (Benk, 2010; Sotannde *et al.*, 2016; Thoms *et al.*, 1999). In Uganda, *Canarium Schweinfurthii* resin is currently used as an incense by the local people and on religious ceremonies (Nagawa *et al.*, 2015). *Canarium Schweinfurthii* resin, being a natural resin has potential for application as an organic binder. There is limited information on use of the resin as a binder for briquette production thus, the need to investigate its potential. This study aimed at production of carbonized briquettes using *Canarium Schweinfurthii* resin as binder as well as testing for ignition and emissions resulting from their utilisation.

1.3 Rationale of the Study

Charcoal is the predominant fuel used in many developing countries for domestic and commercial purposes. Transport and handling of charcoal produces fines about to 10-20% by weight (Rousset *et al.*, 2011). Charcoal fines are also obtained from the production of charcoal from sustainably managed planted eucalyptus forests or from the steel industry, a major consumer of charcoal (Rousset *et al.*, 2011). The fines can be turned into lumps of charcoal by briquetting using suitable binders. Biochar from pyrolysis of biomass waste can also be used in production of briquettes (Fadhil, 2020). For transport, handling, and storage, briquettes with high density and mechanical strength are preferred. High density reduces transport and storage costs while high compressive strength, i.e. >2.56 MPa prevents breakages (Okot *et al.*, 2018). There is limited information on use of the resin as a binder for briquette production thus, the need to investigate its potential. This study aimed at production of carbonized briquettes using *Canarium Schweinfurthii* resin as binder as well as testing for ignition and emissions resulting from their utilisation

1.4 Research Objectives

1.4.1 General Objective

To evaluate carbonized briquettes produced from charcoal fines using *Canarium Schweinfurthii* resin as binder.

1.4.2 Specific Objectives

The specific objectives of the study were to:

- (i) Assess the properties of charcoal fines, and *Canarium Schweinfurthii* resin.

- (ii) Investigate the physical and chemical properties of carbonized briquettes produced from charcoal fines using *Canarium Schweinfurthii* resin as a binder.
- (iii) Analyse the ignition, combustion and emissions of the produced carbonized briquettes.

1.5 Research Questions

- (i) What are the physical and chemical properties of charcoal fines, and binder?
- (ii) How does the mixing ratio of charcoal fines and binder as well as compaction pressure affect the performance of the carbonized briquettes?
- (iii) What is the ignition and combustion performance of the carbonized briquettes?
- (iv) To what extent do the emissions from combustion of carbonized briquettes conform with the standards?

1.6 Significance of the Study

- (i) The research provided baseline information on the use of *Canarium Schweinfurthii* resin as a binder for production of carbonized briquettes.
- (ii) Analysis of the products of combustion provided information towards safe utilisation of the developed carbonized briquettes.
- (iii) Production of briquettes contributes to the economy, in terms of income, tax revenue and employment.

1.7 Delineation of the Study

The research was limited to investigation of *Canarium Schweinfurthii* resin as a binder for production of carbonized briquettes using charcoal fines. Furthermore, the study assessed the emissions resulting from use of carbonized briquettes.

CHAPTER TWO

LITERATURE REVIEW

2.1 Biomass, Biofuels and Bioenergy

Biomass is an organic material which has stored sunlight in the form of chemical energy e.g. herbaceous plant matter, wood, crop and forest residues, and dung. Biofuels are solid, liquid or gaseous fuels produced from biomass. Bioenergy means any usable energy obtained from biofuels (Tilli, 2003). Table 1 shows the proximate analysis (moisture, volatile matter, fixed carbon, ash) of selected biomass (feedstock) and biofuels (carbonized feedstock and briquettes). Table 2 shows the ultimate analysis as well as the higher heating values (HHV) of the feedstock and biofuels. From Table 2, the HHV of the feedstock (uncarbonized) is 12.6-18.89 MJ/kg while the HHV of the feedstock (carbonized) is 14.3-29.10 MJ/kg. Ward *et al.* (2014) produced carbonized briquettes from human waste and reported an HHV of 21-25 MJ/kg. Lubwama and Yiga (2017) reported that high ash content reduces heating value, increases thermal resistance to heat transfer, and leads to generation of slag deposits which requires frequent equipment maintenance.

Table 1: Proximate analysis of selected feedstock and briquettes; FS-UC (feedstock- uncarbonized), FS-C (feedstock-carbonized), B-C (briquettes-carbonized)

| Feedstock | Proximate analysis (FS-UC) | | | | Proximate analysis (FS-C) | | | | Proximate analysis (B-C) | | | | Reference |
|--------------------|----------------------------|--------|--------|---------|---------------------------|--------|--------|---------|--------------------------|--------|--------|---------|-----------------------------------|
| | Moisture (%) | VM (%) | FC (%) | Ash (%) | Moisture (%) | VM (%) | FC (%) | Ash (%) | Moisture (%) | VM (%) | FC (%) | Ash (%) | |
| Low rank coals (1) | 17.6 | 30.4 | 34.7 | 17.3 | 1.1 | 10.2 | 68.7 | 20 | n.a | n.a | n.a | n.a | |
| Low rank coals (2) | 18.4 | 33.7 | 38.3 | 9.6 | 2 | 11.8 | 74.6 | 11.6 | n.a | n.a | n.a | n.a | |
| Sawdust | 9.8 | 77.7 | 9.6 | 2.9 | 3.8 | 27.1 | 60.7 | 7.9 | n.a | n.a | n.a | n.a | Blesa <i>et al.</i> (2001) |
| Straw | 9.6 | 68.3 | 14.2 | 7.9 | 2.9 | 20.8 | 60.5 | 15.8 | n.a | n.a | n.a | n.a | |
| Olive stone | 10.2 | 70.5 | 17.2 | 2.1 | 3.2 | 19.5 | 74.1 | 3.3 | n.a | n.a | n.a | n.a | |
| Almond shell | 9.2 | 70.4 | 18 | 2.4 | 1.2 | 24.8 | 72.6 | 1.4 | n.a | n.a | n.a | n.a | |
| Water hyacinth | n.a | n.a | n.a | n.a | n.a | n.a | n.a | n.a | 18.1 | 47.4 | 15 | 19.5 | Carnaje <i>et al.</i> (2018) |
| Hazelnut shells | 0 | 72 | 21 | 7 | n.a | n.a | n.a | n.a | n.a | n.a | n.a | n.a | Haykiri-Acma and Yaman (2010) |
| Brown seaweed | 5 | 63.3 | 9.2 | 22.5 | 0 | 21.9 | 18.3 | 59.8 | n.a | n.a | n.a | n.a | Haykiri-Acma <i>et al.</i> (2013) |
| Groundnut shells | 9.2 | 67.7 | 19.3 | 3.8 | n.a | n.a | n.a | n.a | 6.7-7.3 | 20-28 | 48-55 | 17-22.5 | Lubwama and Yiga (2017) |
| Bagasse | 22.5 | 62.7 | 12.2 | 2.5 | n.a | n.a | n.a | n.a | 6-6.8 | 32-37 | 48-52 | 11-12.5 | |
| Durian peel | n.a | n.a | n.a | n.a | n.a | n.a | n.a | n.a | 0.01 | 3.94 | 78 | 18.18 | Nuriana <i>et al.</i> (2014) |
| Municipal waste | 8.69 | 69.76 | 10.78 | 10.77 | n.a | n.a | n.a | n.a | 5.88 | 63.94 | 15.8 | 14.39 | Prasityo usil and |

| Feedstock | Proximate analysis (FS-UC) | | | | Proximate analysis (FS-C) | | | | Proximate analysis (B-C) | | | | Reference |
|-----------------------|----------------------------|--------|--------|---------|---------------------------|--------|--------|---------|--------------------------|--------|--------|---------|-------------------------------|
| | Moisture (%) | VM (%) | FC (%) | Ash (%) | Moisture (%) | VM (%) | FC (%) | Ash (%) | Moisture (%) | VM (%) | FC (%) | Ash (%) | |
| composting | | | | | | | | | | | | | Muenjinga (2013) |
| Sawdust | 6.74 | 67.43 | 19.71 | 6.12 | n.a | n.a | n.a | n.a | n.a | n.a | n.a | n.a | |
| Cassava rhizome waste | 11.79 | 59.65 | 24.43 | 4.13 | 7.23 | 46.39 | 32.9 | 13.48 | n.a | n.a | n.a | n.a | Sen and Annachatre (2016) |
| Sugarcane bagasse | n.a | n.a | n.a | n.a | 30-70 | n.a | 34 | 62 | 9.19 | 5.464 | 48.6 | 34.74 | Teixeira <i>et al.</i> (2010) |
| fly ash | | | | | | | | | | | | | Ward <i>et al.</i> (2014) |
| Human waste | n.a | n.a | n.a | n.a | n.a | n.a | 49 | 20 | n.a | n.a | n.a | n.a | |

n.a-not available, VM (volatile matter), FC (fixed carbon)

Table 2: Ultimate analysis and higher heating value (HHV) of selected feedstock and briquettes; feedstock- uncarbonized (FS-UC), feedstock-carbonized (FS-C), briquettes-carbonized (B-C)

| Feedstock | Ultimate analysis (FS-UC) | | | | | HH V (FS- UC) | Ultimate analysis (FS-C) | | | | | HHV (FS-C) | HH V (B- C) | Reference |
|----------------------------------|---------------------------|----------|----------|----------|----------|------------------------|--------------------------|---------------|---------------|-------------------|-----------|-----------------|----------------------|---|
| | C (%) | H (%) | N (%) | S (%) | O (%) | MJ/ kg | C (%) | H (%) | N (%) | S (%) | O (%) | MJ/kg | MJ/ kg | |
| Palm kernel shell | n.a | n.a | n.a | n.a | n.a | n.a | 81.4 | 1.6 | 1.8 | 0.16 | | 27.51- 28.1 | | Bazargan <i>et al.</i> (2014) |
| Hazelnut shells | 54.8 | 6.7 | 1 | 0.1 | 37.4 | 18.8 9 | n.a | n.a | n.a | n.a | n.a | n.a | n.a | Haykiri-Acma and Yaman (2010) |
| Brown seaweed | 42.7 | 6.5 | 4.2 | 1.7 | 44.6 | 12.6 | 84.8 | 2 | 4.2 | 4.8 | 4.2 | 14.3 | n.a | Haykiri-Acma <i>et al.</i> (2013) |
| Palm empty fruit branches | 48.8 | 6.3 | 0.7 | 0.2 | 36.7 | 16.3 8 | | | | | | | | |
| Rice husk | n.a | n.a | n.a | n.a | n.a | n.a | 35.9 - 36.6 | 2.36- 2.42 | 0.41- 0.45 | 0.08 - 0.16 | n.a | 18.43- 24.16 | | Jamradloedluk and Wiriyaumpai wong (2007) |
| Rice straw | n.a | n.a | n.a | n.a | n.a | n.a | 49.4 - 51.8 | 3.43- 3.64 | 0.77- 0.82 | 0.17 - 0.19 | n.a | 21.37- 24.98 | | |
| Water hyacinth | n.a | n.a | n.a | n.a | n.a | n.a | 23.5 - 24.2 | 2.08- 2.13 | 0.70- 0.73 | 0.32 - 0.38 | n.a | 17.04- 22.04 | | |
| Bagasse | n.a | n.a | n.a | n.a | n.a | n.a | 65.3 - 66.4 | 3.53- 3.78 | 0.35- 0.40 | 0.13 - 0.22 | n.a | 22.64- 29.10 | | |
| Human waste | n.a | n.a | n.a | n.a | n.a | n.a | 58.2 3 | 6.1 | 5.19 | 0.43 | 10.0 5 | 25.57 | 21- 25 | Ward <i>et al.</i> (2014) |

2.2 Fundamental Aspects of Briquetting

2.2.1 Overview

Briquetting is one of the agglomeration/ densification technologies which increases the density of residues for energy production. Briquetting utilizes raw materials such as loose biomass, waste from wood industries, and other combustible waste products (Grover & Mishra, 1996). The diameter of a briquette is 50-80 mm (Tilli, 2003). Prasityousil and Muenjina (2013) produced carbonized briquettes from municipal waste composting char and sawdust char and the cylindrical briquettes had an outside diameter of 3.8 cm, inside diameter of 1.3 cm and height of 15 cm. Teixeira *et al.* (2010) produced carbonized briquettes from sugarcane bagasse fly ash having a diameter of 30 mm. Figure 1 shows the different types of briquettes.

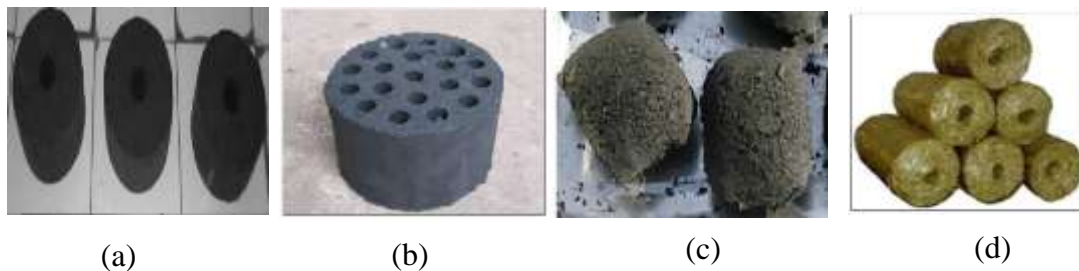


Figure 1: (a) Carbonized briquettes with a hole at the centre (Suhartini *et al.*, 2011), (b) carbonized honey comb briquette with multiple holes (Ferguson, 2012), (c) carbonized briquette without a hole (Carnaje *et al.*, 2018), (d) uncarbonized straw briquette with a hole at the centre (Ferguson, 2012)

2.2.2 Properties of Solids Important to Densification

According to Grover and Mishra (1996), the properties of solids that are important to densification are:

- (i) Flow ability and cohesiveness (binders and lubricants can impart these characteristics for compaction)
- (ii) Surface forces (important to agglomeration for strength)
- (iii) Particle size (too fine a particle means higher cohesion, causing poor flow)
- (iv) Hardness (too hard a particle leads to difficulties in agglomeration)
- (v) Adhesiveness

- (vi) Particle size distribution (sufficient fines are needed to cement larger particles together for a stronger unit).

2.2.3 Compaction Characteristics of Biomass and their Significance

(i) Particle size

Generally, biomass material of 10-20% powdery component (< 4 mesh) with 6-8 mm size gives the best results. The packing dynamics is improved due to the different size particles which also contributes to high static strength. Fine and powdered particles of size less than 1 mm are not suitable for a screw extruder since they are less dense, more cohesive, non-free flowing entities. (Grover & Mishra, 1996). Bazargan *et al.* (2014) did a study on compaction of palm kernel shell biochars for application as solid fuel and considered the following particle sizes; $S_1 > 3000 \mu\text{m}$, $700 < S_2 < 3000 \mu\text{m}$, $300 < S_3 < 700 \mu\text{m}$ and $S_4 < 300 \mu\text{m}$. The results showed that particle size $S_4 < 300 \mu\text{m}$ had the highest splitting tensile strength. Blesa *et al.* (2001) did a study on effect of the pyrolysis process on the physicochemical and mechanical properties of smokeless fuel briquettes and the particle size of the pyrolysed materials considered were: coals (0.5–0.25 mm), sawdust (<1 mm), olive stone (<0.83 mm). Prasityousil and Muenjina (2013) produced carbonized briquettes from municipal waste composting char and sawdust char using an ASTM sieve no. 4 (pore size 4.75 mm).

(ii) Moisture

When the feed moisture content is 8-10 %, the briquettes will have 6-8% moisture, will be strong and free of cracks and the briquetting process is smooth. Moreover, water acts as a film type binder by strengthening the bonding in briquettes. For organic and cellular products, water helps in promoting bonding by van der Waals' forces by increasing the true area of contact of the particles (Grover & Mishra, 1996). From Table 1, the moisture content of uncarbonized feedstock is 5-22.5%, carbonized feedstock is 0-70% and for carbonized briquettes is 0.01-18.1%. Teixeira *et al.* (2010) produced carbonized briquettes from sugarcane bagasse fly ash and reported that moisture content of the feedstock was 30-70%. However, the feedstock was passed through a filter press or belt press extruder to reduce the moisture and final drying was done using a gas washer to achieve the recommended moisture content for briquette production.

(iii) Temperature of Biomass

Variation of the temperature of biomass affects the briquette moisture stability, density, and crushing strength. High pressure conditions cause the moisture in the biomass to form steam which

then hydrolyses the lignin and hemicellulose parts of biomass into lower lignin products, molecular carbohydrates, sugar polymers and other derivatives which provide a bonding effect “in situ”. The die temperature should be in the range of 280-290°C (Grover & Mishra, 1996). Maize cob briquettes densified between 20-80°C showed that at a temperature of 80°C, the produced briquettes had high density and durability/ mechanical strength (Kpalo *et al.*, 2020a).

(iv) Temperature of the Die

This is important for medium pressure compaction with a heating device and no binder is necessary (Grover & Mishra, 1996). The die temperature facilitates the release of components such as cellulose, lignin, and hemicellulose and the lignin acts as binder (Kpalo *et al.*, 2020a). The screw type briquetting machine can be operated with less power leading to a longer life of the die. Furthermore, the surface of the briquette is partially carbonized/torrefied to a dark brown colour making the briquette resistant to atmospheric moisture during storage. The temperature should be in the range 280-290°C (Grover & Mishra, 1996).

(v) External Additives

Addition of coal and charcoal in very fine form improves the heating value and combustibility of the briquettes. About 10-20% char fines can be used in briquetting without impairing their quality. In addition, only screw pressed briquettes can be carbonized (Grover & Mishra, 1996). From Table 1, it can be noted that briquettes are made from a single feedstock or blending different feedstock. This is mainly done to supplement different feedstock due to scarcity and to ensure sustainability as well as enhance the HHV of the resulting briquettes. Lubwama *et al.* (2020) did a study on effects and interactions of the agricultural waste residues and binder type on physical properties and calorific values of carbonized briquettes. Experiments with cassava starch binder and wheat starch binder showed that the physical properties of the developed briquettes were affected significantly by the carbonized agricultural residue used and binder type. Also, calorific values of groundnut shell and bagasse briquettes were found to be significantly affected by the agricultural residue type.

2.2.4 Types of Binders

Briquetting at low pressure requires a binding agent to aid in the formation of bonds between the biomass particles. The binders are classified into organic, inorganic and compound binders (Zhang *et al.*, 2018).

(i) Organic Binders

These are classified into four types, namely; biomass binders, tar pitch and petroleum bitumen binders, lignosulphonate binders and polymer binders. Biomass binders include; agricultural waste, forestry biomass, aquatic plants, Tar pitch and petroleum bitumen binders include; petroleum bitumen, coal tar, coal tar pitch, tar residue, lignin liquor. Lignosulphonate binders include; lignin derivative, paper mill, lignin liquor. Polymer binders include starch and polyvinyl acetate (PVA). The advantages of organic binders are; good bonding, good combustion performance, high drop test strength, high crush strength, low ash. The disadvantages of organic binders are; high price, decompose easily and burn when heated (mechanical strength and thermal stability of organic binder briquettes are poor) (Zhang *et al.*, 2018).

(ii) Inorganic Binders

They are classified into three types, namely; industrial binders, civilian binders and environmental protection binders. Industrial binders include; clay, limestone, bentonite, cement. Civilian binders include; clay and limestone. Environmental protection binders include; calcium oxide, limestone, iron oxide, magnesium oxide. The merits of inorganic binders include; low cost, strong adhesion, abundant resource, non-pollution, excellent thermal stability, and good hydrophilicity. The demerit of inorganic binders is the increased amount of ash (Zhang *et al.*, 2018).

(iii) Compound Binders

They are composed of at least two binders each performing a different role. The merits of compound binders are; improve the quality of briquettes, reduce the amount of inorganic binder, reduce the cost of organic binder and better performance of briquettes (Zhang *et al.*, 2018).

2.2.5 Binding Mechanisms of Densification

The behaviour of biomass as a fuel is influenced by its chemical and physical properties. Chemical properties include proximate analysis, ultimate analysis, and HHV. Physical properties include bulk density, moisture content, void volume, and thermal properties. The binding mechanisms under high pressure are divided into attractive forces between solid particles, adhesion and cohesion forces, and interlocking bonds (Grover & Mishra, 1996). Two hypotheses of briquette forming mechanisms have been proposed namely; non-binder briquetting mechanism, and cold-press briquetting mechanism with binder (Zhang *et al.*, 2018).

(i) Non-Binder Briquetting Mechanism

The hypotheses have been proposed for lignite and include; bituminous/ humic acid hypothesis, capillary hypothesis, colloid hypothesis, and adhesion molecules hypothesis (Zhang *et al.*, 2018).

Bituminous/ Humic Acid Hypothesis

Young lignite is easy to briquette due to its high content of humic acid and asphaltine. In addition, the asphaltine will soften and become a plastic substance in the temperature range of 70–90°C. Asphaltine and humic acid thus act as its own binder. Furthermore, pitch in lignite acts as binder, which holds coal particles together under the action of external force and suitable temperature. Also, the free humic acid in lignite has strong polarity and colloid properties, which could hold coal particles together during briquetting. The limitation of the hypothesis is that, pulverized coal used for briquetting is still very good after the extraction of humic acid, and the resulting briquettes have high strength (Zhang *et al.*, 2018).

Capillary Hypothesis

It postulates that there is a large number of hydrated capillary precocities in lignite. During briquetting under an applied pressure, the capillaries will crush; the water is squeezed out from the capillaries, and covers the surface of the coal particles to form a water film. Consequently, the water film will fill the voids between coal particles, and become the interaction force between molecules. When the pressure is released, the capillary regains a little dilation, some water will return into the capillaries, and the rest will remain on the surface of coal particles to form the crescent shape because of the effect of surface tension. Finally, the coal grains are bonded into a solid lump under the action of capillary force. The limitation of the hypothesis is that the formability of European lignite is better than Yunnan lignite, although they were formed at the same time. In addition, the capillary force disappears when lignite is dried but the lignite can still shape under high pressure, and the briquette strength is high (Zhang *et al.*, 2018).

Colloid Hypothesis

This hypothesis postulates that lignite comprises solid and liquid colloidal material. The solid material consists of tiny granular humic acid which comes together and produces intermolecular cohesion under the action of external force. Since these cohesions possess charge, it makes the solution contact with crystal molecules, combining to form jellylike colloidal particles. The intermolecular cohesion varies with the coal rank and coal's property. Coal particles are bonded together under pressure by means of Van der Waals force or molecular adhesive force. The smaller

the particle size, the larger is the specific surface area and increased bonding of binder resulting in greater strength of the briquette. The limitation of the hypothesis is that some non-colloid materials such as metal powder and salt crystals are also easy to shape. In addition, lignite is not a crystalline polymer with a regular molecular structure thus, it is not sufficient to explain lignite shaping only by colloid hypothesis (Zhang *et al.*, 2018).

Adhesion Molecules Hypothesis

It postulates that the bonding force of particles is due to water forced from primary capillary pores and filled in the gap between particles under pressure. The water between the particles produces a surface tension resulting in the formation of secondary capillary adsorption force. As a result, Van der Waals and capillary force bond the coal particles together. The molecular adhesive force is a result of coal particles coming close to each other. However, the hypothesis can't explain non-binder lignite briquetting of north-east Inner Mongolia and Yunnan (Zhang *et al.*, 2018).

(ii) The Cold-Press Briquetting Mechanism with Binder

The hypotheses of briquetting mechanism with binder are mainly proposed for lignite, anthracite, and bituminous coal. They include; soaking and bridging, mechanic and chemical bonding force, and the minimal contact angle and maximum bonding power.

Soaking and Bridging Mechanism

The quality of briquette is directly influenced by the soaking and bonding between coal particles and binder. Materials with high viscosity such as organic solvents and asphalt are used as binder. When the pores and surface of the coal particles are covered with binder, solid bridge is formed at the coal particle contact point. The viscosity, water content, and components of tar have significant effects on caking property and wetting degree when tar is used as binder. The viscosity of bitumen affects the compressive strength of briquette, and the content of coke-forming components affects the thermal stability of briquette. Briquettes prepared with corn starch binder and silicon-containing binder showed that silicon-oxygen bonds formed between silica acid gel particles after the curing reaction have the effect on connection bridge (negative ion connection bridge), which can connect the gel particles and coal particles into a complex net structure (Fig. 2 and 3) (Zhang *et al.*, 2018).

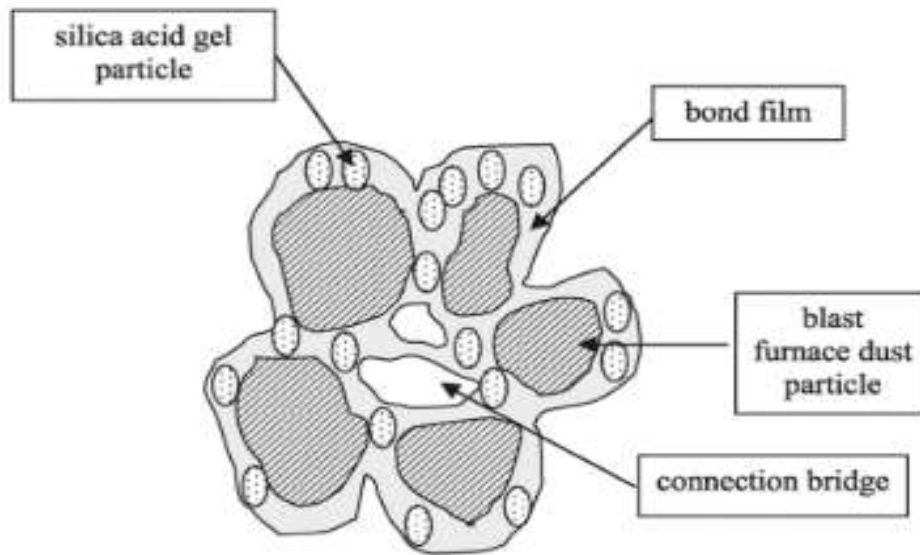


Figure 2: The bonding mechanism of sodium silicate (Zhang *et al.*, 2018)

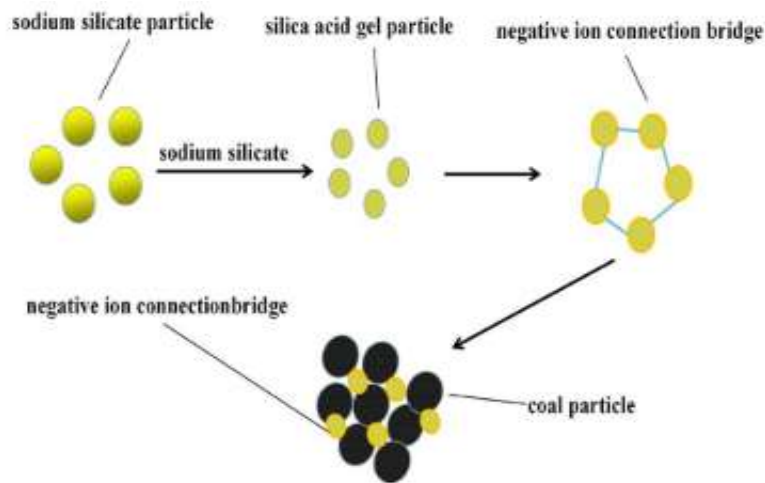


Figure 3: The bonding mechanism of sodium silicate (Zhang *et al.*, 2018)

The Mechanic and Chemical Bonding Force

This postulates that the interaction between coal particles and binder is a complex process, including wetting, mass transfer as well as combination of both factors. The adhesive strength between binder and coal particles is comprehensive. Mechanical power plays a major role for nonpolar coal particles in briquetting process. During pressing of the briquette, the binder/adhesive penetrates the pores and the cured briquettes, as a result of mechanical bonding, have improved strength. The strength of briquette is influenced by the curing conditions and water content. During the drying process, with the reduction of water from coal particles, the distance between the coal particles is reduced, the friction between the coal particles is increased, and briquette strength is increased (Zhang *et al.*, 2018).

Adding inorganic adhesives to coal with a certain amount of water and applying an external force, results in relative slip between the minerals and the binders in coal particles, leading to simultaneous increase in attraction and repulsion as a result of the decrease of the distance between coal particles. Attraction is mainly capillary forces, covalent, and ionic bonding forces on the contact surface. The crushing strength of the briquette is higher when the attractive force is greater than the repulsive force. According to solvent solubility parameter close principle, as solvents to dissolve coating finishing agents, organic binder has strong affinity for coal particles. A covalent or hydrogen bond forms when binder molecules with active groups share a pair of electrons with coal's active groups. Figure 4 shows the hydroxyl groups on the surface of kaolin. The hydroxyl groups could combine with functional groups on coal surface to produce hydrogen bond, which contributes to briquetting. In addition, the organic binder can penetrate into coal's small cell, mesh force is generated in the interface after drying and solidifying, which improves the briquetting strength (Zhang *et al.*, 2018).

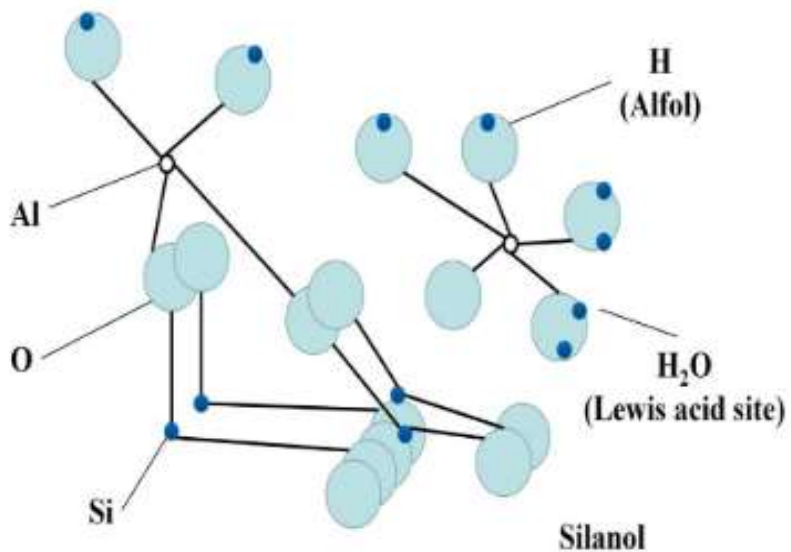


Figure 4: The hydroxyl groups on the surface of kaolin (Zhang *et al.*, 2018)

The texture of briquettes and the briquetting forming mechanism was analysed by means of an Optical microscope and Thermogravimetric analysis (Zhang *et al.*, 2018). The results showed that the addition of inorganic components assist in absorbing organic components, and then form chemical bonds with the coal particles, as shown in Fig. 5. The generation of a continuous gel-phase is important to promote the thermal stability of the briquette through the agglomeration of coal particles.

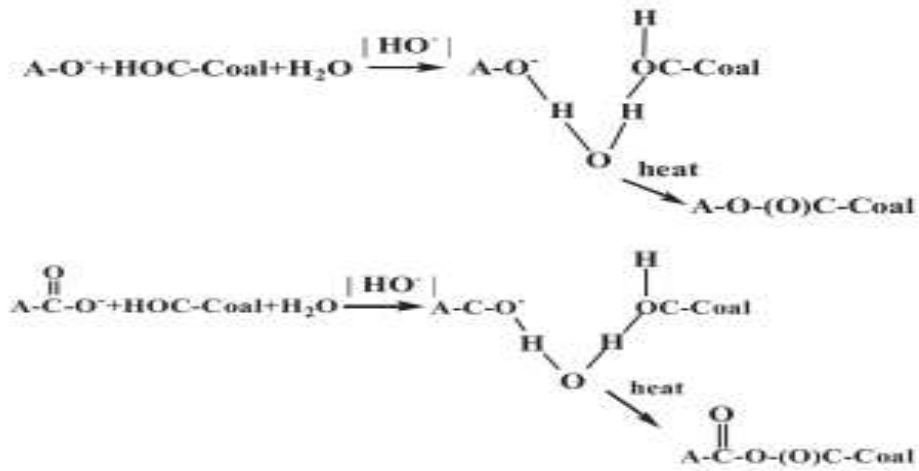


Figure 5: The chemical bond between binder and coal particles (Zhang *et al.*, 2018)

The bonding mechanism of corn starch is shown in Fig. 6. Corn starch can improve the briquette strength at room temperature and after drying as a result of the expansibility after absorbing water, viscosity and compatibility after gelatinization. After 200°C, corn starch gradually transforms into a continuous solid connection bridge, which connects the blast furnace dust particles closely. When the temperature is above 1000°C, the solid connection bridge disappears gradually and strength of the briquettes decreases (Zhang *et al.*, 2018).

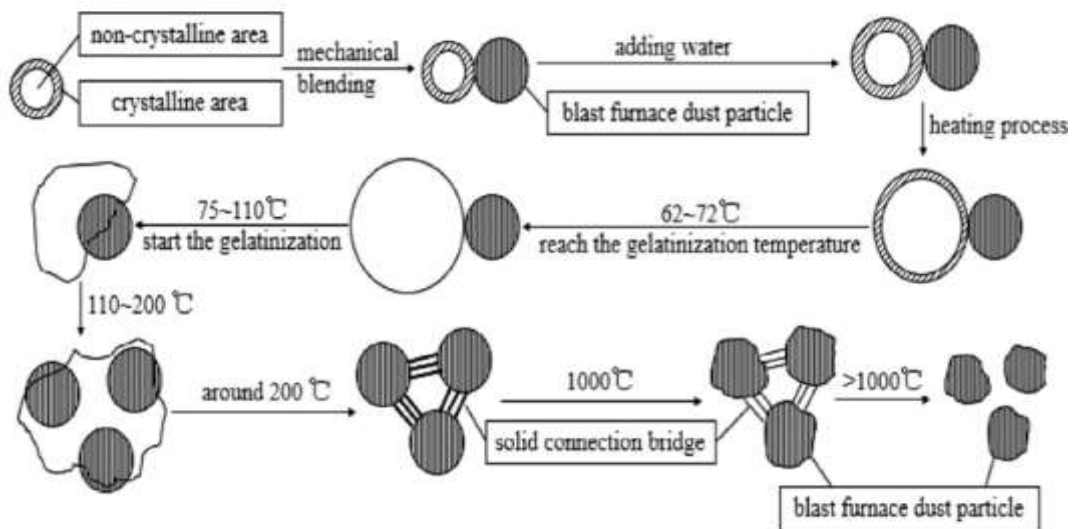


Figure 6: The bonding mechanism of corn starch (Zhang *et al.*, 2018)

The Minimal Contact Angle and Maximum Bonding Power

This hypothesis compares the wetting property of coal to the compressive strength of briquettes. The higher the degree of coalification, the higher the compressive strength of briquettes, because of the difference of the properties of wetting of coal. With the increase of coalification of the coals, the contact angle between coal and the binder decreases, the energy of adhesion and the degree of

wetting of coal increases. Thus, the compressive strength of briquettes increases. The relation between the compressive strength and the critical surface tension of wetting of coal has been investigated (Zhang *et al.*, 2018). The results showed that the higher the critical surface tension, the higher the degree of wetting of coal and hence the compressive strength of briquettes increases. With the increase of the hydrophobic group, the contact angle between coal and the starch binder increases, the wettability of coal particle, the compressive strength of briquette and adhesive performance of briquette decrease (Zhang *et al.*, 2018).

2.2.6 Briquetting Technology

Briquetting technologies are classified into low pressure compaction with a binder, medium pressure compaction with a heating device and high pressure compaction. Solid particles are the starting materials in all these compaction techniques. Briquetting and extrusion both represent compaction i.e., the pressing together of particles in a confined volume (Fagbemi *et al.*, 2014; Grover & Mishra, 1996). Initially, when pressure is applied during compaction, it will lead to some non-permanent elastic deformation of the sample that lasts only as long as the force is applied. As the pressure increases, permanent plastic deformation begins to occur. Bonding arising from the diffusion of molecules from one particle to the next and the formation of solid bridges is more probable under higher pressures. Therefore, high pressures (and temperatures) cause better connection at the points of contact resulting in denser and durable products. Furthermore, higher pressures are known to decrease sample porosity (Bazargan *et al.*, 2014). Table 3 shows the feedstock, binder, binder concentration, compaction pressure, compressive strength, splitting tensile strength, bulk density, impact resistance index, and water resistance index of various carbonized briquettes. Briquetting technology includes screw press extruder, mechanical piston press, hydraulic piston press, roller press, and manual press (Kpalo *et al.*, 2020a).

(i) Screw Press Extruder

It consists of a die and screw extruder. There are three types of screw presses namely; cylindrical screw press with heated dies, conical screw press, and one without externally heated dies. In the screw extruder, the biomass is continuously fed into a screw, which forces the material into a heated cylindrical die to the point where lignin flow occurs (Kpalo *et al.*, 2020a). Figure 7 shows a screw extruder.

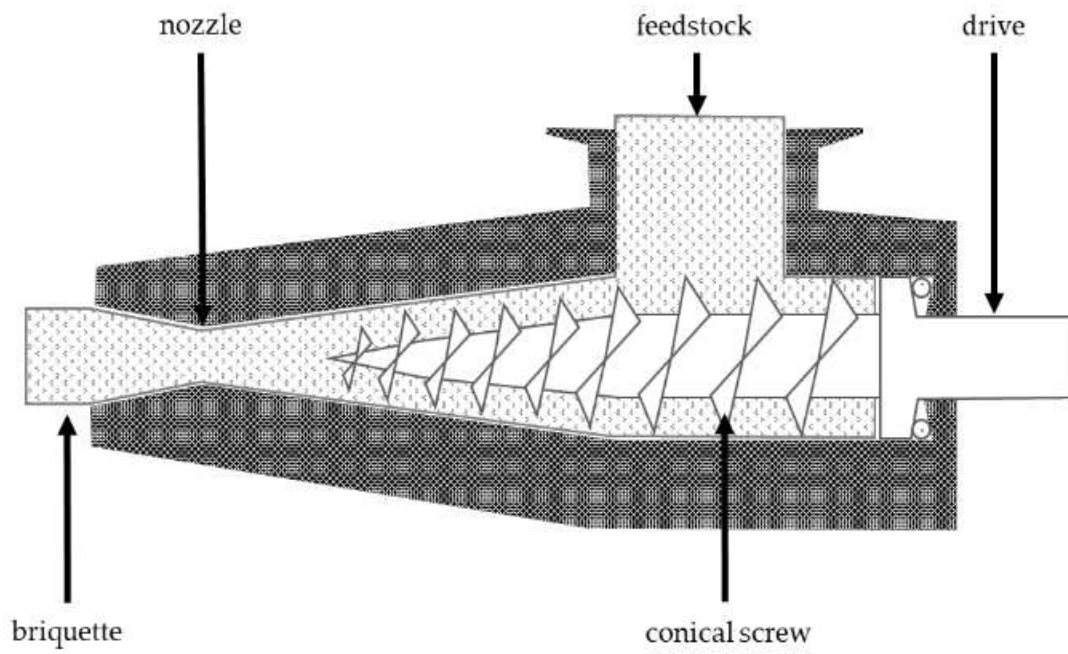


Figure 7: Screw extruder (Kpalo *et al.*, 2020a)

Table 3: Feedstock, binder, binder concentration (BC), compaction pressure (CP), compressive strength (CS), splitting tensile strength (STS), bulk density (ρ), impact resistance index (IRI), and water resistance index (WRI) of selected carbonized briquettes

| Feedstock | Binder | BC (%) | CP (MPa) | CS (kPa) | STS (kPa) | ρ (g/cm ³) | IRI | WRI | Reference |
|--|---------------------------------------|-----------|----------|----------------|-----------|-----------------------------|---------|--------|---|
| Palm kernel shell | Cassava starch | 10 | 20-100 | n.a | 17-38 | 0.288-0.747 | 167 | <50% | Bazargan <i>et al.</i> (2014) |
| Low rank coals and biomass (sawdust, straw, olive stone and almond shell) | humates | 15 | 125 | 1250-5000 | | n.a | 150-700 | 95% | Blesa <i>et al.</i> (2001) |
| Water hyacinth | molasses | 20-40 | 0.827 | 390-1910 | | 0.84-0.89 | n.a | n.a | Carnaje <i>et al.</i> (2018) |
| Rubber seed shell | cassava starch | 25 | n.a | 1080 | 284 | 6.48 | n.a | n.a | Fagbemi <i>et al.</i> (2014) |
| hazelnut shells | molasses and pyrolytic liquid | 10-15 | 5-10 | 8100 | n.a | n.a | n.a | n.a | Haykiri-Acma and Yaman (2010) |
| Brown seaweed | sulfite liquor, molasses and linobind | 2-10 | 187 | 35 400-10 8700 | n.a | n.a | 20-100 | 11-31s | Haykiri-Acma <i>et al.</i> (2013) |
| Rice straw, bagasse and water hyacinth | cassava starch | 22.22 | n.a | 264-2609 | n.a | 0.578-0.925 | n.a | n.a | Jamradloedluk and Wiriyampaiwong (2007) |
| Groundnut shells and bagasse | Cassava & wheat starch | 2.91-8.25 | ≤ 7 | n.a | n.a | 0.2-1.0 | 44-97.5 | n.a | Lubwama and Yiga (2017) |
| Durian peel | starch | 10 | n.a | 146.5- 151 | n.a | 0.99 | n.a | n.a | Nuriana <i>et al.</i> (2014) |

| Feedstock | Binder | BC (%) | CP (MPa) | CS (kPa) | STS (kPa) | ρ (g/cm³) | IRI | WRI | Reference |
|---|---|---------------|-----------------|-----------------|------------------|---|-------------|------------|----------------------------------|
| Municipal waste composting char and sawdust char | slop waste | 10-20 | n.a | 1250-2000 | n.a | 0.85-1.24 | n.a | 136 min | Prasityousil and Muenjina (2013) |
| Cassava rhizome waste | molasses, starch gel, concentrated slop, Cassava pulp and soybean residue | 0-40 | n.a | 851 – 1494 | n.a | 0.69-0.91 | 153.7-416.7 | n.a | Sen and Annachhatre (2016) |
| Sugarcane bagasse fly ash | Cassava starch | 8 | 69.43 | n.a | n.a | 1.12 | n.a | n.a | Teixeira <i>et al.</i> (2010) |
| Human waste | molasses, lime, corn starch and wheat starch | 3-20 | 9.65 | >375 | n.a | n.a | 10-700 | n.a | Ward <i>et al.</i> (2014) |

*n. a -not available

(ii) Mechanical Piston Press

This consists of a ram (piston) and a die and it is driven by an electric motor. Biomass feedstock is compressed in a die by a reciprocating ram with a very high compaction pressure to obtain a briquette. The machine develops a compression pressure of about 196.1 MPa and is typically used for large scale production in the range 200–2500 kg/h. The density of the produced briquettes is 1000 -1200 kg/m³ (Kpalo *et al.*, 2020a). Figure 8 shows a piston press.

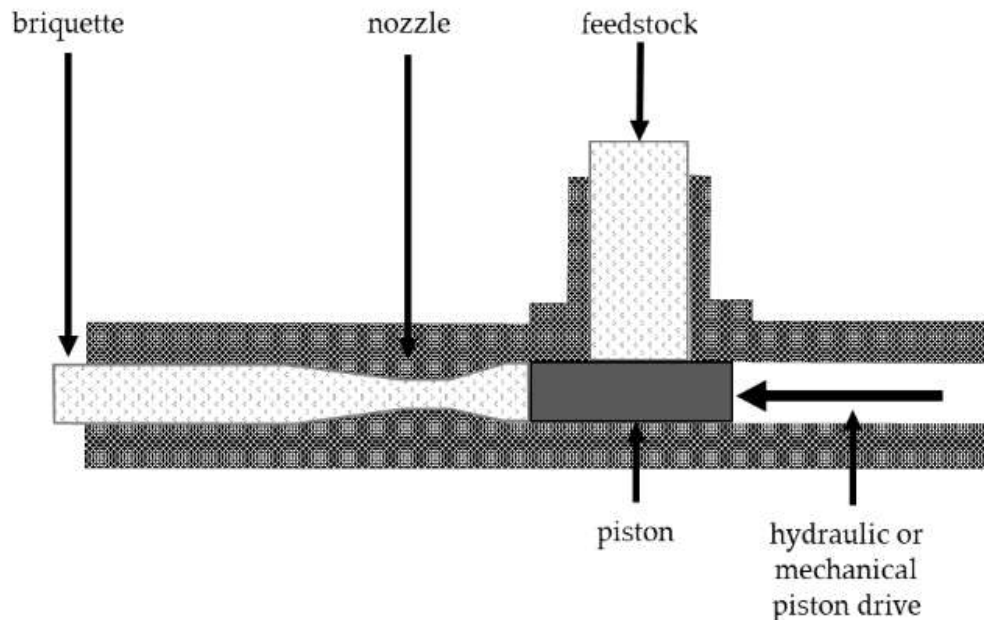


Figure 8: Piston press (Kpalo *et al.*, 2020a)

(iii) Hydraulic Piston Press

Its mode of operation is similar to the mechanical piston press except that the energy to the piston is exerted by a cylinder operated by a hydraulic system. The briquetting pressure in the hydraulic system is normally limited to 30 MPa. The piston head can exert a higher pressure when it is of a smaller diameter than the hydraulic cylinder, but the gearing up of pressure in commercial applications is modest. These machines have production capacities of 50–400 kg/h and can tolerate moisture content greater than 15% which is common for mechanical piston presses. The bulk density of the produced briquettes is lower than 1000 kg/m³ due to limited pressure. In addition, the briquettes have a uniform shape and size, typically using 40 × 40 mm cylinders, and the quality of the product is much higher compared to mechanical presses (Kpalo *et al.*, 2020a).

(iv) Roller Press

This technology is used to produce pillow-shaped briquettes. It comprises two cylindrical rollers of the same diameter, rotating in opposite direction on parallel axes. The rollers are positioned

with a small gap between them and the distance from each other depends on factors such as the binder used, type of biomass, moisture content, and particle size. During operation, the raw material is fed into the press and forced through the gap between the rollers on one side. It is then pressed into a die forming the densified product, on the opposite side. The bulk density of the briquettes is in the range 450-550 kg/m³ (Kpalo *et al.*, 2020a). Figure 9 shows a roller press.

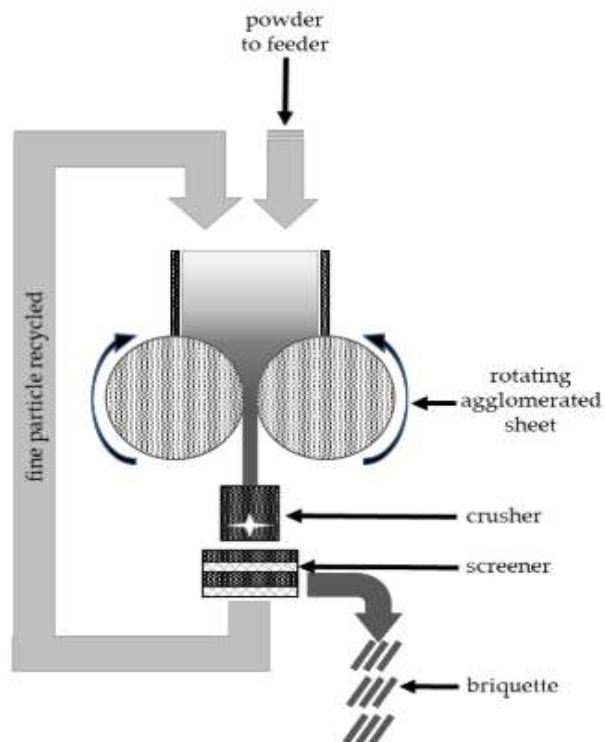


Figure 9: Roller press (Kpalo *et al.*, 2020a)

(v) Manual Press

These include piston or screw presses which are operated manually and hardly use electricity. Manual presses are designed for the purpose of briquette making or adapted from existing implements used for other purposes e.g., the manual clay brick making press can be used to make briquettes from both carbonized and uncarbonized biomass feedstock. Another common example is the Washington University (WU)-presser. The press is made from both metal and wood with the latter being the most common. These machines operate with very minimal pressure and the feedstock requires binder. The advantages of a manual press include; low capital, low operating costs, low level of skill to operate. The disadvantage of a manual press is the low production capacity of about 5 kg/h (Kpalo *et al.*, 2020a). Figure 10 shows a manual press.

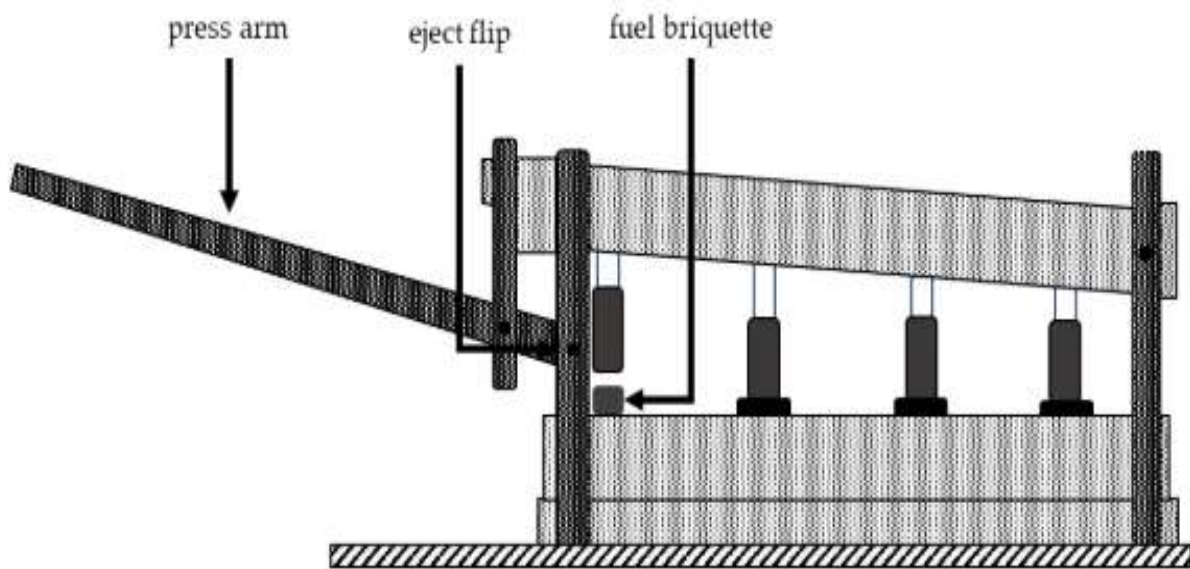


Figure 10: Manual press (WU-presser) (Kpalo *et al.*, 2020a)

2.3 Ignition of Carbonized Briquettes

Ignition can be defined as a rapid transition process by which an exothermic oxidation reaction and self-supported combustion is initiated (Moqbel *et al.*, 2010). The steps of solids ignition include an increase in solids temperature, decomposition of the solid phase, escape of volatiles from the solid surface, diffusion of pyrolyzed species from the solid surface into the gas phase, diffusion of oxygen to the reaction sites on the solid surface followed by gaseous reactions and heterogeneous reactions at the solid surface (Moqbel *et al.*, 2010). In auto-ignition, a reaction mixture will ignite spontaneously without the presence of an external ignition source. This occurs at the auto-ignition temperature needed to supply the activation energy. Induced ignition is caused by an ignition source (e.g. spark, flame, hot surface) which supplies the minimum ignition energy (Lackner, 2011). Ignition temperature depends on volatile matter, particle size, sample size, bed height, heating rate, oxygen concentration, and pressure (Pandey & Dhakal, 2013). Ignition temperature is reduced with increasing pressure and oxygen concentration (Lackner, 2011). In briquette making, a hole at the centre of the fuel improves the combustion characteristics of the briquette through rapid drying, easy ignition and highly efficient burning due to the draft and insulated combustion chamber that the hole creates (Romallosa & Kraft, 2017). Carnaje *et al.* (2018) did a study on charcoal briquettes from water hyacinth (*Eichhornia crassipes*) using molasses as binder and the following volumes of kerosene were applied as ignition agent: 5 mL, 10 mL, and 15 mL. The results showed that ignition time was 2.22-3.3 min. Rotich (1998) did a study on carbonization and briquetting of sawdust for use in domestic cookers using starch as binder with paraffin/wood chips/pieces of paper as ignition agents. The results showed that ignition time was between 7-10 min. Onchieku *et al.* (2012) studied optimum parameters for the production

of charcoal briquettes from bagasse using clay as binder. Molasses were used as a filler and ignition enhancer. Results showed that the ignition time was 4.4-7.35 min.

Chirchir *et al.* (2013) did a study on effect of binder types and amount on physical and combustion characteristics of rice husk-bagasse-charcoal dust composite briquettes using three binders (molasses, cow dung and clay) with paraffin as ignition agent. The ignition time depended on the amount and type of binder with the following results; molasses (7.5-14 min), clay (15-25 min) and cow dung (10-15 min). Onuegbu *et al.* (2011) did a study on ignition time and Water Boiling Test of bio-coal and biomass briquette blends with cassava starch as binder using elephant grass (*pennisetum purpurem*) and spear grass (*imperata cylindrica*) as ignition agent. The results showed that ignition time was 0.33-3.1 min and increased proportionally to the plant material (volatile matter). Onuegbu *et al.* (2010) ignited coal briquettes using a cigarette lighter and the time required to ignite the briquettes was recorded as the ignition time. Gesase *et al.* (2019) performed ignition tests on briquettes by pouring bioethanol gel on a briquette sample placed in a beaker to allow infiltration of the gel into the briquette thus, the successful ignition was achieved using 15-20 ml of bioethanol gel with ignition time of 2.06-2.72 min.

2.4 Combustion Products and Pollutants

Combustion is described as self-sustained, exothermic reaction between fuel and oxidizer (Moqbel *et al.*, 2010). The combustion behaviour of biomass is affected by the following factors: (a) the geometrical shape of the fuel, the porosity, and the tendency of the fuel to undergo fragmentation. The external surface area of the fuel particle determines the rate of initial devolatilization as well as the subsequent progress of the flame front into the particle and combustion of the char formed. These determine the burning rate and consequently the temperature in the combustion chamber, (b) the supply of air and operating conditions especially the fuel load which determines the air/fuel ratio, and (c) the chemical composition-C, N, ash content and volatile content (Mitchell *et al.*, 2016).

Control of pollutant emissions is a major factor in the design of modern combustion systems. Pollutants of concern include particulate matter (PM), such as soot, fly ash, metal fumes, various aerosols; carbon monoxide; oxides of nitrogen, NO_x , which consist of NO and NO_2 ; the sulphur oxides, SO_2 and SO_3 ; unburned and partially burned hydrocarbons, such as aldehydes; and greenhouse gases such as N_2O , but particularly CO_2 (Chen *et al.*, 2016; Khlifi *et al.*, 2019; Turns, 2000). Primary pollutants (emitted directly from the source) and secondary pollutants (those formed via reactions involving primary pollutants in the atmosphere) affect the environment and human health in the following ways; soiling and deterioration of materials, harm to vegetation,

potential increase of morbidity (sickness) and mortality in humans, altered properties of the atmosphere and precipitation (Chen *et al.*, 2016; Turns, 2000).

2.5 Water Boiling Test (WBT)

The WBT comprises three phases i.e., Cold Start High Power (CSHP), Hot Start High Power (HSHP), and Simmer phases (Clean cooking alliance, 2014). Figure 11 shows the temperature profile during the WBT.

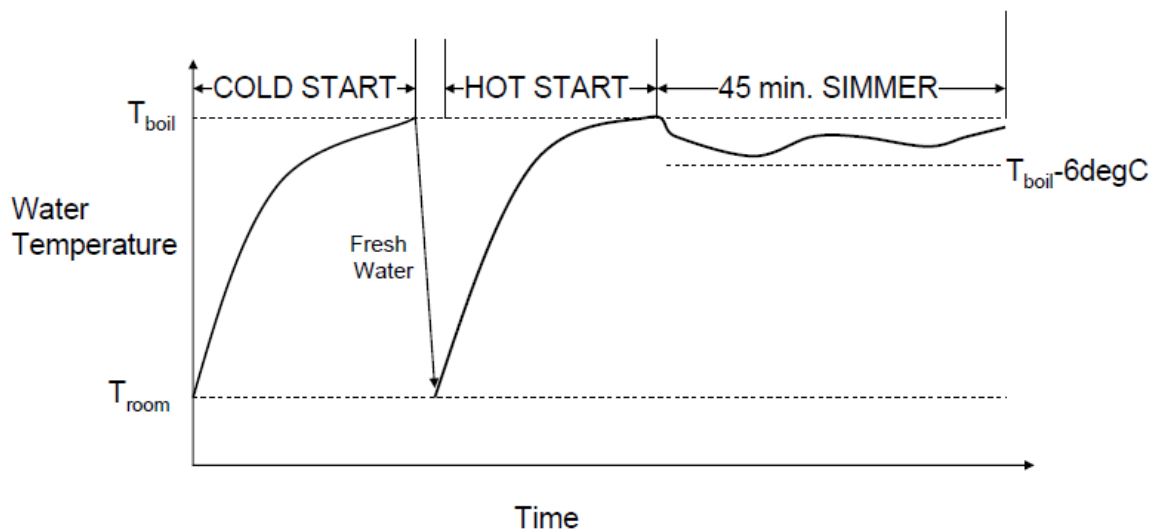


Figure 11: Temperature profile during the WBT (Clean cooking alliance, 2014)

2.5.1 Cold Start High Power (CSHP) Phase

The tester begins with the stove at room temperature and uses a pre-weighed bundle of fuel to boil a measured quantity of water in a standard pot. The tester then replaces the boiled water with a fresh pot of ambient-temperature water for the HSHP phase.

2.5.2 Hot Start High Power (HSHP) Phase

The HSHP phase is performed after the CSHP phase while the stove is still hot. The tester uses a pre-weighed bundle of fuel to boil a measured quantity of water in a standard pot. Repeating the test with a hot stove, results in identifying performance differences between a stove when it is cold and when it is hot. This is particularly important for stoves with high thermal mass, since these stoves may be kept warm in practice.

2.5.3 Simmer Phase

It provides the amount of fuel to simmer a measured amount of water at just below boiling point for 45 min. This phase simulates the long cooking of legumes or pulses common throughout much of the world.

2.5.4 Emissions Testing

This basic testing protocol includes optional instructions for measuring carbon dioxide (CO₂), carbon monoxide (CO), and particulate matter (PM) concentrations in the stove's exhaust and other pollutants.

2.5.5 Water Boil Test Performance Metrics

The subscripts, 'c', 'h', and 's' are used to represent the CSHP, HSHP and Simmer phases respectively (Clean cooking alliance, 2014).

(i) Cold Start High Power (CSHP) Phase

Higher Heating Value, HHV (kJ/Kg)

This is also known as gross calorific value. It is the theoretical maximum amount of energy that can be extracted from the combustion of the moisture-free fuel if it is completely combusted and the combustion products are cooled to room temperature such that the water produced by the reaction of the fuel-bound hydrogen is condensed to the liquid phase.

Lower Heating Value, LHV (kJ/Kg)

Also known as net heating value. This is the theoretical maximum amount of energy that can be extracted from the combustion of the moisture-free fuel if it is completely combusted and the combustion products are cooled to room temperature but the water produced by the reaction of the fuel-bound hydrogen remains in the gas phase. The LHV typically differs from HHV by 1.32 MJ/kg for wood fuels.

Moisture Content, MC_{wet} (%)

This is the percentage of wood moisture on a wet basis, as shown in Equation 1.

$$MC_{wet} = \frac{m_{fuel,wet} - m_{fuel,dry}}{m_{fuel,wet}} \quad (1)$$

Effective Calorific Value, EHV (kJ/kg)

It accounts for the energy required to heat and evaporate the moisture present in the fuel. The EHV is not actually used in any WBT calculations. It is computed using Equation 2.

$$EHV = LHV \times (1 - MC_{wet}) - MC_{wet} \times \Delta h_{H_2O} \quad (2)$$

Where, Δh_{H_2O} is change in specific enthalpy of water shown in Equation 3

$$\Delta h_{H_2O} = h_{H_2O(gas),T_b} - h_{H_2O(liquid),T_{fuel,i}} \quad (3)$$

The specific enthalpy of the liquid water at the initial temperature ($T_{fuel,i}$) and the water vapour at the local boiling temperature (T_b) is found from a steam table (Thermopedia, 2011). A reasonable approximation is given in Equation 4:

$$\Delta h_{H_2O} = \Delta h_{H_2O,fg} + h_{H_2O(liquid),T_b} - h_{H_2O(liquid),T_{fuel,i}} = \Delta h_{H_2O,fg} + C_{p,H_2O}(T_b - T_{fuel,i}) \quad (4)$$

The specific heat capacity of liquid water, C_{p,H_2O} is 4.186 kJ/kg-K, and the specific enthalpy of vaporization of water, $\Delta h_{H_2O,fg}$ is 2260 kJ/kg. Hence, EHV is computed from Equation 5.

$$EHV = LHV \times (1 - MC_{wet}) - MC_{wet}[4.186(T_b - T_{fuel,i}) + 2260] \quad (5)$$

Fuel Consumed (moist), f_{cm} (g)

This is the mass of wood used to heat the water to boiling point. It is computed as shown in Equation 6, where f_{ci} is the pre-weighed bundle of wood, and f_{cf} is the wood remaining at the end of the test phase.

$$f_{cm} = f_{ci} - f_{cf} \quad (6)$$

Net Change in Char during the Test, ΔC_c (g)

This is the mass of char produced during the test, calculated as shown in Equation 7 where, k is the mass of an empty pre-weighed container in which the hot char is placed and C_c is total weight of the char and the container.

$$\Delta C_c = C_c - k \quad (7)$$

Mass of Water Vaporized, w_{cv} (g)

This is the amount of water lost through evaporation during the test. It is obtained using Equation 8. Where, $P1_{ci}$ is the initial weight of pot and water, and $P1_{cf}$ is the final weight of pot and water.

$$w_{cv} = P1_{ci} - P1_{cf} \quad (8)$$

Effective Mass of Water Boiled, w_{cr} (g)

This is the water remaining at end of the test. It is a measure of the amount of water heated to boiling. It is computed as shown in Equation 9 where $P1_{cf}$ is the final weight of pot and water, and $P1$ is the weight of the pot.

$$w_{cr} = P1_{cf} - P1 \quad (9)$$

Time to Boil, Δt_c (min)

This is the difference between start, t_{ci} and finish, t_{cf} times as shown in Equation 10.

$$\Delta t_c = t_{cf} - t_{ci} \quad (10)$$

Temperature-Corrected Time to Boil, Δt_c^T (min)

It is the same as Equation 10, but adjusts the result to a standard 75°C temperature change (25-100°C). The results are thus standardized and a comparison can be made between tests that may have used water with higher or lower initial temperatures as shown in Equation 11.

$$\Delta t_c^T = \Delta t_c \times \frac{75}{T1_{cf} - T1_{ci}} \quad (11)$$

Equivalent Dry Fuel Consumed, f_{cd} (g)

It adjusts the amount of dry fuel that was burned in order to account for two factors: (a) the energy that was needed to remove the moisture in the fuel and (b) the amount of char remaining unburned. The mass of dry fuel consumed is the moist fuel consumed, f_{cm} minus the mass of water in the fuel as shown in Equation 12.

$$dry\ fuel = f_{cm} \times (1 - MC_{wet}) \quad (12)$$

The energy that was needed to remove the moisture in the fuel ($\Delta E_{H_2O,c}$) is obtained from Equation 13.

$$\Delta E_{H_2O,c} = m_{H_2O,c} [C_{p,H_2O}(T_b - T_{fuel,i}) + \Delta h_{H_2O,fg}] \quad (13)$$

In similar fashion to Equation 5,

$$T_{fuel,i} \approx T_a \quad (14)$$

$$\text{The mass of water in the fuel is: } m_{H_2O,c} = f_{cm} \times MC_{wet} \quad (15)$$

Thus:

$$\Delta E_{H_2O,c} = f_{cm} \times MC_{wet} [4.186(T_b - T_a) + 2260] \quad (16)$$

The fuel required to remove the moisture in the fuel is computed as shown in Equation 17.

$$\mathbf{fuel\ to\ evaporate\ water} = \frac{\Delta E_{H_2O,c}}{LHV} \quad (17)$$

The fuel energy stored in the char remaining, $\Delta E_{char,c}$ is computed as shown in Equation 18 where ΔC_c is the mass of char and LHV_{char} is the energy content of the char.

$$\Delta E_{char,c} = \Delta C_c \times LHV_{char} \quad (18)$$

The equivalent amount of unburned fuel remaining in the form of char is calculated as shown in Equation 19.

$$\mathbf{fuel\ in\ char} = \frac{\Delta E_{char,c}}{LHV} \quad (19)$$

Hence:

$$\mathbf{f_{cd} = dry\ fuel - fuel\ to\ evaporate\ water - fuel\ in\ char} \quad (20)$$

Substituting Equations: 12, 16, 17, 18 and 19 into Equation 20 gives:

$$f_{cd} = f_{cm} \times (1 - MC_{wet}) - \frac{f_{cm} \times MC_{wet} [4.186(T_b - T_a) + 2260]}{LHV} - \frac{\Delta C_c \times LHV_{char}}{LHV} \quad (21)$$

$$f_{cd} = \frac{f_{cm} \{LHV(1 - MC_{wet}) - MC_{wet} [4.186(T_b - T_a) + 2,260]\} - \Delta C_c \times LHV_{char}}{LHV} \quad (22)$$

Thermal Efficiency, h_c (%)

This is a ratio of the work done by heating and evaporating water to the energy consumed by burning fuel. It is computed using Equation 23.

$$h_c = \frac{\Delta E_{H_2O,heat} + \Delta E_{H_2O,evap}}{E_{released,c}} \quad (23)$$

The energy to heat the water, $\Delta E_{H_2O,heat}$ is computed as shown in Equation 24 where, m_{H_2O} is the mass of water, C_{p,H_2O} is the specific heat capacity, ΔT is the change in temperature.

$$\Delta E_{H_2O,heat} = m_{H_2O} \times C_{p,H_2O} \times \Delta T$$

$$\Delta E_{H_2O,heat} = (P1_{ci} - P1) \times 4.186 \times (T1_{cf} - T1_{ci}) \quad (24)$$

The energy to evaporate the water, $\Delta E_{H_2O,evap}$ is obtained from Equation 25 where w_{cv} is the mass of water evaporated.

$$\Delta E_{H_2O,evap} = w_{cv} \times \Delta h_{H_2O,fg}$$

$$\Delta E_{H_2O,evap} = w_{cv} \times 2260 \quad (25)$$

The energy consumed, $E_{released,c}$ is obtained from Equation 26 where, f_{cd} is the equivalent mass of dry fuel consumed.

$$E_{released,c} = f_{cd} \times LHV \quad (26)$$

Thus:

$$h_c = \frac{4.186(P1_{ci}-P1)(T1_{cf}-T1_{ci})+w_{cv} \times 2260}{f_{cd} \times LHV} \quad (27)$$

Burning Rate, r_{cb} (g/min)

This is a measure of the rate of fuel consumption while bringing water to a boil. It is calculated as shown in Equation 28 where, f_{cd} is equivalent dry fuel consumed, and Δt_c is the time of the test.

$$r_{cb} = \frac{f_{cd}}{\Delta t_c} \quad (28)$$

Specific Fuel Consumption, SC_c (g /L)

Specific consumption can be defined for any number of cooking tasks and should be considered “the fuel required to produce a unit output” whether the output is cooked beans, boiled water, or loaves of bread. For the CSHP, it is a measure of the amount of wood required to produce one litre (or kilo) of boiling water starting with cold stove. It is obtained from Equation 29.

$$SC_c = \frac{f_{cd}}{w_{cr}} \quad (29)$$

Temperature-Corrected Specific Fuel Consumption, SC_c^T (g /L)

This corrects specific consumption to account for differences in initial water temperatures. It enables comparison of stoves tested on different days or in different environmental conditions. The correction is a simple factor that “normalizes” the temperature change observed in test

conditions to a “standard” temperature change of 75°C (25-100°C). It is obtained from Equation 30.

$$SC_c^T = SC_c \times \frac{75}{(T_{1cf} - T_{1ci})} \quad (30)$$

Temperature-Corrected Specific Energy Consumption, SE_c^T (kJ /L)

This is a measure of the amount of fuel energy required to produce one litre (or kilo) of boiling water starting with cold stove. This is computed as shown in Equation 31.

$$SE_c^T = SC_c^T \times \frac{LHV}{1000} \quad (31)$$

Firepower, FP_c (W)

This is the fuel energy consumed to boil the water divided by the time to boil, Δt_c as shown in Equation 32. It tells the average power output of the stove during the High Power test. By using f_{cd} in this calculation, the remaining char and the fuel moisture content are both accounted.

$$FP_c = \frac{f_{cd} \times LHV}{\Delta t_c \times 60} \quad (32)$$

Total Exhaust Flow, V_c (m^3)

The total exhaust flow, V_c is the volumetric flow rate through the hood, Q multiplied by the time of the test period, Δt_c as shown in Equation 33.

$$V_c = Q \times \frac{\Delta t_c}{60} \quad (33)$$

Exhaust Carbon Concentration, CC_c (ppm)

This is the average concentration of carbon atoms in the stove exhaust which accounts for the carbon atoms present in the CO₂, CO, and PM as shown in Equation 34.

$$CC_c = CO_{2carbon,c} + CO_{carbon,c} + PM_{carbon,c} \quad (34)$$

One molecule of CO₂ contains one carbon atom. Thus, the concentration of carbon from CO₂ [ppm_v] is the same as the concentration of CO₂. The CO₂ concentration, $CO_{2carbon,c}$ is computed as shown in Equation 35, where CO_{2c} is the concentration measured during the test, and CO_{2b} is the background concentration.

$$CO_{2carbon,c} = CO_{2c} - CO_{2b} \quad (35)$$

The CO carbon concentration, $CO_{carbon,c}$ is calculated using Equation 36.

$$CO_{carbon,c} = CO_c - CO_b \quad (36)$$

The PM is measured as a mass concentration $\left[\frac{\mu g}{m^3}\right]$. It is assumed that the PM is 80% carbon by mass, so the PM mass carbon concentration is computed as shown in Equation 37.

$$PM_{carbon,c} \left[\frac{\mu g}{m^3}\right] = 0.8 (PM_c - PM_b) \quad (37)$$

To convert the mass concentration $\left[\frac{\mu g}{m^3}\right]$ to $[ppm_v]$ the following steps are followed. The mass concentration of a gas is the mass of the gas per unit volume. The parts per million by volume of a gas is the volume fraction of space that the gas occupies multiplied by 1 000 000 as shown in Equation 38.

$$Conc_{carbon} \left[\frac{g}{m^3}\right] = \frac{m_{gas}}{V_{total}} \quad Conc_{carbon} [ppm_v] = \frac{V_{gas}}{V_{total}} \times 10^6 \quad (38)$$

To convert from $\left[\frac{g}{m^3}\right]$ to $[ppm_v]$, the ideal gas law is used to convert m_{gas} to V_{gas} as shown in Equation 39.

$$P_{total}V_{gas} = n_{gas}RT \quad (39)$$

The number of moles of the gas, n_{gas} is computed as shown in Equation 40 where, m_{gas} is the mass of the gas, and MW_{gas} is the molecular weight.

$$n_{gas} = \frac{m_{gas}}{MW_{gas}} \quad (40)$$

Substituting Equation 40 into Equation 39 gives:

$$P_{total}V_{gas} = \frac{m_{gas}}{MW_{gas}} RT$$

Thus:

$$V_{gas} = \frac{m_{gas} RT}{MW_{gas} P_{total}} \quad (41)$$

Where temperature of the gas, $T = T_{cd} + 273.15 K$; universal gas constant, $R = 0.008314 \left[\frac{kJ}{mol-K}\right]$; $MW_{gas} = MW_{carbon} = 12 g/mol$; atmospheric pressure, $P_{total} = P_{atm} [kPa]$

$$V_{gas} = \frac{m_{gas} \times 0.008314 \times (T_{cd} + 273.15)}{12 \times P_{atm}} \quad (42)$$

Then, substitute Equation 42 into the Equation 38 to give:

$$PM_{carbon,c} [ppm_v] = \frac{\frac{m_{gas} \times 0.008314 \times (T_{cd} + 273.15)}{12 \times P_{atm}}}{V_{total}} \times 10^6$$

$$PM_{carbon,c} [ppm_v] = \frac{m_{gas}}{V_{total}} \times \frac{0.008314 \times (T_{cd} + 273.15)}{12 \times P_{atm}} \times 10^6 \quad (43)$$

Combining Eq. 37 and 38 gives,

$$\left(\frac{m_{gas}}{V_{total}}\right) \left[\frac{g}{m^3}\right] = \frac{PM_{carbon,c} \left[\frac{\mu g}{m^3}\right]}{10^6 \left[\frac{\mu g}{g}\right]} = \frac{0.8 (PM_c - PM_b)}{10^6} \left[\frac{g}{m^3}\right] \quad (44)$$

Thus:

$$PM_{carbon,c} [ppm_v] = \frac{0.8 (PM_c - PM_b)}{10^6} \times \frac{0.008314 \times (T_d + 273.15)}{12 \times P_{atm}} \times 10^6$$

$$PM_{carbon,c} [ppm_v] = \frac{(PM_c - PM_b) \times 0.008314 \times (T_d + 273.15)}{15 \times P_{atm}} \quad (45)$$

Putting it all together results in Equation 46.

$$CC_c = (CO_{2c} - CO_{2b}) + (CO_c - CO_b) + \frac{(PM_c - PM_b) \times 0.008314 \times (T_{cd} + 273.15)}{15 \times P_{atm}} \quad (46)$$

Total Carbon in Exhaust, CE_c (g/m^3)

It is the mass concentration of carbon in the exhaust. It is calculated by using the ideal gas law to convert the volumetric exhaust carbon concentration [ppm_v] (CC_c calculated above) to a mass concentration. In the calculation of CC_c , it is shown that the volumetric concentration [ppm_v] is related to the mass concentration (g/m^3) by the formula:

$$Conc_{carbon} [ppm_v] = Conc_{carbon} \left[\frac{g}{m^3}\right] \times \frac{0.008314 \times (T_{cd} + 273.15) \times 10^6}{12 \times P_{atm}}$$

Rearranging,

$$Conc_{carbon} \left[\frac{g}{m^3}\right] = \frac{Conc_{carbon} [ppm_v]}{\frac{0.008314 \times (T_{cd} + 273.15) \times 10^6}{12 \times P_{atm}}}$$

$$CE_c = \frac{CC_c \times 12 \times P_{atm} \times 10^{-6}}{0.008314 \times (T_{cd} + 273.15)} \quad (47)$$

Dry Fuel Consumed Estimated from Emissions, f_{ce} (g)

This is the estimate of dry fuel consumed based on the total carbon mass collected in the emission hood as shown in Equation 48. The total carbon mass is the product of mass concentration, CE_c and the total volume collected, V_c . $FuelFracC$ is the fuel carbon fraction.

$$f_{ce} [g_{fuel}] = \frac{CE_c \left[\frac{g_{carbon}}{m^3} \right] \times V_c [m^3]}{FuelFracC \left[\frac{g_{carbon}}{g_{fuel}} \right]} \quad (48)$$

Hood Carbon Balance, CB_c (%)

This is the ratio of carbon collected in the emission hood to carbon consumed. The carbon balance is equivalent to the ratio of burned fuel collected in the emission hood to fuel consumed.

$$\begin{aligned} Carbon\ Balance &= \frac{carbon\ emission\ collected}{total\ carbon\ consumed} \\ &= \frac{(dry\ fuel\ collected\ in\ emission) \times (carbon\ fraction\ of\ fuel)}{(dry\ fuel\ consumed) \times (carbon\ fraction\ of\ fuel)} \\ &= \frac{dry\ fuel\ collected\ in\ emissions}{dry\ fuel\ consumed} \end{aligned} \quad (49)$$

The dry fuel collected in the emissions is the quantity, f_{ce} calculated in Equation 48. The dry fuel consumed is determined by weighing the fuel and char before and after the test period. The dry fuel consumed is the moist fuel consumed minus the mass of moisture in the fuel minus the mass of fuel remaining in the form of char as shown in Equation 50.

$$dry\ fuel\ consumed = f_{cm}(1 - MC_{wet}) - \frac{\Delta C_c \times CharFracC}{FuelFracC} \quad (50)$$

Thus:

$$CB_c = \frac{f_{ce}}{f_{cm}(1 - MC_{wet}) - \frac{\Delta C_c \times CharFracC}{FuelFracC}} \quad (51)$$

The value of CB_c is formatted as a percent in WBT_data-calculation_sheet_4.2.3.xls (Aprovecho Research Center, 2020). The carbon balance indicates what fraction of the stove emissions are captured by the hood.

CO₂ emission Factor, EF_{CO_2c} (g/ kg)

This is the average grams of CO₂ emitted per kilogram of fuel burned. It is calculated from the ratio of CO₂ concentration to carbon concentration as shown in Equation 52.

$$\frac{Conc_{CO_2} [ppm_v]}{Conc_{Carbon} [ppm_v]} = \frac{(CO_{2c} - CO_{2b})}{CC_c} \quad (52)$$

$$Conc_{Carbon} [ppm_v] = \frac{n_{gas}}{n_{Total}} \times 10^6 \quad (53)$$

Hence, the volumetric concentration ratio of two gases is equivalent to the molar ratio as shown in Equation 54.

$$\frac{Conc_{CO_2} [ppm_v]}{Conc_{Carbon} [ppm_v]} = \frac{\frac{n_{CO_2} \times 10^6}{n_{Total}}}{\frac{n_{Carbon} \times 10^6}{n_{Total}}} = \frac{n_{CO_2c}}{n_{Carbon,c}} \quad (54)$$

From Equation 54, the moles of CO₂, n_{CO_2c} is converted to grams of CO₂, m_{CO_2} as shown in Equation 55. The moles of carbon, $n_{Carbon,c}$ is converted to kilograms of fuel, m_{fuel} as shown in Equation 56.

$$m_{CO_2} [g_{CO_2}] = n_{CO_2c} [mol_{CO_2}] \times \frac{44 [g_{CO_2}]}{1 [mol_{CO_2}]} \quad (55)$$

$$m_{fuel} [kg] = n_{Carbon,c} [mol_{Carbon}] \times \frac{12 [g_{Carbon}]}{1 [mol_{Carbon}]} \times \frac{1 [g_{fuel}]}{FuelFracC [g_{Carbon}]} \times \frac{1 [kg_{fuel}]}{1000 [g_{fuel}]} \quad (56)$$

Putting it all together:

$$\begin{aligned} EF_{CO_2c} \frac{[g_{CO_2}]}{[kg_{fuel}]} &= \frac{m_{CO_2} [g_{CO_2}]}{m_{fuel} [kg]} \\ &= \frac{n_{CO_2c} [mol_{CO_2}] \times 44 \left[\frac{g_{CO_2}}{mol_{CO_2}} \right]}{n_{Carbon,c} [mol_{Carbon}] \times 12 \left[\frac{g_{Carbon}}{mol_{Carbon}} \right] \times \frac{1 [g_{fuel}]}{FuelFracC [g_{Carbon}]} \times \frac{1 [kg_{fuel}]}{1000 [g_{fuel}]}} \end{aligned} \quad (57)$$

From Equation 52 and 54,

$$\frac{n_{CO_2c} [mol_{CO_2}]}{n_{Carbon,c} [mol_{Carbon}]} = \frac{(CO_{2c} - CO_{2b})}{CC_c} \quad (58)$$

Hence:

$$EF_{CO_2c} = \frac{(CO_{2c} - CO_{2b})}{CC_c} \times \frac{44}{12} \times FuelFracC \times 1000 \quad (59)$$

CO Emission Factor, EF_{COc} (g/ kg)

This is the average grams of CO emitted per kilogram of fuel burned calculated as shown in Equation 60.

$$EF_{CO_c} = \frac{(CO_c - CO_b)}{CC_c} \times \frac{28}{12} \times FuelFracC \times 1000 \quad (60)$$

Particulate Matter emission Factor, EF_{PM_c} (mg/ kg)

This is the average grams of PM emitted per kilogram of fuel burned. The PM concentration is a mass concentration with units $\mu g/m^3$. If the ratio of the mass concentration of PM to the mass concentration of carbon is considered, then:

$$\frac{(PM_c - PM_b) \left[\frac{\mu g_{PM}}{m_{air}^3} \right]}{CE_c \left[\frac{g_{carbon}}{m_{air}^3} \right]} = \frac{(PM_c - PM_b)}{CE_c} \left[\frac{\mu g_{PM}}{g_{carbon}} \right] \quad (61)$$

The numerator of Equation 61 can be converted from micrograms to grams of PM as shown in Equation 62.

$$m_{PM} [g_{PM}] = \frac{m_{PM} [\mu g_{PM}]}{1\,000\,000 \left[\frac{\mu g_{PM}}{g_{PM}} \right]} \quad (62)$$

The denominator of Equation 61 can be converted from grams of carbon to kilograms as shown in Equation 63.

$$m_{fuel} [kg_{fuel}] = \frac{m_{carbon} [g_{carbon}]}{FuelFracC \left[\frac{g_{carbon}}{g_{fuel}} \right] \times 1000 \left[\frac{g_{fuel}}{kg_{fuel}} \right]} \quad (63)$$

Putting it all together results in Equation 64:

$$EF_{PM_c} = \frac{m_{PM} [g_{PM}]}{m_{fuel} [kg_{fuel}]} = \frac{(PM_c - PM_b) \times FuelFracC \times 1000}{CE_c \times 1\,000\,000} \quad (64)$$

CO₂ Mass Produced, $m_{CO_{2c}}$ (g)

This is the total mass of CO₂ emitted during the test phase calculated as shown in Equation 65.

$$m_{CO_{2c}} = EF_{CO_{2c}} \times \left[f_{cm}(1 - MC_{wet}) - \Delta C_c \times \frac{charFracC}{fuelFracC} \right] \times \frac{1}{1000} \quad (65)$$

CO Mass Produced, m_{CO_c} (g)

This is the total mass of CO emitted during the test phase calculated as shown in Equation 66.

$$m_{CO_c} = EF_{CO_c} \times \left[f_{cm}(1 - MC_{wet}) - \Delta C_c \times \frac{CharFracC}{fuelFracC} \right] \times \frac{1}{1000} \quad (66)$$

Particulate Matter Mass Produced, m_{PM_c} (g)

This is the total mass of PM emitted during the test phase calculated as shown in Equation 67.

$$m_{PM_c} = EF_{PM_c} \times \left[f_{cm}(1 - MC_{wet}) - \Delta C_c \times \frac{CharFracC}{fuelFracC} \right] \times \frac{1}{1000} \quad (67)$$

CO₂ Emission per Water Boiled, $E_{CO_{2c}}$ (g/L)

It is calculated as shown in Equation 68 where $m_{CO_{2c}}$ is the total mass of CO₂ emitted, and w_{cr} is the effective mass of water boiled.

$$E_{CO_{2c}} \left[\frac{g_{CO_2}}{L_{H_2O}} \right] = \frac{m_{CO_{2c}} [g_{CO_2}]}{w_{cr} [g_{H_2O}]} \times 1000 \left[\frac{g_{H_2O}}{L_{H_2O}} \right] \quad (68)$$

CO Emission per Water Boiled, E_{CO_c} (g/L)

It is obtained using Equation 69 where m_{CO_c} is the total mass of CO emitted, and w_{cr} is the effective mass of water boiled.

$$E_{CO_c} \left[\frac{g_{CO}}{L_{H_2O}} \right] = \frac{m_{CO_c} [g_{CO}]}{w_{cr} [g_{H_2O}]} \times 1000 \left[\frac{g_{H_2O}}{L_{H_2O}} \right] \quad (69)$$

Emission per Water Boiled, E_{PM_c} (g/L)

It is computed using Equation 70 where m_{PM_c} is the total mass of PM emitted, and w_{cr} is the effective mass of water boiled.

$$E_{PM_c} \left[\frac{g_{PM}}{L_{H_2O}} \right] = \frac{m_{PM_c} [g_{PM}]}{w_{cr} [g_{H_2O}]} \times 1000 \left[\frac{g_{H_2O}}{L_{H_2O}} \right] \quad (70)$$

(ii) Hot Start High Power (HSHP) phase

In this test, measurements and calculations are identical to the CSHP phase except that the char remaining is not extracted and weighed. The char remaining is assumed to be the same as the char remaining from the CSHP phase.

Fuel Consumed (Moist), f_{hm} (g)

$$f_{hm} = f_{hi} - f_{hf} \quad (71)$$

change in char during the test, ΔC_h (g)

$$\Delta C_h = \Delta C_c \quad (72)$$

mass of water vaporized, w_{hv} (g)

$$w_{hv} = P1_{hi} - P1_{hf} \quad (73)$$

Effective mass of water boiled, w_{hr} (g)

$$w_{hr} = P1_{hf} - P1 \quad (74)$$

Time to boil, Δt_h (min)

$$\Delta t_h = t_{hf} - t_{hi} \quad (75)$$

Temperature-Corrected Time to Boil, Δt_h^T (min)

$$\Delta t_h^T = \Delta t_h \times \frac{75}{T1_{hf} - T1_{hi}} \quad (76)$$

Equivalent Dry Fuel Consumed, f_{hd} (g)

$$f_{hd} = \frac{f_{hm}\{LHV(1-MC_{wet})-MC_{wet}[4.186(T_b-T_a)+2260]\}-\Delta C_h \times LHV_{char}}{LHV} \quad (77)$$

Thermal efficiency, h_h (%)

$$h_h = \frac{4.186(P1_{hi}-P1)(T1_{hf}-T1_{hi})+w_{hv} \times 2260}{f_{hd} \times LHV} \quad (78)$$

Burning Rate, r_{hb} (g/min)

$$r_{hb} = \frac{f_{hd}}{\Delta t_h} \quad (79)$$

Specific Fuel Consumption, SC_h (g /L)

$$SC_h = \frac{f_{hd}}{w_{hr}} \quad (80)$$

Temperature- corrected specific fuel consumption, SC_h^T (g /L)

$$SC_h^T = SC_h \times \frac{75}{(T1_{hf}-T1_{hi})} \quad (81)$$

Temperature- Corrected Specific Energy Consumption, SE_h^T (Kj/L)

$$SE_h^T = SC_h^T \times \frac{LHV}{1000} \quad (82)$$

Firepower, FP_h (W)

$$FP_h = \frac{f_{hd} \times LHV}{\Delta t_h \times 60} \quad (83)$$

Total exhaust flow, V_h (m^3)

$$V_h = Q \times \frac{\Delta t_h}{60} \quad (84)$$

Exhaust Carbon Concentration, CC_h (ppm)

$$CC_h = (CO_{2h} - CO_{2b}) + (CO_h - CO_b) + \frac{(PM_h - PM_b) \times 0.008314 \times (T_{hd} + 273.15)}{15 \times P_{atm}} \quad (85)$$

Total Carbon in Exhaust, CE_h (g/m^3)

$$CE_h = \frac{CC_h \times 12 \times P_{atm} \times 10^{-6}}{0.008314 \times (T_{hd} + 273.15)}$$

(86)

Dry Fuel Consumed Estimated from Emissions, f_{he} (g)

$$f_{he} = \frac{C_h \times V_h}{FuelFracC} \quad (87)$$

Hood Carbon Balance, CB_h (%)

$$CB_h = \frac{f_{he}}{f_{hm}(1 - MC_{wet}) - \frac{\Delta C_h \times CharFracC}{FuelFracC}} \quad (88)$$

CO_2 Emission Factor, $EF_{CO_{2h}}$ (g/g)

$$EF_{CO_{2h}} = \frac{(CO_{2h} - CO_{2b})}{CC_h} \times \frac{44}{12} \times FuelFracC \times 1000 \quad (89)$$

CO Emission Factor, EF_{CO_h} (g/g)

$$EF_{CO_h} = \frac{(CO_h - CO_b)}{CC_h} \times \frac{28}{12} \times FuelFracC \times 1000 \quad (90)$$

PM Emission Factor, EF_{PM_h} (g/g)

$$EF_{PM_h} = \frac{(PM_h - PM_b) \times FuelFracC \times 1000}{CE_h \times 1,000,000} \quad (91)$$

CO_2 Mass Produced, $m_{CO_{2h}}$ (g)

$$m_{CO_{2h}} = EF_{CO_{2h}} \times \left[f_{hm}(1 - MC_{wet}) - \Delta C_h \times \frac{CharFracC}{fuelFracC} \right] \times \frac{1}{1000} \quad (92)$$

CO Mass Produced, m_{CO_h} (g)

$$m_{CO_h} = EF_{CO_h} \times \left[f_{hm}(1 - MC_{wet}) - \Delta C_h \times \frac{CharFracC}{fuelFracC} \right] \times \frac{1}{1000} \quad (93)$$

Particulate Matter Mass Produced, $m_{PM,h}$ (g)

$$m_{PM,h} = EF_{PM,h} \times \left[f_{hm}(1 - MC_{wet}) - \Delta C_h \times \frac{CharFracC}{fuelFracC} \right] \times \frac{1}{1000} \quad (94)$$

CO₂ Emission per Water Boiled, $E_{CO_{2h}}$ (g/L)

$$E_{CO_{2h}} = \frac{m_{CO_{2h}}}{w_{hr}} \times 1000 \quad (95)$$

CO Emission per Water Boiled, E_{CO_h} (g/L)

$$E_{CO_h} = \frac{m_{CO_h}}{w_{hr}} \times 1000 \quad (96)$$

Particulate Matter Emission per Water Boiled, E_{PM_h} (g/L)

$$E_{PM_h} = \frac{m_{PM_h}}{w_{hr}} \times 1000 \quad (97)$$

(iii) Variables For Low Power (Simmering) Phase

The assumption made in this test is based on the amount of char present at the start of the Simmer phase. At the end of the HSHP phase, when the water comes to a boil, it is quickly weighed without disturbing the char and then the fire is tended to maintain the water within a few degrees of boiling for 45 min. There will be char remaining in the stove from the wood that was used to bring the water to a boil during the Hot Start. Removing that char from the stove, weighing it, and relighting it disturbs the fire and may result in the water temperature dropping too far below boiling. Therefore, the recommended procedure is to assume that the char present at the start of the Simmer phase is the same as the char that was measured after the CSHP test (ΔC_c). While this is not entirely accurate, the error introduced by this assumption should be minimal – especially if the tester(s) followed an identical procedure in the CSHP and HSHP phases.

Fuel Consumed (Moist), f_{sm} (g)

$$f_{sm} = f_{si} - f_{sf} \quad (98)$$

Change in Char during the Test, ΔC_s (g)

$$\Delta C_s = C_s - k \quad (99)$$

Mass of Water Vaporized, w_{sv} (g)

$$w_{sv} = P1_{si} - P1_{sf} \quad (100)$$

Effective Mass of Water Simmered, w_{sr} (g)

$$w_{sr} = P1_{sf} - P1 \quad (101)$$

Time to Boil, Δt_s (min)

$$\Delta t_s = t_{sf} - t_{si} \quad (102)$$

Equivalent Dry Fuel Consumed, f_{sd} (g)

$$f_{sd} = \frac{f_{sm}\{LHV(1-MC_{wet})-MC_{wet}[4.186(T_b-T_a)+2260]\}-\Delta C_s \times LHV_{char}}{LHV} \quad (103)$$

Thermal Efficiency, h_s (%)

$$h_s = \frac{4.186(T1_{sf}-T1_{si})(P1_{si}-P1+w_{sr})/2+w_{sv} \times 2260}{f_{sd} \times LHV} \quad (104)$$

The thermal efficiency should not be used to evaluate the Low power stove performance. Instead, the Turn down ratio and the IWA Low power specific fuel consumption should be used.

Burning Rate, r_{sb} (g/min)

$$r_{sb} = \frac{f_{sd}}{\Delta t_s} \quad (105)$$

Specific Fuel Consumption, SC_s (g /L)

$$SC_s = \frac{f_{sd}}{w_{sr}} \quad (106)$$

The specific consumption in the Simmer phase (SC_s) indicates the mass of fuel required to maintain each litre (or kilo) of water three degrees below boiling temperature. The same is true for other indicators, like burning rate and firepower.

Specific Energy Consumption, (kJ /L)

$$SE_s = SC_s \times \frac{LHV}{1000} \quad (107)$$

Firepower, FP_s (W)

$$FP_s = \frac{f_{sd} \times LHV}{\Delta t_s \times 60} \quad (108)$$

Turn Down Ratio, TDR

This is the ratio of average High firepower, FP_c to average Low firepower, FP_s as shown in Equation 109. It represents the degree to which the firepower of the stove can be controlled by the user.

$$TDR = \frac{FP_c}{FP_s} \quad (109)$$

Total Exhaust Flow, V_s (m^3)

$$V_s = Q \times \frac{\Delta t_s}{60} \quad (110)$$

Exhaust Carbon Concentration, CC_s (ppm)

$$CC_s = (CO_{2s} - CO_{2b}) + (CO_s - CO_b) + \frac{(PM_s - PM_b) \times 0.008314 \times (T_{sd} + 273.15)}{15 \times P_{atm}} \quad (111)$$

Total Carbon in Exhaust, CE_s (g/m^3)

$$CE_s = \frac{CC_s \times 12 \times P_{atm} \times 10^{-6}}{0.008314 \times (T_{sd} + 273.15)} \quad (112)$$

Dry Fuel Consumed Estimated from Emissions, f_{se} (g)

$$f_{se} = \frac{C_s \times V_s}{FuelFracC} \quad (113)$$

Hood Carbon Balance, CB_s (%)

$$CB_s = \frac{f_{se}}{f_{sm}(1 - MC_{wet}) - \frac{\Delta C_s \times CharFracC}{FuelFracC}} \quad (114)$$

CO_2 Emission Factor, $EF_{CO_{2s}}$ (g/g)

$$EF_{CO_{2s}} = \frac{(CO_{2s} - CO_{2b})}{CC_s} \times \frac{44}{12} \times FuelFracC \times 1000 \quad (115)$$

CO Emission Factor, EF_{CO_s} (g/g)

$$EF_{CO_s} = \frac{(CO_s - CO_b)}{CC_s} \times \frac{28}{12} \times FuelFracC \times 1000 \quad (116)$$

PM Emission Factor, EF_{PM_s} (g/ g)

$$EF_{PM_s} = \frac{(PM_s - PM_b) \times FuelFracC \times 1000}{C_s \times 1,000,000} \quad (117)$$

CO₂ Mass Produced, $m_{CO_{2s}}$ (g)

$$m_{CO_{2s}} = EF_{CO_{2s}} \times \left[f_{sm}(1 - MC_{wet}) - \Delta C_s \times \frac{charFracC}{FuelFracC} \right] \times \frac{1}{1000} \quad (118)$$

CO Mass Produced, m_{CO_s} (g)

$$m_{CO_s} = EF_{CO_s} \times \left[f_{sm}(1 - MC_{wet}) - \Delta C_s \times \frac{charFracC}{FuelFracC} \right] \times \frac{1}{1000} \quad (119)$$

Particulate Matter Mass Produced, m_{PM_s} (g)

$$m_{PM_s} = EF_{PM_s} \times \left[f_{sm}(1 - MC_{wet}) - \Delta C_s \times \frac{charFracC}{FuelFracC} \right] \times \frac{1}{1000} \quad (120)$$

CO₂ Emission per Water Simmered, $E_{CO_{2s}}$ (g/ L)

$$E_{CO_{2s}} = \frac{m_{CO_{2s}}}{w_{sr}} \times 1000 \quad (121)$$

CO Emission Per Water Simmered, E_{CO_s} (g/ L)

$$E_{CO_s} = \frac{m_{CO_s}}{w_{sr}} \times 1000 \quad (122)$$

PM Emission per Water Simmered, E_{PM_s} (g/ L)

$$E_{PM_s} = \frac{m_{PM_s}}{w_{sr}} \times 1000 \quad (123)$$

(iv) International Workshop Agreement (IWA) performance metrics

High Power Thermal Efficiency (%)

If the Hot Start phase is omitted, then the Cold Start efficiency is reported as shown in Equation 124.

$$\text{High power thermal efficiency} = h_c \quad (124)$$

If the Hot Start phase is not omitted, then the average of the Cold Start efficiency, h_c and Hot Start efficiency, h_h is reported as shown in Equation 125.

$$\text{High power thermal efficiency} = \frac{h_c + h_h}{2} \quad (125)$$

Low Power Specific Fuel Consumption (MJ/min/L)

It is the energy consumed per litre of water Simmered per minute. It is calculated according to Equation 126.

$$\text{Low power specific fuel consumption} = \frac{f_{sd} \times LHV}{w_{sr} \times \Delta t_s \times 1000} \quad (126)$$

High Power CO (g/MJ)

This metric is the CO emission per unit of energy delivered to the cooking pot.

$$\text{High power CO} = \frac{\text{CO emission [g]}}{\text{Energy delivered to pot [MJ]}} \quad (127)$$

$$\text{Energy delivered to pot [MJ]} = h_c \times f_{cd} [\text{g}] \times LHV \left[\frac{\text{kJ}}{\text{kg}} \right] \times \frac{1}{1000} \left[\frac{\text{MJ}}{\text{kJ}} \right] \times \frac{1}{1000} \left[\frac{\text{kg}}{\text{g}} \right] \quad (128)$$

If the Hot Start phase is omitted, then the metric is calculated for the Cold Start.

$$\text{High power CO} = \frac{m_{CO_c} \times 1000000}{h_c \times f_{cd} \times LHV} \quad (129)$$

If the Hot Start phase is not omitted, then the metric is calculated for the Cold Start and Hot Start and the average of the two is reported.

$$\text{High power CO} = \frac{\frac{m_{CO_c} \times 1000000}{h_c \times f_{cd} \times LHV} + \frac{m_{CO_h} \times 1000000}{h_h \times f_{hd} \times LHV}}{2} = \frac{1000000}{LHV \times 2} \times \left(\frac{m_{CO_c}}{h_c \times f_{cd}} + \frac{m_{CO_h}}{h_h \times f_{hd}} \right) \quad (130)$$

High Power PM (mg/MJ)

This is the PM emission per unit of energy delivered to the cooking pot as shown in Equation 131.

$$\text{High power PM} \left[\frac{\text{mg}}{\text{MJ}} \right] = \frac{\text{PM emissions [mg]}}{\text{Energy delivered to pot [MJ]}} \quad (131)$$

If the Hot Start phase is omitted, then the metric is calculated for the Cold Start as shown in Equation 132.

$$\text{High power PM} = \frac{m_{PM_c} \times 10^9}{h_c \times f_{cd} \times LHV} \quad (132)$$

If the Hot Start phase is not omitted, then the metric is calculated for the Cold Start and Hot Start and the average of the two is reported as shown in Equation 133.

$$\text{High power PM} = \frac{\frac{m_{PM_c} \times 10^9}{h_c \times f_{cd} \times LHV} + \frac{m_{PM_h} \times 10^9}{h_h \times f_{hd} \times LHV}}{2} = \frac{10^9}{LHV \times 2} \times \left(\frac{m_{PM_c}}{h_c \times f_{cd}} + \frac{m_{PM_h}}{h_h \times f_{hd}} \right) \quad (133)$$

Low Power PM (mg/min/L)

It is the PM emission per litre of water Simmered per minute as shown in Equation 134. By normalizing for the amount of water and the time of Simmer, this metric can be used to compare stove performance even when the amount of water and length of the Simmer is different between stoves.

$$\text{Low power PM} = \frac{m_{PM_s}}{\Delta t_s \times w_{sr}} \times 1000000 \quad (134)$$

Indoor CO Emissions (g/min)

This metric reports the High Power or Low Power CO emission rate into the kitchen, whichever is greater as shown in Equation 135.

$$\text{Indoor CO Emissions} = \max(ER_{CO,high}, ER_{CO,low}) \quad (135)$$

If the Hot Start phase is omitted, then the High Power emission rate is calculated for the Cold Start.

$$ER_{CO,high} = \frac{m_{CO,indoor,c}}{\Delta t_c} \quad (136)$$

Where, $m_{CO,indoor,c}$ is the total mass of CO emitted into the kitchen during the test period. If the Hot Start phase is not omitted, then the High Power emission rate is calculated for the Cold Start and Hot Start and the average of the two is reported as shown in Equation 137.

$$ER_{CO,high} = \frac{\frac{m_{CO,indoor,c}}{\Delta t_c} + \frac{m_{CO,indoor,h}}{\Delta t_h}}{2} \quad (137)$$

The Low Power emission rate is calculated from the Simmer period.

$$ER_{CO,low} = \frac{m_{CO,indoor,s}}{\Delta t_s} \quad (138)$$

For non-chimney stoves that vent 100% of emissions into the kitchen, the total mass emitted into the kitchen is equal to the total mass emitted from the stove ($m_{CO,indoor,c} = m_{CO_c}$, $m_{CO,indoor,h} = m_{CO_h}$, $m_{CO,indoor,s} = m_{CO_s}$). For other stoves that vent outdoors, the fugitive emissions into the kitchen must be measured separately from the total emissions and the formula in WBT_data-calculation_sheet_4.2.3.xls (Aprovecho Research Center, 2020) corrected accordingly.

Indoor Particulate Matter Emissions (mg/min)

This metric reports the High Power or Low Power PM_{2.5} emission rate into the kitchen, whichever is greater as shown in Equation 139.

$$\text{Indoor PM emissions} = \max(ER_{PM,high}, ER_{PM,low}) \quad (139)$$

It is computed in the same manner as the indoor CO emissions except a factor of 1000 is added to convert grams to milligrams. If the Hot Start phase is omitted, then the High Power emission rate is calculated for the Cold Start.

$$ER_{PM,high} = \frac{m_{PM,indoor,c}}{\Delta t_c} \times 1000 \quad (140)$$

Where, $m_{PM,indoor,c}$ is the total mass of PM emitted into the kitchen during the test period. If the Hot Start phase is not omitted, then the High Power emission rate is calculated for the Cold Start and Hot Start and the average of the two is reported.

$$ER_{PM,high} = \frac{\frac{m_{PM,indoor,c} \times 1000}{\Delta t_c} + \frac{m_{PM,indoor,h} \times 1000}{\Delta t_h}}{2} \quad (141)$$

The Low Power emission rate is calculated from the Simmer period:

$$ER_{PM,low} = \frac{m_{PM,indoor,s}}{\Delta t_s} \times 1000 \quad (142)$$

For non-chimney stoves that vent 100% of emissions into the kitchen, the total mass emitted into the kitchen is equivalent to the total mass emitted from the stove ($m_{PM,indoor,c} = m_{PM_c}$, $m_{PM,indoor,h} = m_{PM_h}$, $m_{PM,indoor,s} = m_{PM_s}$). For other stoves that vent outdoors, the fugitive emissions into the kitchen must be measured separately from the total emissions and the formula in WBT_data-calculation_sheet_4.2.3.xls (Aprovecho Research Center, 2020) corrected accordingly.

2.6 Conclusion

Binders have been used for production of briquettes in the range of 2-40%. The organic binders reported for production of briquettes are; starch, molasses, humates, slop waste, pyrolytic liquid, sulfite liquor, cow dung and soybean residue. Starch and molasses are the most common binders used. Starch is used as food while the molasses may be in limited supply from the sugarcane industry. The inorganic binders mainly used for production of briquettes are lime and clay. The inorganic binders have high ash content. In addition, some studies combine more than two binders (compound binders) in the production of briquettes. However, very few studies have been done on the production of carbonized briquettes using natural resins. The compressive strength of the briquettes is 146.5-108700 kPa while the splitting tensile strength is 17-284 kPa. The ignition agents mentioned in different studies include; molasses, elephant grass, spear grass, kerosene

(paraffin), bioethanol gel, cigarette lighter. The ignition times reported are 0.33-25 min. In addition, some of the binders also act as ignition enhancers e.g. molasses contain volatile matter which acts as ignition enhancer.

CHAPTER THREE

MATERIALS AND METHODS

3.1 Conceptual Framework

Figure 12 shows the conceptual framework followed to execute the research.

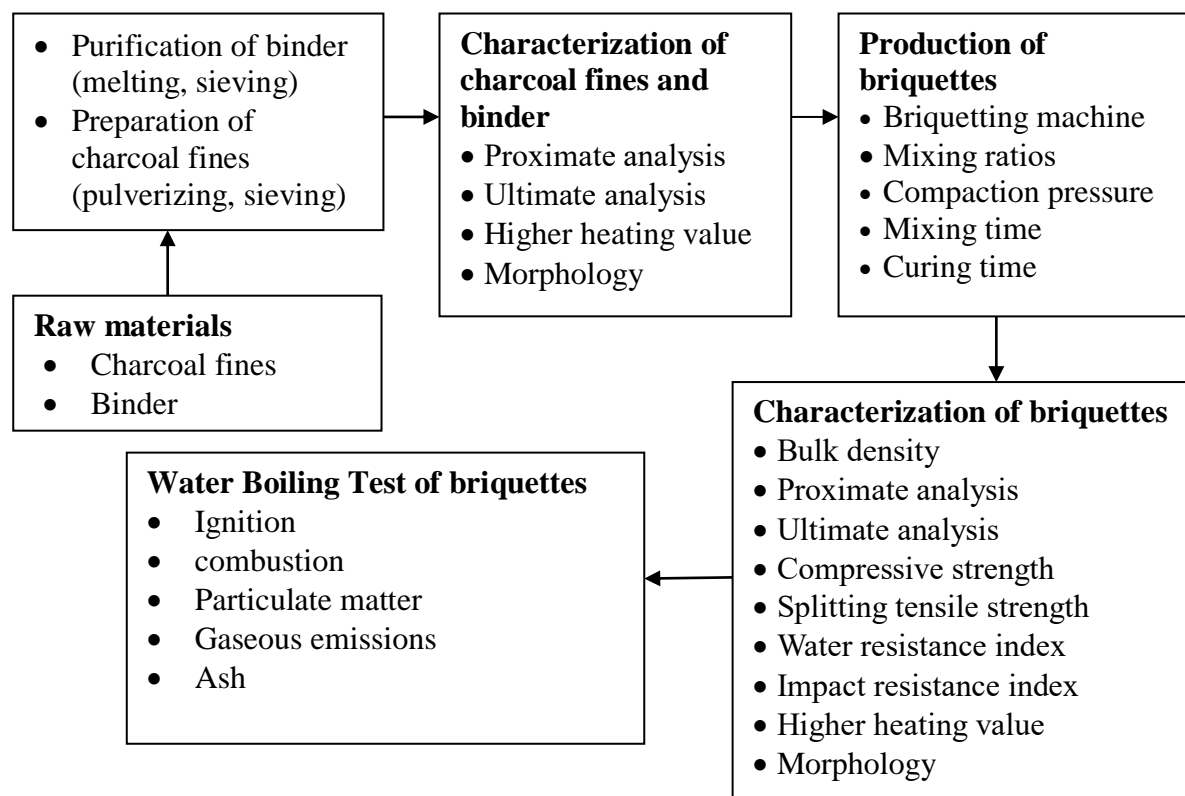


Figure 12: Conceptual framework

3.2 Purification of the *Canarium schweinfurthii* Resin (Binder)

The crude *Canarium schweinfurthii* resin mixed with impurities of bark was obtained from St. Balikuddembe (Owino) market in Kampala, Uganda. The crude resin was heated in a pan placed on a Hotplate Stirrer (Corning, PC 420D) to a boiling point of about 163°C (Appendix 1) measured with an Infrared Thermometer (Wintact, WT900). The melted crude resin was sieved with a 1.99 mm square wire mesh to remove the impurities of bark and the purified resin (gum rosin) was collected in a pan and allowed to cool to room temperature and solidify. Figure 13 shows the preparation of the binder.

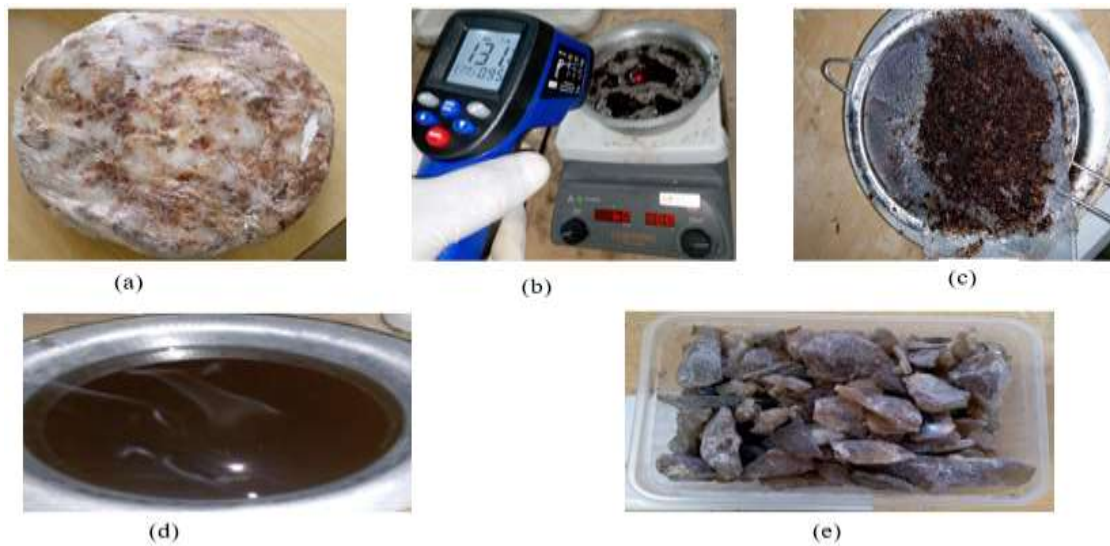


Figure 13: Binder preparation: (a) as-received, (b) melting/boiling, (c) sieving, (d) liquid binder (e) solid binder

3.3 Preparation of the Charcoal Fines

Due to poor handling, the charcoal fines (by-product of charcoal made from carbonized wood) sourced from consumers were mixed with sand making it difficult to sieve thus, lumps of wood charcoal were purchased from the retailers, pulverized, and sieved to obtain a representative sample. A sack of charcoal was obtained from Tengeru market in Arusha, Tanzania. The charcoal was pulverized using a Sealing Type Swinging Pulveriser (DXF-20D) to obtain fine particles. The ground charcoal was sieved using a 355 μm sieve placed on an Electromagnetic sieve shaker (ES-04) to obtain fines recommended for the production of high strength briquettes (Bazargan *et al.*, 2014). The sieved material was stirred thoroughly to produce a homogeneous mixture. Figure 14 shows the procedure for preparation of charcoal fines.

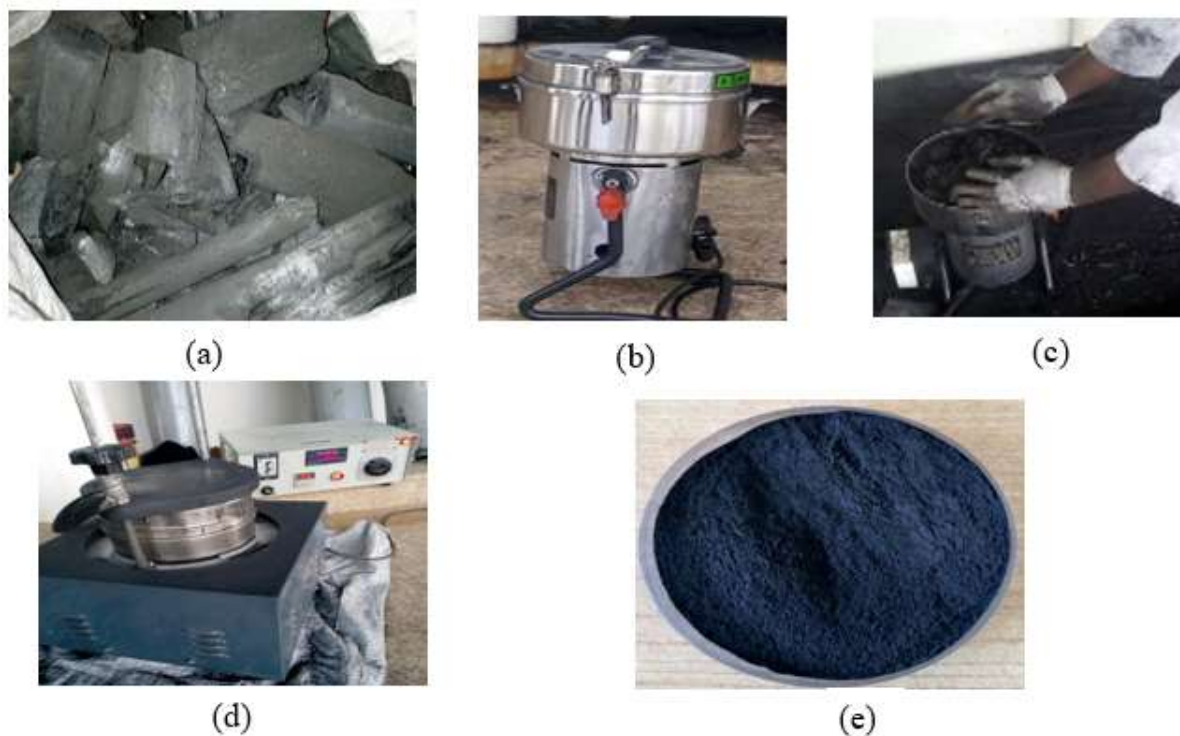


Figure 14: Preparation of charcoal fines: (a) lumps of charcoal, (b) Sealing Type Swinging Pulveriser (c) loading the lumps of charcoal in the pulveriser, (d) Electromagnetic sieve shaker, (e) charcoal fines

3.4 Characterization of Charcoal Fines and *Canarium schweinfurthii* Resin (Binder)

The equipment used for characterization is shown in Appendix 2. Proximate analysis was done using a Thermogravimetric Analyser (Eltra Thermostep) to determine the moisture, volatiles, fixed carbon, and ash content of charcoal fines and binder according to the American Society for Testing and Materials (ASTM E1131-08) standard (ASTM, 2014a). This was done in a nitrogen atmosphere followed by an oxidising atmosphere and the experiment was conducted at Nelson Mandela African Institution of Science and Technology (NM-AIST). The moisture content in the charcoal fines was classified under highly volatile matter as recommended by the ASTM E1131-08 standard (ASTM, 2014a). The TG (Thermogravimetric) and DTG (Differential Thermogravimetric) thermograms from proximate analysis were also analysed. The ultimate analysis was done at NM-AIST using the Elemental Analyser (Flash, 2000) to determine the elemental composition of the binder and charcoal fines following the ASTM D3176-15 standard (American Society for Testing and Materials [ASTM], 2015). The higher heating value (HHV) of the binder and charcoal fines was determined at NM-AIST using the Bomb Calorimeter (IKA, C2000) according to the ASTM D5865-13 standard (ASTM, 2013). Three replicates were considered. The morphology of the charcoal fines and binder was examined at Busitema University, Faculty of Engineering using Scanning Electron Microscopy (SEM) (Vega 3 Tescan). An accelerating voltage of 20.0 kV was used.

3.5 Physical and Chemical Properties of Carbonized Briquettes

3.5.1 Production of Carbonized Briquettes

The production of briquettes was conducted at NM-AIST Laboratory as shown in Fig. 15. The charcoal fines and solid binder (*Canarium Schweinfurthii* resin) were weighed using an Analytical Balance (Explorer, EX 124) with an accuracy of ± 0.0001 g. Below the binder concentration of 25 wt%, the resulting briquettes disintegrated during ejection from the die and their strength was undesirable. Above the binder concentration of 40 wt%, the produced briquettes become stronger. Moreover, it is logical to use a small quantity of binder for production of briquettes as this is economical (Sen *et al.*, 2016). The binder concentrations of 25, 30, 35 and 40 wt% were considered to form four briquette samples (B25, B30, B35 and B40) with the following ratio of charcoal fines: Binder, respectively; 3:1, 7:3, 13:7, 3:2. The binder was first melted in a pan on a Hotplate Stirrer (Stuart, CB162) set at 400°C. Charcoal fines were then added and the mixture stirred manually for 4-5 min to obtain a homogeneous mixture before pouring it into the die of the briquetting machine. The pouring temperature of the mixture was 125-134°C (Appendix 3), recorded using an Infrared Thermometer (Wintact, WT900). After pouring in the die, the mixture was compressed for 5 min (Sotande *et al.*, 2010) using a 20 ton hydraulic jack. The compaction pressure after 5 min was 5.92-7.96 MPa (Appendix 4) recorded with a Pressure Gauge (Nuoha Fina, EN887-1). The cured briquettes were then ejected from the die and stored at room temperature.

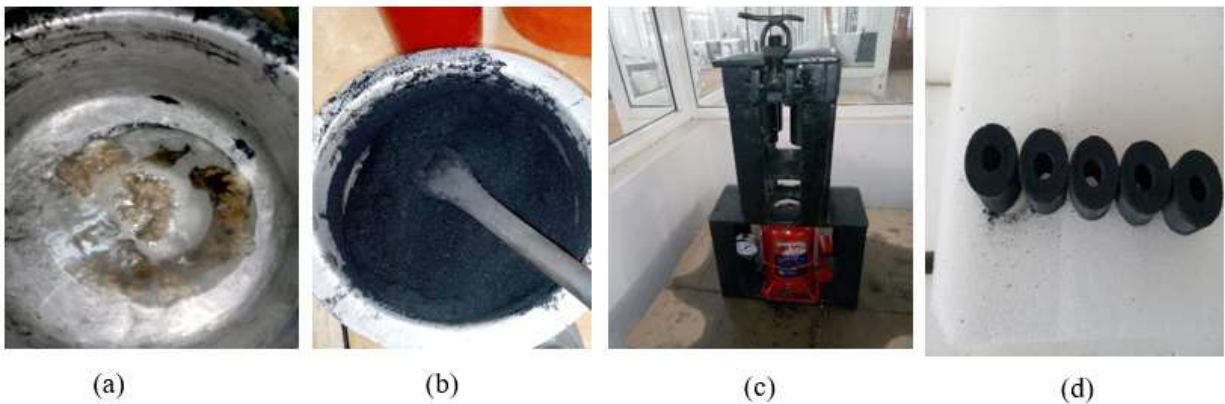


Figure 15: Production of briquettes: (a) melting binder, (b) mixing binder/charcoal fines, (c) compaction, (d) sample briquettes

3.5.2 Physical and Chemical Properties of the Carbonized Briquettes

(i) Physical Properties

Bulk Density

The mass of briquette was measured using an Analytical Balance (Explorer, EX124). The dimensions (height, outside diameter, inside diameter) of the cylindrical briquette to determine volume were measured using a Vernier Caliper (HVC01200) with an accuracy of 0.05 mm. The ASTM 2395-14 standard was followed (ASTM, 2014b). Five replicates were considered. The density, ρ (g/cm³) was computed using Equation 143.

$$\rho = \frac{m}{\frac{\pi}{4}(d_1^2 - d_2^2)h} \quad (143)$$

where d_1 -Outside diameter (cm), d_2 -Inside diameter (cm), h - Height (cm), m -mass (g)

Impact Resistance Index (IRI)

The IRI was determined by repeatedly dropping the briquettes from a height of 2 m onto a tiled floor until they fractured (Bazargan *et al.*, 2014). Five replicates were considered. The IRI was computed according to Equation 144.

$$IRI = \frac{n_d}{n_p} \times 100 \quad (144)$$

where n_d -Average number of drops, n_p - Average number of pieces

Compressive and Splitting Tensile Strength

The dimensions (height, outside diameter, inside diameter) of the cylindrical briquette were measured using a Vernier Caliper (HVC01200) with an accuracy of 0.05 mm. The compressive and splitting tensile forces of the briquette were determined using a 300 kN (Testometric, FS300AT) and 25 kN (Testometric, M500-25) materials testing machines, following the ASTM C39/C39M-17b and ASTM C496/C496M-11 standards, respectively (ASTM, 2011, 2017). For compressive and splitting tensile forces, the flat and curved surfaces of the briquette sample, respectively were placed between horizontal metal plates of the machine as shown in Fig. 16 and Appendices 14 and 15. This was followed by applying an increasing load at a rate of 0.5 mm/min until the briquette failed by cracking or breaking. Three replicates were considered. The compressive strength (F) and splitting tensile strength (T) were calculated using Equation 145 and 146, respectively (Gilvari *et al.*, 2019).

$$F = \frac{P}{\frac{\pi}{4}(d_1^2 - d_2^2)} \quad (145)$$

$$T = \frac{2P}{\pi d_1 h} \quad (146)$$

where d_1 -Outside diameter (mm), d_2 -Inside diameter (mm), h -Height (mm), P -Load (N)

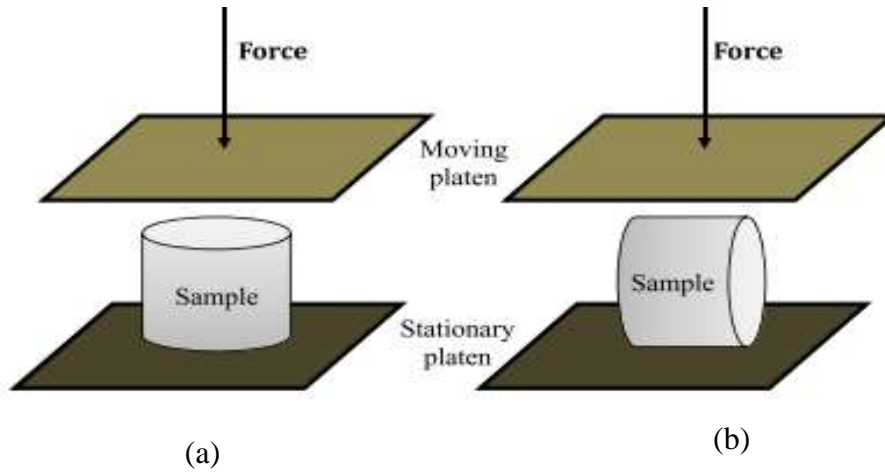


Figure 16: (a) compressive strength (b) splitting tensile strength (Bazargan *et al.*, 2014)

Water Resistance Index (WRI)

A weighed briquette was immersed in tap-water contained in a beaker at room temperature for 30 min (Bazargan *et al.*, 2014) as shown in Fig. 17. It was then withdrawn, wiped to remove surface moisture, and reweighed. Five replicates were considered. The percentage of water absorbed was calculated using Equation 147 while the WRI was computed according to Equation 148 (Kpalo *et al.*, 2020b).

$$\%water\ absorbed = \frac{w_2 - w_1}{w_1} \times 100 \quad (147)$$

Where w_1 - weight of briquette before immersion (g), w_2 - weight of briquette after immersion (g).

$$WRI = 100 - \%water\ absorbed \quad (148)$$



Figure 17: Water resistance index; briquettes immersed in water contained in a beaker

Morphology of the Briquettes

The experiment was carried out at Busitema University, Faculty of Engineering. The morphology of the briquettes was examined using SEM (Vega 3 Tescan) shown in Appendix 2d. An accelerating voltage of 20.0 kV was used.

(ii) Chemical Properties

Proximate Analysis, Ultimate Analysis, Higher Heating Value, and Energy Density

The equipment used for characterization is shown in Appendix 2. Sample briquettes were pulverized using a Planetary Ball Mill (Retsch PM100) to obtain a homogeneous mixture for proximate analysis, ultimate analysis, higher heating value, and energy density. Proximate analysis, ultimate analysis and higher heating value of the briquettes were determined using the same procedure used for characterization of the *Canarium Schweinfurthii* resin and charcoal fines. The TG and DTG thermograms from proximate analysis were also analysed. The energy density was calculated by multiplying the density with the HHV of the briquettes (Kambo & Dutta, 2014). Three replicates were considered.

3.5.3 Statistics of Proximate Analysis, Ultimate Analysis and HHV of Briquettes

The data for proximate analysis, ultimate analysis and HHV obtained from simple random sampling of the briquettes were subjected to a one-way Analysis of Variance (ANOVA) and Fisher's Least Significance Difference (LSD) using OriginPro 9 software to determine the significant differences between the various treatments of the briquettes. All significance tests in this study were conducted with $P < 0.05$. For ANOVA, the following hypothesis was tested; Null Hypothesis: The means of all levels are equal, Alternative Hypothesis: the means of one or more levels are different.

3.5.4 Effect of Binder Concentration and Compaction Pressure on Physical Properties of Briquettes

The two factors considered were binder concentration (A) and compaction pressure (B). The responses were the physical properties i.e., Bulk density (ρ), Impact resistance index (IRI), compressive strength (F), splitting tensile strength (T), and water resistance index (WRI). Design Expert software was used to analyse the effect of binder concentration and compaction pressure on physical properties of the briquettes. The experimental data for the responses was considered in three replicates.

3.6 Water Boiling Test of the Carbonized Briquettes

3.6.1 Experimental Setup

The research was carried out at the Centre for Research in Energy and Energy Conservation (CREEC), Makerere University. The experiment was conducted using the Laboratory Emission Monitoring System (LEMS) as shown in Appendix 5 and Fig. 18, according to the ISO 19867-1 standard (Aprovecho Research Center, 2018). The schematic diagram in Fig. 18 was drawn using Microsoft Visio. A blower (Dayton, 1TDU2) on the LEMS was used to push the air/exhaust through the system. The hood face velocity was less than 0.25 m/s measured with a hot wire anemometer (TPI, SP565) while the blower is running (Aprovecho Research Center, 2018).

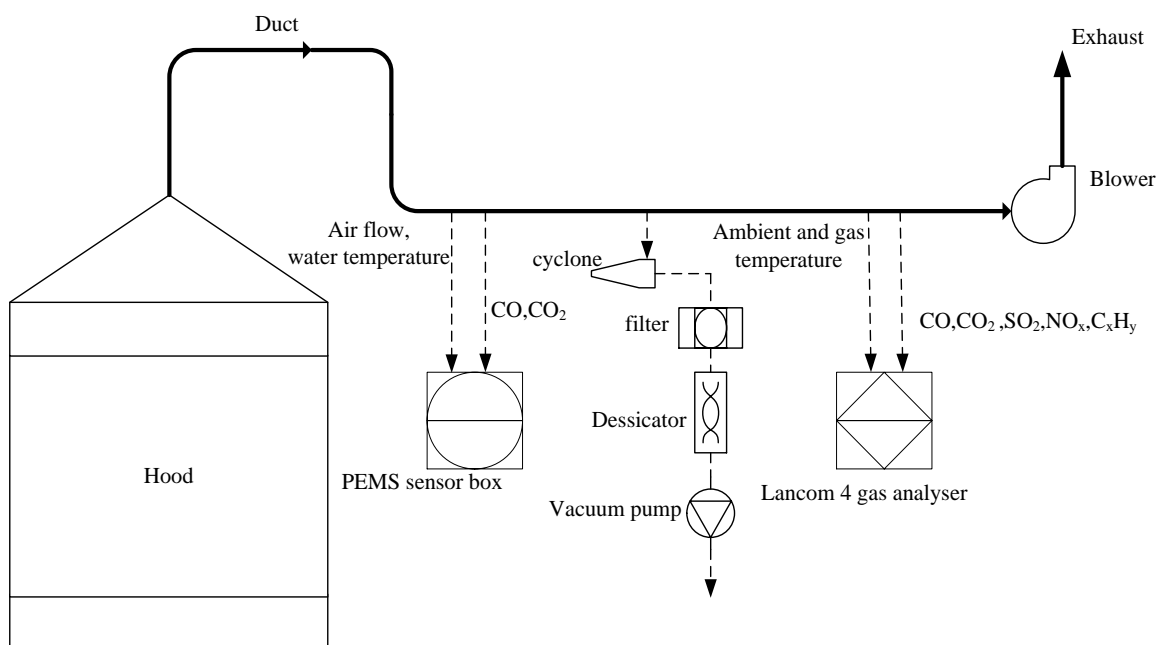


Figure 18: Schematic diagram of the Laboratory Emission Monitoring System

3.6.2 Ignition of Briquettes

A natural draft cookstove (Burn) shown in Fig. 19a was selected for the experiment and its weight measured using an electric weighing scale (Hiweigh, WPS). The four briquette samples (B25, B30, B35, B40) were placed in turn in the combustion chamber of the cookstove. Four briquettes were loaded on the cookstove. The stove was reweighed to determine the weight of the samples and placed under the hood of the LEMS. The bioethanol gel used for ignition of the briquettes was 5% of the briquette weight according to the ISO 19867-1 standard (ISO, 2018). The bioethanol gel was weighed on the ash tray of the cookstove using the electric weighing scale (Hiweigh, WPS). The ash tray with the bioethanol gel was lighted with a match and then placed into the ash chamber

of the cookstove to ignite the briquettes. Three replicates were considered and the time taken for the bioethanol gel to burn to completion was recorded as the ignition time using a stopwatch.



Figure 19: (a) Cookstove (Burn), (b) Weighing water, (c) gas analyser (PEMS, 2000) , (d) gas analyser (Ametek Land, lancom 4), (e) Filter holder, (f) Drying the filter paper, (g) furnace, (h) XRD/XRF analyser

3.6.3 Combustion

The local boiling point was determined empirically according to the WBT 4.2.3 protocol (Clean cooking alliance, 2014) and found to be 95°C at an altitude of 1240 m (Wikipedia, 2021) where the experiment was carried out. The WBT 4.2.2 and 4.2.3 protocols were considered during the combustion experiment (Clean cooking alliance, 2014). The phases of the WBT considered were Cold Start High Power (CSHP), Hot Start High Power (HSHP) and Simmer phases. An electric weighing scale (Hiweigh, WPS) was used to measure 2.5 kg (2.5 L) of water in a pot as shown in Fig. 19b. A thermocouple (26AWG K type, chromel, Alumel) with 260 PTFE insulation was placed 5 cm from the bottom of the pot (Clean cooking alliance, 2013) to measure the temperature of the water. The thermocouple was connected to a Portable Emission Monitoring System (PEMS) sensor box (PEMS, 2000) shown in Fig. 19c and the water temperature was monitored from a computer using the PEMS software. After ignition, the pot with water was placed on the cookstove and the water temperature (T_{water}) was recorded with the PEMS software. The gas temperature (T_{gas}) and ambient temperature (T_{ambient}) were recorded with the gas analyser (Ametek Land, lancom 4) shown in Fig. 19d. During combustion of the briquettes, smoke, flame, soot, and ash from the burning briquettes were monitored.

3.6.4 Gaseous Emissions and Particulate Matter During the Water Boiling Test

Gaseous emissions and PM were measured during ignition, CSHP, HSHP, and Simmer phases. The gaseous emissions measured by the gas analyser (Ametek Land, Lancom 4) included CO, CO₂, SO₂, NO_x, and C_xH_y while the PEMS sensor box was used to record CO and CO₂ for evaluation of WBT performance metrics. For PM measurement, the electronic weighing scale (Citrizon, CX265) was first calibrated using a 500 mg class 1 weight (Troemner, 7026-1W). A filter paper (HI-Q, FPAE-102) was then weighed using the calibrated electronic weighing scale considering three replicates. The filter paper was placed in a filter holder (ILPH-102) shown in Fig. 19e and fixed on the LEMS. A vacuum pump (Gast, 71R655-V10-C222TX) was used to push the exhaust from the duct through the filter at a speed of 16.7 Lpm. The PM collected by the filter paper was 2.5 µm while the larger PM (>2.5 µm) was collected with a cyclone (URG-2000-30EHS). After the experiment, the filter paper was removed from the filter holder and placed in a dessicator (Igloo, FR320) as shown in Fig. 19f to absorb the moisture from the collected PM_{2.5}. The temperature and relative humidity inside the dessicator were monitored using a white digital indoor-outdoor temperature and humidity gauge (AcuRite, 00611A3).

After drying, the filter paper was reweighed to determine the amount of PM_{2.5} captured. The WBT performance metrics were analysed using the excel workbook titled WBT_data-calculation_sheet_4.2.3.xls (Appendix 6) (Aprovecho Research Center, 2020). A sample of charcoal fines was heated in a box furnace (Cole-Parmer, CBFL516C) as shown in Fig. 19g at a temperature of 600°C to obtain ash following the ASTM D1102 standard. The ash and charcoal fines were then sieved with a 150 µm sieve to obtain a sample which was analysed using a portable X-ray diffraction/X-ray fluorescence (XRD/XRF) analyser (Olympus, Terra II) shown in Fig. 19h to determine its chemical composition. The XRD data was analysed using X Powder software and the experiment was conducted at NM-AIST Laboratory. The XRD plots were drawn using OriginPro 9 software.

CHAPTER FOUR

RESULTS AND DISCUSSION

4.1 Characterization of the *Canarium Schweinfurthii* Resin (Binder) and Charcoal Fines

4.1.1 Thermogravimetric and Differential Thermogravimetric Thermograms from Proximate Analysis

Appendices 7, 8 show the TG and DTG data while Fig. 20a, b shows the TG and DTG thermograms for charcoal fines and binder, respectively. Figure 20c shows the temperature profile of the TG and DTG analysis. The first weight loss at around 105°C was due to removal of the highly volatile matter as a result of dehydration in association with the degradation of thermally unstable organic constituents below 200°C (Haykiri-Acma *et al.*, 2013) and the corresponding peak on the DTG thermogram was 0.003 g/min for charcoal fines. The second weight loss for heating the sample from 105-915°C and cooling to 750°C was attributed to removal of medium volatile matter and the corresponding peaks on the DTG thermograms were 0.012 g/min and 0.188 g/min for charcoal fines and binder, respectively. The third weight loss for heating the sample at around 750°C was due to char combustion as reported by Zhu *et al.* (2019) and the corresponding peak on the DTG thermogram was 0.009 g/min for charcoal fines. On the contrary, heating the binder to 915°C resulted in complete devolatilization and there was negligible mass of the sample remaining after that temperature as shown by the TG thermogram thus, there was no char combustion. This is due to the fact that the binder contains terpenoids which are highly volatile. The residual mass was ash as reported by Wu *et al.* (2018) for the charcoal fines and negligible mass was observed for the binder as shown by the TG thermograms.

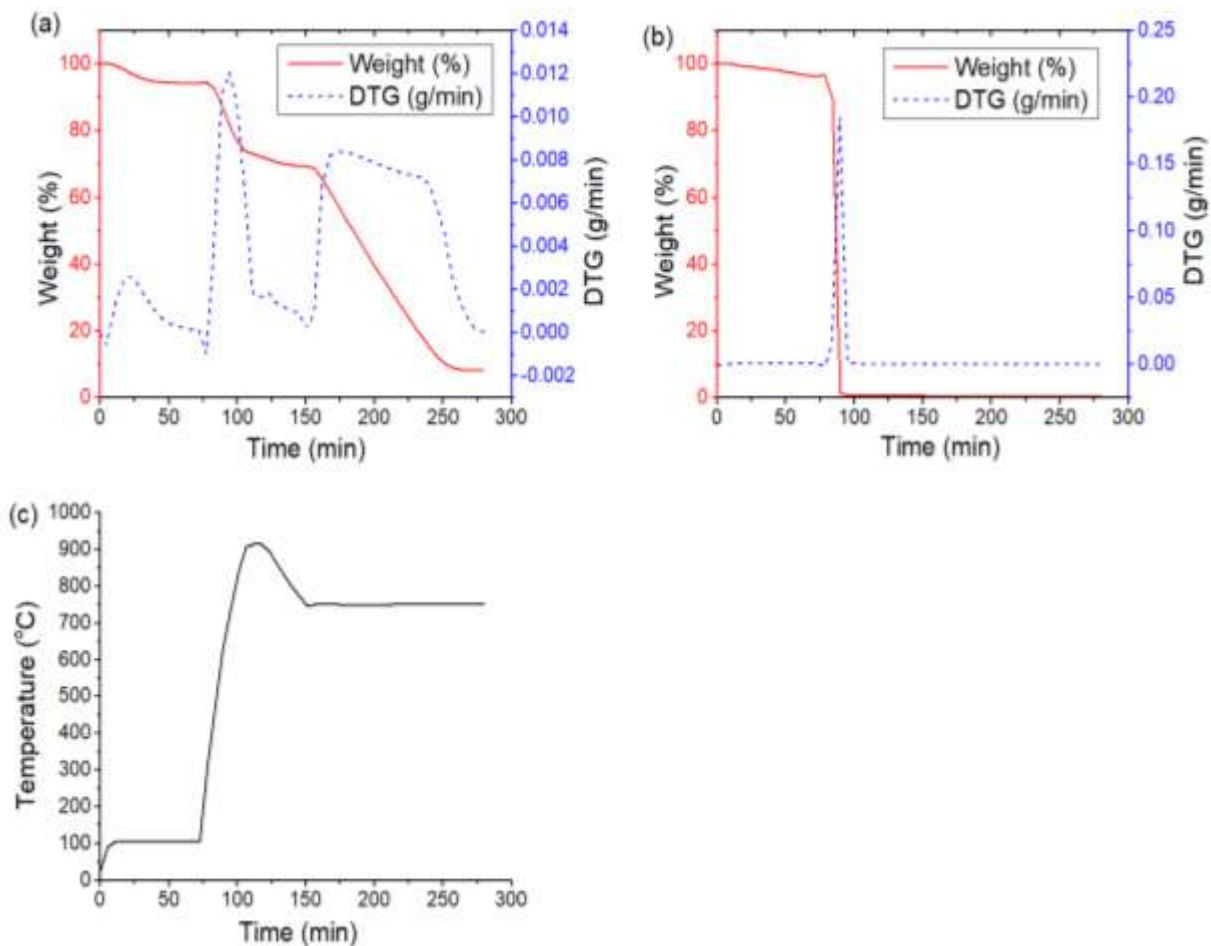


Figure 20: (a) & (b); TG and DTG thermograms for charcoal fines and binder, respectively, (c) temperature profile during TG and DTG analysis

4.1.2 Proximate Analysis of Binder and Charcoal Fines

The proximate analysis results of the charcoal fines and binder are shown in Table 4 and Appendix 9. It was observed that the charcoal fines contained a significant amount of medium volatile matter which is attributed to the inefficient local methods of pyrolysis of wood to produce charcoal. The binder had a high percentage of medium volatile matter since it contains terpenoids which are highly volatile. The zero amount of ash in the binder implies that the heating value of the binder is not affected by the ash as reported by Samadi *et al.* (2019). Hu *et al.* (2015) produced biochar pellets using organic binders (lignin and starch) and reported that the biochar pellets had higher volatile matter, but lower ash content and fixed carbon similar to this study. Pereira *et al.* (2012) also reported volatile matter in charcoal produced from six Eucalyptus clones in a laboratory kiln.

4.1.3 Ultimate Analysis, and Higher Heating Value of Binder and Charcoal Fines

The ultimate analysis, and HHV results of the charcoal fines and binder are shown in Table 4, and Appendices 10, 11. The nitrogen found in the charcoal fines is attributed to the fuel-N incorporated mainly in pyrrolic and pyridinic structures (Glarborg *et al.*, 2003). The nitrogen in the *Canarium*

Schweinfurthii resin was also identified by Ameh (2018) using GC-MS. The hydrogen and oxygen in charcoal fines is attributed to the medium volatile matter in the raw material as noted from the proximate analysis. Idris *et al.* (2015) produced charcoal from oil palm biomass with a heating value of 23-25 MJ/kg while Pereira *et al.* (2012) produced charcoal from Eucalyptus clones with a heating value of 29.60-31.89 MJ/kg and these results are close to the heating value of 28.11 MJ/kg for charcoal fines obtained in this study. Zhao *et al.* (2012) reported that terpenoids are extremely flammable, with high heating value, for instance, α -pinene has a heating value of 45 MJ/kg which is close to the value of 40.17 MJ/kg obtained in this study for the *Canarium Schweinfurthii* resin containing a mixture of terpenoids.

Table 4: Proximate analysis, ultimate analysis, and HHV of binder and charcoal fines

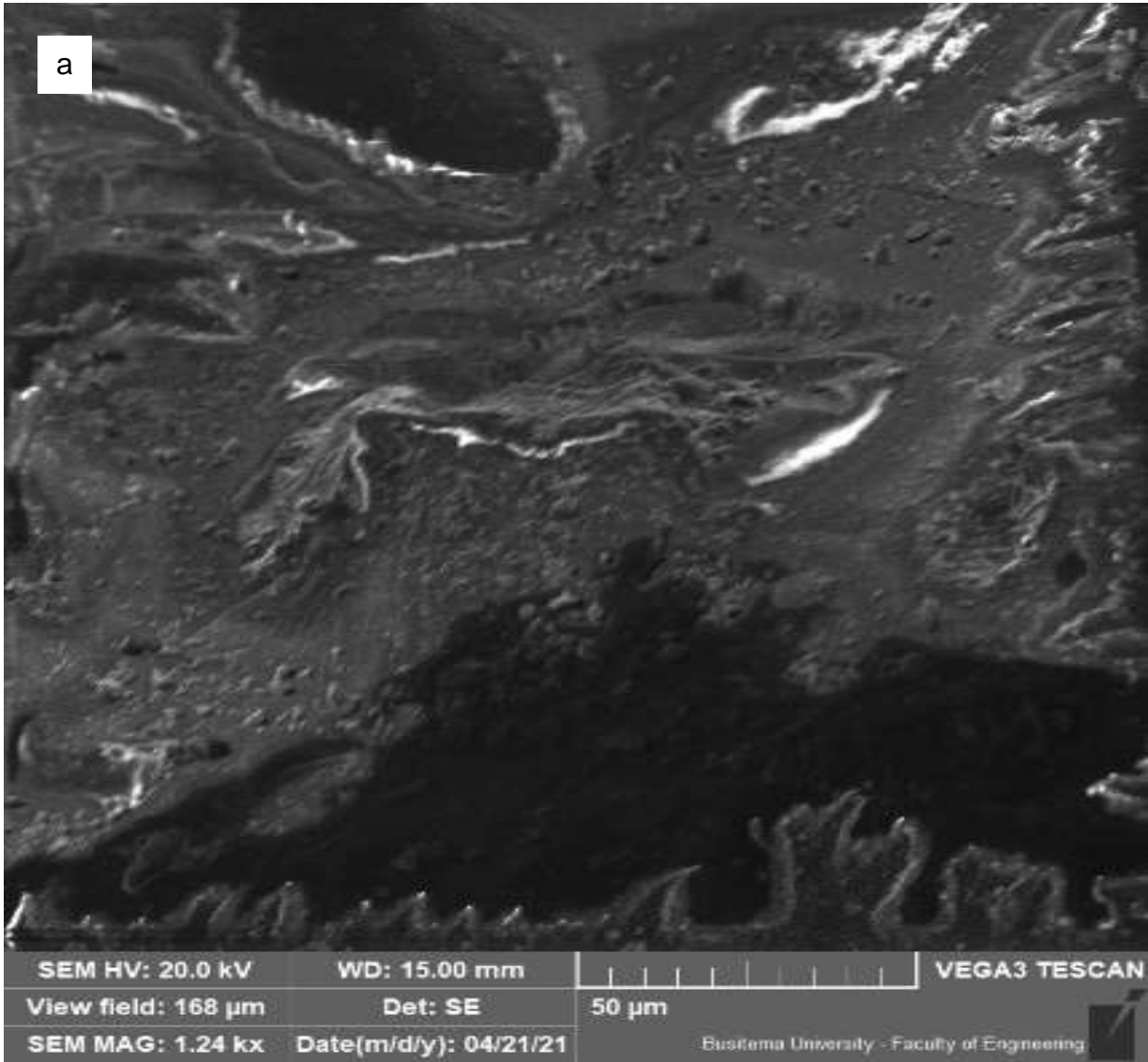
| Sample | Proximate analysis (wt %, as received) | | | | Ultimate analysis (wt%, db*) | | | | | HHV (MJ/k) |
|----------------|--|------------------------|------|--------------|------------------------------|-----------|----------|----------|---------|------------|
| | Highly volatile matter | Medium volatile matter | Ash | Fixed Carbon | C | H | N | O | S | |
| Charcoal fines | 6.06 | 21.95 | 7.69 | 64.30 | 71.7 3 | 2.17 | 1.7 2 | 6.9 1 | ND * | 28.11 |
| Binder | 4.71 | 95.30 | 0 | 0 | 81.0 4 | 10.8 4 | 1.1 1 | 6.2 9 | ND * | 40.17 |

*db-dry basis

*ND-Not Detected

4.1.4 Morphology of Binder and Charcoal Fines

Figure 21a, b shows the SEM micrographs for binder and charcoal fines. Figure 21a shows that the solid binder exhibited a smooth appearance with some regions having dendrites and a pore. Figure 21b shows that the charcoal fines exhibited regions with a fibrous and porous structure (Gani & Naruse, 2007) while other regions were amorphous. This could be attributed to the volatile matter (Raju *et al.*, 2014) in the charcoal fines as shown from the proximate analysis results in Table 4.



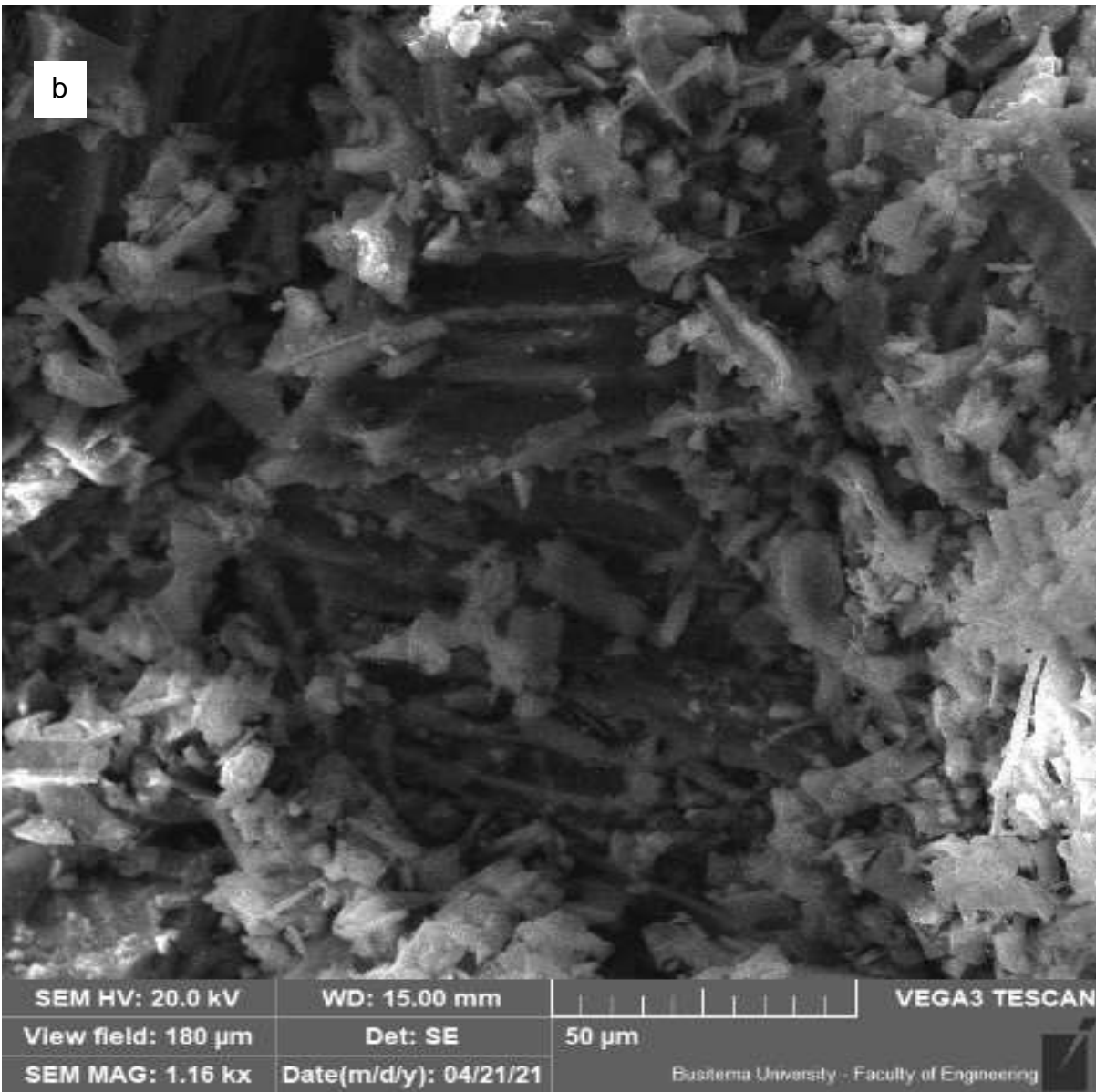


Figure 21: SEM micrographs; (a) Binder, (b) charcoal fines

4.2 Physical Properties of the Carbonized Briquettes

4.2.1 Bulk density

Appendix 12 shows the results for the outside diameter (d_1), inside diameter (d_2), height (h), volume (V), mass (m), and density (ρ) of briquettes. It was observed that the bulk density increased with increasing binder concentration (Fig. 22) since the same amount of charcoal fines were used, and there was a slight increase in volume while the mass of briquette increased greatly as more binder was added (Appendix 12). The bulk density was 0.770, 0.877, 0.951, 1.036 g/cm³ for briquettes B25, B30, B35 and B40 respectively. Kpalo *et al.* (2020a) reported that briquettes can be produced with binders with a density ≥ 1.0 g/cm³. Using other binders, the density of

briquettes obtained by other researchers as detailed in Table 3 was in the range of 0.2-1.24 g/cm³ and this is comparable to the values (0.770-1.036 g/cm³) obtained in this study.

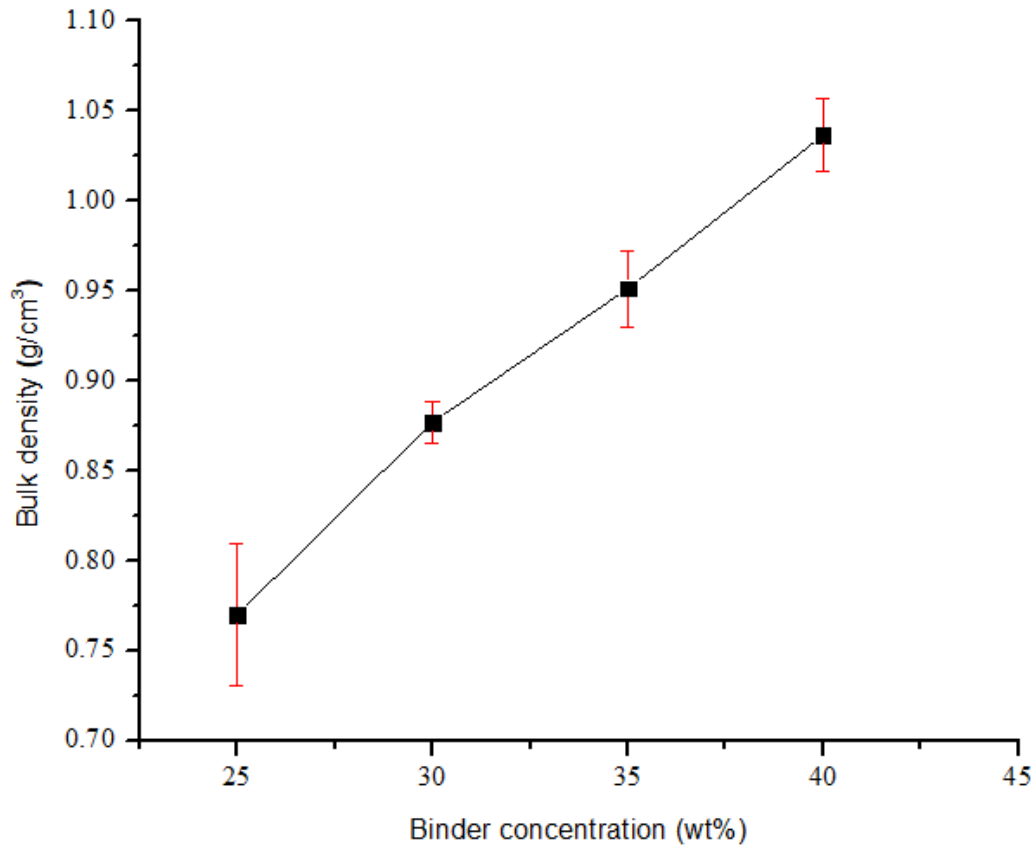


Figure 22: Bulk density versus binder concentration

4.2.2 Impact Resistance Index (IRI)

The IRI of the briquettes is shown in Fig. 23 and Appendix 13. It was observed that the IRI increased with binder concentration due to improved bond performance (Zhang *et al.*, 2018). Briquette B25 broke into 30-40 pieces on the first time of impact with IRI of 2.90. Briquette B30 broke into 4-13 pieces on the first/second time of impact with IRI of 16.97. Briquettes B35 and B40 broke into 2-4 pieces on the first/second time of impact with IRI of 60.00 and 73.33, respectively. These results concurred with the findings reported previously by Sen *et al.* (2016) that as the density of the briquettes increases, the IRI also increases. Briquettes B35 and B40 passed the recommended IRI value of 50 (Bazargan *et al.*, 2014).

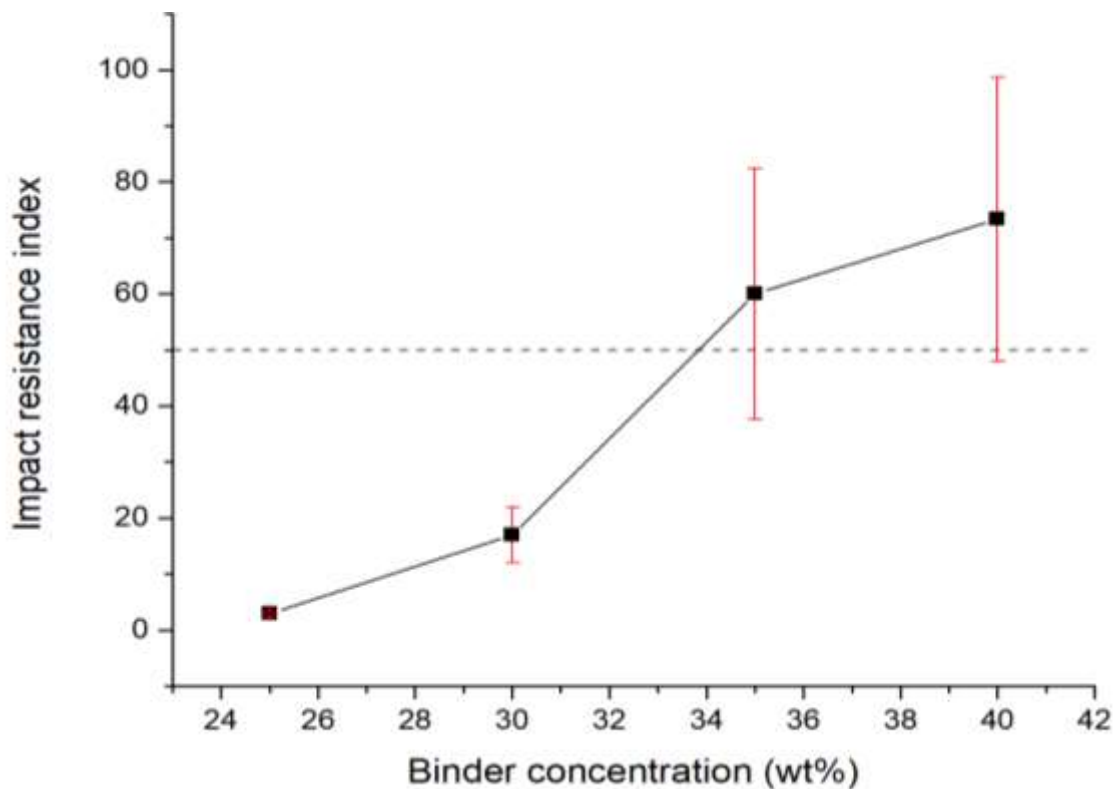


Figure 23: Impact resistance index (IRI) versus binder concentration (wt%)

4.2.3 Compressive and Splitting Tensile Strength

The compressive and splitting tensile strength results are shown in Fig. 24a, b and Appendix 14-19. The compressive strength was 2.25, 3.93, 8.06 and 10.94 MPa for briquettes B25, B30, B35 and B40, respectively. The splitting tensile strength was 0.09, 0.21, 0.32 and 0.42 MPa for briquettes B25, B30, B35 and B40, respectively. Generally, the compressive and splitting tensile strengths increased with increasing binder concentration due to improved bond performance (Zhang *et al.*, 2018). In addition, compressive strength was greater than the splitting tensile strength as reported by Gilvari *et al.* (2019). Bazargan *et al.* (2014) reported splitting tensile strengths of 0.017-0.035 MPa for briquettes with 30-40% moisture content produced using 10 wt% cassava starch as binder and those results are less than the ones (0.09-0.42 MPa) obtained in this study. According to Turkish Standard (TS)12055, Class I briquettes should have a compressive strength greater than 13 MPa, while Class II briquettes should withstand a compressive strength not lower than 10 MPa (Haykiri-Acma *et al.*, 2013). Thus, briquette B40 met the Class II standard while briquette B35 was close to Class II standard. Briquettes B25 and B30 were below the TS. For compressive strength, all the briquettes met the recommended minimum value of 0.375 MPa reported for commercial charcoal briquettes (Ward *et al.*, 2014).

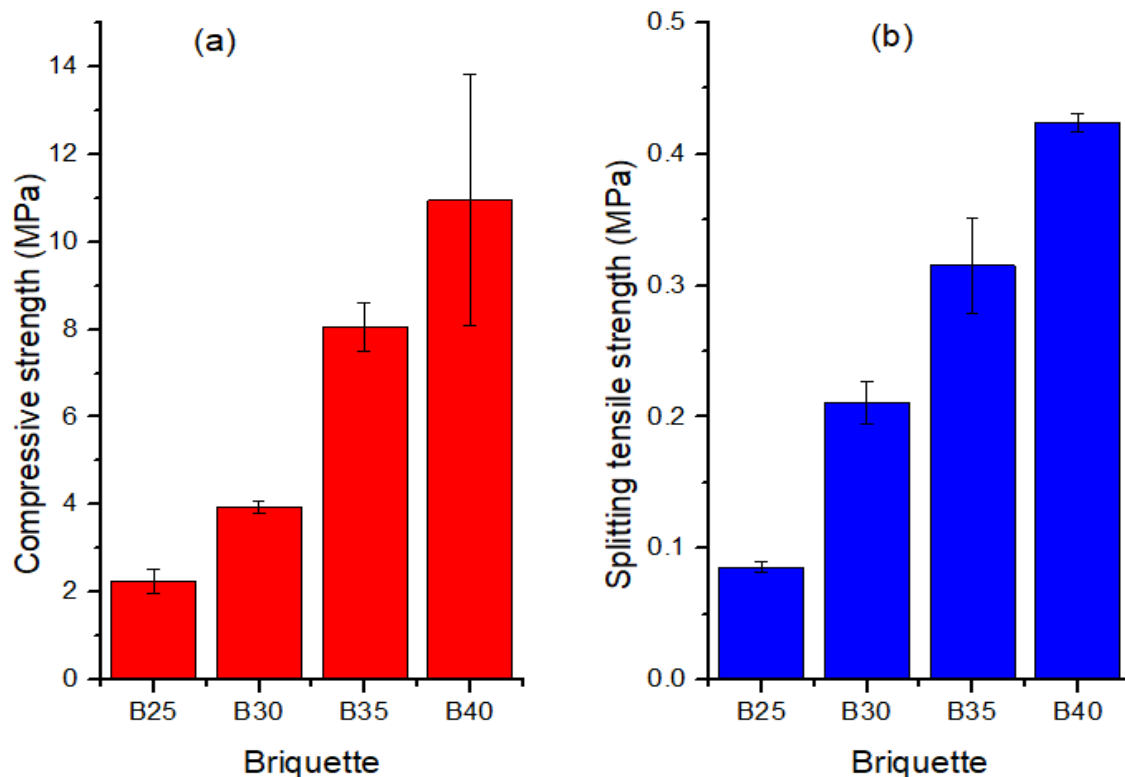


Figure 24: (a) Compressive strength, (b) splitting tensile strength

4.2.4 Water Resistance Index (WRI)

The WRI results are shown in Fig. 25 and Appendix 20. It was observed that the WRI for all the briquettes was between 99.26-99.29 % which met the recommended WRI of 95 % (Gilvari *et al.*, 2019). The high WRI is attributed to the binder used which contains terpenoids that are insoluble in water. Bhattacharya *et al.* (1989) reported that *Canarium Schweinfurthii* resin is an organic binder that is hydrophobic thus, the binder coated the charcoal fines making the briquettes impervious to water. Thoms *et al.* (1999) produced cold cured anthracite/coke breeze briquettes using coal tar acid resin and the briquettes had excellent water-proofing characteristics similar to the ones in this study. Fichan *et al.* (1999) reported that at 25°C, water solubility of terpenes showed low solubility (0.037-0.22 mmol/L), whereas oxygenated monoterpenes exhibited 20 times higher solubility (2-20 mmol/L) and this agrees with the WRI results for the briquettes in this study made with *Canarium Schweinfurthii* resin containing terpenoids. Furthermore, briquettes B25 and B30 were loosely bound thus, some particles broke from the briquettes during the experiment and this could partly explain their low WRI. Bazargan *et al.* (2014) produced briquettes from palm kernel shell biochars using starch as binder and obtained a WRI below 50% implying that the briquettes were less resistant to water absorption compared to this study. Haykiri-Acma *et al.* (2013) produced biobriquettes from carbonized brown seaweed using molasses,

sulphide liquor, and linobind as binders and the WRI revealed that the times for disintegration in water were between 11-31 s which is less than the time considered in this study.

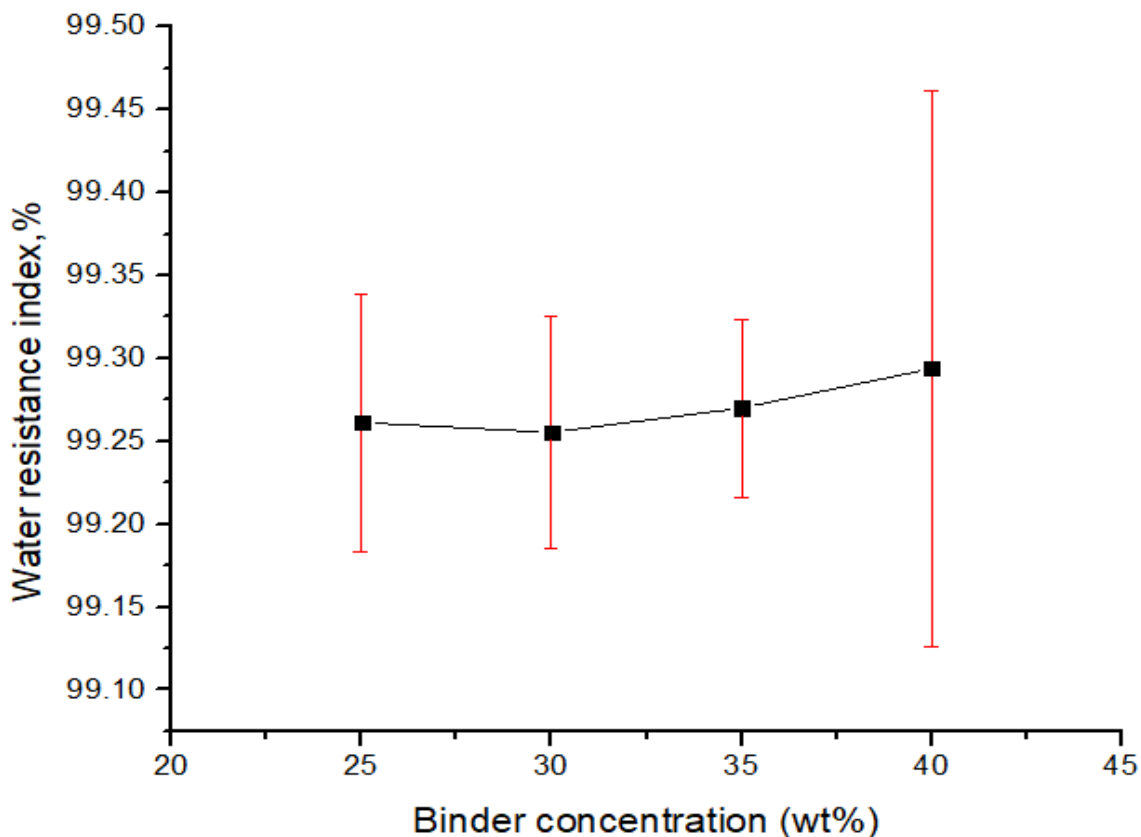
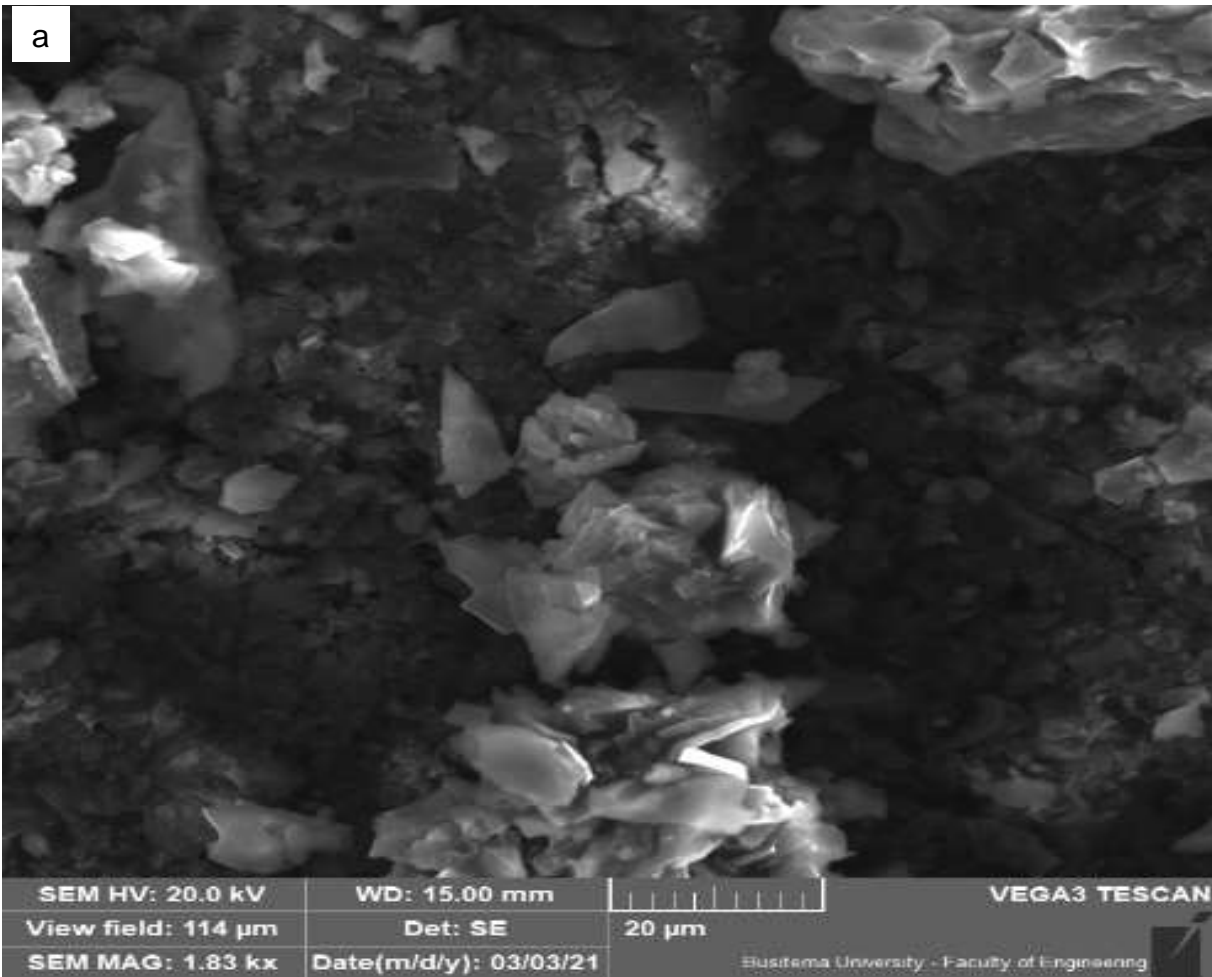


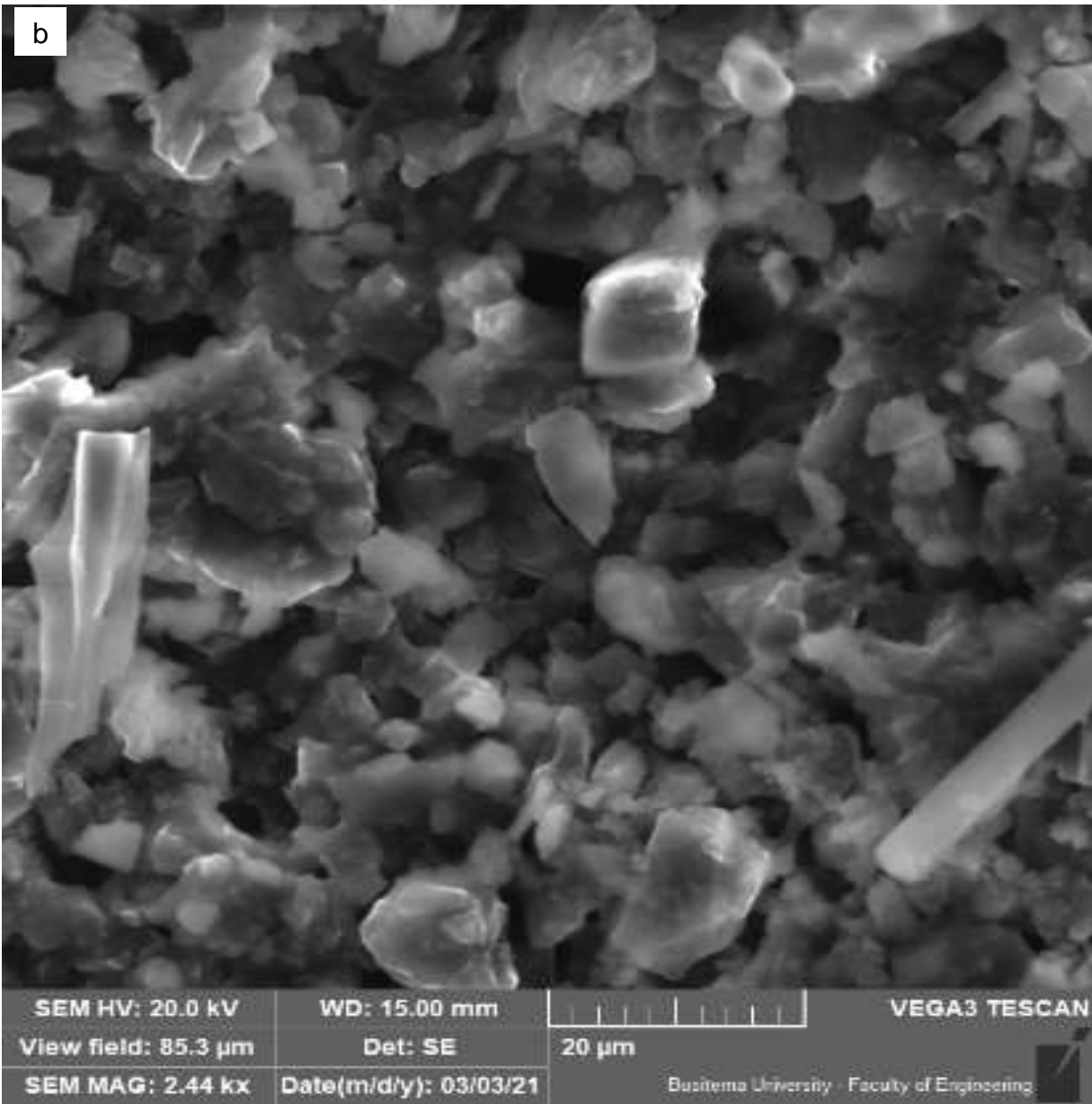
Figure 25: Water resistance index versus binder concentration

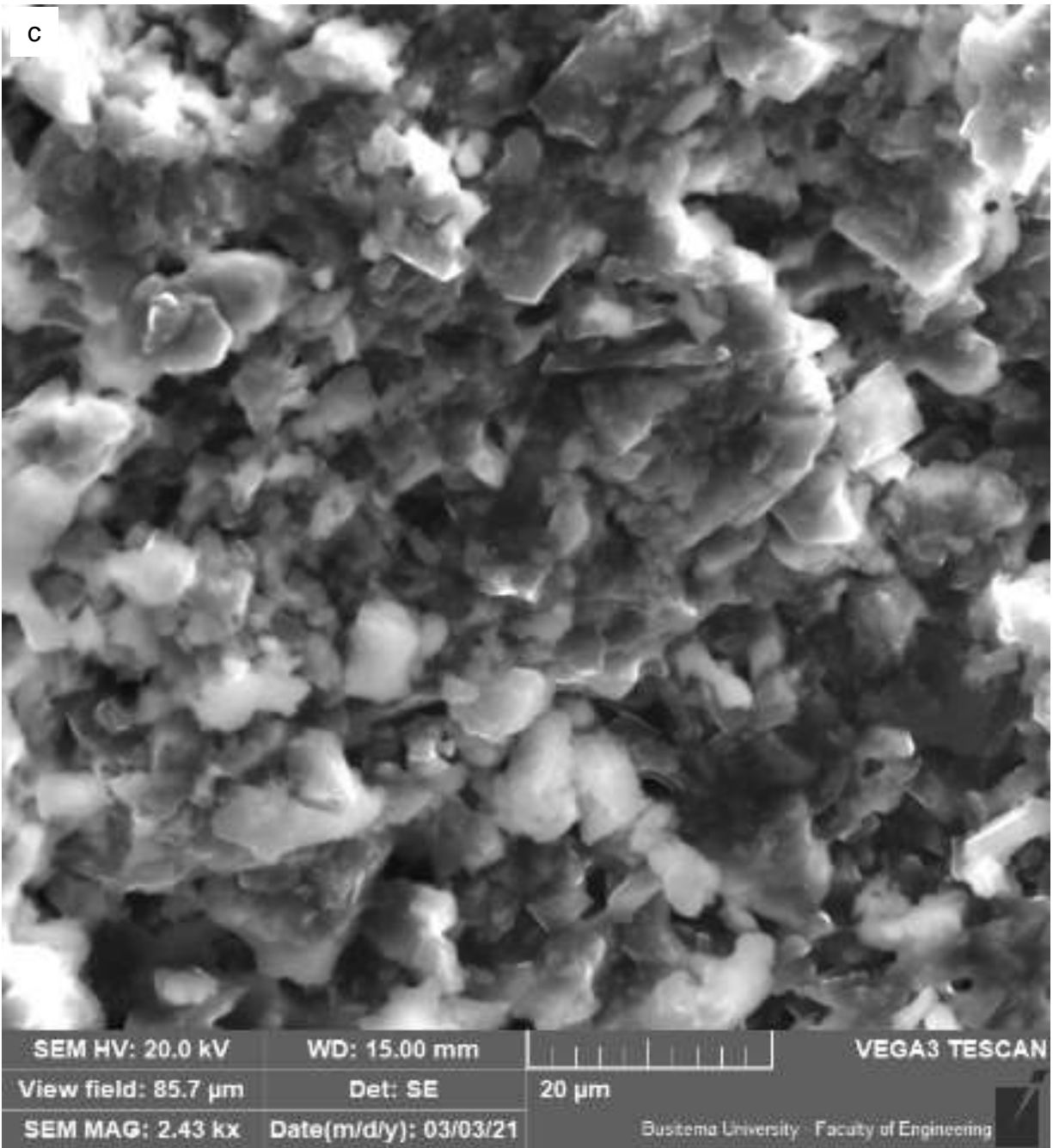
4.2.5 Morphology of Briquettes

Figure 26a-d shows the SEM micrographs for briquettes B25, B30, B35 and B40. The charcoal fines were coated with the binder during mixing. In addition, there was agglomeration of the mixture resulting in the granular appearance (Blesa *et al.*, 2001). The compaction of the granules in the briquetting machine resulted in a porous structure which enhances burning efficiency of the briquettes since it provides more paths for airflow allowing more oxygen and air to circulate inside of the briquettes (Carnaje *et al.*, 2018). The soaking and bridging mechanism for briquettes made from coal and binder postulates that coal particles were wetted by binder and then particles were bonded together through “binder bridge” (Zhang *et al.*, 2018). The same mechanism applies to the charcoal fines and binder in this study. Huang and Hao (2012) analysed gasification briquettes prepared with Shenmu bituminous coal using SEM. The results showed that the cured binder plays a role of “bridge bond” among coal particles which applies to the briquettes in this study. Mixing of the charcoal fines with binder at high temperature and the resulting compaction at high pressure resulted in diffusion of molecules at the point of contact from one particle to another, thus forming solid bridges (Okot *et al.*, 2018). Hu *et al.* (2015) reported that the bonding forces involved in the

biochar pellets densified with lignin mainly related to the attraction and cohesion forces that include hydrogen bonds, Van Der Waals forces, and mechanical interlock. Similar bonding forces are possible for briquettes produced in this study.







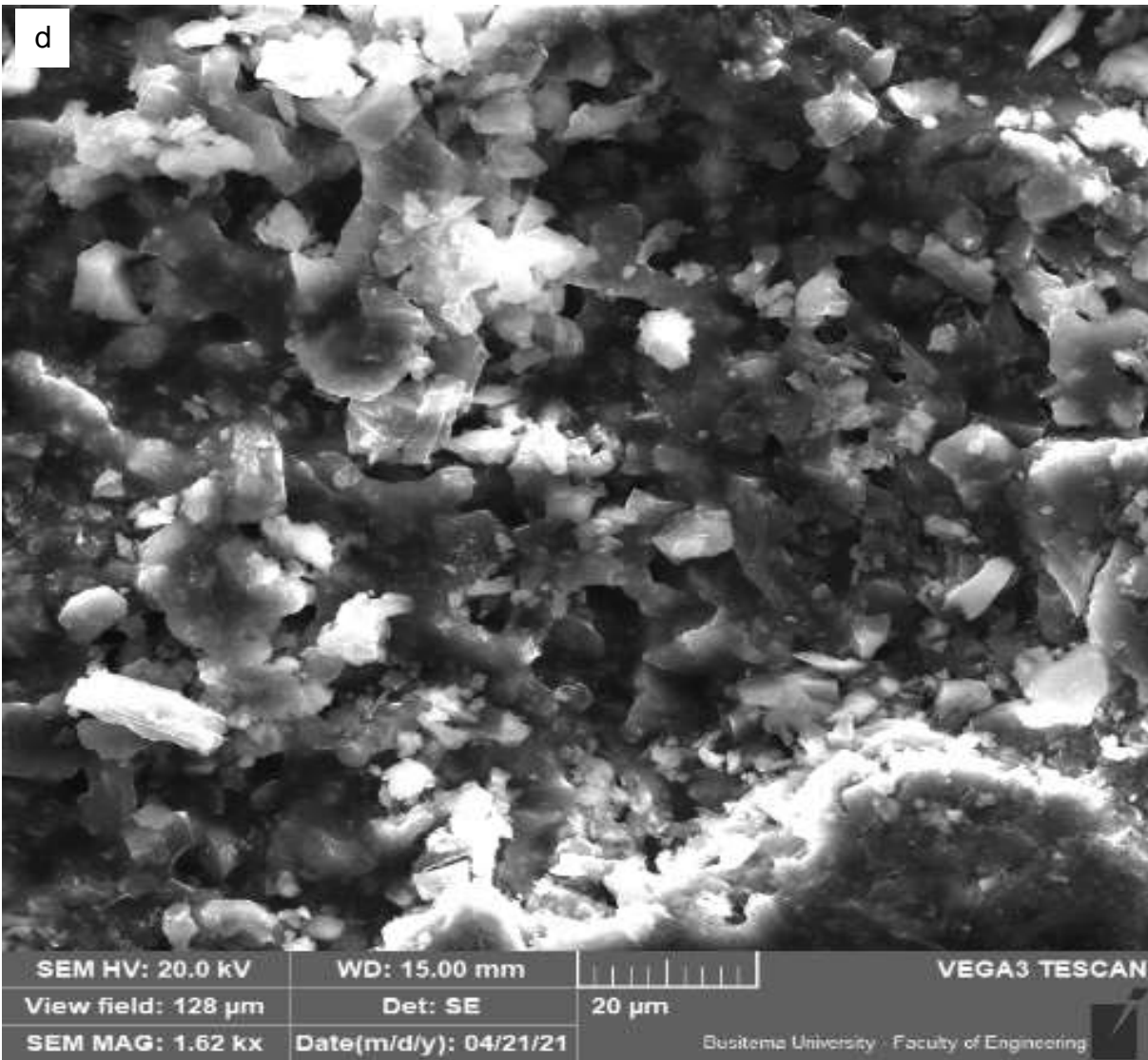


Figure 26: SEM micrographs of briquettes; (a) B25, (b) B30, (c) B35, (d) B40

4.3 Chemical Properties of the Carbonized Briquettes

4.3.1 Thermogravimetric and Differential Thermogravimetric Thermograms from Proximate Analysis

Figure 27a-d shows the TG and DTG thermograms while Appendices 21-24 show the TG and DTG data for the briquettes. The TG and DTG analysis followed the same temperature profile shown in Fig. 20c. The first weight loss at around 105°C was due to release of the highly volatile matter (Hu *et al.*, 2015) and the corresponding peaks on the DTG thermograms were 0.0025 g/min for all the briquette samples. The second weight loss on heating the sample from 105-915°C and cooling back to 750°C was due to release of medium volatile matter (Kivevele & Huan, 2013) and the corresponding peaks on the DTG thermograms were 0.05 g/min, 0.0425 g/min, 0.0575 g/min, 0.0775 g/min for briquettes B25, B30, B35 and B40, respectively. The third weight loss for heating the sample at around 750°C was due to char combustion (Mitchell *et al.*, 2016) and the

corresponding peaks on the DTG thermograms were approximately 0.0075 g/min for all the briquette samples. The residual mass was ash for all the briquette samples as shown in Table 6.

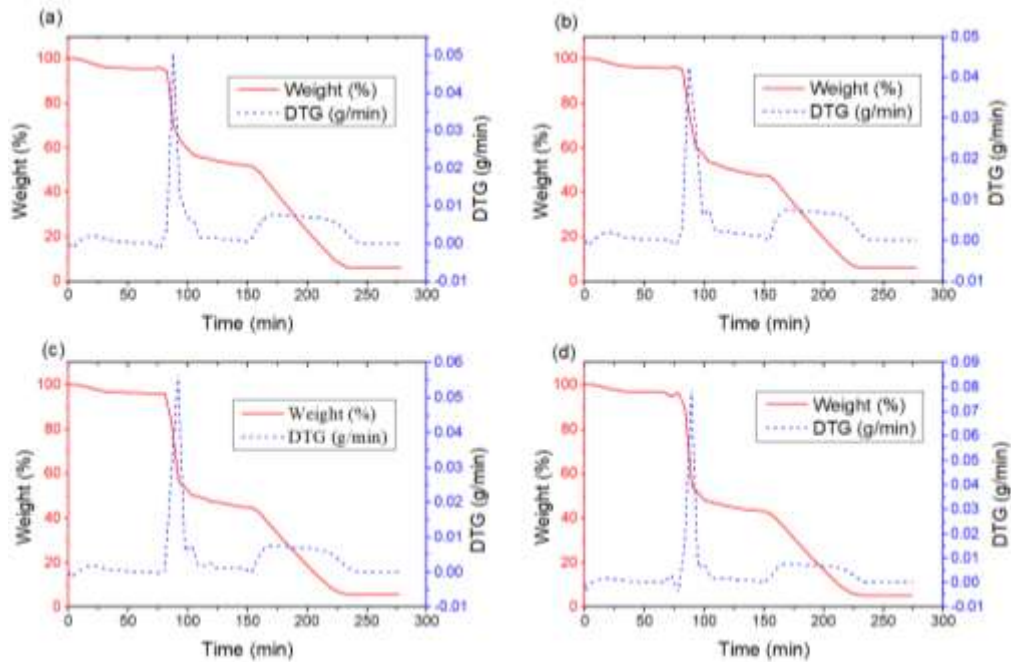


Figure 27: TG and DTG thermograms for briquettes; (a) B25, (b) B30, (c) B35, (d) B40

4.3.2 Proximate Analysis of Briquettes

Proximate analysis results of carbonized briquettes are shown in Tables 5, 6 and Appendix 25. From Table 5, ANOVA showed that there was significant difference between the means of briquette samples for all the properties. From Table 6, for highly volatile matter, LSD showed that the difference of the means was not significant for briquettes B35/B30. For medium volatile matter, LSD showed that there was significant difference between the means for all the briquette samples. The medium volatile matter increased with increasing binder concentration from B25 to B40 as a result of the binder used which contains terpenoids that are highly volatile. For fixed carbon, LSD showed that there was significant difference between the means for all the briquette samples. The amount of fixed carbon decreased with increase in the binder concentration since the binder has no fixed carbon as observed from the proximate analysis results of Table 4. For ash, LSD showed that the difference of the means was not significant for briquettes B30/B25, B35/B25, B35/B30 and B40/B35. The percentage of ash decreased slightly between the binder concentrations since the same amount of charcoal fines was used in all the experiments and the binder used does not contain ash as seen from the proximate analysis results in Table 4 thus, the combustion of the briquettes is only affected by ash from the charcoal fines as reported by Obi (2015).

4.3.3 Ultimate Analysis, Higher Heating Value, and Energy Density of Briquettes

Ultimate analysis, HHV, and energy density results of carbonized briquettes are shown in Tables 5, 6 and Appendices 26-28. From Table 5, ANOVA showed that there was significant difference between the means of briquette samples for all the properties except nitrogen. From Table 6, for carbon, LSD showed that the difference of the means was not significant for briquettes B30/B25, B35/B30 and B40/B35. For hydrogen, LSD showed that the difference of the means was not significant for briquettes B30/B25 and B35/B30. The percentage of carbon and hydrogen increased with binder concentration due to the terpenoids that contain a high amount of carbon and hydrogen. The nitrogen found in the briquettes is attributed to the fuel-N found in charcoal fines (Glarborg *et al.*, 2003) as well as nitrogen-containing compounds in the *Canarium Schweinfurthii* resin (Ameh, 2018). For oxygen, LSD showed that the difference of the means was not significant for briquettes B30/B25, B35/B25 and B35/B30.

For heating value, LSD showed that the difference of the means was not significant for briquettes B35/B30, B40/B30 and B40/B35. The increase in binder concentration initially led to an increase in the HHV and after it remained constant. The variability in fixed carbon of feedstock has a greater impact on the HHV as compared to variability in other feedstock parameters such as volatile matter and ash content as shown in Table 6 (Samadi *et al.*, 2019). The incoherency in the results of oxygen, and nitrogen could be attributed to manually mixing the binder and charcoal fines and agglomeration of the mixture with increasing binder concentration which could have resulted in the mixture which is not homogeneous. The energy density of the briquettes was 22.83, 27.68, 29.79, 32.04 GJ/m³ for briquettes B25, B30, B35 and B40. The energy density of the briquettes increased with increase in the binder concentration due to an increase in the bulk density of the briquettes as shown in Fig. 22. Wu *et al.* (2018) reported energy density and HHV (15.3–27.6 GJ/m³, 17.3-27.9 MJ/kg) for charcoal briquettes prepared from hydrothermal pretreated biomass wastes without binder and these are comparable to the ones (22.83–32.04 GJ/m³, 29.66-31.56 MJ/kg) obtained in this study. Sotannde *et al.* (2010) produced charcoal briquettes from neem wood residues using starch and gum arabica as binders and the HHV (32.27-33.54 MJ/kg) of the briquettes were close to the ones obtained in this study.

Table 5: One-way ANOVA for proximate analysis, ultimate analysis, and HHV of briquettes

| Property | Parameters | DF | Sum of Squares | Mean Square | F-value | P-value |
|------------------------|------------|----|----------------|-------------|---------|-----------------------|
| Highly volatile matter | Model | 3 | 1.91 | 0.64 | 19.38 | 5.01E-04 ^b |
| | Error | 8 | 0.26 | 0.03 | | |
| | Total | 11 | 2.17 | | | |
| medium volatile matter | Model | 3 | 172.36 | 57.45 | 346.65 | 8.33E-09 ^b |
| | Error | 8 | 1.33 | 0.17 | | |
| | Total | 11 | 173.69 | | | |
| Ash | Model | 3 | 0.62 | 0.21 | 4.49 | 3.98E-02 ^b |
| | Error | 8 | 0.37 | 0.05 | | |
| | Total | 11 | 0.99 | | | |
| Fixed carbon | Model | 3 | 121.42 | 40.47 | 326.09 | 1.06E-08 ^b |
| | Error | 8 | 0.99 | 0.12 | | |
| | Total | 11 | 122.42 | | | |
| C | Model | 3 | 48.26 | 16.09 | 8.79 | 6.52E-03 ^b |
| | Error | 8 | 14.64 | 1.83 | | |
| | Total | 11 | 62.90 | | | |
| H | Model | 3 | 4.12 | 1.37 | 15.11 | 1.17E-03 ^b |
| | Error | 8 | 0.73 | 0.09 | | |
| | Total | 11 | 4.85 | | | |
| N | Model | 3 | 0.75 | 0.25 | 1.45 | 2.99E-01 ^a |
| | Error | 8 | 1.37 | 0.17 | | |
| | Total | 11 | 2.12 | | | |

| Property | Parameters | DF | Sum of Squares | Mean Square | F-value | P-value |
|----------|------------|----|----------------|-------------|---------|-----------------------|
| O | Model | 3 | 6.11 | 2.04 | 22.91 | 2.79E-04 ^b |
| | Error | 8 | 0.71 | 0.09 | | |
| | Total | 11 | 6.82 | | | |
| HHV | Model | 3 | 6.49 | 2.16 | 7.62 | 9.88E-03 ^b |
| | Error | 8 | 2.27 | 0.28 | | |
| | Total | 11 | 8.76 | | | |

^a Not significant (P > 0.05), ^b significant (P < 0.05)

Table 6: Fishers LSD test for proximate analysis, ultimate analysis, and HHV of briquettes

| Briquette | Proximate analysis (wt %, as received) | | | | Ultimate analysis (wt%, db [*]) | | | | | HHV (MJ/kg) |
|------------|--|------------------------|--------------------|--------------------|---|--------------------|-------------------|-----|-------------------|--------------------|
| | Highly volatile matter | medium volatile matter | Ash | Fixed carbon | C | H | N | S | O | |
| B25 | 4.68 ^a | 40.46 ^d | 5.48 ^a | 49.38 ^a | 74.62 ^c | 4.40 ^c | 2.17 ^a | ND* | 7.37 ^a | 29.66 ^b |
| B30 | 4.24 ^b | 44.52 ^c | 5.47 ^a | 45.77 ^b | 75.13 ^{bc} | 4.87 ^{bc} | 1.94 ^a | ND* | 7.34 ^a | 31.56 ^a |
| B35 | 3.94 ^b | 47.86 ^b | 5.15 ^{ab} | 43.04 ^c | 77.37 ^{ab} | 5.27 ^b | 2.37 ^a | ND* | 7.41 ^a | 31.32 ^a |
| B40 | 3.59 ^c | 50.61 ^a | 4.94 ^b | 40.86 ^d | 79.67 ^a | 6.00 ^a | 1.70 ^a | ND* | 5.73 ^b | 30.92 ^a |

Means with the same letter(s) in a column for briquette properties are not significantly different (P < 0.05)

*db- dry basis *ND-Not Detected

4.4 Effect of Binder Concentration and Compaction Pressure on Physical Properties of Briquettes

The experimental data for binder concentration (A) and compaction pressure (B) was extracted from Appendices 3 and 4 respectively. The experimental data for bulk density (ρ), impact resistance index (IRI), compressive strength (F), splitting tensile strength (T), and water resistance index (WRI) was extracted from Appendices 12, 13, 16, 17, and 20 respectively and is shown in Table 7.

Table 7: Data for factors and responses analysed in Design Expert

| Run | A (%) | B (MPa) | ρ (g/cm ³) | IRI | F (MPa) | T (MPa) | WRI (%) |
|-----|-------|---------|-----------------------------|--------|---------|---------|---------|
| 1 | 25 | 8.2 | 0.788 | 3.33 | 1.97 | 0.09 | 99.32 |
| 2 | 25 | 7.6 | 0.767 | 3.13 | 2.53 | 0.08 | 99.14 |
| 3 | 25 | 8.0 | 0.826 | 2.50 | 2.25 | 0.08 | 99.24 |
| 4 | 30 | 7.6 | 0.858 | 25.00 | 3.91 | 0.19 | 99.30 |
| 5 | 30 | 7.8 | 0.879 | 11.11 | 3.80 | 0.22 | 99.18 |
| 6 | 30 | 7.8 | 0.885 | 16.67 | 4.09 | 0.22 | 99.18 |
| 7 | 35 | 6.2 | 0.954 | 50.00 | 8.38 | 0.31 | 99.30 |
| 8 | 35 | 7.0 | 0.933 | 50.00 | 7.42 | 0.35 | 99.31 |
| 9 | 35 | 7.8 | 0.974 | 50.00 | 8.37 | 0.28 | 99.27 |
| 10 | 40 | 5.8 | 1.025 | 50.00 | 9.67 | 0.42 | 99.32 |
| 11 | 40 | 6.0 | 1.063 | 50.00 | 14.23 | 0.42 | 99.02 |
| 12 | 40 | 6.2 | 1.053 | 100.00 | 8.92 | 0.43 | 99.45 |

4.4.1 Development of Model

Based on the experimental data from Table 7, Design Expert developed model equations showing the empirical relationship between factors and responses as described in Equations 149-153. Linear models were developed by Design Expert for bulk density, impact resistance index, compressive strength, and splitting tensile strength. For water resistance index, a model based on the mean was suggested.

$$\rho = 0.9150 + 0.1386A + 0.0157B$$

(149)

$$IRI = 41.74 + 32.52A - 13.46B \quad (150)$$

$$F = 6.39 + 3.96A - 0.6923B \quad (151)$$

$$T = 0.2593 + 0.1652A - 0.0032B \quad (152)$$

$$WRI = 99.25 \quad (153)$$

Table 8 shows the ANOVA for the models. The R^2 -values, F-values, and P-values were used to assess the quality of the models. The R^2 is used to compare the experimental and predicted values and models with $R^2 > 0.9$ are considered to exhibit a high correlation (Karungi *et al.*, 2020). The model R^2 values of 0.9670, 0.9253, 0.8747 and 0.9817 respectively for bulk density, impact resistance index, compressive strength and splitting tensile strength, are close to unity. It indicates that the experimental and predicted values are similar, as further illustrated in Appendix 29. For bulk density, the model F-value of 131.95 implies the model is significant. There is only a 0.01% chance that an F-value this large could occur due to noise. Binder concentration was a significant model term with P-value less than 0.0500. Compaction pressure was an insignificant model term with P-value greater than 0.1000. The Lack of Fit F-value of 30.51 implies the Lack of Fit is not significant relative to the pure error. There is a 13.92% chance that a Lack of Fit F-value this large could occur due to noise.

For impact resistance index, the model F-value of 55.72 implies the model is significant. There is only a 0.01% chance that an F-value this large could occur due to noise. Binder concentration was a significant model term with P-value less than 0.0500. Compaction pressure was an insignificant model term with P-value greater than 0.1000. The Lack of Fit F-value of 8.30 implies the Lack of Fit is not significant relative to the pure error. There is a 26.25% chance that a Lack of Fit F-value this large could occur due to noise. For compressive strength, the model F-value of 31.42 implies the model is significant. There is only a 0.01% chance that an F-value this large could occur due to noise. Binder concentration was a significant model term with P-value less than 0.0500. Compaction pressure was an insignificant model term with P-value greater than 0.1000. The Lack of Fit F-value of 59.38 implies the Lack of Fit is not significant relative to the pure error. There is a 10.01% chance that a Lack of Fit F-value this large could occur due to noise.

For splitting tensile strength, the model F-value of 241.15 implies the model is significant. There is only a 0.01% chance that an F-value this large could occur due to noise. Binder concentration was a significant model term with P-value less than 0.0500. Compaction pressure was an insignificant model term with P-value greater than 0.1000. The Lack of Fit F-value of 12.73 implies the Lack of Fit is not significant relative to the pure error. There is a 21.37% chance that a Lack of Fit F-value this large could occur due to noise. For water resistance index, there were no significant model terms. The Lack of Fit F-value of 27601.26 implies the Lack of Fit is significant. There is only a 0.47% chance that a Lack of Fit F-value this large could occur due to noise.

4.4.2 Diagnostics

The developed models were checked to ascertain their validity. For a good model, the residuals should be randomly and normally distributed. To ascertain this, plots of the normal % probability versus externally studentized residuals, externally studentized residuals versus predicted values, and predicted versus actual values of the responses were analysed as shown in Fig. 28-30 respectively. Figure 28a–e shows that the points conform to a straight line, implying normal distribution of the data (Menya *et al.*, 2020).

Figure 29a-d shows that the results do not show any particular pattern, suggesting random distribution of the residuals which is a requirement of a good model (Menya *et al.*, 2020). On the contrary, Fig. 29e shows a particular pattern, thus there was no random distribution of the residuals. This is attributed to the Lack of fit of the data as shown in Table 8. The plots for Fig. 30a-d show minimal divergence of points from the straight line. Thus, the resulting response surface plots can be used to predict the interaction between the factors and responses (Menya *et al.*, 2020). The data for Fig. 30e could not follow a linear trend due to a Lack of Fit of the data.

Table 8: ANOVA for the models of the experimental design

| Source | sum of squares | Degrees of freedom | Mean square | F-value | P-value | |
|---|----------------|--------------------|-------------|----------|---------|-----------------|
| (a) Bulk density: $R^2=0.9670$, Adjusted $R^2=0.9597$, predicted, $R^2= 0.9445$ | | | | | | |
| Model | 0.1059 | 2 | 0.0529 | 131.95 | <0.0001 | significant |
| A-Binder | 0.0312 | 1 | 0.0312 | 77.86 | <0.0001 | |
| B-Pressure | 0.0004 | 1 | 0.0004 | 0.88 | 0.3723 | |
| Lack of Fit | 0.0036 | 8 | 0.0004 | 30.51 | 0.1392 | not significant |
| (b) Impact resistance index: $R^2=0.9253$, Adjusted $R^2=0.9087$, predicted $R^2= 0.8587$) | | | | | | |
| Model | 12884.8692 | 2 | 6442.4346 | 55.72 | <0.0001 | significant |
| A-Binder | 1718.9940 | 1 | 1718.9940 | 14.87 | 0.0039 | |
| B-Pressure | 259.7978 | 1 | 259.7978 | 2.25 | 0.1681 | |
| Lack of Fit | 1025.0696 | 8 | 128.1337 | 8.30 | 0.2625 | not significant |
| (c) Compressive strength: $R^2=0.8747$, Adjusted $R^2=0.8469$, Predicted, $R^2= 0.7547$ | | | | | | |
| Model | 137.5046 | 2 | 68.7523 | 31.42 | <0.0001 | significant |
| A-Binder | 25.5472 | 1 | 25.5472 | 11.67 | 0.0077 | |
| B-Pressure | 0.6871 | 1 | 0.6871 | 0.31 | 0.5889 | |
| Lack of Fit | 19.6529 | 8 | 2.4566 | 59.38 | 0.1001 | not significant |
| (d) Splitting tensile strength: $R^2=0.9817$, Adjusted $R^2=0.9776$, predicted, $R^2= 0.9575$ | | | | | | |
| Model | 0.1878 | 2 | 0.0939 | 241.15 | <0.0001 | significant |
| A-Binder | 0.0444 | 1 | 0.0444 | 113.94 | <0.0001 | |
| B-Pressure | 0.0000 | 1 | 0.0000 | 0.04 | 0.8506 | |
| Lack of Fit | 0.0035 | 8 | 0.0004 | 12.73 | 0.2137 | not significant |
| (e) Water resistance index: $R^2=0.0000$, Adjusted $R^2=0.0000$, predicted, $R^2= -0.1901$) | | | | | | |
| Model | 0.0000 | 0 | | | | |
| Lack of Fit | 0.1301 | 10 | 0.0130 | 27601.26 | 0.0047 | significant |

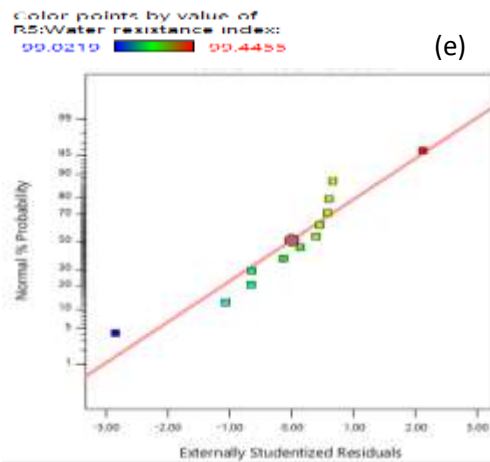
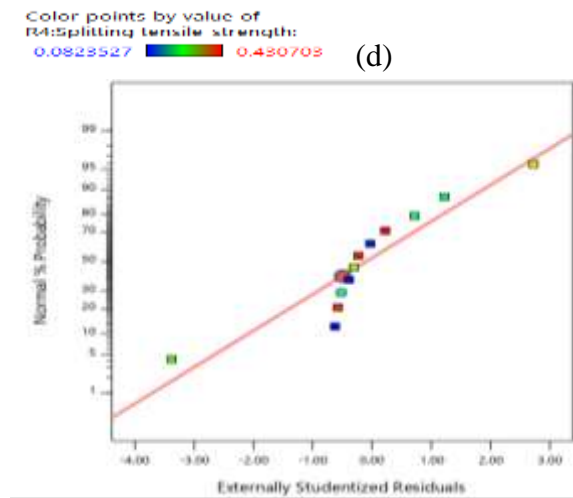
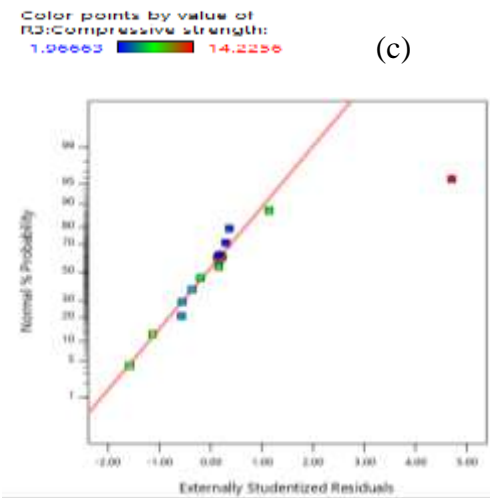
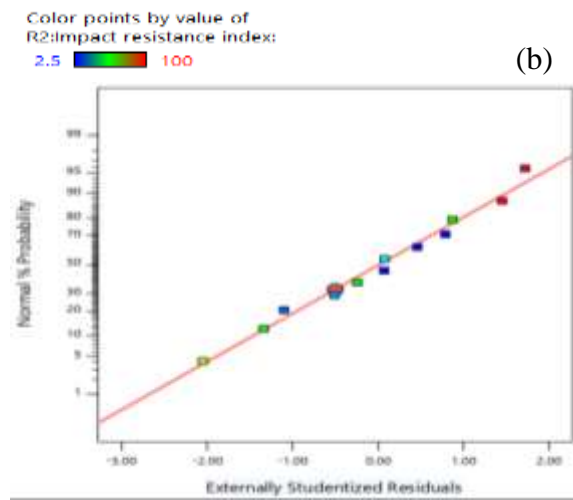
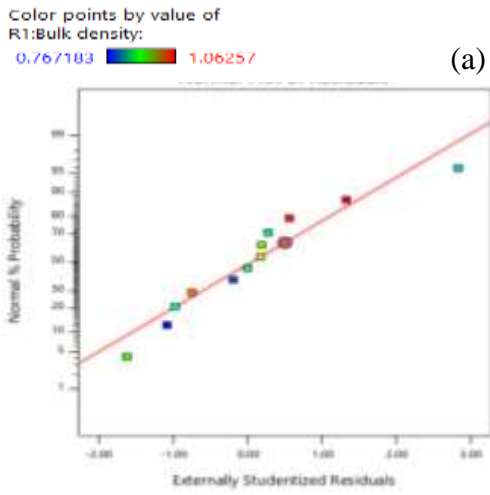


Figure 28: Normal % probability vs Externally studentized residuals; (a) Bulk density, (b) Impact resistance index, (c) Compressive strength, (d) Splitting tensile strength, (e) Water resistance index

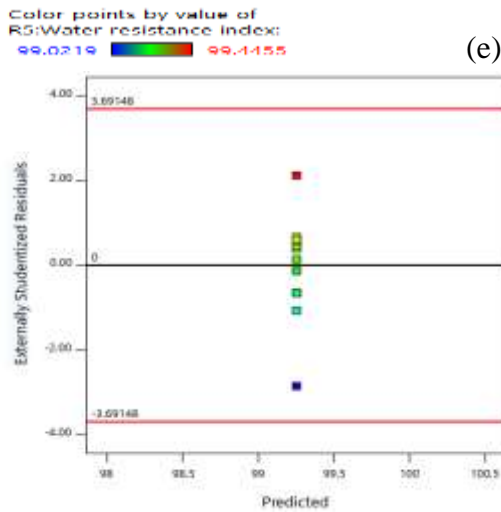
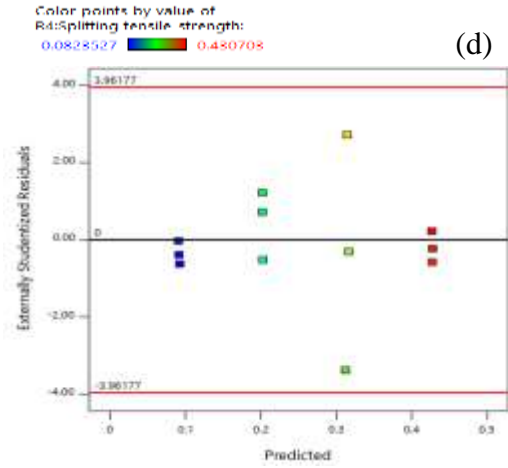
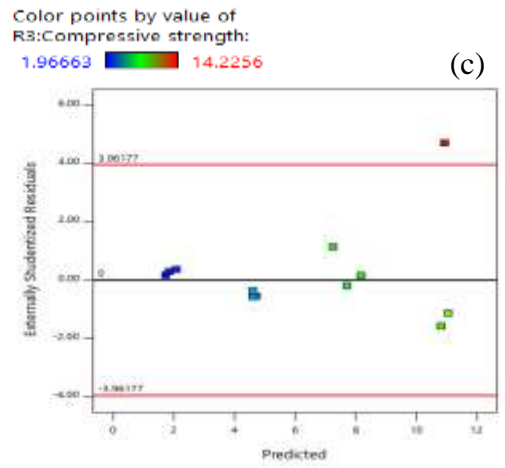
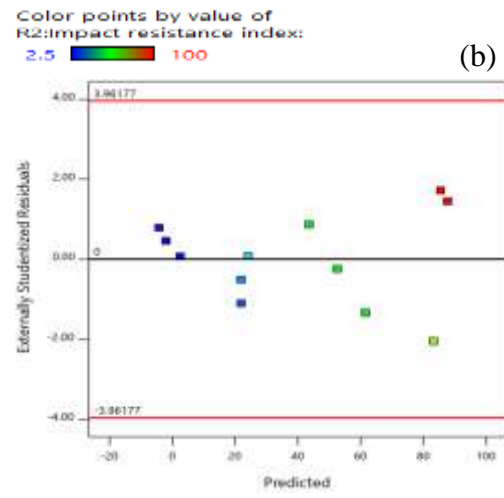
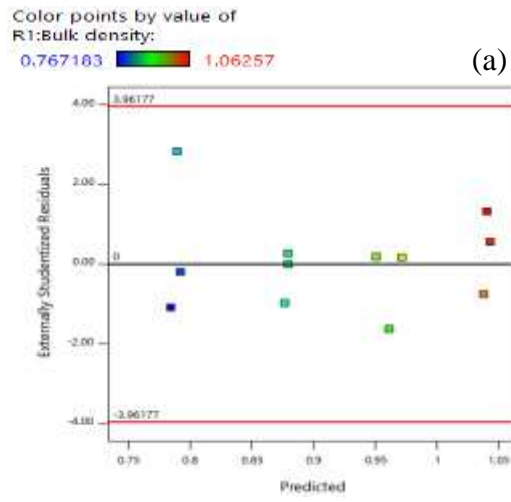


Figure 29: Externally studentized residuals vs predicted; (a) Bulk density, (b) Impact resistance index, (c) Compressive strength, (d) Splitting tensile strength, (e) Water resistance index

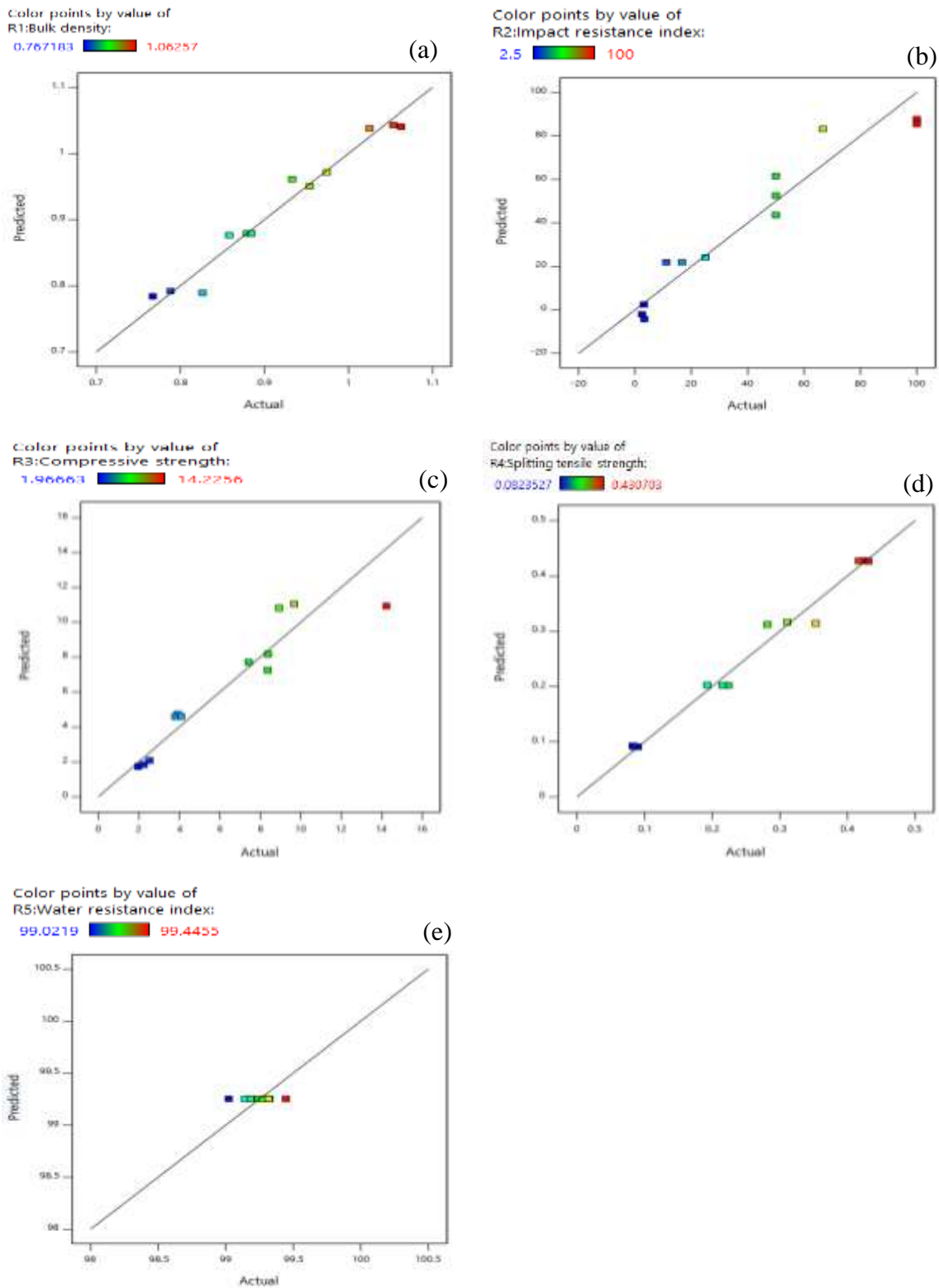


Figure 30: Predicted vs actual;(a) Bulk density, (b) Impact resistance index, (c) Compressive strength, (d) Splitting tensile strength, (e) Water resistance index

4.4.3 Response Surface Plots

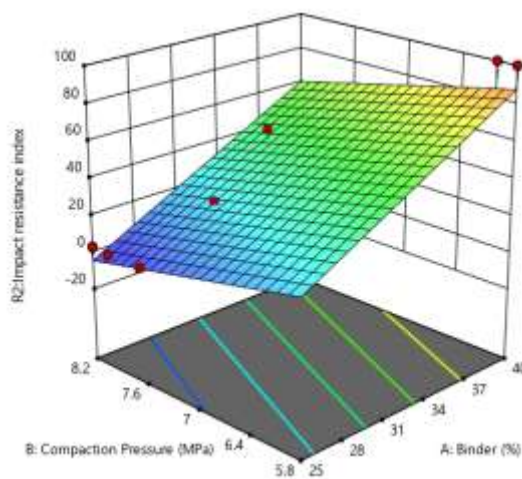
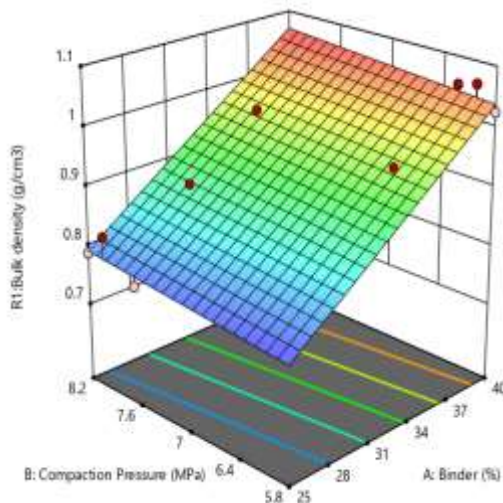
Three-dimensional response surface plots were analysed to show the effect of binder concentration and compaction pressure on physical properties of briquettes, as shown in Fig. 31a–e. The response surface plots are useful in the efficient tracking of optimal levels of variables to obtain the best

response range. The shapes of the plots depict the extent of interactions between variables in determining the response (Karungi *et al.*, 2020). Figure 31a shows that for a compaction pressure of 5.8-8.2 MPa, bulk density of the briquettes increases with binder concentration and the optimum bulk density is predicted at a binder concentration of 40% and compaction pressure of 8.2 MPa. Figure 31b shows that for a compaction pressure of 5.8-8.2 MPa the IRI of the briquettes increases with binder concentration and the optimum IRI is predicted at a binder concentration of 40% and compaction pressure of 5.8 MPa.

Figure 31c shows that for compaction pressure of 5.8-8.2 MPa the compressive strength of the briquettes increases with binder concentration and the optimum compressive strength is predicted at a binder concentration of 40% and compaction pressure of 5.8 MPa. Figure 31d shows that for a compaction pressure of 5.8-8.2 MPa splitting tensile strength of the briquettes increases with binder concentration and the optimum splitting tensile strength is predicted at a binder concentration of 40% and compaction pressure of 5.8-8.2 MPa. Figure 31e shows that the water resistance index is independent of binder concentration and compaction pressure. This is attributed to the model using the mean value predicted by Design Expert since there was a Lack of Fit for the experimental data.



(b)



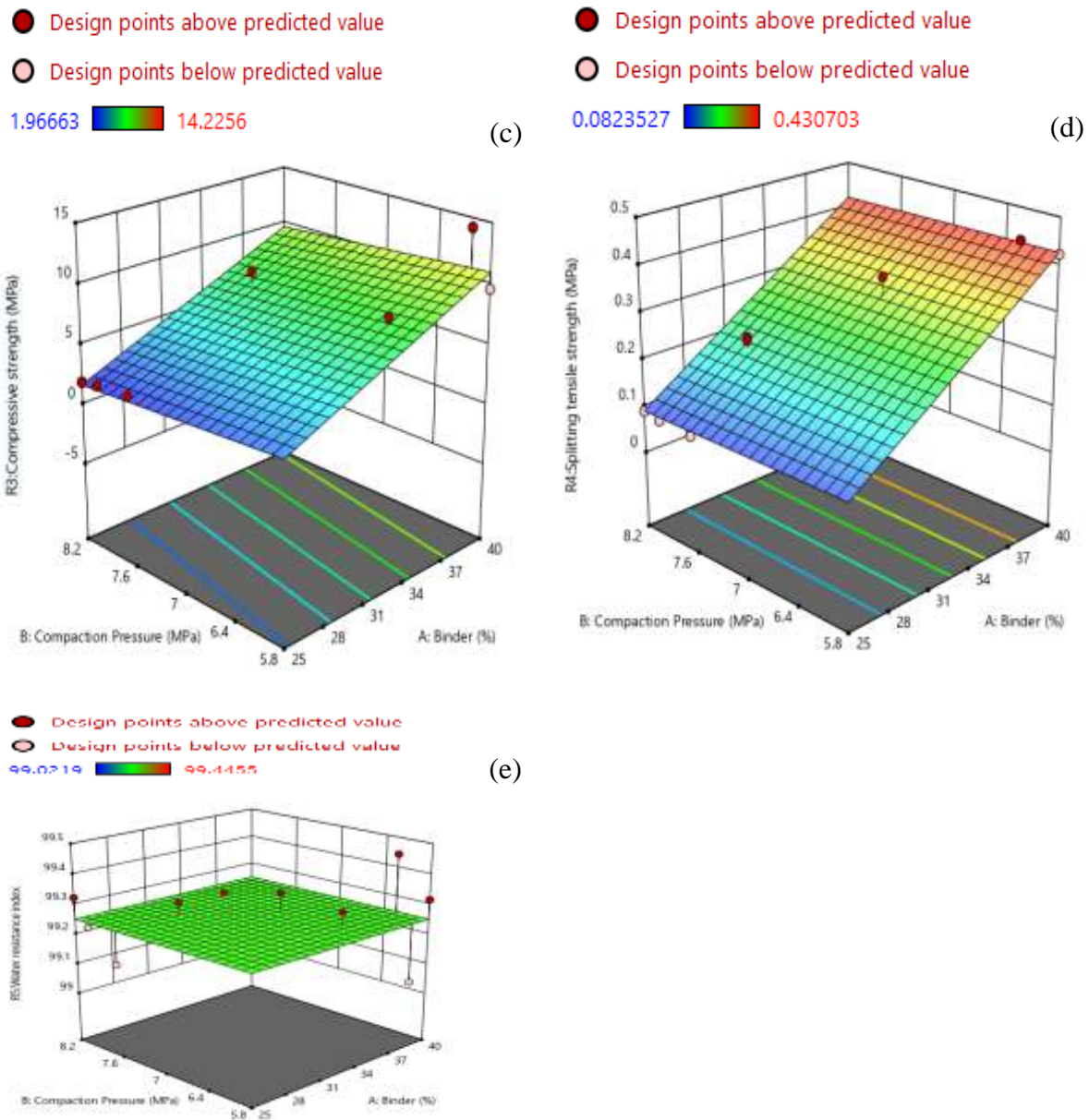


Figure 31: Response surface plots; (a) bulk density, (b) impact resistance index, (c) compressive strength, (d) splitting tensile strength, and (e) water resistance index

4.5 Water Boiling Test of the Carbonized Briquettes

4.5.1 Ignition

Figure 32a-e shows the ignition images. Figure 32a shows the bioethanol gel ($\text{CH}_3\text{CH}_2\text{OH}$, yellow in colour) before ignition (Balat, 2011). Figure 32b shows the cookstove loaded with the briquettes before ignition. Figure 32c shows that after igniting the bioethanol gel with a match, it burned with a blue flame to provide the ignition energy required to ignite the briquettes. The blue radiation is due to excited CH radicals in the high temperature zone (Turns, 2000). The OH radicals also contribute to visible radiation (Turns, 2000). Figure 32d shows the ignited briquettes burning with a yellow flame due to the highly volatile terpenoids in the binder used. Furthermore, briquette B40

was observed to burn with a more intense yellow flame due to the increase of volatile matter with binder concentration.

The ignition time of the briquettes was 6.47-7.01 min (Appendix 32). Nwabue *et al.* (2017) produced smokeless bio-coal briquettes incorporating plastic waste materials using cassava starch as binder. The briquettes were ignited using a lighter and found that the ignition time was 0.88-2.60 min. The low ignition time was attributed to the added biomass and plastic materials and the results are comparable to the ones obtained in this study. Ormeño *et al.* (2009) reported that at relatively low temperatures and concentrations, liquid terpenes can generate an ignitable mixture, leading to a flame in the presence of an ignition source. The same observation was made in this ignition experiment (Fig. 32d) where the binder containing terpenoids is a solid at room temperature. The formation of the yellow flame can be attributed to the high volatile content of the briquette which is an indication of easy ignition of the briquette and proportionate increase in flame length (Obi, 2015). Blasi (1993) reported that to get a flaming ignition as shown in Fig. 32d, three conditions must be met: (a) the gas phase temperature must attain values sufficiently high to initiate and accelerate the combustion reaction, (b) fuel and oxidizer must be available at a proper level of concentration to give a mixture within the flammability limits, and (c) the extent of the heated zone must be sufficiently large to overcome heat losses. Figure 32e shows the ignited briquette with a red glow in the central hole as well as at the curved surface. Fernandez-Anez *et al.* (2018) studied ignition sensitivity of solid fuel mixtures and one of the criteria to confirm ignition was observation of visible flame or incandescence which are the features observed in Fig. 32 d, e respectively.

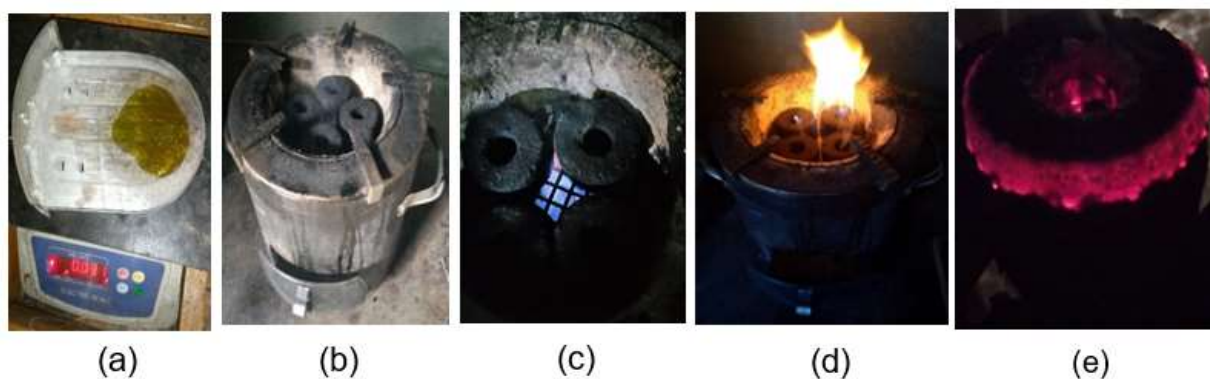


Figure 32: Ignition images; (a) Weighing bioethanol gel, (b) Briquettes loaded on the cookstove, (c) Bioethanol gel burning with a blue flame (d) Briquettes burning with a yellow flame, (e) ignited briquette with a red glow

4.5.2 Combustion

Figure 33a-e shows the combustion images. At the start of the CSHP phase, briquette B25 burned with white smoke and no flame as shown in Fig. 33a while briquettes B30, B35 and B40 burned with a yellow flame and soot as shown in Fig. 33b. Briquette B40 burned with a more intense yellow flame and produced the highest amount of soot since it contained more binder. Briquette B25 burned with a yellow flame and soot towards the end of the CSHP phase. The yellow flame and soot are attributed to the binder used that contains volatile terpenoids with a high molecular weight thus, resulting in a rich air/fuel mixture forming soot with its consequent blackbody continuum radiation (Turns, 2000). Although the soot radiation has its maximum intensity in the infrared (Wiens Law), the spectral sensitivity of the human eye causes us to see a bright yellow to dull orange emission depending on the flame temperature (Turns, 2000). Part of the soot was trapped on the pot as shown in Fig. 33b, c. Mitchell *et al.* (2016) reported that the high volatile wood fuels release a high concentration of highly carbonaceous dark smoke during flaming combustion thus, the combustion characteristics of the briquettes is similar to that of wood fuels. Romallosa and Kraft (2017) reported that a hole at the centre of the fuel improves the combustion characteristics of the briquette through rapid drying, easy ignition and highly efficient burning due to the draft and insulated combustion chamber that the hole creates.

During the HSHP and Simmer phases, there was ash formation creating a layer of insulation around the burning briquettes as shown in Fig. 33d, e. Consequently, there was a reduction in the burning rate and the insulation minimised heat transfer to the pot resulting in a long time to boil during HSHP phase. Ash influences heat transfer and diffusion of oxygen to the surface of fuel during combustion (Obi, 2015). There was also a tendency for the briquettes to undergo fragmentation as shown in Fig. 33d but they remained stable until the end of the combustion process.



Figure 33: Combustion images; (a) Briquette B25 burning with white smoke, (b) Briquettes B25, B30, B35, and B40 burning with a yellow flame and soot (d) Briquettes burning without soot and yellow flame (e) Ash formation around the briquettes

4.5.3 Temperature Profiles and Gaseous Emissions

Figures 34a, 35a, 36a, and 37a show temperature profiles while Appendices 33-36 show temperature data during the WBT. The T_{gas} remained relatively constant and close to the T_{ambient} which is important for measuring PM (Clean cooking alliance, 2014). The spikes in the T_{gas} during the ignition phase occurred due to the pot not being placed on the cookstove as the bioethanol gel was allowed to burn to completion. The spikes in the T_{gas} during the HSHP and Simmer phases occurred during weighing of the pot with water. The T_{water} trends are similar to the international WBT reported by Chen *et al.* (2016). At the start of the experiment, the T_{ambient} and T_{water} corresponded to the dry bulb and wet bulb temperatures respectively. The T_{water} was lower than T_{ambient} due to evaporative cooling (Amer *et al.*, 2015; Yang *et al.*, 2019).

During the CSHP phase, the pot containing water was not covered with a lid as the burning characteristics of the fuel exhibited that of wood fuel and this is in accordance with the WBT 4.2.3 protocol (Clean cooking alliance, 2014). The depression in the T_{water} during the HSHP phase was due to withdrawing of the thermocouple from the hot water to cover the pot with a lid when the yellow flame and soot had stopped and the burning characteristics of the fuel exhibited that of charcoal as shown in Fig. 33d in accordance with the WBT 4.2.2 protocol (Clean cooking alliance, 2013). Moreover, without covering the pot during the HSHP phase, the water would not reach the boiling point. In addition, a high amount of fuel would be required to heat the water to the boiling point and consequently increase the emissions. Quist *et al.* (2020) did a study on influence of variability in testing parameters on cookstove performance metrics based on the WBT and reported that the use of a lid greatly reduced variations in both thermal efficiency associated with heating water and specific consumption metrics even when there were significant variations in the other testing parameters. Quist *et al.* (2020) also reported that, the use of a lid would provide better consistency for cookstove comparisons when using these metrics. The use of a lid reduces the radiation losses with its emissivity of perhaps 0.1, compared to almost 1 for the water surface. Thus, there is more net heat available to heat the water (Hermans, 2012).

Figures 34b, 35b, 36b, and 37b show the profile of gaseous emissions while Appendices 33-36 show the gaseous emissions data during the WBT. Mitchell *et al.* (2016) reported that the route leading to the formation of smoke from biomass involves pyrolysis of the different constituents, cellulose and lignin and can form soot via the HACA (hydrogen abstraction– C_2H_2 addition) route or via aromatic compounds respectively. The concentration of CO_2 , C_xH_y , CO, SO_2 , and NO_x increased with time during ignition and CSHP phase to a maximum and then decreased during the HSHP and Simmer phases and the peak values are shown in Table 9 along with their Occupational

Safety and Health Administration (OSHA) permitted industrial concentration. The peak emissions of SO₂, NO₂, and CO₂ from the briquettes met this standard. The NO_x found in the briquettes is attributed to the fuel-N found in charcoal fines (Glarborg *et al.*, 2003) as well as nitrogen-containing compounds in the *Canarium Schweinfurthii* resin (Ameh, 2018). The SO₂ is attributed to the Sulphur in the charcoal fines (Deac *et al.*, 2016). Arora *et al.* (2014) tested CO emissions from ignition materials (wood, kerosene, mustard stalks) in a natural draft cookstove (Philips) and found that the highest amount of CO emission was 1100 ppm generated using mustard stalks and this is higher than the value of 25 ppm obtained in this study during the ignition phase. Oketch *et al.* (2014) did a study on fuel efficiency and emissions comparison from bioethanol gel stoves and detected presence of CO and CO₂. Thus, the bioethanol gel used for ignition in this study contributed to the CO and CO₂ emissions during ignition.

Household coal combustion, even with the cleaner coals and higher quality stoves more commonly used in cities, still produces relatively high levels of emissions of PM, SO₂, and black carbon (World Health Organization [WHO], 2014). Similar emissions are reported for the briquettes in this study. World Health Organization (2014) reported that many products of incomplete combustion components exert a radiative forcing of climate, either because they are greenhouse gases (GHGs) able to trap long-wave heat radiation from the earth (methane, N₂O), they indirectly affect GHGs via chemical processes in the atmosphere (CO, non-methane volatile organic compounds), or because they interfere with short-wave solar radiation and/or they affect climate through impacts on clouds (particulate matter/aerosols – including black carbon). These components (except N₂O) are often referred to as short-lived climate pollutants.

Table 9: Peak concentration (ppm) of the gaseous emissions

| Briquette | CO ₂ | C _x H _y | CO | SO ₂ | NO _x |
|---|-----------------|-------------------------------|-----|-----------------|-----------------|
| B25 | 775 | 325 | 150 | 0.325 | 0.125 |
| B30 | 950 | 250 | 150 | 2.75 | 6.25 |
| B35 | 1650 | 225 | 150 | 2.375 | 2.375 |
| B40 | 1500 | 300 | 175 | 3.125 | 1.375 |
| Permitted industrial concentrations, 15 min peak* | - | - | 400 | 5 | 5 |

*(El-Mahallawy & El-Din Habik, 2002)

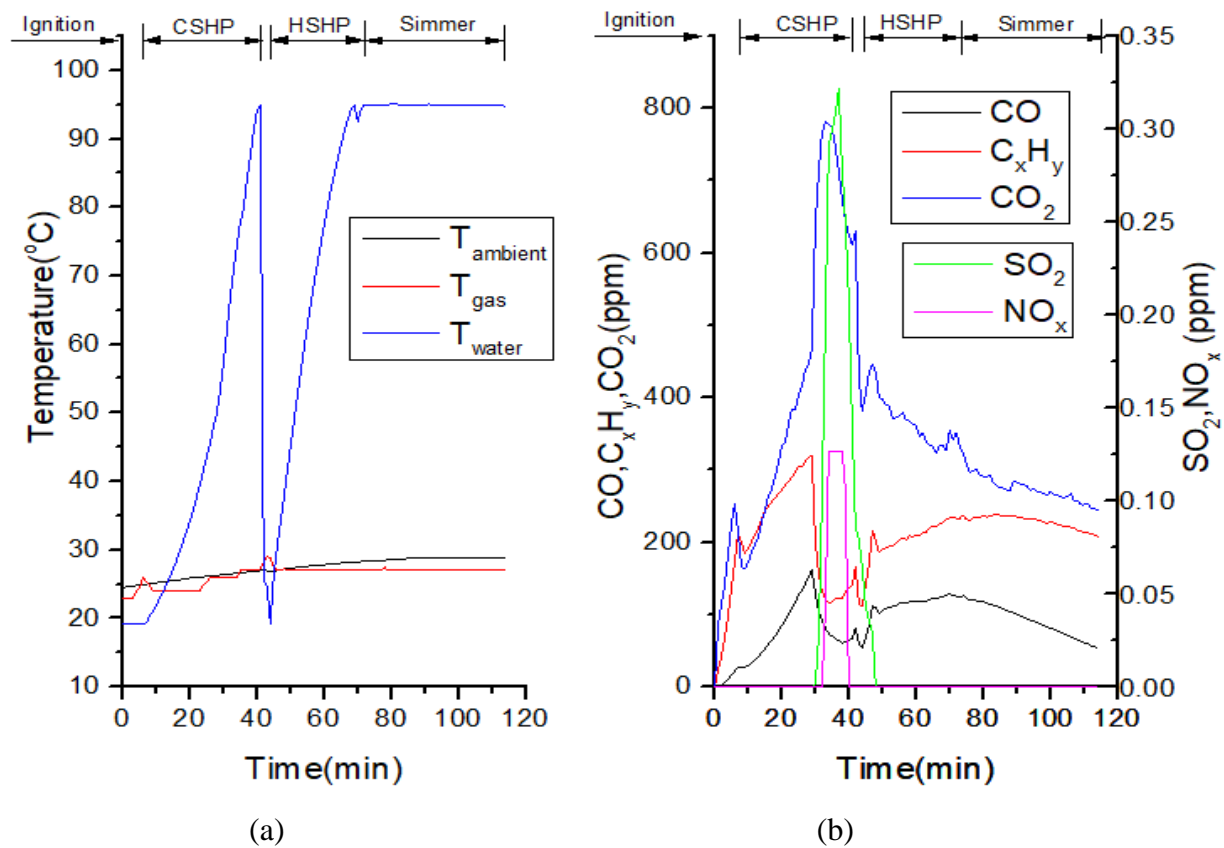


Figure 34: Briquette B25 during ignition, CSHP, HSHP, and Simmer phases; (a) Temperature profiles, (b) Gaseous emissions

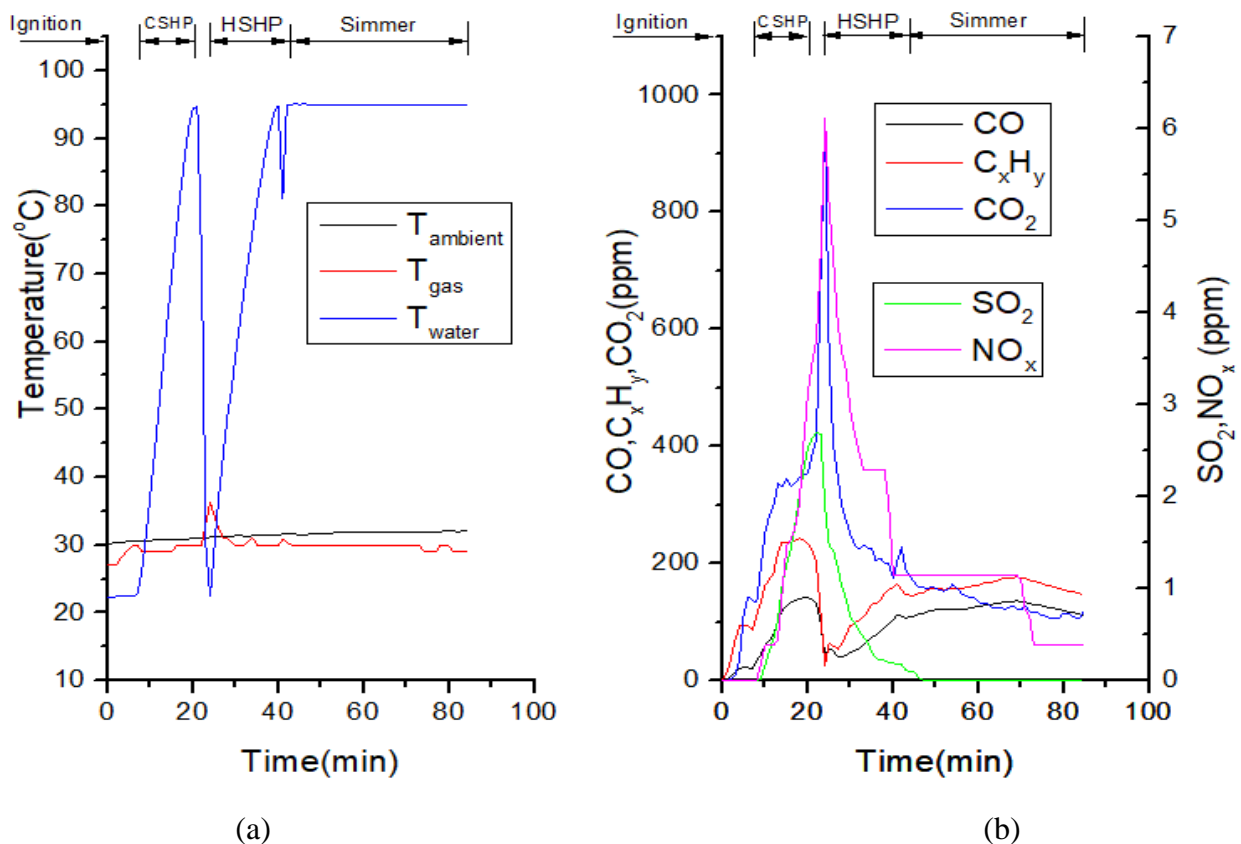


Figure 35: Briquette B30 during ignition, CSHP, HSHP, and Simmer phases; (a) Temperature profiles, (b) Gaseous emissions

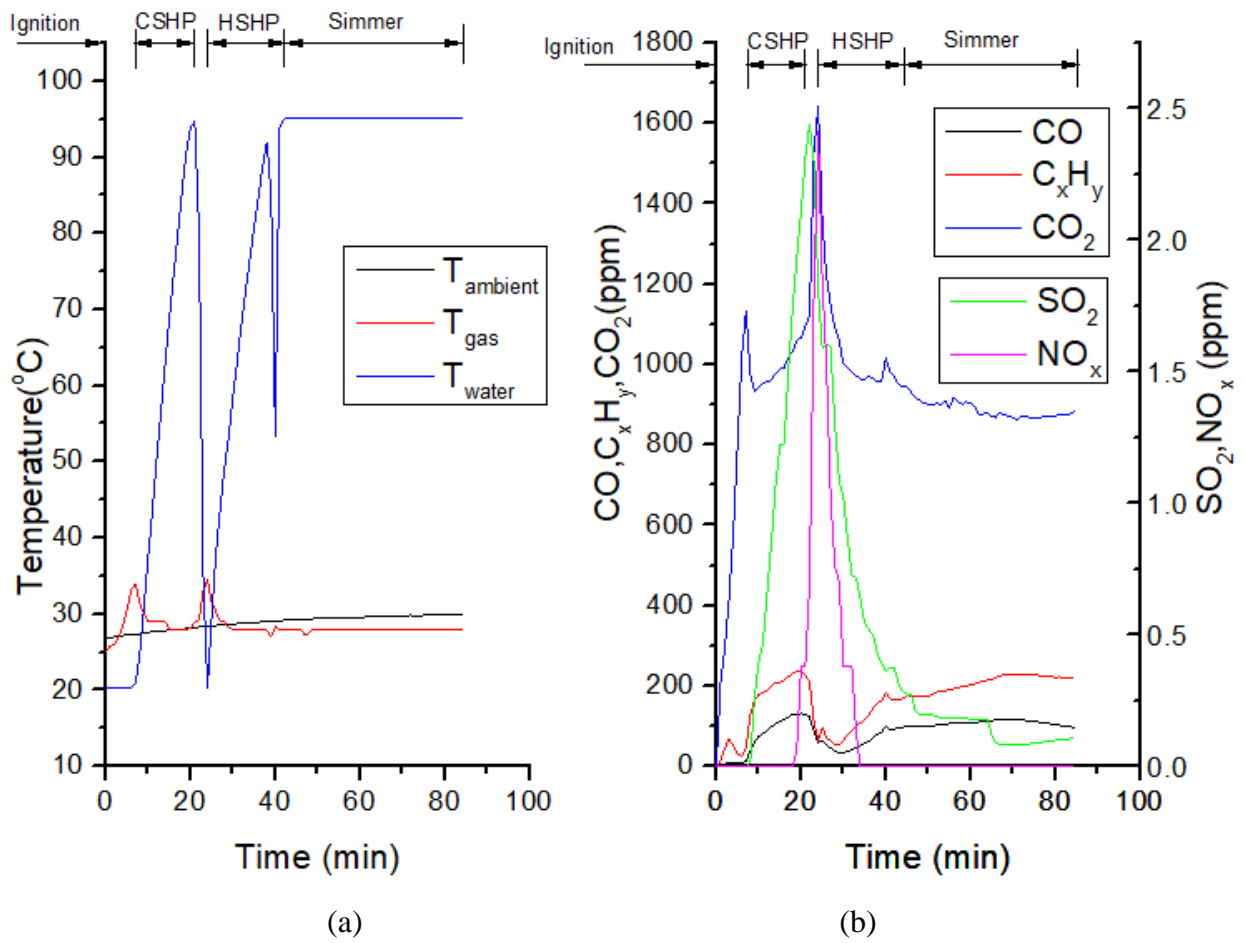


Figure 36: Briquette B35 during ignition, CSHP, HSHP, and Simmer phases; (a) Temperature profiles, (b) Gaseous emissions

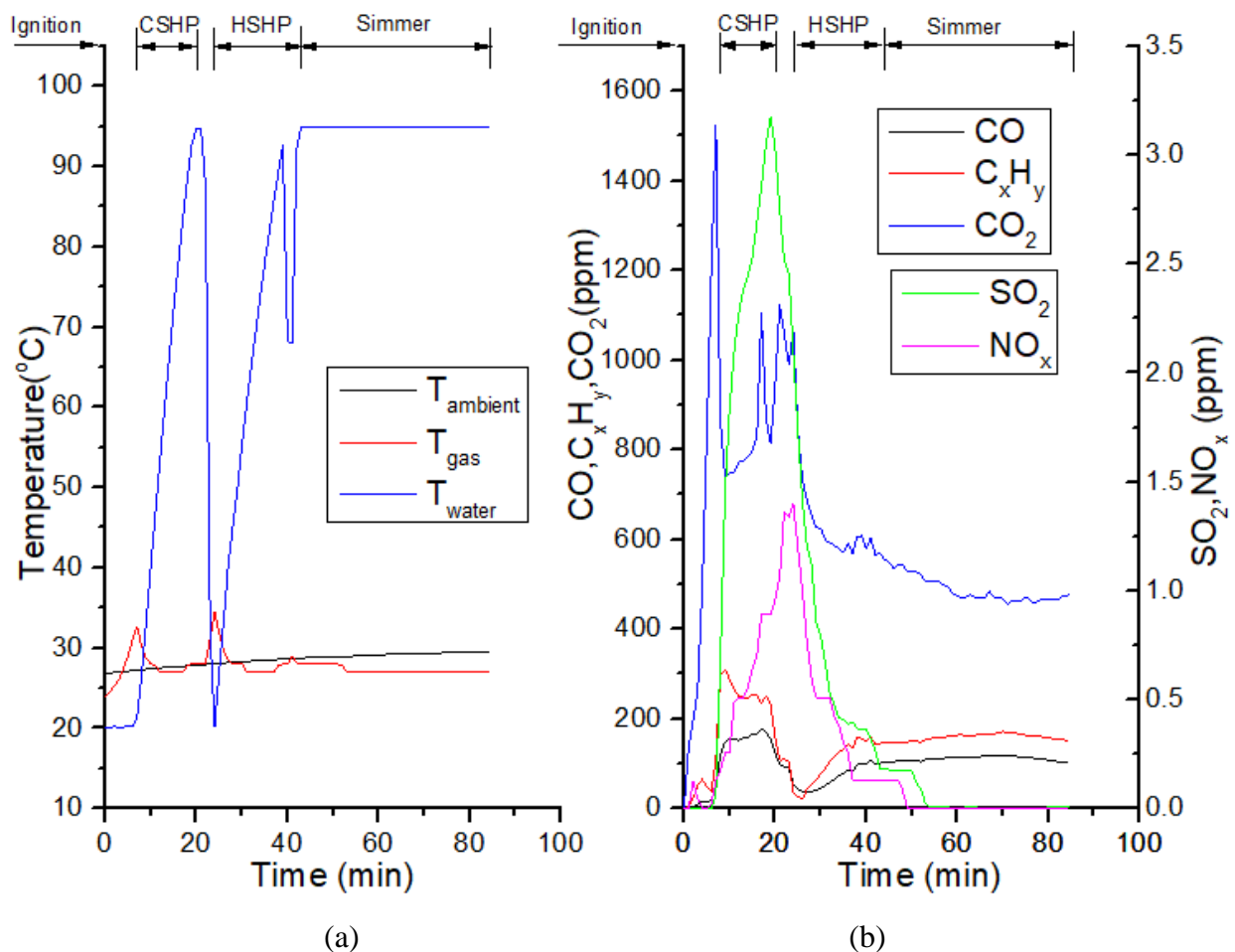


Figure 37: Briquette B40 during ignition, CSHP, HSHP, and Simmer phases; (a) Temperature profiles, (b) Gaseous emissions

4.5.4 WBT Performance Metrics

Appendix 37 shows results of the WBT performance metrics. Appendix 38 shows images of the filter paper for briquettes B25, B30, B35 and B40 during CSHP, HSHP and Simmer phases.

(i) Time to Boil

Figure 38 shows the results of time to boil. The time to boil during the HSHP phase was shorter than for CSHP phase for all the briquettes since a lid was used during the HSHP phase. During the CSHP phase, briquettes B30, B35 and B40 boiled water faster than briquette B25 due to the exothermic reaction resulting from the flaming combustion of the terpenoids in the binder as shown in Fig. 33b. Furthermore, briquette B40 boiled water in the shortest time during the CSHP and HSHP phases since it contained more binder implying that it generated more heat. On the contrary, briquette B25 took a long time to boil water during the CSHP since it contained the least amount of binder and initially burned with white smoke and no flame for about 23 min as shown in Fig. 33a. The Simmer phase considered the same boiling time of 45 min for all briquette samples (Clean cooking alliance, 2014). The time to boil was 20.3- 41.9 min, 14.7-25.2 min for CSHP and

HSHP phases, respectively. Lask *et al.* (2015) tested an improved charcoal cookstove (EcoRecho) to boil 2.5 L of water and found that the boiling time was 30-50 min implying that the cookstove and briquettes used in this study boiled water faster (14.7-41.9 min) during CSHP and HSHP phases.

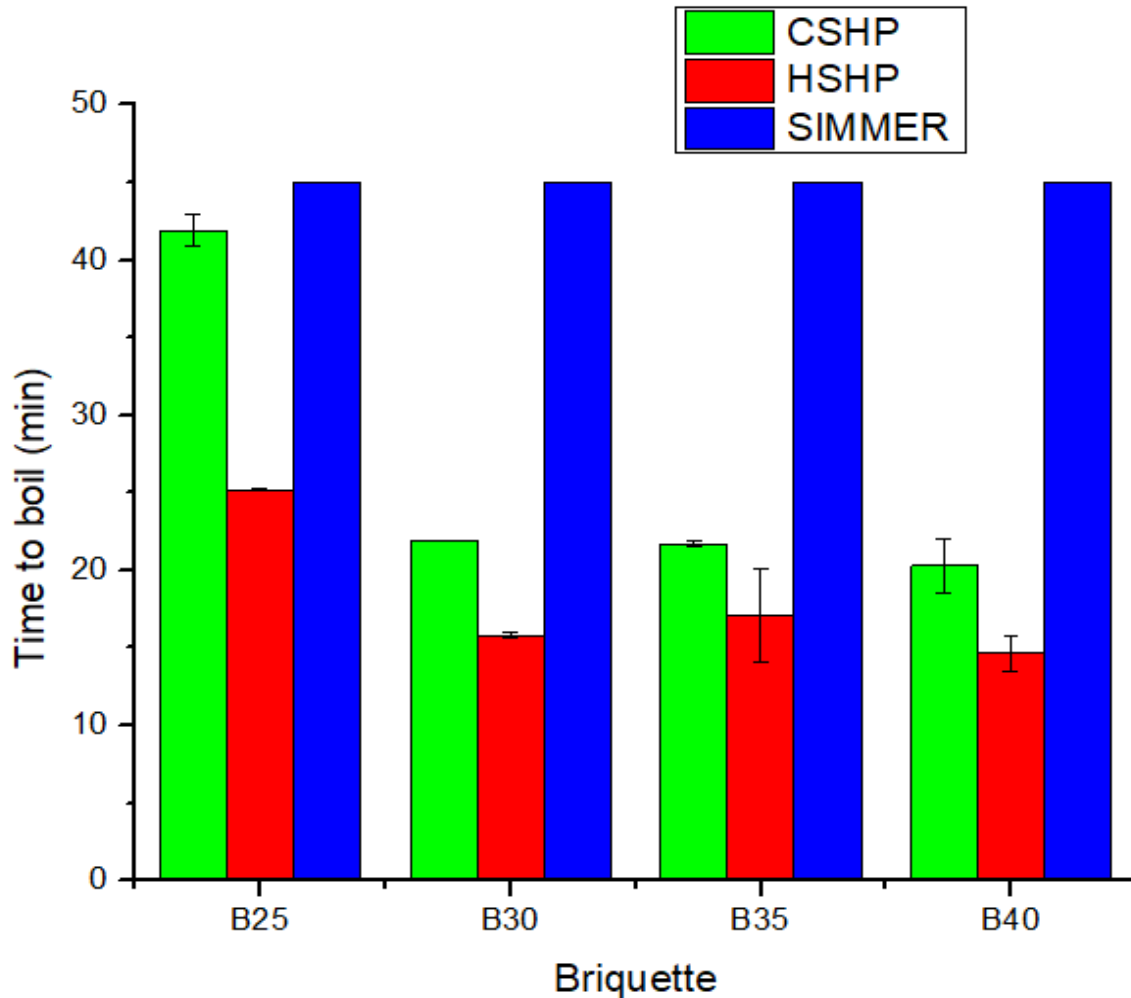


Figure 38: Time to boil

(ii) Burning rate

Figure 39 shows the results of burning rate. During the CSHP and HSHP phases, the burning rate of briquettes increased with the binder concentration as a result of increase in the volatile matter in the binder used. Lubwama and Yiga (2017) reported that high volatile matter eases ignition and enhances combustion due to increased chemical reactivity. During the Simmer phase, the burning rate of briquettes B30, B35 and B40 was higher than that of briquette B25 since the later had taken a long time to boil during the CSHP and HSHP phases thus, the briquette had been covered with ash which minimised heat transfer and limited diffusion of oxygen to the briquette to support combustion. Furthermore, briquettes B30, B35 and B40 had the same burning rate during the Simmer phase since they had a slight difference in time to boil during the CSHP and HSHP phases,

thus could have been covered with the same amount of ash. The burning rate was 3.7-8.2 g/min, 2.1-4.2 g/min, 1.1-1.7 g/min for CSHP, HSHP and Simmer phases, respectively. Nwabue *et al.* (2017) obtained a burning rate of 1300-3800 g/min for smokeless bio-coal briquettes incorporating plastic waste materials. This implies that the briquettes used in this study burn slower (1.1-8.2 g/min), thus the cookstove does not have to be loaded with fuel frequently.

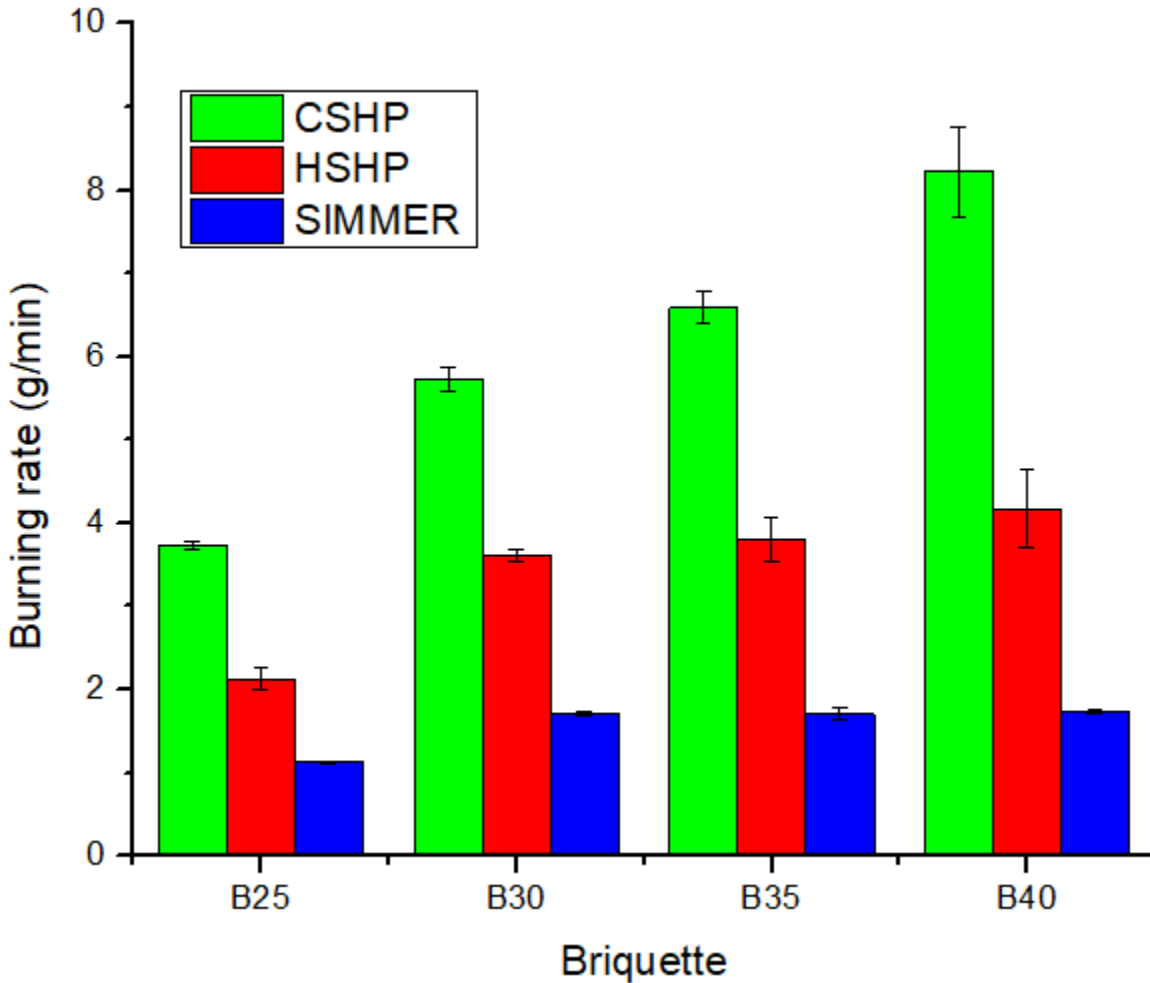


Figure 39: Burning rate

(iii) Thermal Efficiency, Dry Fuel Used, Effective Mass of Water Boiled and Specific Fuel Consumption

Figure 40a-d shows the results of thermal efficiency, dry fuel used, effective mass of water boiled, and specific fuel consumption (SC). The thermal efficiency (Fig. 40a) of the cookstove during the CSHP phase was lower than during the HSHP phase due to covering of the pot with a lid in the later phase which reduced the time to boil and consequently minimised on the amount of dry fuel used (Fig. 40b). During the CSHP and HSHP phases, the thermal efficiency of the cookstove fluctuated with binder concentration as a result of fluctuation in the dry fuel consumed. Considering the CSHP and HSHP phases for each briquette type, there was a slight difference in

the amount of water evaporated as shown in Fig. 40c. Hermans (2012) reported that whether or not there is a lid on the pan, the heat supply to the water remains the same. Except for the (relatively small) heat losses by radiation and conduction, all heat is used for evaporation when approaching boiling point. This means that there should be no difference in the amount of water evaporated, irrespective of the details of condensation and backflow that occur under the lid. The amount of water evaporated during the Simmer phase was higher than that during the CSHP and HSHP phases since the Simmer phase took a long time of 45 min.

Clean cooking alliance (2014) recommends considering SC instead of thermal efficiency, especially during the Simmer phase of the WBT. This is because a stove that is very slow to boil may have a very good-looking thermal efficiency because a great deal of water was evaporated. However, the fuel used per water remaining may be too high since so much water was evaporated and so much time was taken while bringing the pot to a boil. From Fig. 40d, during the Simmer phase, the SC of the cookstove for briquette B25 was lower than that for briquettes B30, B35 and B40 since B25 had the lowest amount of dry fuel consumed and highest amount of effective mass of water boiled (Fig. 40c). Furthermore, briquettes B30, B35 and B40 had approximately the same value of SC since they had approximately the same amount of dry fuel consumed and effective mass of water boiled.

The thermal efficiency was 21.79-30.86%, 44.62-54.61%, 39.14-50.34% during CSHP, HSHP, and Simmer phases, respectively. Lask *et al.* (2015) obtained an average thermal efficiency of 40% using a charcoal cookstove (Prakti) implying that the cookstove and fuel used in this study performed better during the HSHP. The SC was 53.2-70.1 g/L, 21.7-26.1 g/L, 22.8-39.4 g/L during CSHP, HSHP and Simmer phases, respectively. Grimsby *et al.* (2016) obtained SC values for CSHP of 83 and 102 g/L for the traditional charcoal stove (no liner) and improved charcoal stove (jiko bora-ceramic liner), respectively implying that the stove used in this study requires less fuel to boil a litre of water (53.2-70.1 g/L).

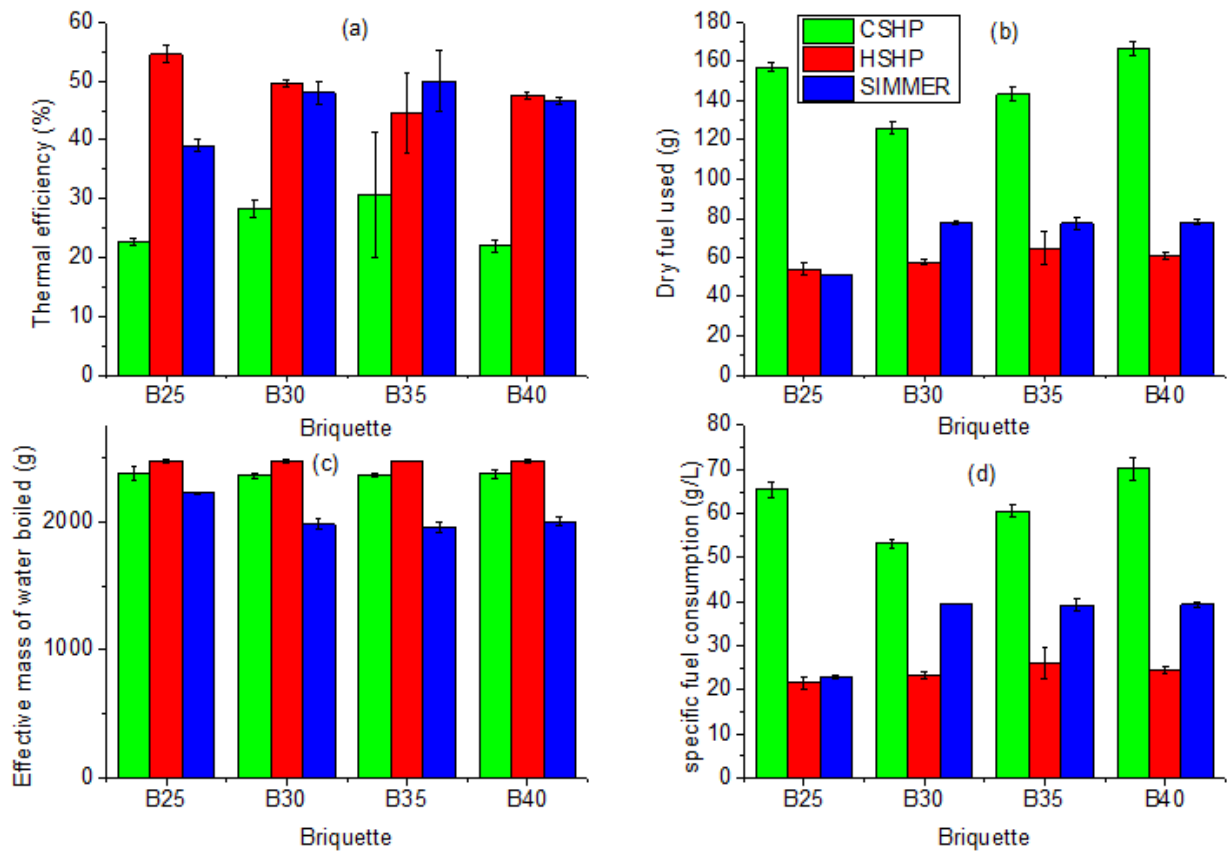


Figure 40: (a) Thermal efficiency, (b) Dry fuel used, (c) Effective mass of water boiled, (d) Specific fuel consumption

(iv) Firepower

Figure 41 shows the results of firepower. The firepower increased with binder concentration during CSHP and HSHP phases for briquettes B25, B30, B35 and B40, respectively. During the Simmer phase, there was negligible difference in the firepower for briquettes B30, B35 and B40 since they had the same time to boil and approximately the same amount of dry fuel used as shown in Fig.38 and Fig. 40b, respectively. However, the firepower for briquettes B30, B35 and B40 was higher than that for briquettes B25 since the later had the lowest amount of dry fuel used. Each briquette type showed a decreasing firepower during CSHP, HSHP and Simmer phases. The firepower was 1775.0-4123.2 W, 1011.5-2091.8 W, 535.9-867.8 W for the CSHP, HSHP and Simmer phases, respectively. Grimsby *et al.* (2016) obtained values of firepower for CSHP of 4200 W and 3000 W for the traditional charcoal stove (no liner) and improved charcoal stove (jiko bora-ceramic liner), respectively which are within the range (535.9-4123.2 W) of the cookstove used in this study.

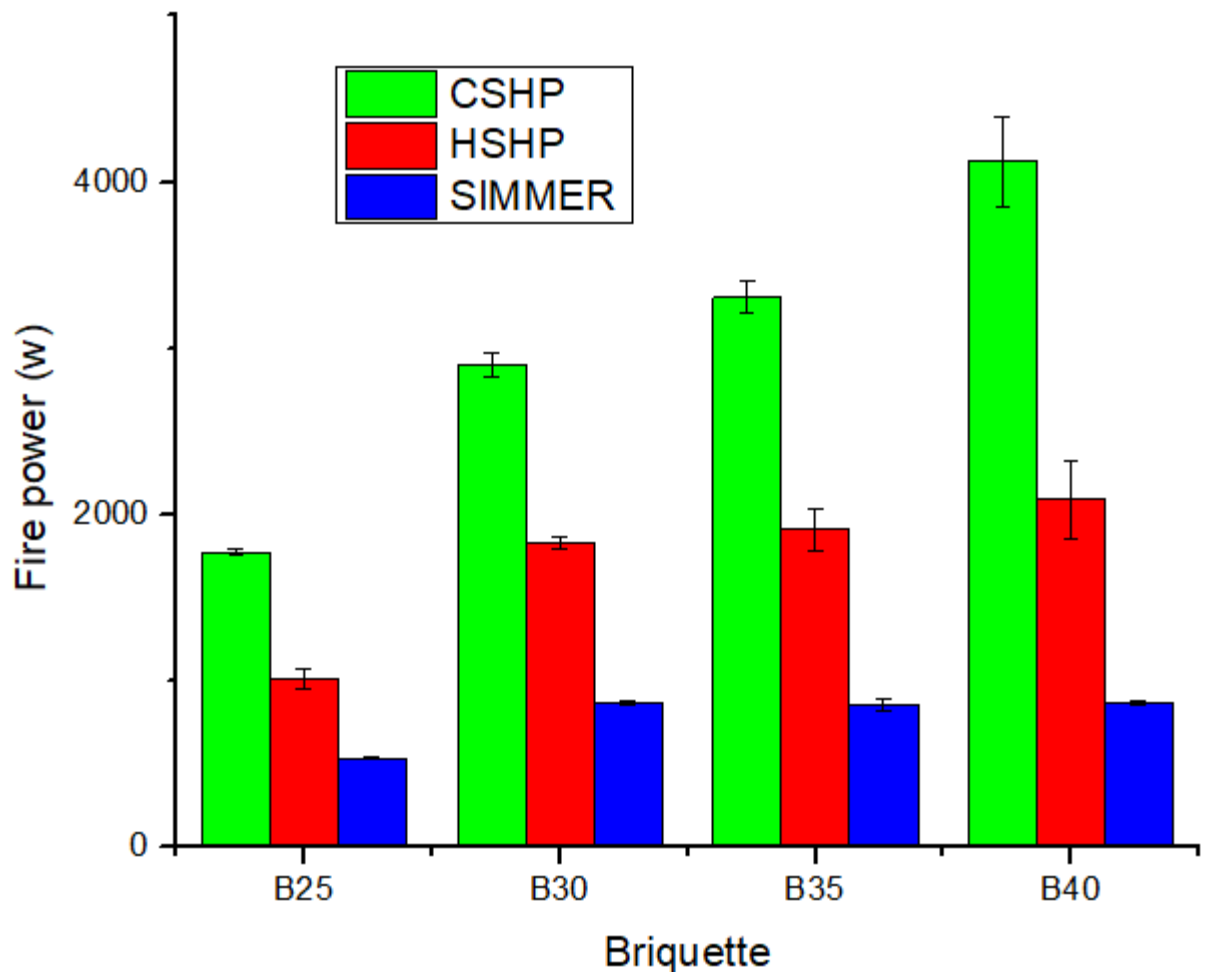


Figure 41: Firepower

(v) Total Emissions

Figure 42 shows the results of total emissions. From Fig. 42a it was observed that generally, the amount of $PM_{2.5}$ increased with binder concentration during CSHP, HSHP, and Simmer phases. Moreover, briquettes B40 produced the highest amount of $PM_{2.5}$ for all the phases since it contained the highest amount of binder. The highest amount of $PM_{2.5}$ was captured during the CSHP phase since the fuel burned with a yellow flame accompanied with emission of soot. During the HSHP and Simmer phases, the soot emission had reduced considerably since most of the binder had been combusted. The total emissions of $PM_{2.5}$ were 10.5-25.5 mg, 0.5-1.9 mg, 0.3-0.8 mg for the CSHP, HSHP, and Simmer phases respectively.

Figure 42b shows that during the CSHP phase, the amount of CO emitted fluctuated with binder concentration for briquettes B25, B30, B35 and B40 since the binder contains terpenoids thus there was not enough air to combust them. During the HSHP phase the amount of CO decreased with binder concentration. During the Simmer phase there was fluctuation of CO for briquettes B25, B30, B35, and B40. Figure 42c shows that generally, during the CSHP phase, the amount of CO_2 increased with binder concentration for briquettes B25, B30, B35, and B40. During the HSHP

phase there was fluctuation in the amount of CO₂. During the Simmer phase, the amount of CO₂ increased with binder concentration. Briquette B40 produced the greatest amount of CO₂ since it contained more binder.

From Fig. 34b, 35b, 36b and 37b, a significant level of hydrocarbons was still detectable in the fuel during the HSHP phase and this could explain the high amount of CO and CO₂ measured during this phase. The total emissions of CO and CO₂ during the Simmer phase was higher than during the CSHP and HSHP phases due to the fact that the Simmer phase takes a long time of 45 min. The total emissions of CO were 21.0-28.9 g, 9.3-28.9 g and 44.5-58.0 g for the CSHP, HSHP, and Simmer phases, respectively. The total emissions of CO₂ were 104.2-172.4 g, 92.4-110.1 g and 123.5-173.3 g for the CSHP, HSHP, and Simmer phases, respectively. Mitchell *et al.* (2016) reported that the level of CO emitted depends on the time-temperature history above the burning bed and this agrees with the results of the Simmer phase considering the time taken. Furthermore, the carbon monoxide in the exhaust could be attributed to dissociation of the carbon dioxide formed during combustion (Turns, 2000).

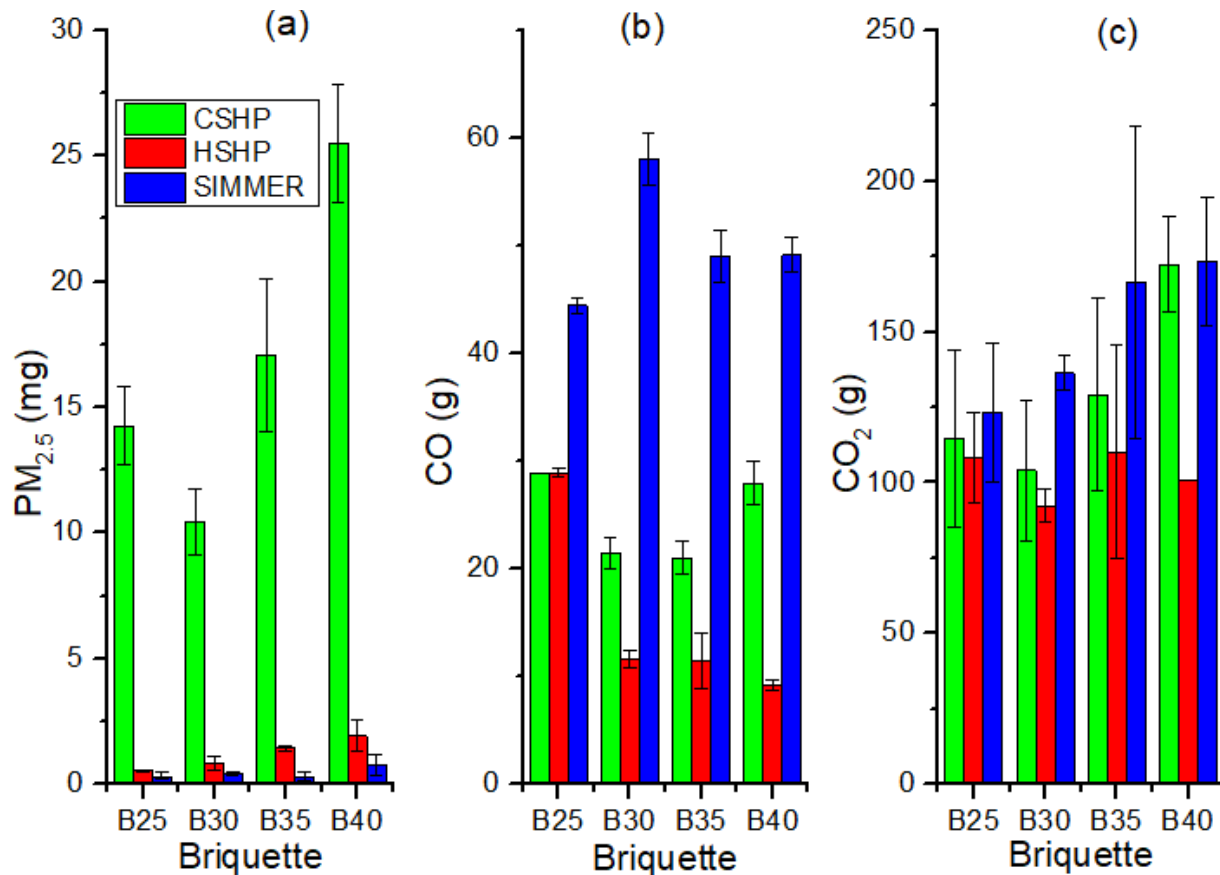


Figure 42: Total Emissions; (a) PM_{2.5}, (b) CO, (c) CO₂

(vi) Emissions per MJ

Figure 43a-c shows the results of emissions per MJ delivered to the cooking pot. From Fig. 43a it was observed that the emissions per MJ for $PM_{2.5}$ fluctuated with binder concentration during CSHP phase and increased with binder concentration during HSHP phase. During the Simmer phase the emissions per MJ for $PM_{2.5}$ of briquettes B25, B30 B35, and B40 fluctuated with binder concentration. Moreover, briquettes B40 produced the highest emissions per MJ for $PM_{2.5}$ for all the phases since it contained the highest amount of binder. The highest emissions per MJ for $PM_{2.5}$ was captured during the CSHP phase since the fuel burned with a yellow flame accompanied with emission of soot. The emissions per MJ for $PM_{2.5}$ were 9.6-23.6 mg/MJ, 0.7-2.2 mg/MJ, 0.3-0.7 mg/MJ for the CSHP, HSHP and Simmer phases, respectively. Mitchell *et al.* (2016) obtained total particulate matter ($PM_{2.5}$ and PM_{10}) values of 15-47.5 mg/MJ during flaming and smouldering after combustion of torrefied wood briquettes in a fixed bed domestic stove. Thus, the PM was quite higher than the one (0.3-23.6 mg/MJ) obtained in this study.

From Fig. 43b, c it was observed that generally, during the CSHP phase, the emissions per MJ for CO and CO_2 fluctuated with binder concentration for briquettes B25, B30, B35 and B40. During the HSHP phase, the emissions per MJ of CO decreased while that of CO_2 fluctuated with binder concentration. During the Simmer phase, the emissions per MJ for CO and CO_2 fluctuated with binder concentration. The emissions per MJ for CO were 16.8-28.8 g/MJ, 10.7-34.7 g/MJ, 42.4-78.6 g/MJ for the CSHP, HSHP and Simmer phases, respectively. The emissions per MJ for CO_2 were 95.5-160.4 g/MJ, 107.0-129.3 g/MJ, 121.2-218.4 g/MJ for the CSHP, HSHP and Simmer phases, respectively. Mitchell *et al.* (2016) obtained CO values of 500-7000 mg/MJ during ignition, flaming and smouldering after combustion of torrefied wood briquettes in a fixed bed domestic stove. Thus, the CO was quite higher than the one (10.7- 78.6 mg/MJ) obtained in this study.

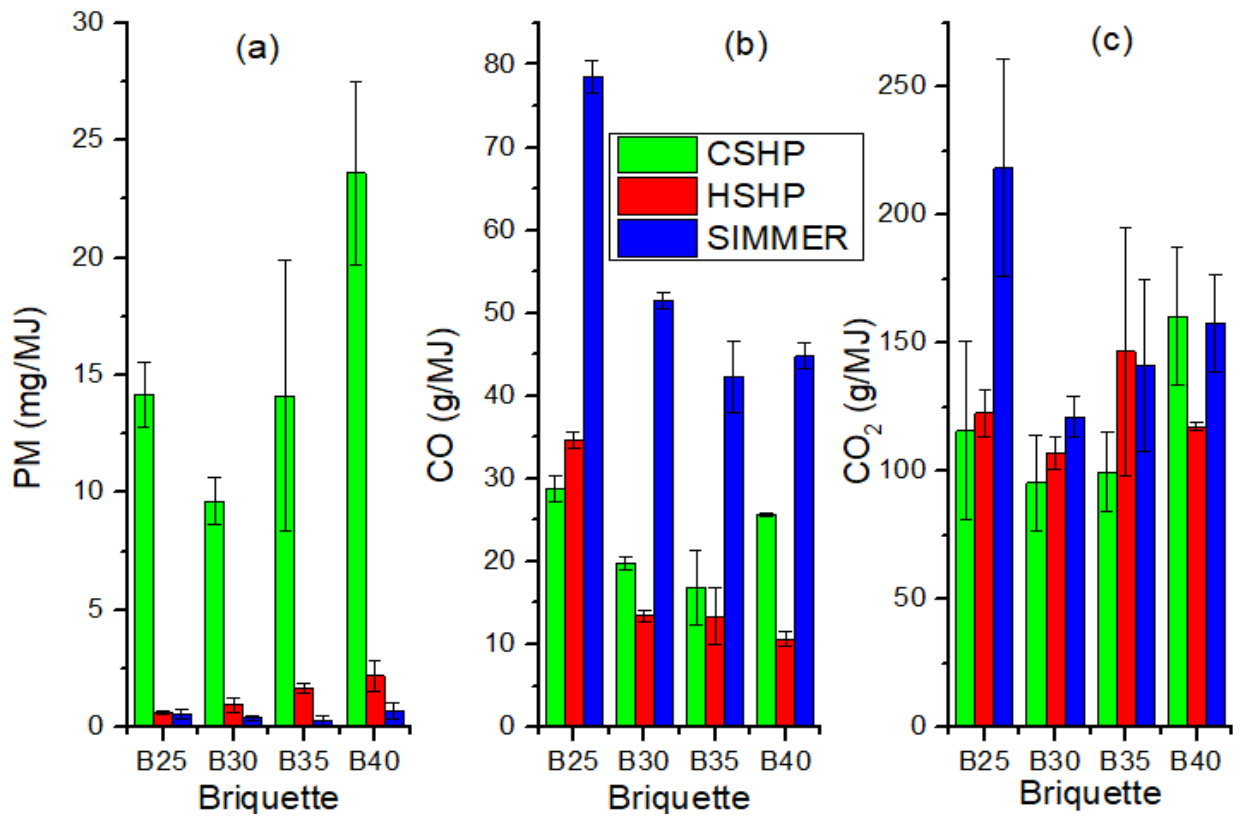


Figure 43: Emissions per MJ; (a) PM_{2.5}, (b) CO and (c) CO₂

(vii) Specific Emissions and Emission Rate

The results of specific emissions and emission rate of PM_{2.5}, CO, and CO₂ are summarized in Table 10. Grimsby *et al.* (2016) did a study on multiple biomass fuels and improved cookstoves from Tanzania assessed with the WBT and used concentrations of CO and PM as values for comparing cleanliness of cooking options. Other researchers have also considered PM_{2.5}, CO, and CO₂ (Chen *et al.*, 2016; Lask *et al.*, 2015; Medina *et al.*, 2016). Burnett *et al.* (2014) did a study on an integrated risk function for estimating the global burden of disease attributable to ambient fine PM exposure and one of the diseases modelled was lung cancer by comparing the predicted and relative risk (RR) vs Log PM_{2.5} (µg/m³). The results showed that below 5 µg/m³, the predicted and RR is about 1 thus, the specific emissions results of the Log PM_{2.5} (µg/m³) from the current study show limited risk to development of lung cancer.

World Health Organization (2014) recommends an annual interim target-1 (IT-1) of 35-75 µg/m³ PM_{2.5} thus, the results of specific emissions obtained in this study were above the standard for CSHP, HSHP and Simmer phases. In comparison to cooking with kerosene for both wick and pressurized stoves, studies of kitchen and personal exposure levels found respirable PM in the range of 340 µg/m³ to more than 1000 µg/m³ (WHO, 2014). These results are similar to the ones (422.1- 1034.9 µg/m³) obtained in this study for the Simmer phase. The WHO (annual average)

air quality guidelines IT-1 for PM_{2.5} (vented) is 0.80 mg/min (WHO, 2014). From the results of the emissions rate, briquettes B25, B30, and B35 met this standard during the CSHP, HSHP and Simmer phases while B40 achieved the same during HSHP and Simmer phases. The 24-hour average air quality guideline for CO (vented) is 0.59 g/min (WHO, 2014). From the results of the emissions rate, briquette B25 was close to this standard during the CSHP phase while briquettes B30, B35 and B40 were close to this standard during the HSHP phase. World Health Organization (2014) reported that CO₂ emissions from non-sustainable use of biomass fuel affects the climate, but does not directly impact health.

Table 10: Specific emissions and emissions rate of PM_{2.5}, CO, and CO₂

| | Unit | B25 | B30 | B35 | B40 |
|---------------------------|-------------------|----------|----------|----------|----------|
| Specific Emissions | | | | | |
| CSHP phase | | | | | |
| CO | g/L | 12.0 | 9.1 | 8.9 | 11.8 |
| CO ₂ | g/L | 47.7 | 44.3 | 54.7 | 72.8 |
| PM _{2.5} | µg/m ³ | 19 904.9 | 28 337.9 | 47 265.8 | 76 692.9 |
| Log (PM _{2.5}) | µg/m ³ | 4.3 | 4.4 | 4.7 | 4.9 |
| HSHP phase | | | | | |
| CO | g/L | 11.7 | 4.7 | 4.6 | 3.8 |
| CO ₂ | g/L | 43.7 | 37.5 | 44.5 | 40.9 |
| PM _{2.5} | µg/m ³ | 1288.3 | 3050.1 | 5071.4 | 7857.4 |
| Log (PM _{2.5}) | µg/m ³ | 3.1 | 3.5 | 3.7 | 3.9 |
| simmer phase | | | | | |
| CO | g/L | 20.0 | 29.6 | 25.1 | 24.8 |
| CO ₂ | g/L | 55.6 | 69.5 | 85.4 | 87.6 |
| PM _{2.5} | µg/m ³ | 422.1 | 570.6 | 404.8 | 1034.9 |
| Log (PM _{2.5}) | µg/m ³ | 2.6 | 2.8 | 2.6 | 3.0 |
| Emissions Rate | | | | | |
| CSHP phase | | | | | |
| CO | g/min | 0.7 | 1.0 | 1.0 | 1.4 |
| CO ₂ | g/min | 2.8 | 4.8 | 5.9 | 8.6 |
| PM _{2.5} | mg/min | 0.34 | 0.48 | 0.79 | 1.26 |
| HSHP phase | | | | | |
| CO | g/min | 1.1 | 0.7 | 0.7 | 0.6 |
| CO ₂ | g/min | 4.3 | 5.8 | 6.4 | 6.9 |
| PM _{2.5} | mg/min | 0.02 | 0.05 | 0.09 | 0.14 |
| simmer phase | | | | | |
| CO | g/min | 1.0 | 1.3 | 1.1 | 1.1 |
| CO ₂ | g/min | 2.7 | 3.0 | 3.7 | 3.8 |
| PM _{2.5} | mg/min | 0.01 | 0.010 | 0.01 | 0.02 |

4.6 Ash

Figure 44 shows the XRD results for ash and charcoal fines. The properties of wood ash depend on various factors; type of plant, part of plant combusted (bark, wood, leaves), type of waste

(wood, pulp or paper residue), combination with other fuel sources, type of soil, climate, conditions of combustion, collection and of storage (Demeyer *et al.*, 2001; Pitman, 2006). Steenari *et al.* (1999) reported that Ca and Si are the most dominant elements in wood ash, but significant amounts of other important nutrients, such as Mg, K, P and Mn, are also present. The ash contained mainly CaCO_3 (76.6 wt%) followed by CaO (13.1 wt%) and the remainder was the amorphous compounds (10.3 wt%). Steenari and Lindqvist (1997) reported that calcium in wood ash is present mainly in a CaCO_3 form which agrees with the results in this study. Misra *et al.* (1993) did a study on wood ash composition as a function of furnace temperature and considered temperatures of 600 and 1300°C. At a temperature of 600°C the XRD analysis of the wood ash showed a relative intensity of the strongest peaks as 100% for CaCO_3 and this is similar to the results obtained in this study.

The charcoal fines contained CaCO_3 (70%) and the remainder was the amorphous compounds (30 wt%). Tongpoothorn *et al.* (2011) did a study on preparation of activated carbon derived from *Jatropha curcas* fruit shell and the XRD analysis of the activated carbon exhibited broad peaks and absence of a sharp peak that revealed predominantly amorphous structure. Thus, the disappearance of peaks for CaO could be attributed to the high percentage of amorphous carbon in the charcoal fines. Etiégni and Campbell (1991) did a study on physical and chemical characteristics of wood ash from Lodgepole pine saw dust and found that ash yield and chemical composition changed with temperature. In addition, XRD analysis of a dry sample as well as a sample hydrated and air dried for 24 h showed that the most probable major components of the wood ash were lime (CaO), calcite (CaCO_3), portlandite (Ca(OH)_2) and calcium silicate (Ca_2SiO_4). The Ca(OH)_2 could have formed as a result of the hydration reaction between CaO and water as reported by Steenari *et al.* (1999). Steenari *et al.* (1999) reported that combustion temperatures of 1000-1200°C result in the formation of calcium silicates thus Ca_2SiO_4 reported by Etiégni and Campbell (1991) could have formed as a result of heating the samples between 538-1093°C.

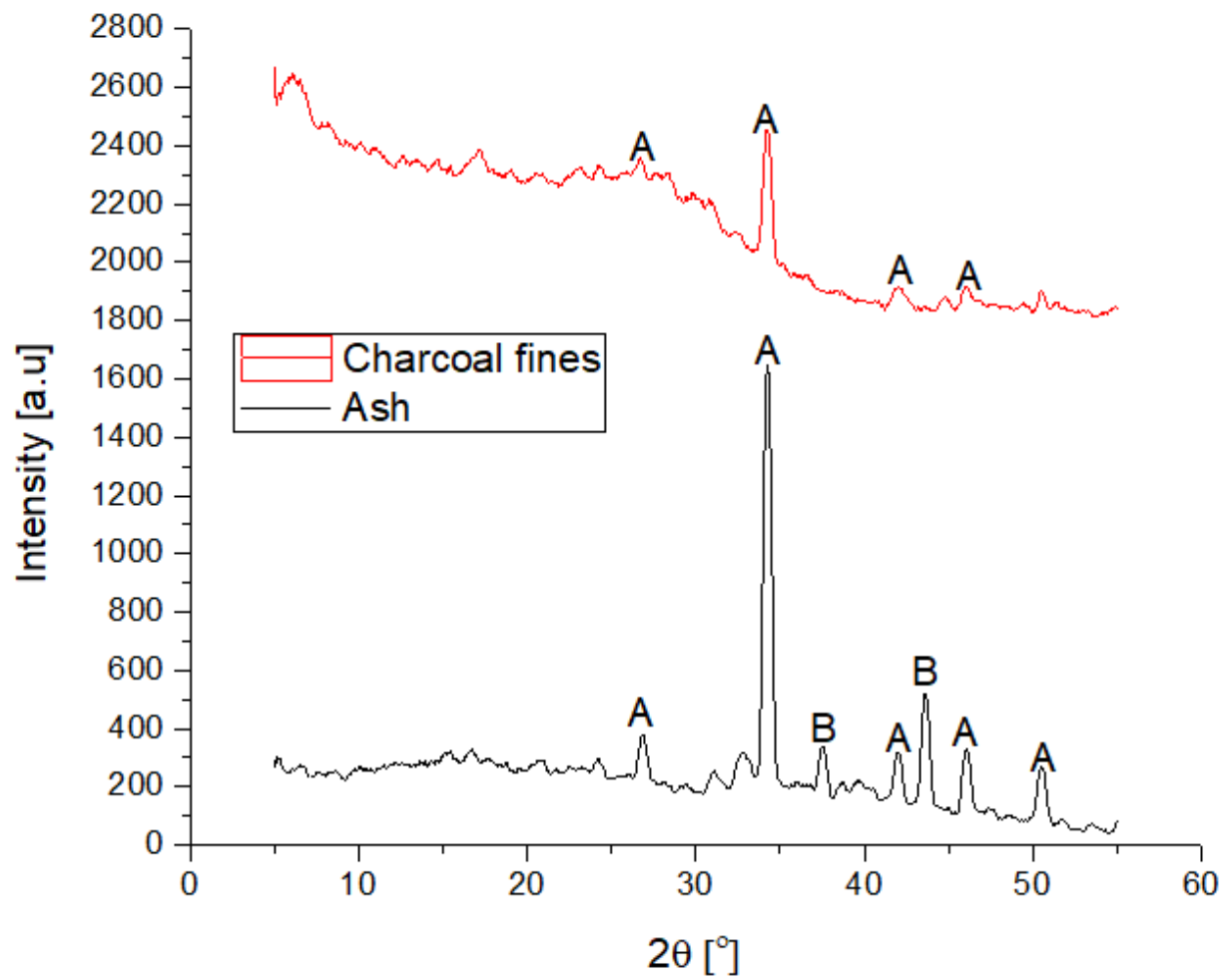


Figure 44: XRD analysis of ash and charcoal fines; A- Calcite (CaCO_3), B- lime (CaO)

CHAPTER FIVE

CONCLUSION AND RECOMMENDATIONS

5.1 Conclusion

The study showed that *Canarium Schweinfurthii* resin is a suitable binder for production of carbonized briquettes using charcoal fines as feedstock. Alternatively, biomass waste can be carbonized to provide the char which can supplement the charcoal fines. The charcoal fines contained medium volatile matter as a result of the inefficient local methods of carbonization of wood to produce charcoal. In addition, the binder does not contain ash which interferes with the combustion of the briquettes. The heating value of the binder was higher than that of the charcoal fines and hence improved the higher heating value of the briquettes in addition to acting as binder.

The briquettes were found to cure instantly since the binder used is a solid at room temperature and does not need water in its preparation thus, the briquettes can be used as soon as they are ejected from the die. The increased strength and density of the briquettes with binder concentration implies that they can easily be stored and transported. The increased density of the briquettes with binder concentration implies that briquettes burn longer thus, reducing the loading time of the cookstove. For compressive strength, all the briquettes met the recommended minimum value of 0.375 MPa reported for commercial charcoal briquettes. The high WRI showed that the briquettes are impervious to water which would cause easy disintegration as well as difficulty during ignition of the briquettes.

Since the binder is combustible, it contributes to the heat energy from the briquettes as observed by the flaming combustion during ignition and CSHP phases. The briquettes were found to ignite easily and burned with white smoke, yellow flame and soot during CSHP phase and later burned without a yellow flame and soot during the HSHP and Simmer phases. Briquettes B40 were found to boil water faster during CSHP and HSHP phase though they also contribute the highest emissions in terms of PM_{2.5}. The sulphur in the charcoal fines as well as the nitrogen in the charcoal fines and binder contributed to the SO₂ and NO_x emissions respectively. During the WBT, the terpenoids in the binder contributed to the high amount of soot, hydrocarbons, CO and CO₂ during ignition and combustion of the briquettes.

5.2 Recommendations

Briquettes B35 and B40 passed the recommended IRI value of 50. To mitigate the emission of PM_{2.5}, briquettes B25 and B30 with a lower binder concentration are recommended. The briquettes

can be used as an alternative source of fuel to firewood since they exhibit similar combustion behaviour. To improve indoor air quality when using the developed briquettes, it is recommended that a chimney should be installed on the kitchen to vent outdoor these pollutant emissions during cooking. Furthermore, individuals involved in cooking are advised to stay away from the kitchen especially during the CSHP phase to avoid exposure to the pollutant emissions. This would however, be practical only when cooking food that does not require close attention to be near the cookstove such as boiling water. The ash can be a potential fertilizer to replenish the soil thus, increasing harvests and neutralising soil acidity.

Due to scarcity of the resin, its synthesis in the laboratory should be investigated to ensure sustainability. During mixing of binder and charcoal fines, there was agglomeration of the mixture and this can be avoided by using deflocculants which need to be studied. In addition, techno-economic and life-cycle assessment should be done. The effect of soot on heat transfer to the pot should also be investigated. The gas analyser (Ametek Land, lancom 4) could not identify the exact species of the hydrocarbons from the combustion products thus their chemical formulae could not be determined. Analysis of the gaseous emissions to identify these species using more sophisticated equipment is recommended. Further research to understand the chemical composition and more binding properties (softening point, quinoline insoluble, toluene insoluble; physicochemical and rheological properties i.e. colour, odour, taste, pH, solubility (in hot water, cold water, acetone, chloroform, ethanol), intrinsic viscosity, protein, percentage yield, swelling capacity, melting temperature, tannin content, total soluble fibre) of the resin is suggested. Thus, this study has shown that *Canarium Schweinfurthii* resin can be used as a binder for converting of waste material such as charcoal fines to energy through the production of briquettes.

REFERENCES

- Amech, P. O. (2018). Electrochemical and computational study of gum exudates from *Canarium schweinfurthii* as green corrosion inhibitor for mild steel in HCl solution . *Journal of Taibah University for Science*, 12(6), 783–795. <https://doi.org/10.1080/16583655.2018.1514147>
- Amer, O., Boukhanouf, R., & Ibrahim, H. G. (2015). A review of evaporative cooling technologies. *International Journal of Environmental Science and Development*, 6(2), 111–117. <https://doi.org/10.7763/ijesd.2015.v6.571>
- Aprovecho Research Center. (2018). *Instructions for use of the Laboratory Emissions Monitoring System*. <https://www.google.com>
- Aprovecho Research Center. (2020). *Sensor Box Processing WBT 4.2.3 apr.28.20.xls* (4.2.3). <http://aprovecho.org/software/>
- Arora, P., Das, P., Jain, S., & Kishore, V. V. N. (2014). A laboratory based comparative study of Indian biomass cookstove testing protocol and water boiling test. *Energy for Sustainable Development*, 21, 81–88. <https://doi.org/10.1016/j.esd.2014.06.001>
- ASTM. (2011). *Standard Test Method for Splitting Tensile Strength of Cylindrical Concrete Specimens*. https://doi.org/10.1520/C0496_C0496M-11
- ASTM. (2013). *Standard Test Method for Gross Calorific Value of Coal and Coke*. <https://doi.org/10.1520/D5865-13>
- ASTM. (2014a). *Standard Test Method for Compositional Analysis By Thermogravimetry*. <https://doi.org/10.1520/E1131-08R14>
- ASTM. (2014b). *Standard Test Methods for Density and Specific Gravity (Relative Density) of Wood And Wood-Based Materials*. <https://doi.org/10.1520/D2395-14>
- ASTM. (2015). *Standard Practice for Ultimate Analysis of Coal and Coke*. <https://doi.org/10.1520/D3176-15>
- ASTM. (2017). *Standard Test Method for Compressive Strength of Cylindrical Concrete Specimens*. https://doi.org/10.1520/C0039_C0039M-17B
- Balat, M. (2011). Production of bioethanol from lignocellulosic materials via the biochemical pathway: A review. *Energy Conversion and Management*, 52(2), 858–875.

<https://doi.org/10.1016/j.enconman.2010.08.013>

- Bazargan, A., Rough, S. L., & McKay, G. (2014). Compaction of palm kernel shell biochars for application as solid fuel. *Biomass and Bioenergy*, *70*, 489–497. <https://doi.org/10.1016/j.biombioe.2014.08.015>
- Benk, A. (2010). Utilisation of the binders prepared from coal tar pitch and phenolic resins for the production metallurgical quality briquettes from coke breeze and the study of their high temperature carbonization behaviour. *Fuel Processing Technology*, *91*(9), 1152–1161. <https://doi.org/10.1016/j.fuproc.2010.03.030>
- Bhattacharya, S. C., Sett, S., & Shrestha, R. M. (1989). State of the art for biomass densification. *Energy Sources*, *11*(3), 161–182. <https://doi.org/10.1080/00908318908908952>
- Blasi, C. D. (1993). Modeling and simulation of combustion processes of charring and non-charring solid fuels. *Progress in Energy and Combustion Science*, *19*(1), 71–104. [https://doi.org/10.1016/0360-1285\(93\)90022-7](https://doi.org/10.1016/0360-1285(93)90022-7)
- Blesa, M. J., Fierro, V., Miranda, J. L., Moliner, R., & Palacios, J. M. (2001). Effect of the pyrolysis process on the physicochemical and mechanical properties of smokeless fuel briquettes. *Fuel Processing Technology*, *74*(1), 1–17. [https://doi.org/10.1016/S0378-3820\(01\)00209-0](https://doi.org/10.1016/S0378-3820(01)00209-0)
- Burnett, R. T., Arden, P. C., Ezzati, M., Olives, C., Lim, S. S., Mehta, S., Shin, H. H., Singh, G., Hubbell, B., Brauer, M., Ross Anderson, H., Smith, K. R., Balmes, J. R., Bruce, N. G., Kan, H., Laden, F., Prüss-Ustün, A., Turner, M. C., Gapstur, S. M., ... Cohen, A. (2014). An integrated risk function for estimating the global burden of disease attributable to ambient fine particulate matter exposure. *Environmental Health Perspectives*, *122*(4), 397–403. <https://doi.org/10.1289/ehp.1307049>
- Carnaje, N. P., Talagon, R. B., Peralta, J. P., Shah, K., & Paz-Ferreiro, J. (2018). Development and characterisation of charcoal briquettes from water hyacinth (*Eichhornia crassipes*)-molasses blend. *PloS One*, *13*(11), e0207135.
- Chen, Y., Shen, G., Su, S., Du, W., Huangfu, Y., Liu, G., Wang, X., Xing, B., Smith, K. R., & Tao, S. (2016). Efficiencies and pollutant emissions from forced-draft biomass-pellet semi-gasifier stoves: Comparison of International and Chinese water boiling test protocols. *Energy for Sustainable Development*, *32*, 22–30. <https://doi.org/10.1016/j.esd.2016.02.008>

- Chirchir, D. K., Nyaanga, D. M., & Githeko, J. M. (2013). Effect of binder types and amount on physical and combustion characteristics. *International Journal of Engineering Research and Science and Technology*, 2(1), 12–20.
- Clean cooking alliance. (2013). *Guidelines for Testing Charcoal Stoves with WBT 4.2.2*. <http://cleancookingalliance.org/binary-data/document/file/000/000/401-1.pdf>
- Clean cooking alliance. (2014). *The Water Boiling Test version 4.2.3*. <https://www.cleancookingalliance.org/technology-and-fuels/testing/protocols.html>
- Da Silva Rodrigues-Corrêa, K. C., De Lima, J. C., & Fett-Neto, A. G. (2013). Oleoresins from pine: Production and industrial uses. *Natural Products*, 136, 4037-4060.
- Deac, T., Fechete-tutunaru, L., & Gaspar, F. (2016). Environmental impact of sawdust briquettes use - experimental approach. *Energy Procedia*, 85, 178–183.
- Demeyer, A., Voundi Nkana, J. C., & Verloo, M. G. (2001). Characteristics of wood ash and influence on soil properties and nutrient uptake: An overview. *Bioresource Technology*, 77(3), 287–295. [https://doi.org/10.1016/S0960-8524\(00\)00043-2](https://doi.org/10.1016/S0960-8524(00)00043-2)
- Drobíková, K., Plachá, D., Motyka, O., Gabor, R., Kutlákova, K. M., Vallová, S., & Seidlerová, J. (2015). Recycling of blast furnace sludge by briquetting with starch binder: Waste gas from thermal treatment utilizable as a fuel. *Waste Management*, 48, 471–477.
- El-Mahallawy, F., & El-Din Habik, S. (2002). *Fundamentals and Technology of Combustion* (V. Thame (1stEd.) Elsevier. <https://www.google.com>
- Etiégni, L., & Campbell, A. G. (1991). Physical and chemical characteristics of wood ash. *Bioresource Technology*, 37(2), 173–178. [https://doi.org/10.1016/0960-8524\(91\)90207-Z](https://doi.org/10.1016/0960-8524(91)90207-Z)
- Fadhil, A. B. (2020). Production and characterization of liquid biofuels from locally available nonedible feedstocks. *Asia-Pacific Journal of Chemical Engineering*, 16(1), 1–21. <https://doi.org/10.1002/apj.2572>
- Fagbemi, E., Ayeke, P., Omonigho, B., Udokpo, N., Iseru, E., Akpovwovwo, T., & Awolola, E. (2014). Determination of physical and mechanical properties of briquettes produced from carbonized rubber seed shell using local binder. *American Journal of Materials Research*, 1(3), 44–47. <http://www.aascit.org/journal/ajmr>
- Ferguson, H. (2012). *Briquette Businesses in Uganda; The potential for briquette enterprises to*

address the sustainability of the Ugandan biomass fuel market. [www. gvepinternational.org%0A](http://www.gvepinternational.org%0A)

- Fernandez-Anez, N., Slatter, D. J. F., Saeed, M. A., Phylaktou, H. N., Andrews, G. E., & Garcia-Torrent, J. (2018). Ignition sensitivity of solid fuel mixtures. *Fuel*, 223, 451–461. <https://doi.org/10.1016/j.fuel.2018.02.106>
- Fichan, I., Larroche, C., & Gros, J. B. (1999). Water solubility, vapor pressure, and activity coefficients of terpenes and terpenoids. *Journal of Chemical and Engineering Data*, 44(1), 56–62. <https://doi.org/10.1021/je980070+>
- Gani, A., & Naruse, I. (2007). Effect of cellulose and lignin content on pyrolysis and combustion characteristics for several types of biomass. *Renewable Energy*, 32(4), 649–661. <https://doi.org/10.1016/j.renene.2006.02.017>
- Gesase, L. E., King'ondou, C. K., & Jande, Y. A. C. (2019). Manihot glaziovii-Bonded and Bioethanol-Infused Charcoal Dust Briquettes: A New Route of Addressing Sustainability, Ignition, and Food Security Issues in Briquette Production. *Bioenergy Research*, 13, 378–386. <https://doi.org/10.1007/s12155-019-10076-9>
- Gilvari, H., De Jong, W., & Schott, D. L. (2019). Quality parameters relevant for densification of bio-materials: Measuring methods and affecting factors: A review. *Biomass and Bioenergy*, 120, 117–134. <https://doi.org/10.1016/j.biombioe.2018.11.013>
- Glarborg, P., Jensen, A. D., & Johnsson, J. E. (2003). Fuel nitrogen conversion in solid fuel fired systems. *Progress in Energy and Combustion Science*, 29(2), 89–113.
- Grimsby, L. K., Rajabu, H. M., & Treiber, M. U. (2016). Multiple biomass fuels and improved cook stoves from Tanzania assessed with the water boiling test. *Sustainable Energy Technologies and Assessments*, 14, 63–73. <https://doi.org/10.1016/j.seta.2016.01.004>
- Grover, P. D., & Mishra, S. K. (1996). *Biomass Briquetting: Technology and Practices*. (No.46). FAO Regional Wood Energy Development Programme in Asia. <https://www.google.com>
- Haykiri-Acma, H., Yaman, S., & Kucukbayrak, S. (2013). Production of biobriquettes from carbonized brown seaweed. *Fuel Processing Technology*, 106, 33–40.
- Heinimö, J., & Junginger, M. (2009). Production and trading of biomass for energy: An overview of the global status. *Biomass and Bioenergy*, 33(9), 1310–1320.

- Hermans, L. J. F. (2012). Boiling water. *Europhysics News*, 43(2), 13–13.
- Hu, Q., Shao, J., Yang, H., Yao, D., Wang, X., & Chen, H. (2015). Effects of binders on the properties of bio-char pellets. *Applied Energy*, 157, 508–516.
- Huang, G., & Hao, Y. (2012). Preparation and principle of Shenmu bituminous coal gasification briquette. *China Coal*, 38, 83–90.
- Idris, J., Shirai, Y., Andou, Y., Ali, A. A. M., Othman, M. R., Ibrahim, I., & Hassan, M. A. (2015). Self-sustained carbonization of oil palm biomass produced an acceptable heating value charcoal with low gaseous emission. *Journal of Cleaner Production*, 89, 257–261. <https://doi.org/10.1016/j.jclepro.2014.11.016>
- ISO. (2018). *Clean cookstoves and clean cooking solutions: Harmonized laboratory test protocols: Part 1: Standard test sequence for emissions and performance, safety and durability*. <https://www.google.com>
- Kambo, H. S., & Dutta, A. (2014). Strength, storage, and combustion characteristics of densified lignocellulosic biomass produced via torrefaction and hydrothermal carbonization. *Applied Energy*, 135, 182–191. <https://doi.org/10.1016/j.apenergy.2014.08.094>
- Karungi, A., Pogrebnoi, A., & Kivevele, T. (2020). Optimization of microwave-assisted alkali pretreatment followed by acid hydrolysis of sugarcane straw for production of acetone-butanol-ethanol. *Energy Sources, Part A: Recovery, Utilization and Environmental Effects*, 2020, 1–17. <https://doi.org/10.1080/15567036.2020.1760404>
- Khelifi, S., Lajili, M., Tabet, F., Boushaki, T., & Sarh, B. (2019). Investigation of the combustion characteristics of briquettes prepared from olive mill solid waste blended with and without a natural binder in a fixed bed reactor. *Biomass Conversion and Biorefinery*, 10, 535–544. <https://doi.org/10.1007/s13399-019-00449-7>
- Kivevele, T. T., & Huan, Z. (2013). Effects of antioxidants on the cetane number, viscosity, oxidation stability, and thermal properties of biodiesel produced from nonedible oils. *Energy Technology*, 1(9), 537–543. <https://doi.org/10.1002/ente.201300072>
- Kpalo, S. Y., Zainuddin, M. F., Manaf, L. A., & Roslan, A. M. (2020a). A review of technical and economic aspects of biomass briquetting. *Sustainability*, 12(11), 4609. <https://doi.org/10.3390/su12114609>

- Kpalo, S. Y., Zainuddin, M. F., Manaf, L. A., & Roslan, A. M. (2020b). Production and characterization of hybrid briquettes from corncobs and oil palm trunk bark under a low pressure densification technique. *Sustainability*, *12*(6), 2468.
- Kuete, V. (2017). *Canarium schweinfurthii*. <https://doi.org/10.1016/B978-0-12-809286-6.00016-9>
- Lackner, M. (2011). *Combustion: Ullmann's Encyclopedia of Industrial Chemistry*. Wiley-VCH. <https://doi.org/10.1002/14356007.b03>
- Lask, K., Booker, K., Han, T., Granderson, J., Yang, N., Ceballos, C., & Gadgil, A. (2015). Performance comparison of charcoal cookstoves for Haiti: laboratory testing with water boiling and controlled cooking tests. *Energy for Sustainable Development*, *26*, 79–86. <https://doi.org/10.1016/j.esd.2015.02.002>
- Lubwama, M., & Yiga, V. A. (2017). Development of groundnut shells and bagasse briquettes as sustainable fuel sources for domestic cooking applications in Uganda. *Renewable Energy*, *111*, 532–542. <https://doi.org/10.1016/j.renene.2017.04.041>
- Lubwama, M., Yiga, V. A., & Lubwama, H. N. (2020). Effects and interactions of the agricultural waste residues and binder type on physical properties and calorific values of carbonized briquettes. *Biomass Conversion and Biorefinery*, 2020, 1-21.
- Medina, P., Berrueta, V., Martínez, M., Ruiz, V., Edwards, R. D., & Masera, O. (2016). Comparative performance of five Mexican plancha-type cookstoves using water boiling tests. *Development Engineering*, *2*, 20–28. <https://doi.org/10.1016/j.deveng.2016.06.001>
- Menya, E., Olupot, P. W., Storz, H., Lubwama, M., Kiros, Y., & John, M. J. (2020). Optimization of pyrolysis conditions for char production from rice husks and its characterization as a precursor for production of activated carbon. *Biomass Conversion and Biorefinery*, *10*(1), 57–72. <https://doi.org/10.1007/s13399-019-00399-0>
- Misra, M. K., Ragland, K. W., & Baker, A. J. (1993). Wood ash composition as a function of furnace temperature. *Biomass and Bioenergy*, *4*(2), 103–116.
- Mitchell, E. J. S., Lea-Langton, A. R., Jones, J. M., Williams, A., Layden, P., & Johnson, R. (2016). The impact of fuel properties on the emissions from the combustion of biomass and other solid fuels in a fixed bed domestic stove. *Fuel Processing Technology*, *142*, 115–123. <https://doi.org/10.1016/j.fuproc.2015.09.031>

- Moqbel, S., Reinhart, D., & Chen, R. H. (2010). Factors influencing spontaneous combustion of solid waste. *Waste Management*, *30*(8–9), 1600–1607.
- Nagawa, C., Böhmendorfer, S., & Rosenau, T. (2015). Chemical composition and anti-termite activity of essential oil from *Canarium schweinfurthii* Engl. *Industrial Crops and Products*, *71*, 75–79. <https://doi.org/10.1016/j.indcrop.2015.03.078>
- Nwabue, F. I., Unah, U., & Itumoh, E. J. (2017). Production and characterisation of smokeless bio-coal briquettes incorporating plastic waste materials. *Environmental Technology and Innovation*, *8*, 233–245. <https://doi.org/10.1016/j.eti.2017.02.008>
- Obi, O. F. (2015). Evaluation of the effect of palm oil mill sludge on the properties of sawdust briquette. *Renewable and Sustainable Energy Reviews*, *52*, 1749–1758.
- Oketch, P. O., Ndiritu, H. M., & Gathitu, B. B. (2014). Experimental study of fuel efficiency and emissions comparison from bio-ethanol gel Stoves. *European International Journal of Science and Technology*, *3*(7), 328–339.
- Okot, D. K., Bilsborrow, P. E., & Phan, A. N. (2018). Effects of operating parameters on maize cob briquette quality. *Biomass and Bioenergy*, *112*, 61–72.
- Onchieku, J. M., Chikamai, B. N., & Rao, M. S. (2012). Optimum Parameters for the Formulation of Charcoal Briquettes Using Bagasse and Clay as Binder. *European Journal of Sustainable Development*, *1*(3), 477–492. <https://doi.org/10.14207/ejsd.2012.v1i3p477>
- Onuegbu, T. U., Ekpunobi, U. E., Ogbu, I. M., Ekeoma, M. O., & Obumselu, F. O. (2011). Comparative studies of ignition time and water boiling test of coal and biomass briquettes blend. *International Journal of Recent Research and Applied Studies*, *7*(2), 153-159.
- Onuegbu, Theresa Uzoma, Ogbu, I. M., & Ilochi, N. O. (2010). Enhancing the Properties of Coal Briquette Using Spear Grass (*Imperata Cylindrica*). *Leonardo Journal of Sciences*, *17*(2), 47–58. <http://ljs.academicdirect.org>
- Ormeño, E., Céspedes, B., Sánchez, I. A., Velasco-García, A., Moreno, J. M., Fernandez, C., & Baldy, V. (2009). The relationship between terpenes and flammability of leaf litter. *Forest Ecology and Management*, *257*(2), 471–482. <https://doi.org/10.1016/j.foreco.2008.09.019>
- Pandey, S., & Dhakal, R. P. (2013). Pine Needle Briquettes: A Renewable Source of Energy. *International Journal of Energy Science*, *3*(3), 254–260.

- Pereira, B. L. C., Oliveira, A. C., Carvalho, A. M. M. L., Carneiro, A. D. C. O., Santos, L. C., & Vital, B. R. (2012). Quality of wood and charcoal from Eucalyptus clones for ironmaster use. *International Journal of Forestry Research*, 2012, 1-9.
- Pitman, R. M. (2006). Wood ash use in forestry: A review of the environmental impacts. *Forestry*, 79(5), 563–588. <https://doi.org/10.1093/forestry/cpl041>
- Prasityousil, J., & Muenjina, A. (2013). Properties of solid fuel briquettes produced from rejected material of municipal waste composting. *Procedia Environmental Sciences*, 17, 603–610. <https://doi.org/10.1016/j.proenv.2013.02.076>
- Quist, C. M., Jones, M. R., & Lewis, R. S. (2020). Influence of variability in testing parameters on cookstove performance metrics based on the water boiling test. *Energy for Sustainable Development*, 58, 112–118. <https://doi.org/10.1016/j.esd.2020.07.006>
- Raju, A. I. C., Jyothi, R. K., Satya, M., & Praveena, U. (2014). Studies on development of fuel briquettes for household and industrial purpose. *International Journal of Research in Engineering and Technology*, 3(2), 54–63.
- Rezzi, S., Bighelli, A., Castola, V., & Casanova, J. (2005). Composition and chemical variability of the oleoresin of *Pinus nigra* ssp. *laricio* from Corsica. *Industrial Crops and Products*, 21(1), 71–79. <https://doi.org/10.1016/j.indcrop.2003.12.008>
- Romallosa, A. R. D., & Kraft, E. (2017). Feasibility of biomass briquette production from municipal waste streams by integrating the informal sector in the philippines. *Resources*, 6(12), 1–19. <https://doi.org/10.3390/resources6010012>
- Rotich, K. P. (1998). *Carbonization and Briquetting of Sawdust for Use in Domestic Cookers*. University of Nairobi. <https://www.google.com>
- Rousset, P., Caldeira-Pires, A., Sablowski, A., & Rodrigues, T. (2011). LCA of eucalyptus wood charcoal briquettes. *Journal of Cleaner Production*, 19(14), 1647–1653. <https://doi.org/10.1016/j.jclepro.2011.05.015>
- Samadi, S. H., Ghobadian, B., & Nosrati, M. (2019). Prediction of higher heating value of biomass materials based on proximate analysis using gradient boosted regression trees method. *Energy Sources, Part A: Recovery, Utilization and Environmental Effects*, 0(0), 1–10.
- Sen, R., Wiwatpanyaporn, S., & Annachatre, A. P. (2016). Influence of binders on physical

- properties of fuel briquettes produced from cassava rhizome waste. *International Journal of Environment and Waste Management*, 17(2), 158–175.
- Šiler, B., & Mišić, D. (2016). Biologically active compounds from the genus *Centaurium* sl (Gentianaceae): current knowledge and future prospects in medicine. *Studies in Natural Products Chemistry*, 49, 363-397.
- Sotannde, O. A., Oluyeye, A. O., & Abah, G. B. (2010). Physical and combustion properties of charcoal briquettes from neem wood residues. *International Agrophysics*, 24(2), 189–194.
- Sotannde, O. A., Oluyeye, A. O., & Abah, G. B. (2016). Physical and combustion properties of briquettes from sawdust of *Azadirachta indica*. *International Agrophysics*, 21(1), 63–67. <https://doi.org/10.1007/s11676-010-0010-6>
- Steenari, B. M., Karlsson, L. G., & Lindqvist, O. (1999). Evaluation of the leaching characteristics of wood ash and the influence of ash agglomeration. *Biomass and Bioenergy*, 16(2), 119–136. [https://doi.org/10.1016/S0961-9534\(98\)00070-1](https://doi.org/10.1016/S0961-9534(98)00070-1)
- Steenari, B. M., & Lindqvist, O. (1997). Stabilization of biofuel ashes for recycling to forest soil. *Biomass and Bioenergy*, 13(1–2), 39–50.
- Sugumaran, P., & Seshadri, S. (2010). *Biomass Charcoal Briquetting, Technology for Alternative Energy Based Income Generation in Rural Areas*. www.amm-mcrc.org
- Suhartini, S., Hidayat, N., & Wijaya, S. (2011). Physical properties characterization of fuel briquette made from spent bleaching earth. *Biomass and Bioenergy*, 35(10), 4209–4214. <https://doi.org/10.1016/j.biombioe.2011.07.002>
- Teixeira, S. R., Pena, A. F. V., & Miguel, A. G. (2010). Briquetting of charcoal from sugar-cane bagasse fly ash (scbfa) as an alternative fuel. *Waste Management*, 30(5), 804-807.
- Thermopedia. (2011). *Steam Tables: A-to-Z Guide to Thermodynamics, Heat & Mass Transfer, and Fluids Engineering*. https://doi.org/10.1615/AtoZ.s.steam_tables
- Thoms, L. J., Snape, C. E., & Taylor, D. (1999). Physical characteristics of cold cured anthracite/coke breeze briquettes prepared from a coal tar acid resin. *Fuel*, 78(14), 1691–1695. [https://doi.org/10.1016/S0016-2361\(99\)00116-7](https://doi.org/10.1016/S0016-2361(99)00116-7)
- Tilli, A. (2003). *Bioenergy*. <https://www.google.com>

- Tongpoothorn, W., Sriuttha, M., Homchan, P., Chanthai, S., & Ruangviriyachai, C. (2011). Preparation of activated carbon derived from *Jatropha curcas* fruit shell by simple thermo-chemical activation and characterization of their physico-chemical properties. *Chemical Engineering Research and Design*, 89(3), 335–340.
- Turns, S. R. (2000). *An introduction to combustion; concepts and applications* (2nd Ed.). McGraw-Hill. <https://www.google.com>
- Ward, B. J., Yacob, T. W., & Montoya, L. D. (2014). Evaluation of solid fuel char briquettes from human waste. *Environmental Science and Technology*, 48(16), 9852–9858. <https://doi.org/doi.org/10.1021/es500197h>
- WHO. (2014). *WHO Guidelines for Indoor Air Quality: Household Fuel Combustion*. WHO Document Production Services. <https://www.google.com>
- Wikipedia. (2021). *Makerere*. <https://en.wikipedia.org/wiki/Makerere>
- Wu, S., Zhang, S., Wang, C., Mu, C., & Huang, X. (2018). High-strength charcoal briquette preparation from hydrothermal pretreated biomass wastes. *Fuel Processing Technology*, 171, 293–300. <https://doi.org/10.1016/j.fuproc.2017.11.025>
- Yadav, N., Yadav, R., & Goyal, A. (2014). Chemistry of terpenoids. *International Journal of Pharmaceutical Sciences Review and Research*, 27(2), 272–278.
- Yang, Y., Cui, G., & Lan, C. Q. (2019). Developments in evaporative cooling and enhanced evaporative cooling: A review. *Renewable and Sustainable Energy Reviews*, 113, 1–10. <https://doi.org/10.1016/j.rser.2019.06.037>
- Yousuf, S., Kamdem, R. S. T., Ngadjui, B. T., Wafo, P., & Fun, H. K. (2011). 3a-Hydroxytirucalla-8,24-dien-21-oic acid. *Acta Crystallographica*, 67(4), o937–o938.
- Zhang, G., Sun, Y., & Xu, Y. (2018). Review of briquette binders and briquetting mechanism. *Renewable and Sustainable Energy Reviews*, 82(Part 1), 477–487.
- Zhao, F. J., Shu, L. F., & Wang, Q. H. (2012). Terpenoid emissions from heated needles of *Pinus sylvestris* and their potential influences on forest fires. *Acta Ecologica Sinica*, 32(1), 33–37. <https://doi.org/10.1016/j.chnaes.2011.06.002>
- Zhu, P., Quan, S., Lei, Z., & Zhang, J. (2019). Structural and pyrolysis behaviors analysis of coal pretreated with a weak acid. *Energy Sources, Part A: Recovery, Utilization and*

APPENDICES

Appendix 1: Boiling point of the binder

| Sample | Top | Middle | Bottom | AVG | STD |
|--------|-----|--------|--------|-----|-----|
| 1 | 98 | 100 | 275 | 158 | 101 |
| 2 | 107 | 112 | 284 | 168 | 100 |
| 3 | 102 | 108 | 279 | 163 | 100 |
| | | | | 163 | |

Appendix 2: Equipment used for characterization: (a)Elemental (CHNSO) analyser, (b)Thermogravimetric analyser (c)Bomb Calorimeter, (d) SEM



(a)



(b)



(c)



(d)

Appendix 3: Pouring temperature of the mixture (charcoal fines and binder)

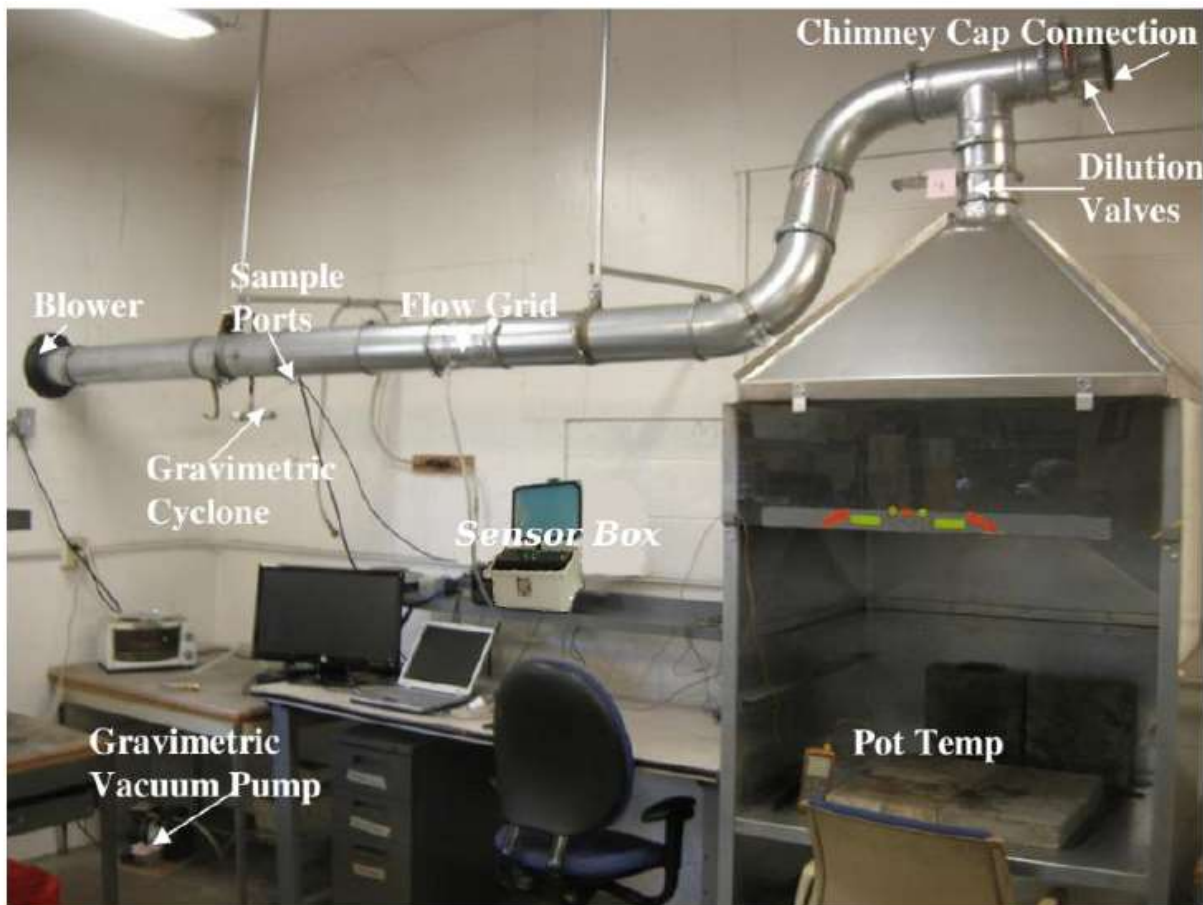
| *Briquette | 1 | 2 | 3 | AVG (°C) | STD |
|-------------------|----------|----------|----------|-----------------|------------|
| B25 | 135 | 123 | 116 | 125 | 10 |
| B30 | 125 | 143 | 112 | 127 | 16 |
| B35 | 128 | 136 | 131 | 132 | 4 |
| B40 | 140 | 123 | 138 | 134 | 9 |

*Briquette; B25-25 wt% binder, B30-30 wt% binder, B35-35 wt% binder, B40-40 wt% binder

Appendix 4: Compaction pressure of the briquettes

| Briquette | Compaction pressure (MPa) | | | | | AVG (MPa) | STD |
|------------------|----------------------------------|-----|-----|-----|-----|------------------|------------|
| B25 | 8.2 | 7.6 | 8 | 8 | 8 | 7.96 | 0.22 |
| B30 | 7.6 | 7.8 | 7.8 | 8 | 7.8 | 7.80 | 0.14 |
| B35 | 6.2 | 7 | 7.8 | 7.6 | 7 | 7.12 | 0.63 |
| B40 | 5.8 | 5.8 | 5.8 | 6 | 6.2 | 5.92 | 0.18 |

Appendix 5: LEMS hood, ducting and gravimetric assembly (Aprovecho Research Centre, 2018)



Appendix 6: WBT 4.2.3 Data Calculation Sheet

(a) Sample data Import sheet

Data Import Sheet

Aprovecho Advanced Studies in Appropriate Technology

Sensor Box -- For PEMS and LEMS

Software Version 4.2.3 for all Sensor Boxes

Updated Dec. 20, 2018 - Final

Background

(before lighting fire)

Start time Verify these times

End time But do not change unless in error

Start row

End row

CO background concentration -0.004165983

PM background concentration -18.44494721

| | Phase 1 (Cold Start) | Phase 2 (Hot Start) | Phase 3 (Simmer) | Entire Measured Period |
|-------------------|-------------------------|------------------------|---------------------|------------------------------|
| Start time | 08:49:31 | 09:33:11 | 09:59:10 | |
| End time | 09:30:23 | 09:58:26 | 10:44:10 | |
| Test length (min) | 40.9 | 25.3 | 45.0 | |
| Start row | 1337 | 2647 | 3427 | |
| End row | 2563 | 3405 | 4777 | |

Total consumption/emission

| | Phase 1 (Cold Start) | Phase 2 (Hot Start) | Phase 3 (Simmer) |
|-----------------|-------------------------|------------------------|---------------------|
| Consumption (g) | | | |
| Emission (g) | | | |

Sensor Box Number

Data file name (without .csv or .txt):

Process Data

Enter PEMS # and data file name

Then Click "Process Data" Button and proceed to "WBT" sheet entry.

Fuel carbon fraction

Wood is about 50%, other fuels differ.

Charcoal carbon fraction

50 - 90%

Flow Data

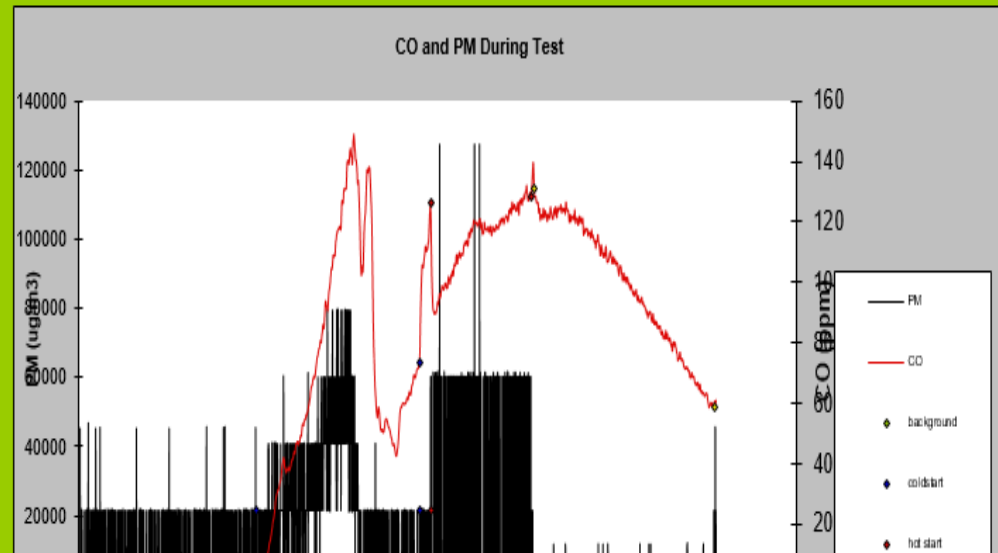
| | |
|------------|---------|
| Magnahelic | Screen |
| Inch Water | Reading |

Zero Flow

Fan on @: minutes

Full Flow

Fan should be turned on between 1 and 4 minutes



(b) Sample WBT sheet

SHELL FOUNDATION HEH PROJECT WATER BOILING TEST

DATA AND CALCULATION FORM (the form can be used with stoves that cook between one and four pots)*

Shaded cells require user input; unshaded cells automatically display outputs

Qualitative data

| | |
|----------------------|------------|
| Name(s) of Tester(s) | Derrick |
| Test Number | 1 |
| Date | 12.12.2020 |
| Stove type/model | Burn |
| Location | Creec |
| Fuel species | 25% Binder |
| Wind conditions | No wind |

note, if you are testing a non pot stove, the data entry places in the simmering test for pots other than the primary pot are left blank intentionally because the simmering test can not account for pots other than the primary pot.

Magnahelic

Full Flow: 0.40 inches H2O

Initial Test Conditions

| Data | value | units | label | Data | value | units | label |
|---|--------|--|-------|-------------------------------|-------|-------|----------------|
| Air temp | 19.9 | °C | | Dry weight of Pot # 1 (grams) | 198 | g | P1 |
| Average dimensions of fuel | | cm x cm x cm | | Dry weight of Pot # 2 (grams) | | g | P2 |
| Gross calorific value (dry fuel) | 29,700 | kJ/kg | HHV | Dry weight of Pot # 3 (grams) | | g | P3 |
| Net calorific value (dry fuel) | 28,500 | kJ/kg | LHV | Dry weight of Pot # 4 (grams) | | g | P4 |
| Wood moisture content (% - wet basis) the fuel) | 4.7% | % | MC | (grams) | - | g | k |
| Net calorific value charcoal (dry fuel) | 27,046 | kJ/kg | EHV | Local boiling point | 94.9 | °C | T _b |
| Fuel type (enter "W","K","G",or "C") | c | W = wood, K = kerosene, G = LPG, C = coal and charcoal | | | | | |

Black Carbon

Gravimetric

Description of stove and other comments: Enter filter info for each phase

Enter filter info for each phase

| | | HIGH POWER TEST (COLD START) | | | |
|----------------------------------|----------|------------------------------|------------------|-------------------------|------------------|
| Measurements | Units | Start | | Finish: w/h Pot #1 boil | |
| | | data | label | data | label |
| Time | hh:mm:ss | 08:49 | t _{ci} | 09:30:23 | t _{cf} |
| Weight of fuel | g | 3293 | f _{ci} | 3130 | f _{cf} |
| Water temperature, Pot # 1 | °C | 19.1 | T1 _{ci} | 94.9 | T1 _{cf} |
| Water temperature, Pot # 2 | °C | | T2 _{ci} | | T2 _{cf} |
| Water temperature, Pot # 3 | °C | | T3 _{ci} | | T3 _{cf} |
| Water temperature, Pot # 4 | °C | | T4 _{ci} | | T4 _{cf} |
| Weight of Pot # 1 with water | g | 2698 | P1 _{ci} | 2627 | P1 _{cf} |
| Weight of Pot # 2 with water | g | | P2 _{ci} | | P2 _{cf} |
| Weight of Pot # 3 with water | g | | P3 _{ci} | | P3 _{cf} |
| Weight of Pot # 4 with water | g | | P4 _{ci} | | P4 _{cf} |
| Fire-starting materials (if any) | -- | | | | |
| Weight of charcoal+container | g | | | | |

| Calculations/Results | Units | COLD START | | HOT START | |
|--------------------------------|-------|------------|-----------------|-----------|-----------------|
| | | data | label | data | label |
| Fuel consumed (moist) | g | 163 | f _{cm} | 60 | f _{hm} |
| Net change in char during test | g | - | D _c | - | D _h |
| Equivalent dry wood consumed | g | 155 | f _{cd} | 57 | f _{hd} |
| Water vaporized from all pots | g | 71 | w _{cv} | 32 | w _{hv} |
| Effective mass of water boiled | g | 2,429 | w _{ev} | 2,471 | w _{hv} |

(c) Sample results sheet

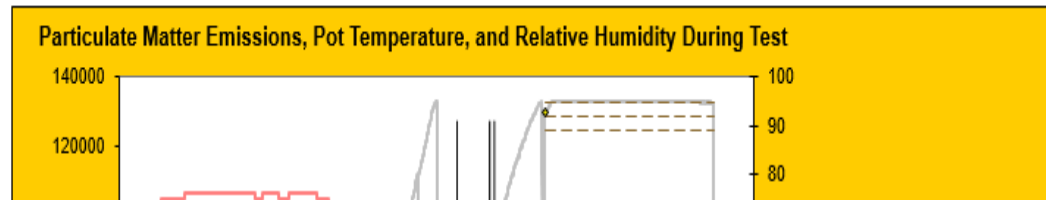
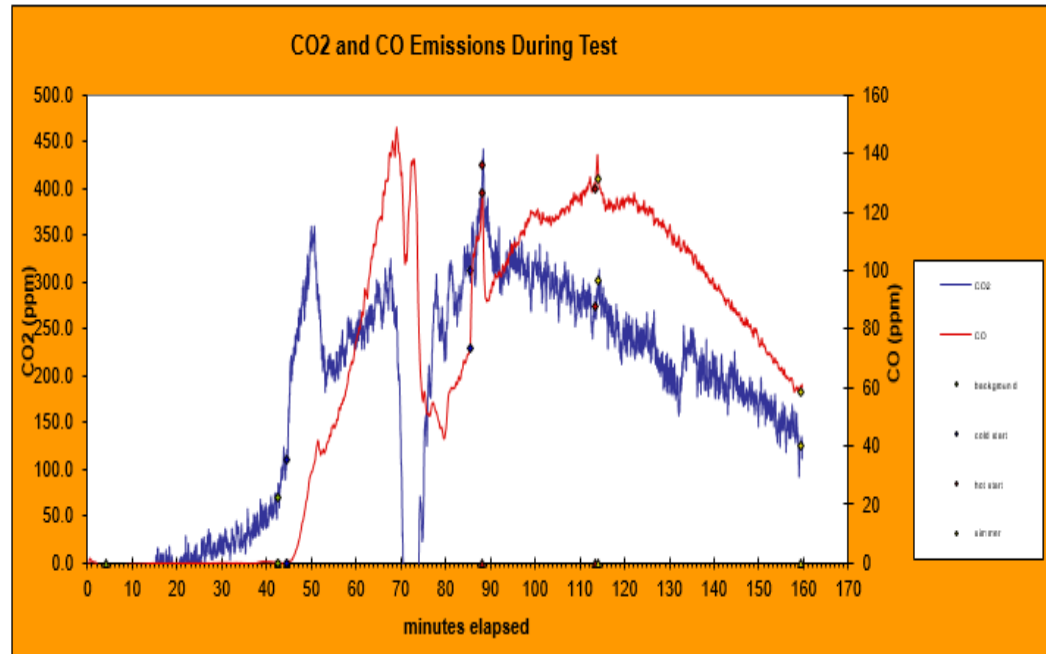
| | |
|------------------|------------|
| Stove type/model | Burn |
| Location | Creec |
| Fuel species | 25% Binder |
| Date | 12.12.2020 |

| IWA Performance Metrics | units | Value |
|-------------------------------------|--------------------|--------|
| High Power Thermal Efficiency | % | 37.5% |
| Low Power Specific Consumption Rate | MJ/min/L | 0.015 |
| High Power CO | g/MJ _d | 32.02 |
| Low Power CO | g/min/L | 0.45 |
| High Power PM | mg/MJ _d | 3740.4 |
| Low Power PM | mg/min/L | 0.92 |
| Indoor Emissions CO | g/min | 1.01 |
| Indoor Emissions PM | mg/min | 88.9 |
| Safety | Index | |

| | Tier |
|-------------------------------------|------|
| High Power Thermal Efficiency | 3.2 |
| Low Power Specific Consumption Rate | 4.1 |
| High Power CO | 0.4 |
| Low Power CO | 0.4 |
| High Power PM | 0.2 |
| Low Power PM | 4.0 |
| Indoor Emissions CO | 0.9 |
| Indoor Emissions PM | 0.4 |
| Safety | 0.0 |

| Standard Performance Measures | | |
|-----------------------------------|-----|--------|
| Fuel to Cook 5L (850/1500) | g | 330.0 |
| CO to Cook 5L (20) | g | 161.3 |
| PM to Cook 5L (1500) | mg | 7518.4 |
| Energy to Cook 5L (15,000/25,000) | kJ | 9,406 |
| Time to Boil | min | 32.7 |

Summarized Data is found at the bottom of this sheet



WA VITA WBT Tier
 High Power Thermal Efficiency
 Low Power Specific Consumption Rate
 High Power CO
 Low Power CO
 High Power PM
 Low Power PM
 Indoor Emissions CO
 Indoor Emissions PM
 Safety

(d) Sample logger data sheet

| Background--> | | | 4046.6 | 0.0 | 0.1 | 114.6 | 4.7 | | | | | |
|-----------------|-----------------|---------|-----------------------|-----------------------------|------------|------------------|------------------|--------------------|---------------|----------|-----------------|---------|
| Time | | | PM | | | | | CO | | | | |
| Seconds Elapsed | Minutes Elapsed | Clock | PM scat coef (1 / Mm) | Zeroed PM scat coef (1 /Mm) | PM (ug/m3) | PM Flow (ug/sec) | PM Flow (mg/min) | Integrated PM (ug) | CO (logunits) | CO (ppm) | Zeroed CO (ppm) | CO (mc) |
| 1 | 0.0 | 8:04:58 | 4048 | 1 | -2490.103 | -8.0 | -0.5 | 0 | -97 | -4 | -9 | |
| 3 | 0.1 | 8:05:00 | 4048 | 1 | -2490.103 | 0.0 | 0.0 | 0 | -23 | -1 | -6 | |
| 5 | 0.1 | 8:05:02 | 4061 | 14 | -26321.01 | -116.9 | -7.0 | -233.71725 | 40 | 2 | -3 | |
| 7 | 0.1 | 8:05:04 | 4048 | 1 | -2490.103 | -11.7 | -0.7 | -257.10979 | 83 | 3 | -1 | |
| 9 | 0.2 | 8:05:06 | 4061 | 14 | -26321.01 | 0.0 | 0.0 | -257.10979 | 112 | 5 | 0 | |
| 11 | 0.2 | 8:05:08 | 4048 | 1 | -2490.103 | -7.0 | -0.4 | -271.15558 | 135 | 6 | 1 | |
| 13 | 0.2 | 8:05:10 | 4061 | 14 | -26321.01 | -114.5 | -6.9 | -500.18037 | 143 | 6 | 1 | |
| 15 | 0.3 | 8:05:12 | 4061 | 14 | -26321.01 | 0.0 | 0.0 | -500.18037 | 150 | 6 | 1 | |
| 17 | 0.3 | 8:05:14 | 4048 | 1 | -2490.103 | -9.9 | -0.6 | -519.97187 | 151 | 6 | 2 | |
| 19 | 0.3 | 8:05:16 | 4048 | 1 | -2490.103 | 0.0 | 0.0 | -519.97187 | 150 | 7 | 2 | |

(e) Sample raw data sheet

| # | 12/12/2020 | | | | | | | | |
|---------|------------|---------|------|-------|----------|-----|-----|-------|---|
| # | 8:04:57 | | | | | | | | |
| ## | ## | | | | | | | | |
| #0 | 0.041394 | 0.00384 | 4.27 | 1 | 0.00384 | 0.1 | 1 | 1 | 1 |
| seconds | CO | GasTemp | PM | Flow | FlueTemp | TC | CO2 | PM_RH | |
| 1 | -97 | 5605 | 316 | 10619 | 5748 | 195 | 533 | 65 | |
| 3 | -23 | 5601 | 316 | 10572 | 5745 | 195 | 539 | 66 | |
| 5 | 40 | 5601 | 317 | 10631 | 5746 | 195 | 537 | 66 | |
| 7 | 83 | 5600 | 316 | 10634 | 5746 | 195 | 545 | 67 | |
| 9 | 112 | 5601 | 317 | 10589 | 5747 | 195 | 543 | 67 | |
| 11 | 135 | 5600 | 316 | 10616 | 5746 | 195 | 539 | 67 | |
| 13 | 143 | 5601 | 317 | 10630 | 5747 | 195 | 531 | 68 | |
| 15 | 150 | 5603 | 317 | 10600 | 5748 | 195 | 527 | 68 | |
| 17 | 151 | 5605 | 316 | 10626 | 5749 | 195 | 527 | 68 | |
| 19 | 159 | 5606 | 316 | 10602 | 5747 | 195 | 519 | 68 | |
| 21 | 157 | 5607 | 316 | 10591 | 5747 | 195 | 514 | 68 | |
| 23 | 153 | 5608 | 316 | 10605 | 5747 | 195 | 516 | 69 | |
| 25 | 156 | 5608 | 314 | 10590 | 5747 | 195 | 512 | 69 | |
| 27 | 152 | 5608 | 316 | 10627 | 5747 | 195 | 510 | 69 | |
| 29 | 153 | 5610 | 317 | 10591 | 5749 | 195 | 505 | 69 | |
| 31 | 153 | 5611 | 316 | 10598 | 5746 | 195 | 503 | 69 | |
| 33 | 144 | 5612 | 315 | 10622 | 5749 | 195 | 503 | 69 | |
| 35 | 143 | 5613 | 316 | 10620 | 5749 | 195 | 498 | 69 | |
| 37 | 142 | 5614 | 316 | 10610 | 5749 | 195 | 490 | 69 | |
| 39 | 142 | 5613 | 316 | 10584 | 5748 | 195 | 490 | 69 | |
| 41 | 138 | 5616 | 317 | 10609 | 5749 | 195 | 490 | 69 | |
| 43 | 137 | 5618 | 316 | 10587 | 5748 | 195 | 494 | 70 | |

(f) Sample assumptions sheet

Worksheet to read real-time data & calculate performance

Tami Bond (UIUC), Nordica MacCarty (Aprovecho), and Ryan Thompson (Aprovecho)

Assumptions:

| | | | |
|---------------------------------|--------|----------------|-------------------|
| Carbon fraction of fuel | 50% | PM Coefficient | 4 (ug/m3)/logunit |
| Scattering cross-section (m2/g) | 3 | | |
| Ambient pressure (Pa) | 101325 | | |
| Altitude (m) | 0 | | |

| | | |
|--------------------------|----------|--------------|
| Delay Time | | minutes |
| CO2 Maximum ppm | | |
| CO Calibration | 0.041394 | ppm/logunit |
| Flue Temp Calibration | 0.00384 | degC/logunit |
| CO2 Calibration | 1 | ppm/logunit |
| Thermocouple Calibration | 0.1 | degC/logunit |

File locations

| | |
|----------------|---------------------|
| Raw data files | C:\Emissions-Output |
| Output files | C:\Emissions-Output |

| | |
|--------------------------------|-----------|
| Sample Pump Flow Rate | 4.4 LPM |
| Gravimetric Flow Rate (actual) | 16.67 LPM |

| | |
|--------------------------|-----|
| Black Carbon Filter Area | cm2 |
| Black Carbon Flow Rate | LPM |

(g) Sample calorific values sheet

| Tree species | Tree species | Common name(s) | Calorific value (kcal/kg kJ/kg) | | |
|--|---|--|---------------------------------|------|---------|
| | | | low | high | average |
| 1 (Select from list) | (select from list or use default value of 20,000 MJ/kg) | | | | |
| 2 LPG | | | | | 48,000 |
| 3 Kerosene | | | | | 43,300 |
| 4 Charcoal | | | | | 29,400 |
| 5 Coal | | | | | 24,700 |
| 6 Crop residues | | | | | 14,700 |
| 7 Dung | | | | | 13,600 |
| Ethanol | | | | | 26,800 |
| 8 Average Hardwood | Average Hardwood | | | | 19,734 |
| 9 Average Softwood (Conifer) | Average Softwood (conifer) | | | | 20,817 |
| 10 Abies Balsamea (Balsam Fir) | Abies Balsamea | balsam fir | | | 18,916 |
| 11 Acacia Auriculiformis (Ear-Leaf Acacia, Ear-Pod Wattle) | Acacia Auriculiformis | ear-leaf acacia, ear-pod wattle | 4800 | 4900 | 4850 |
| 12 Acacia Decurrens (King Wattle, Green Wattle, Sydney Black Wattle) | Acacia Decurrens | king wattle, green wattle, Sydney black wattle | | | 18,700 |
| 13 Acacia Farnesiana (Sweet Acacia, Sweet Wattle) | Acacia Farnesiana | sweet acacia, sweet wattle | | | 19,200 |
| 14 Acacia Leucophloea (Kikar, Kuteera Gum) | Acacia Leucophloea | kikar, kuteera gum | | | 21,800 |
| 15 Acacia Mearnsi (Black Wattle) | Acacia Mearnsi | black wattle | 4650 | | 4650 |
| 16 Acacia Nilotica (Egyptian Thorn, Babul (India), Babar (Pakistan)) | Acacia Nilotica | egyptian thorn, babul (India), babar (P) | 4800 | 4950 | 4875 |
| 17 Acacia Tortilis (Umbrella Thorn) | Acacia Tortilis | umbrella thorn | 4400 | | 4400 |
| 18 Acer Rubrum (Red Maple) | Acer Rubrum | red maple | | | 18,545 |
| 19 Albizia Falcataria (Batai, Malucca Albizia, Placata) | Albizia Falcataria | batai, malucca albizia, placata | | | 18,100 |
| 20 Albizia Lebbek (Lebbek, East Indian Walnut Tree) | Albizia Lebbek | lebbek, East Indian walnut tree; | 5200 | | 5200 |
| 21 Albizia Procera (Albicia, Silver Bark Rain Tree) | Albizia Procera | albicia, silver bark rain tree | | | 19,700 |
| 22 Alnus Nepalensis (Nepal Alder) | Alnus Nepalensis | Nepal alder | | | 17,150 |
| 23 Alnus Rubra (Red Alder) | Alnus Rubra | red alder | 4600 | | 4600 |
| 24 Alnus Rubra (Red Alder) | Alnus Rubra | red alder | | | 18,545 |

(h) Sample change log sheet

| | | | | | | | | | |
|---|--|--|--|--|--|--|--|--|--|
| Fixed an error so that thermocouple calibration is correctly read for all sensor boxes | | | | | | | | | |
| 39. Sensor Box WBT 4.2.3 Feb.3.2015 no catalog | | | | | | | | | |
| Fixed framework of single grav filter for whole test. Further documentation is provided in "Single filter spreadsheet development feb 3.docx" | | | | | | | | | |
| 40. Sensor Box WBT 4.2.3 Jun.18.2015 | | | | | | | | | |
| More inputs for the GACC stove performance catalog were provided in the results tab. | | | | | | | | | |
| 41. Sensor Box WBT 4.2.3 Aug.31.2015 | | | | | | | | | |
| Fixed charcoal remaining catalog entry | | | | | | | | | |
| Added weight of charcoal container to catalog entries | | | | | | | | | |
| 42. Sensor Box WBT 4.2.3 Sep.28.2015 | | | | | | | | | |
| The macro was fixed to work with SB < 2008 | | | | | | | | | |
| 42. Sensor Box WBT 4.2.3 Nov.10.2015 | | | | | | | | | |
| Added support for BC system | | | | | | | | | |
| 43. made PM light scattering results be totally overrided by grav measurements. Realtime graphs are still dependent on the background | | | | | | | | | |
| 44. sensor box processing wbt 4.2.3 Dec.5.2016 | | | | | | | | | |
| removed the gravimetric altitude correction after experiments showed that it was not nessary | | | | | | | | | |
| 45. sensor box processing wbt 4.2.3 Nov. 11. 2017 | | | | | | | | | |
| added support for 3XXX series sensor box | | | | | | | | | |
| 46. sensor box processing wbt 4.2.3 Jan 31. 2018 | | | | | | | | | |

Appendix 7: TG and DTG results for the charcoal fines

| Time (min) | Temperature (°C) | Original weight (g) | Final weight (g) | Weight (%) | ΔT (min) | Weight loss (g) | DTG (g/min) |
|-------------------|-------------------------|----------------------------|-------------------------|-------------------|-----------------|------------------------|--------------------|
| 0.0 | 24.1 | 1.2054 | 1.2054 | 100.0 | 0 | 0 | 0 |
| 4.6 | 86.3 | 1.2054 | 1.2081 | 100.2 | 4.6 | -0.0027 | -0.000586232 |
| 10.2 | 104.1 | 1.2054 | 1.2016 | 99.7 | 5.6 | 0.0065 | 0.0011533 |
| 15.9 | 105.0 | 1.2054 | 1.1887 | 98.6 | 5.6 | 0.0129 | 0.002298124 |
| 21.5 | 104.9 | 1.2054 | 1.1738 | 97.4 | 5.6 | 0.0149 | 0.002651536 |
| 27.1 | 105.4 | 1.2054 | 1.1610 | 96.3 | 5.6 | 0.0128 | 0.002293942 |
| 32.7 | 105.4 | 1.2054 | 1.1515 | 95.5 | 5.6 | 0.0095 | 0.001681657 |
| 38.3 | 104.9 | 1.2054 | 1.1451 | 95.0 | 5.6 | 0.0064 | 0.001144807 |
| 43.9 | 105.0 | 1.2054 | 1.1410 | 94.7 | 5.6 | 0.0041 | 0.000735044 |
| 49.6 | 104.8 | 1.2054 | 1.1382 | 94.4 | 5.6 | 0.0028 | 0.000492095 |
| 55.2 | 104.7 | 1.2054 | 1.1364 | 94.3 | 5.6 | 0.0018 | 0.000325444 |
| 60.8 | 104.6 | 1.2054 | 1.1350 | 94.2 | 5.6 | 0.0014 | 0.00024273 |
| 66.4 | 105.0 | 1.2054 | 1.1341 | 94.1 | 5.6 | 0.0009 | 0.000154014 |
| 72.0 | 105.7 | 1.2054 | 1.1333 | 94.0 | 5.6 | 0.0008 | 0.000143569 |
| 77.7 | 276.3 | 1.2054 | 1.1389 | 94.5 | 5.7 | -0.0055 | -0.00097076 |
| 83.3 | 456.6 | 1.2054 | 1.1150 | 92.5 | 5.6 | 0.0239 | 0.004275149 |
| 88.9 | 615.0 | 1.2054 | 1.0529 | 87.3 | 5.6 | 0.0620 | 0.011111642 |
| 94.5 | 719.5 | 1.2054 | 0.9853 | 81.7 | 5.6 | 0.0676 | 0.012076786 |
| 100.1 | 827.8 | 1.2054 | 0.9270 | 76.9 | 5.6 | 0.0583 | 0.010415476 |
| 105.7 | 903.7 | 1.2054 | 0.8903 | 73.9 | 5.6 | 0.0367 | 0.006550595 |
| 111.3 | 915.5 | 1.2054 | 0.8801 | 73.0 | 5.6 | 0.0102 | 0.001823857 |
| 116.8 | 915.1 | 1.2054 | 0.8709 | 72.2 | 5.6 | 0.0092 | 0.001653134 |
| 122.5 | 898.7 | 1.2054 | 0.8603 | 71.4 | 5.7 | 0.0106 | 0.001869863 |
| 128.1 | 864.7 | 1.2054 | 0.8526 | 70.7 | 5.6 | 0.0076 | 0.001368432 |
| 133.6 | 832.7 | 1.2054 | 0.8458 | 70.2 | 5.6 | 0.0069 | 0.001239 |
| 139.2 | 803.0 | 1.2054 | 0.8399 | 69.7 | 5.6 | 0.0058 | 0.001044179 |
| 144.8 | 775.0 | 1.2054 | 0.8348 | 69.2 | 5.6 | 0.0052 | 0.000928144 |
| 150.4 | 748.2 | 1.2054 | 0.8335 | 69.1 | 5.6 | 0.0013 | 0.000225519 |
| 156.2 | 749.9 | 1.2054 | 0.8285 | 68.7 | 5.8 | 0.0050 | 0.000875362 |
| 161.8 | 749.6 | 1.2054 | 0.7910 | 65.6 | 5.6 | 0.0375 | 0.006690476 |
| 167.4 | 749.9 | 1.2054 | 0.7450 | 61.8 | 5.6 | 0.0460 | 0.008183383 |
| 173.0 | 750.1 | 1.2054 | 0.6978 | 57.9 | 5.6 | 0.0473 | 0.00842495 |
| 178.6 | 749.7 | 1.2054 | 0.6508 | 54.0 | 5.6 | 0.0470 | 0.008359091 |
| Time (min) | Temperat ure (°C) | Original weight (g) | Final weight (g) | Weight (%) | ΔT (min) | Weight loss (g) | DTG (g/min) |

| Time (min) | Temperature (°C) | Original weight (g) | Final weight (g) | Weight (%) | ΔT (min) | Weight loss (g) | DTG (g/min) |
|-------------------|-------------------------|----------------------------|-------------------------|-------------------|-----------------|------------------------|--------------------|
| 184.2 | 749.7 | 1.2054 | 0.6044 | 50.1 | 5.6 | 0.0464 | 0.008285714 |
| 189.8 | 749.7 | 1.2054 | 0.5588 | 46.4 | 5.6 | 0.0456 | 0.008142262 |
| 195.4 | 749.7 | 1.2054 | 0.5138 | 42.6 | 5.6 | 0.0449 | 0.008000593 |
| 201.0 | 749.7 | 1.2054 | 0.4699 | 39.0 | 5.6 | 0.0440 | 0.007873433 |
| 206.6 | 749.7 | 1.2054 | 0.4264 | 35.4 | 5.6 | 0.0434 | 0.00771767 |
| 212.2 | 750.1 | 1.2054 | 0.3842 | 31.9 | 5.6 | 0.0422 | 0.007572311 |
| 217.8 | 750.0 | 1.2054 | 0.3426 | 28.4 | 5.6 | 0.0416 | 0.007452789 |
| 223.4 | 750.0 | 1.2054 | 0.3015 | 25.0 | 5.6 | 0.0411 | 0.007346574 |
| 229.0 | 750.1 | 1.2054 | 0.2607 | 21.6 | 5.6 | 0.0408 | 0.007300199 |
| 234.5 | 750.2 | 1.2054 | 0.2208 | 18.3 | 5.6 | 0.0399 | 0.0071886 |
| 240.1 | 750.2 | 1.2054 | 0.1823 | 15.1 | 5.6 | 0.0385 | 0.006859941 |
| 245.7 | 750.2 | 1.2054 | 0.1497 | 12.4 | 5.6 | 0.0325 | 0.005803766 |
| 251.4 | 750.1 | 1.2054 | 0.1241 | 10.3 | 5.6 | 0.0257 | 0.004578791 |
| 257.0 | 750.0 | 1.2054 | 0.1099 | 9.1 | 5.6 | 0.0141 | 0.002524405 |
| 262.5 | 750.0 | 1.2054 | 0.1020 | 8.5 | 5.6 | 0.0079 | 0.001420299 |
| 268.1 | 750.0 | 1.2054 | 0.0983 | 8.2 | 5.6 | 0.0037 | 0.000654113 |
| 273.8 | 749.9 | 1.2054 | 0.0978 | 8.1 | 5.6 | 0.0005 | 9.5549E-05 |
| 279.4 | 749.9 | 1.2054 | 0.0975 | 8.1 | 5.6 | 0.0003 | 5.85222E-05 |

Appendix 8: TG and DTG results for the binder

| Time (min) | Temperature (°C) | Original weight (g) | Final weight (g) | Weight (%) | Weight loss (g) | ΔT (min) | DTG (g/min) |
|-------------------|-------------------------|----------------------------|-------------------------|-------------------|------------------------|-----------------|--------------------|
| 0.0 | 24.1 | 1.1763 | 1.1763 | 100.0 | 0 | 0.0 | 0 |
| 5.3 | 90.5 | 1.1763 | 1.1772 | 100.1 | -0.0009 | 5.3 | -0.0001683 |
| 10.9 | 104.1 | 1.1763 | 1.1747 | 99.9 | 0.0025 | 5.6 | 0.0004467 |
| 16.6 | 105.3 | 1.1763 | 1.1712 | 99.6 | 0.0034 | 5.6 | 0.0006115 |
| 22.2 | 105.4 | 1.1763 | 1.1676 | 99.3 | 0.0037 | 5.6 | 0.0006537 |
| 27.8 | 104.9 | 1.1763 | 1.1644 | 99.0 | 0.0032 | 5.6 | 0.0005727 |
| 33.4 | 105.3 | 1.1763 | 1.1603 | 98.6 | 0.0040 | 5.6 | 0.0007169 |
| 39.0 | 105.3 | 1.1763 | 1.1565 | 98.3 | 0.0039 | 5.6 | 0.0006855 |
| 44.6 | 105.3 | 1.1763 | 1.1527 | 98.0 | 0.0038 | 5.6 | 0.0006706 |
| 50.3 | 105.1 | 1.1763 | 1.1481 | 97.6 | 0.0046 | 5.6 | 0.0008216 |
| 55.9 | 104.7 | 1.1763 | 1.1444 | 97.3 | 0.0037 | 5.6 | 0.0006636 |
| 61.5 | 104.6 | 1.1763 | 1.1392 | 96.8 | 0.0051 | 5.6 | 0.000911 |
| 67.1 | 105.8 | 1.1763 | 1.1346 | 96.5 | 0.0046 | 5.6 | 0.0008269 |
| 72.7 | 105.0 | 1.1763 | 1.1309 | 96.1 | 0.0037 | 5.6 | 0.0006678 |
| 78.4 | 304.8 | 1.1763 | 1.1381 | 96.8 | -0.0072 | 5.7 | -0.0012623 |
| 84.0 | 476.4 | 1.1763 | 1.0512 | 89.4 | 0.0868 | 5.6 | 0.0155543 |
| 89.6 | 630.6 | 1.1763 | 0.0165 | 1.4 | 1.0347 | 5.6 | 0.1853257 |
| 95.2 | 732.2 | 1.1763 | 0.0118 | 1.0 | 0.0047 | 5.6 | 0.0008452 |
| 100.8 | 840.8 | 1.1763 | 0.0086 | 0.7 | 0.0032 | 5.6 | 0.0005655 |
| 106.4 | 907.5 | 1.1763 | 0.0083 | 0.7 | 0.0003 | 5.6 | 5.991E-05 |
| 112.0 | 915.5 | 1.1763 | 0.0088 | 0.7 | -0.0005 | 5.6 | -8.571E-05 |
| 117.5 | 914.9 | 1.1763 | 0.0084 | 0.7 | 0.0004 | 5.6 | 7.164E-05 |
| 123.2 | 894.1 | 1.1763 | 0.0069 | 0.6 | 0.0014 | 5.7 | 0.0002532 |
| 128.8 | 860.4 | 1.1763 | 0.0069 | 0.6 | 0.0000 | 5.6 | -1.796E-06 |
| 134.3 | 828.6 | 1.1763 | 0.0067 | 0.6 | 0.0002 | 5.6 | 4.054E-05 |
| 139.9 | 799.3 | 1.1763 | 0.0068 | 0.6 | -0.0001 | 5.6 | -2.593E-05 |
| 145.5 | 771.5 | 1.1763 | 0.0065 | 0.5 | 0.0004 | 5.6 | 7.096E-05 |
| 151.1 | 744.9 | 1.1763 | 0.0076 | 0.6 | -0.0012 | 5.6 | -0.0002044 |
| 156.9 | 749.3 | 1.1763 | 0.0048 | 0.4 | 0.0028 | 5.8 | 0.0004878 |
| 162.5 | 749.3 | 1.1763 | 0.0048 | 0.4 | -0.0001 | 5.6 | -8.929E-06 |
| 168.1 | 749.2 | 1.1763 | 0.0048 | 0.4 | 0.0000 | 5.6 | 0 |
| 173.7 | 749.3 | 1.1763 | 0.0048 | 0.4 | 0.0000 | 5.6 | 0 |
| 179.3 | 748.9 | 1.1763 | 0.0048 | 0.4 | 0.0001 | 5.6 | 8.902E-06 |
| Time (min) | Temperature (°C) | Original weight (g) | Final weight (g) | Weight (%) | Weight loss (g) | ΔT (min) | DTG (g/min) |

| Time (min) | Temperature (°C) | Original weight (g) | Final weight (g) | Weight (%) | Weight loss (g) | ΔT (min) | DTG (g/min) |
|-------------------|-------------------------|----------------------------|-------------------------|-------------------|------------------------|-----------------|--------------------|
| 184.9 | 749.0 | 1.1763 | 0.0047 | 0.4 | 0.0000 | 5.6 | 8.902E-06 |
| 190.5 | 749.0 | 1.1763 | 0.0048 | 0.4 | 0.0000 | 5.6 | -8.929E-06 |
| 196.1 | 749.0 | 1.1763 | 0.0048 | 0.4 | -0.0001 | 5.6 | -8.902E-06 |
| 201.7 | 749.0 | 1.1763 | 0.0049 | 0.4 | 0.0000 | 5.6 | -8.955E-06 |
| 207.3 | 748.9 | 1.1763 | 0.0048 | 0.4 | 0.0000 | 5.6 | 8.915E-06 |
| 212.9 | 749.2 | 1.1763 | 0.0048 | 0.4 | 0.0000 | 5.6 | 0 |
| 218.5 | 749.2 | 1.1763 | 0.0049 | 0.4 | 0.0000 | 5.6 | -8.969E-06 |
| 224.1 | 749.2 | 1.1763 | 0.0047 | 0.4 | 0.0002 | 5.6 | 3.571E-05 |
| 229.7 | 749.3 | 1.1763 | 0.0048 | 0.4 | -0.0002 | 5.6 | -2.683E-05 |
| 235.2 | 749.5 | 1.1763 | 0.0048 | 0.4 | 0.0000 | 5.6 | 0 |
| 240.8 | 750.0 | 1.1763 | 0.0048 | 0.4 | 0.0000 | 5.6 | 0 |
| 246.4 | 749.7 | 1.1763 | 0.0048 | 0.4 | 0.0000 | 5.6 | 0 |
| 252.1 | 749.6 | 1.1763 | 0.0048 | 0.4 | 0.0000 | 5.6 | 0 |
| 257.7 | 749.5 | 1.1763 | 0.0050 | 0.4 | -0.0001 | 5.6 | -2.675E-05 |
| 263.2 | 750.0 | 1.1763 | 0.0049 | 0.4 | 0.0001 | 5.6 | 1.791E-05 |
| 268.8 | 749.9 | 1.1763 | 0.0049 | 0.4 | 0.0000 | 5.6 | 0 |
| 274.5 | 750.0 | 1.1763 | 0.0048 | 0.4 | 0.0000 | 5.6 | 8.902E-06 |
| 280.1 | 749.9 | 1.1763 | 0.0049 | 0.4 | 0.0000 | 5.6 | -8.876E-06 |

Appendix 9: Proximate analysis of charcoal fines (C), and binder (B)

| Sample | Weight (g) | Highly volatile matter (%) | Medium volatile matter (%) | Ash (%) | Fixed carbon (%) |
|-----------------------|-------------------|-----------------------------------|-----------------------------------|----------------|-------------------------|
| Charcoal fines | | | | | |
| C1 | 1.328 | 6.03 | 22.13 | 7.72 | 64.12 |
| C2 | 1.1282 | 6.07 | 21.78 | 7.70 | 64.44 |
| C3 | 1.1601 | 6.07 | 21.94 | 7.66 | 64.33 |
| AVG | | 6.06 | 21.95 | 7.69 | 64.30 |
| STD | | 0.02 | 0.18 | 0.03 | 0.17 |
| Binder | | | | | |
| B1 | 1.1266 | 4.05 | 95.93 | 0.04 | -0.02 |
| B2 | 1.1667 | 5.05 | 95.01 | -0.09 | 0.03 |
| B3 | 1.1834 | 5.04 | 94.96 | -0.02 | 0.01 |
| AVG | | 4.71 | 95.30 | -0.03 | 0.01 |
| STD | | 0.58 | 0.54 | 0.06 | 0.02 |

Appendix 10: Ultimate analysis of charcoal fines (C), and binder (B)

| Sample | Weight (mg) | Nitrogen (N) | Carbon (C) | Hydrogen (H) | Oxygen (O) |
|-----------------------|--------------------|---------------------|-------------------|---------------------|-------------------|
| Binder | | | | | |
| B1 | 2.5 | 1.04 | 70.83 | 9.57 | 6.82 |
| B2 | 2.6 | 1.20 | 84.53 | 11.53 | 6.47 |
| B3 | 2.8 | 1.07 | 83.56 | 11.43 | 5.59 |
| B4 | 2.5 | 1.00 | 91.92 | 9.57 | |
| B5 | 2.4 | 1.06 | 79.30 | 11.53 | |
| B6 | 2.7 | 1.30 | 76.08 | 11.43 | |
| AVG | | 1.11 | 81.04 | 10.84 | 6.29 |
| STD | | 0.11 | 7.33 | 0.99 | 0.63 |
| Charcoal fines | | | | | |
| C1 | 2.1 | 1.95 | 73.39 | 2.06 | 7.19 |
| C2 | 2.8 | 1.67 | 75.97 | 2.13 | 6.98 |
| C3 | 2.8 | 1.63 | 67.57 | 1.93 | 6.55 |
| C4 | 2.7 | 1.68 | 70.50 | 2.26 | |
| C5 | 2.3 | 1.69 | 68.57 | 2.25 | |
| C6 | 2.6 | 1.71 | 74.39 | 2.41 | |
| AVG | | 1.72 | 71.73 | 2.17 | 6.91 |
| STD | | 0.11 | 3.36 | 0.17 | 0.33 |

Appendix 11: Higher heating value of charcoal fines (C), and binder (B)

| Sample | m±0.0001 g | HHV (MJ/kg) |
|-----------------------|-------------------|--------------------|
| Charcoal fines | | |
| C1 | 0.7955 | 27.9 |
| C2 | 0.8244 | 27.9 |
| C3 | 0.6123 | 28.2 |
| C4 | 0.6635 | 28.2 |
| C5 | 0.7823 | 28.3 |
| AVG | | 28.1 |
| STD | | 0.2 |
| Binder | | |
| B1 | 0.6238 | 40.2 |
| B2 | 0.6022 | 39.9 |
| B3 | 0.539 | 40.5 |
| B4 | 0.7336 | 39.9 |
| B5 | 0.6561 | 40.4 |
| AVG | | 40.2 |
| STD | | 0.3 |

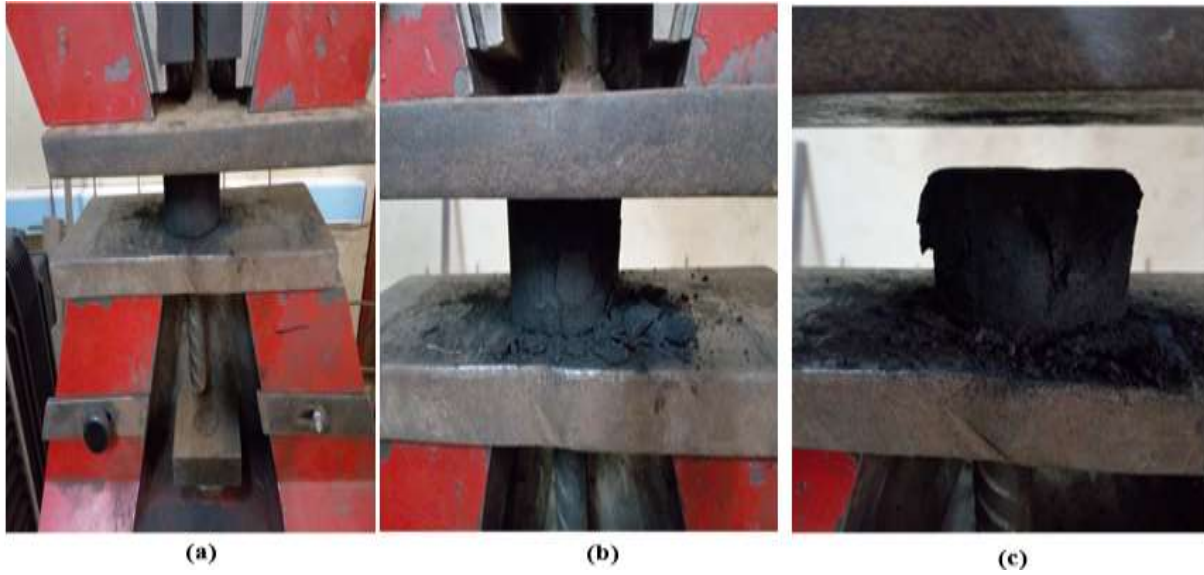
Appendix 12: Outside diameter (d_1), inside diameter (d_2), height (h), mass (m), volume (V), and density (ρ) of the briquettes

| Briquette | $d_1 \pm 0.005 \text{cm}$ | $d_2 \pm 0.005 \text{cm}$ | $h \pm 0.005 \text{cm}$ | V, cm^3 | $m \pm 0.0001 \text{gm}$ | ρ , g/cm^3 |
|------------|---------------------------|---------------------------|-------------------------|------------------|--------------------------|--------------------------|
| B25 | 5.47 | 2 | 4.36 | 88.72 | 64.5046 | 0.727 |
| B25 | 5.5 | 1.94 | 4.565 | 94.91 | 70.2795 | 0.740 |
| B25 | 5.41 | 1.9 | 3.7 | 74.52 | 58.7551 | 0.788 |
| B25 | 5.55 | 2.1 | 4.435 | 91.88 | 70.4925 | 0.767 |
| B25 | 5.45 | 2.2 | 4.645 | 90.66 | 74.9162 | 0.826 |
| AVG | 5.476 | 2.028 | 4.341 | 88.14 | 67.78958 | 0.770 |
| STD | 0.053 | 0.122 | 0.375 | 7.937 | 6.259 | 0.039 |
| B30 | 5.5 | 1.94 | 4.45 | 92.52 | 79.3883 | 0.858 |
| B30 | 5.5 | 1.96 | 4.43 | 91.84 | 80.735 | 0.879 |
| B30 | 5.435 | 2 | 4.51 | 90.42 | 79.9786 | 0.885 |
| B30 | 5.49 | 2 | 4.4 | 90.29 | 80.2153 | 0.888 |
| B30 | 5.485 | 1.995 | 4.465 | 91.50 | 80.005 | 0.874 |
| AVG | 5.482 | 1.979 | 4.451 | 91.31 | 80.06444 | 0.877 |
| STD | 0.027 | 0.027 | 0.041 | 0.952 | 0.485 | 0.012 |
| B35 | 5.49 | 1.95 | 4.43 | 91.59 | 87.3779 | 0.954 |
| B35 | 5.475 | 1.985 | 4.52 | 92.38 | 86.1845 | 0.933 |
| B35 | 5.45 | 1.985 | 4.41 | 89.19 | 86.8743 | 0.974 |
| B35 | 5.505 | 2 | 4.535 | 93.65 | 86.717 | 0.926 |
| B35 | 5.51 | 2 | 4.425 | 91.57 | 88.6533 | 0.968 |
| AVG | 5.486 | 1.984 | 4.464 | 91.67 | 87.1614 | 0.951 |
| STD | 0.024 | 0.020 | 0.059 | 1.628 | 0.936 | 0.021 |
| B40 | 5.46 | 1.99 | 4.545 | 92.23 | 94.5426 | 1.025 |
| B40 | 5.48 | 1.98 | 4.355 | 89.26 | 94.8467 | 1.063 |
| B40 | 5.47 | 1.985 | 4.35 | 88.72 | 93.4495 | 1.053 |
| B40 | 5.49 | 1.97 | 4.45 | 91.73 | 93.6252 | 1.021 |
| B40 | 5.48 | 1.99 | 4.35 | 89.02 | 90.8448 | 1.020 |
| AVG | 5.476 | 1.983 | 4.410 | 90.19 | 93.46176 | 1.036 |
| STD | 0.011 | 0.008 | 0.087 | 1.654 | 1.578 | 0.020 |

Appendix 13: Impact resistance index (IRI) of the briquettes

| Briquette | Drops, n_d | Pieces, n_p | IRI |
|------------------|--------------------------------|---------------------------------|------------|
| B25 | 1 | 30 | 3.33 |
| B25 | 1 | 32 | 3.13 |
| B25 | 1 | 40 | 2.50 |
| B25 | 1 | 35 | 2.86 |
| B25 | 1 | 37 | 2.70 |
| AVG | | | 2.90 |
| STD | | | 0.33 |
| B30 | 1 | 4 | 25.00 |
| B30 | 1 | 9 | 11.11 |
| B30 | 2 | 12 | 16.67 |
| B30 | 1 | 6 | 16.67 |
| B30 | 2 | 13 | 15.38 |
| AVG | | | 16.97 |
| STD | | | 5.04 |
| B35 | 1 | 2 | 50.00 |
| B35 | 1 | 2 | 50.00 |
| B35 | 2 | 4 | 50.00 |
| B35 | 4 | 4 | 100.00 |
| B35 | 2 | 4 | 50.00 |
| AVG | | | 60.00 |
| STD | | | 22.36 |
| B40 | 1 | 2 | 50.00 |
| B40 | 1 | 2 | 50.00 |
| B40 | 2 | 2 | 100.00 |
| B40 | 2 | 2 | 100.00 |
| B40 | 2 | 3 | 66.67 |
| AVG | | | 73.33 |
| STD | | | 25.28 |

Appendix 14: Testing compressive strength of briquettes; (a) flat surface of briquette placed between horizontal metal plates, (b) beginning of experiment, (c) end of experiment



Appendix 15: Testing splitting tensile strength of briquettes; (a) &(b) curved surface of briquette placed between horizontal metal plates



(a)



(b)

Appendix 16: Compressive strength of briquettes

| Briquette | Outside diameter, $d_1 \pm 0.05\text{mm}$ | Inside diameter, $d_2 \pm 0.05\text{mm}$ | Height, $h \pm 0.05\text{mm}$ | Area, mm^2 | Force at break, F_b (N) | Force at peak, F_p (N) | Stress at break, S_b (N/mm^2) | Stress at peak, S_p (N/mm^2) |
|------------|---|--|-------------------------------|---------------------|---------------------------|--------------------------|---|--|
| B25 | 55.35 | 19.95 | 43.1 | 2094.44 | 3176 | 4119 | 1.52 | 1.97 |
| B25 | 54.8 | 20 | 42 | 2045.27 | 3738 | 5169 | 1.83 | 2.53 |
| B25 | 54.95 | 20 | 42 | 2058.21 | 2789 | 5888 | 1.36 | 2.25 |
| AVG | | | | | | | | 2.25 |
| STD | | | | | | | | 0.28 |
| B30 | 54.5 | 19.9 | 43.65 | 2022.64 | 7221 | 7915 | 3.57 | 3.91 |
| B30 | 55 | 20 | 41.1 | 2062.53 | 6889 | 7837 | 3.34 | 3.80 |
| B30 | 54.9 | 20 | 41.4 | 2053.89 | 6787 | 8395 | 3.30 | 4.09 |
| AVG | | | | | | | | 3.93 |
| STD | | | | | | | | 0.14 |
| B35 | 54.65 | 20 | 44.55 | 2032.37 | 15351 | 17032 | 7.55 | 8.38 |
| B35 | 55 | 20.2 | 41.45 | 2056.21 | 14639 | 15257 | 7.12 | 7.42 |
| B35 | 55 | 19.9 | 43.35 | 2065.66 | 16917.999 | 17283.001 | 8.19 | 8.37 |
| AVG | | | | | | | | 8.06 |
| STD | | | | | | | | 0.55 |
| B40 | 54.6 | 20 | 42.45 | 2028.08 | 19005 | 19617 | 9.37 | 9.67 |
| B40 | 54.6 | 19.95 | 42.42 | 2029.65 | 28687 | 28873 | 14.13 | 14.23 |
| B40 | 54.9 | 20 | 43.3 | 2053.89 | 18269 | 18324 | 8.89 | 8.92 |
| AVG | | | | | | | | 10.94 |
| STD | | | | | | | | 2.87 |

Appendix 17: Splitting tensile strength of briquettes

| Briquette | Outside diameter, $d_1 \pm 0.05 \text{ mm}$ | Inside diameter, $d_2 \pm 0.05 \text{ mm}$ | Height, $h \pm 0.05 \text{ mm}$ | Area, mm^2 | Force at peak, F_p (N) | Stress at peak, S_p (N/mm^2) |
|------------|--|---|------------------------------------|---------------------|-----------------------------|--|
| B25 | 54.9 | 19.9 | 42.55 | 3667.51 | 331 | 0.09 |
| B25 | 54.5 | 19.9 | 43 | 3679.30 | 303 | 0.08 |
| B25 | 55 | 19.8 | 43.5 | 3756.23 | 317 | 0.08 |
| AVG | | | | | | 0.09 |
| STD | | | | | | 0.00 |
| B30 | 55 | 19.95 | 43.5 | 3756.23 | 723 | 0.19 |
| B30 | 54.8 | 19.6 | 41.6 | 3579.10 | 801 | 0.22 |
| B30 | 54.6 | 19.9 | 41.62 | 3567.75 | 769 | 0.22 |
| AVG | | | | | | 0.21 |
| STD | | | | | | 0.02 |
| B35 | 54.8 | 20 | 43.15 | 3712.45 | 1155 | 0.31 |
| B35 | 55 | 20 | 42.35 | 3656.92 | 1291 | 0.35 |
| B35 | 54.5 | 20 | 42.7 | 3653.63 | 1029 | 0.28 |
| AVG | | | | | | 0.32 |
| STD | | | | | | 0.04 |
| B40 | 54.45 | 20 | 42.35 | 3620.35 | 1534 | 0.42 |
| B40 | 54.6 | 20 | 42 | 3600.32 | 1501 | 0.42 |
| B40 | 54.45 | 20 | 41.5 | 3547.69 | 1528 | 0.43 |
| AVG | | | | | | 0.42 |
| STD | | | | | | 0.01 |

Appendix 18: Sample results from the materials testing machine (Testometric, FS300AT)

a) Compressive strength test results for briquettes B25

Testometric
materials testing machines

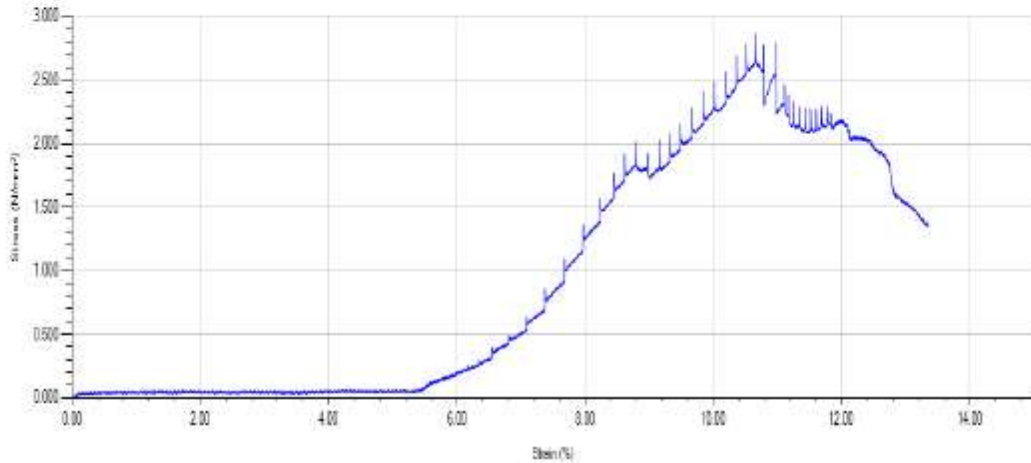
winTest™
Analysis

25%binder
SPECIEN 1

Sample : 1
Height : 42
Outer Diameter : 54.95
Inner Diameter : 20

Machine No. : 0300-02032
Test Name : Compression For Briquettes
Test Type : Compression
Test Date : 23/01/2020 09:41
Test Speed : 0.500 mm/min
Preload : Off
Sample Height : 42.000 mm

| Test No | Area (m ²) | Force @ Break (N) | EN826 Comp. Modulus of Elasticity (N/mm ²) | Def. @ Break (mm) | Force @ Peak (N) | Energy to Break (J) | Measured Volume (m ³) |
|---------|------------------------|-------------------|--|-------------------|------------------|---------------------|-----------------------------------|
| 1 | 0.002 | 2789.000 | 79.172 | 5.607 | 5888.000 | 10.456 | 0.000 |



b) Compressive strength test results for briquettes B30

Testometric
materials testing machines

winTest™
Analysis

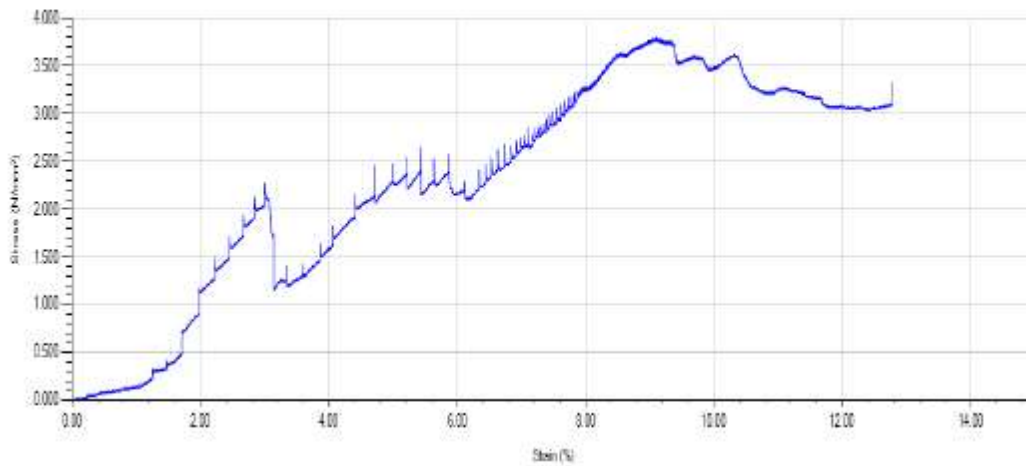
30% Binder

Briquette Sample1

Sample : 1
Height : 41.1
Outer Diameter : 55
Inner Diameter : 20

Machine No. : 0300-02032
Test Name : Compression For Briquettes
Test Type : Compression
Test Date : 23/01/2020 16:22
Test Speed : 0.500 mm/min
Preload : Off
Sample Height : 41.100 mm

| Test No | Area (m ²) | Force @ Break (N) | EN826 Comp. Modulus of Elasticity (N/mm ²) | Def. @ Break (mm) | Force @ Peak (N) | Energy to Break (J) | Measured Volume (m ³) |
|---------|------------------------|-------------------|--|-------------------|------------------|---------------------|-----------------------------------|
| 1 | 0.002 | 6889.000 | 107.820 | 5.250 | 7837.000 | 24.730 | 0.000 |



c) Compressive strength test results for briquettes B35

Testometric
materials testing machines

winTest™
Analysis

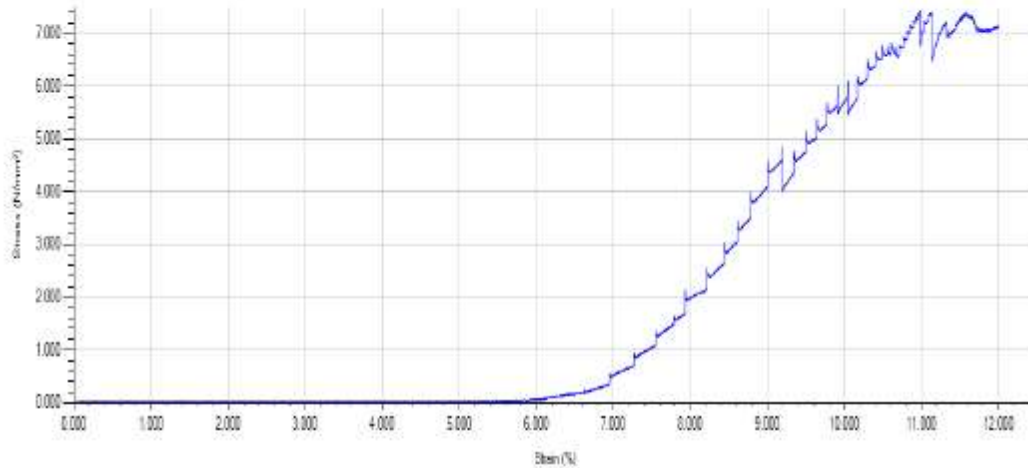
35% Binder

Briquette Sample 1

Sample : 1
Height : 41.45
Outer Diameter : 55
Inner Diameter : 20.2

Machine No. : 0300-02032
Test Name : Compression For Briquettes
Test Type : Compression
Test Date : 23/01/2020 15:47
Test Speed : 0.500 mm/min
Preload : Off
Sample Height : 41.450 mm

| Test No | Area (m ²) | Force @ Break (N) | EN826 Comp. Modulus of Elasticity (N/mm ²) | Def. @ Break (mm) | Force @ Peak (N) | Energy to Break (J) | Measured Volume (m ³) |
|---------|------------------------|-------------------|--|-------------------|------------------|---------------------|-----------------------------------|
| 1 | 0.002 | 14639.000 | 180.479 | 4.972 | 15257.000 | 19.410 | 0.000 |



d) Compressive strength test results for briquettes B40

Testometric
materials testing machines

winTest™
Analysis

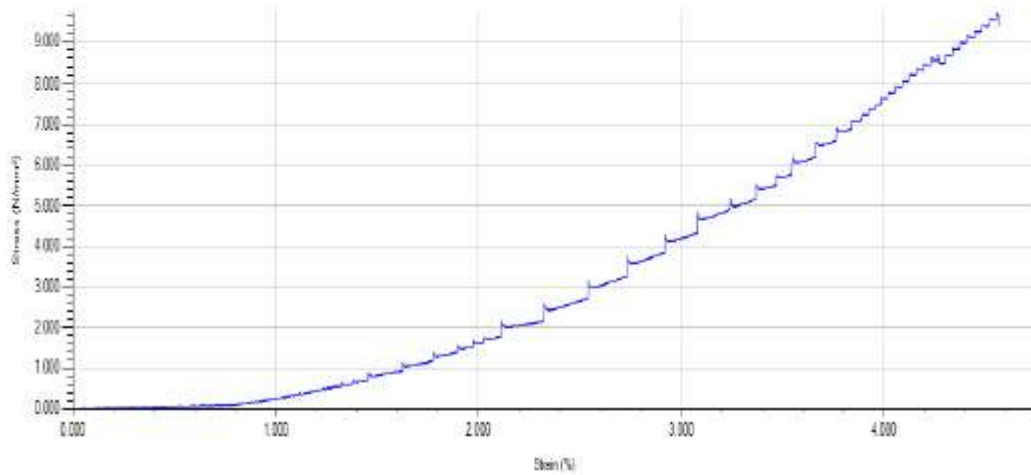
40% Binder

Briquette Sample1

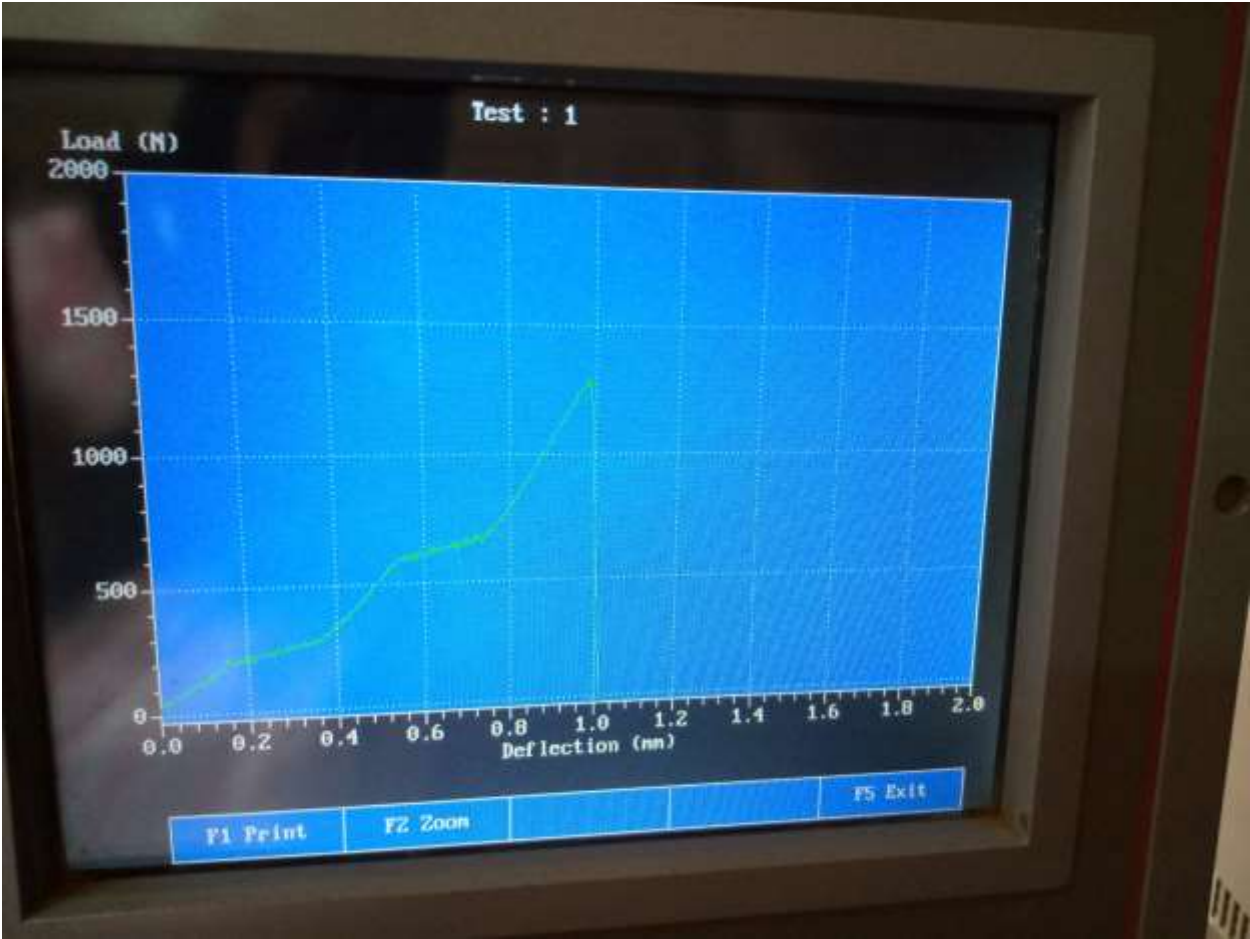
Sample : 2
Height : 42.45
Outer Diameter : 54.60
Inner Diameter : 20

Machine No. : 0300-02032
Test Name : Compression For Briquettes
Test Type : Compression
Test Date : 23/01/2020 15:06
Test Speed : 0.500 mm/min
Preload : Off
Sample Height : 42.450 mm

| Test No | Area (m ²) | Force @ Break (N) | EN826 Comp. Modulus of Elasticity (N/mm ²) | Def. @ Break (mm) | Force @ Peak (N) | Energy to Break (J) | Measured Volume (m ³) |
|---------|------------------------|-------------------|--|-------------------|------------------|---------------------|-----------------------------------|
| 1 | 0.002 | 19004.999 | 323.636 | 1.941 | 19617.001 | 12.453 | 0.000 |



Appendix 19: Sample results from the materials testing machine (Testometric, M500-25)



Appendix 20: Water resistance index (WRI) of the briquettes

| Briquette | Weight of briquette before, $w_1 \pm 0.0001$ g | Weight of briquette after, $w_2 \pm 0.0001$ g | Percentage of water absorbed, (%) | WRI (%) |
|------------|---|--|--------------------------------------|------------|
| B25 | 70.4905 | 70.967 | 0.68 | 99.32 |
| B25 | 60.2395 | 60.756 | 0.86 | 99.14 |
| B25 | 67.758 | 68.274 | 0.76 | 99.24 |
| B25 | 67.425 | 67.872 | 0.66 | 99.34 |
| B25 | 64.512 | 64.987 | 0.74 | 99.26 |
| AVG | | | | 99.26 |
| STD | | | | 0.08 |
| B30 | 77.676 | 78.223 | 0.70 | 99.30 |
| B30 | 78.8515 | 79.495 | 0.82 | 99.18 |
| B30 | 78.819 | 79.463 | 0.82 | 99.18 |
| B30 | 76.5746 | 77.132 | 0.73 | 99.27 |
| B30 | 74.3089 | 74.798 | 0.66 | 99.34 |
| AVG | | | | 99.26 |
| STD | | | | 0.07 |
| B35 | 88.993 | 89.614 | 0.70 | 99.30 |
| B35 | 88.2008 | 88.805 | 0.69 | 99.31 |
| B35 | 88.022 | 88.666 | 0.73 | 99.27 |
| B35 | 88.287 | 88.918 | 0.71 | 99.29 |
| B35 | 90.9385 | 91.685 | 0.82 | 99.18 |
| AVG | | | | 99.27 |
| STD | | | | 0.05 |
| B40 | 91.0731 | 91.6945 | 0.68 | 99.32 |
| B40 | 91.505 | 92.4 | 0.98 | 99.02 |
| B40 | 90.5797 | 91.082 | 0.55 | 99.45 |
| B40 | 92.6403 | 93.315 | 0.73 | 99.27 |
| B40 | 90.5175 | 91.05 | 0.59 | 99.41 |
| AVG | | | | 99.29 |
| STD | | | | 0.17 |

Appendix 21: TG and DTG results for briquette B25

| Time (min) | Temperature (°C) | Original weight (g) | Final weight (g) | Weight (%) | weight loss (g) | ΔT (min) | DTG (g/min) |
|-------------------|-------------------------|----------------------------|-------------------------|-------------------|------------------------|-----------------|--------------------|
| 0.0 | 24.1 | 1.1340 | 1.1340 | 100.0 | 0 | 0 | 0.000000 |
| 3.8 | 83.8 | 1.1340 | 1.1379 | 100.3 | -0.0039 | 3.8 | -0.001045 |
| 9.4 | 104.2 | 1.1340 | 1.1329 | 99.9 | 0.0050 | 5.6 | 0.000887 |
| 15.0 | 104.6 | 1.1340 | 1.1227 | 99.0 | 0.0102 | 5.6 | 0.001816 |
| 20.6 | 104.8 | 1.1340 | 1.1105 | 97.9 | 0.0122 | 5.6 | 0.002179 |
| 26.2 | 105.0 | 1.1340 | 1.1008 | 97.1 | 0.0097 | 5.6 | 0.001735 |
| 31.9 | 104.8 | 1.1340 | 1.0942 | 96.5 | 0.0066 | 5.6 | 0.001175 |
| 37.5 | 104.5 | 1.1340 | 1.0901 | 96.1 | 0.0040 | 5.6 | 0.000719 |
| 43.1 | 104.9 | 1.1340 | 1.0875 | 95.9 | 0.0027 | 5.6 | 0.000475 |
| 48.7 | 105.3 | 1.1340 | 1.0856 | 95.7 | 0.0019 | 5.6 | 0.000332 |
| 54.4 | 104.8 | 1.1340 | 1.0843 | 95.6 | 0.0013 | 5.6 | 0.000237 |
| 60.0 | 104.7 | 1.1340 | 1.0833 | 95.5 | 0.0009 | 5.6 | 0.000166 |
| 65.6 | 104.6 | 1.1340 | 1.0826 | 95.5 | 0.0007 | 5.6 | 0.000130 |
| 71.2 | 105.9 | 1.1340 | 1.0819 | 95.4 | 0.0007 | 5.6 | 0.000125 |
| 76.9 | 237.7 | 1.1340 | 1.0900 | 96.1 | -0.0081 | 5.7 | -0.001428 |
| 82.4 | 434.7 | 1.1340 | 1.0692 | 94.3 | 0.0208 | 5.6 | 0.003715 |
| 88.0 | 594.7 | 1.1340 | 0.7873 | 69.4 | 0.2819 | 5.6 | 0.050538 |
| 93.6 | 703.6 | 1.1340 | 0.7177 | 63.3 | 0.0696 | 5.6 | 0.012448 |
| 99.2 | 811.5 | 1.1340 | 0.6781 | 59.8 | 0.0396 | 5.6 | 0.007057 |
| 104.8 | 896.7 | 1.1340 | 0.6438 | 56.8 | 0.0344 | 5.6 | 0.006142 |
| 110.4 | 915.6 | 1.1340 | 0.6352 | 56.0 | 0.0085 | 5.6 | 0.001526 |
| 116.0 | 915.0 | 1.1340 | 0.6272 | 55.3 | 0.0081 | 5.6 | 0.001445 |
| 121.7 | 904.2 | 1.134 | 0.6172 | 54.4 | 0.0100 | 5.7 | 0.001753 |
| 127.3 | 869.7 | 1.134 | 0.6109 | 53.9 | 0.0063 | 5.6 | 0.001124 |
| 132.8 | 837.4 | 1.134 | 0.6047 | 53.3 | 0.0063 | 5.5 | 0.001133 |
| 138.4 | 807.0 | 1.134 | 0.5993 | 52.8 | 0.0054 | 5.6 | 0.000963 |
| 144.0 | 779.1 | 1.134 | 0.5945 | 52.4 | 0.0048 | 5.6 | 0.000859 |
| 149.6 | 751.9 | 1.134 | 0.5923 | 52.2 | 0.0022 | 5.6 | 0.000398 |
| 155.3 | 749.3 | 1.134 | 0.5807 | 51.2 | 0.0116 | 5.7 | 0.002011 |
| 160.9 | 750.1 | 1.134 | 0.5493 | 48.4 | 0.0314 | 5.6 | 0.005605 |
| 166.5 | 749.6 | 1.134 | 0.5064 | 44.7 | 0.0429 | 5.6 | 0.007610 |
| 172.2 | 749.7 | 1.134 | 0.4635 | 40.9 | 0.0429 | 5.6 | 0.007645 |
| 177.8 | 749.6 | 1.134 | 0.4211 | 37.1 | 0.0425 | 5.6 | 0.007584 |
| 183.4 | 749.5 | 1.134 | 0.3791 | 33.4 | 0.0420 | 5.6 | 0.007493 |
| 189.0 | 749.6 | 1.134 | 0.3377 | 29.8 | 0.0414 | 5.6 | 0.007386 |

| Time (min) | Temperature (°C) | Original weight (g) | Final weight (g) | Weight (%) | weight loss (g) | ΔT (min) | DTG (g/min) |
|-------------------|-------------------------|----------------------------|-------------------------|-------------------|------------------------|-----------------|--------------------|
| 194.6 | 749.6 | 1.134 | 0.2971 | 26.2 | 0.0406 | 5.6 | 0.007222 |
| 200.2 | 749.6 | 1.134 | 0.2573 | 22.7 | 0.0398 | 5.6 | 0.007114 |
| 205.8 | 749.7 | 1.134 | 0.2183 | 19.2 | 0.0390 | 5.6 | 0.006956 |
| 211.4 | 749.4 | 1.134 | 0.1806 | 15.9 | 0.0377 | 5.6 | 0.006739 |
| 217.0 | 749.8 | 1.134 | 0.1445 | 12.7 | 0.0361 | 5.6 | 0.006479 |
| 222.5 | 749.7 | 1.134 | 0.1111 | 9.8 | 0.0334 | 5.6 | 0.005982 |
| 228.1 | 750.0 | 1.134 | 0.0860 | 7.6 | 0.0251 | 5.6 | 0.004490 |
| 233.7 | 750.2 | 1.134 | 0.0719 | 6.3 | 0.0141 | 5.6 | 0.002532 |
| 239.3 | 750.0 | 1.134 | 0.0683 | 6.0 | 0.0036 | 5.6 | 0.000642 |
| 244.9 | 750.1 | 1.134 | 0.0681 | 6.0 | 0.0002 | 5.6 | 0.000030 |
| 250.5 | 750.1 | 1.134 | 0.0679 | 6.0 | 0.0002 | 5.6 | 0.000036 |
| 256.1 | 750.1 | 1.134 | 0.0676 | 6.0 | 0.0003 | 5.6 | 0.000047 |
| 261.7 | 749.9 | 1.134 | 0.0674 | 5.9 | 0.0002 | 5.6 | 0.000041 |
| 267.3 | 749.9 | 1.134 | 0.0672 | 5.9 | 0.0002 | 5.6 | 0.000036 |
| 272.9 | 750.0 | 1.134 | 0.0670 | 5.9 | 0.0002 | 5.6 | 0.000030 |
| 278.6 | 750.0 | 1.134 | 0.0669 | 5.9 | 0.0001 | 5.6 | 0.000018 |

Appendix 22: TG and DTG results for briquette B30

| Time (min) | Temperature (°C) | Original weight (g) | Final weight (g) | Weight (%) | Weight loss (g) | ΔT (min) | DTG (g/min) |
|-------------------|-------------------------|----------------------------|-------------------------|-------------------|------------------------|-----------------|--------------------|
| 0.0 | 24.1 | 1.1417 | 1.1417 | 100.0 | 0 | 0 | 0.000000 |
| 2.9 | 72.6 | 1.1417 | 1.1451 | 100.3 | -0.0034 | 2.9 | -0.001169 |
| 8.6 | 105.6 | 1.1417 | 1.1424 | 100.1 | 0.0027 | 5.6 | 0.000487 |
| 14.2 | 105.7 | 1.1417 | 1.1334 | 99.3 | 0.0090 | 5.6 | 0.001597 |
| 19.8 | 105.4 | 1.1417 | 1.1220 | 98.3 | 0.0114 | 5.6 | 0.002034 |
| 25.4 | 105.1 | 1.1417 | 1.1124 | 97.4 | 0.0095 | 5.6 | 0.001701 |
| 31.0 | 105.0 | 1.1417 | 1.1060 | 96.9 | 0.0064 | 5.6 | 0.001143 |
| 36.6 | 105.3 | 1.1417 | 1.1020 | 96.5 | 0.0040 | 5.6 | 0.000712 |
| 42.3 | 105.4 | 1.1417 | 1.0994 | 96.3 | 0.0026 | 5.6 | 0.000457 |
| 47.9 | 105.4 | 1.1417 | 1.0977 | 96.2 | 0.0017 | 5.6 | 0.000303 |
| 53.5 | 104.8 | 1.1417 | 1.0965 | 96.0 | 0.0012 | 5.6 | 0.000219 |
| 59.1 | 105.0 | 1.1417 | 1.0955 | 96.0 | 0.0010 | 5.6 | 0.000178 |
| 64.7 | 104.6 | 1.1417 | 1.0947 | 95.9 | 0.0008 | 5.6 | 0.000137 |
| 70.3 | 105.3 | 1.1417 | 1.0942 | 95.8 | 0.0006 | 5.6 | 0.000102 |
| 76.0 | 193.9 | 1.1417 | 1.1006 | 96.4 | -0.0064 | 5.7 | -0.001127 |
| 81.6 | 410.9 | 1.1417 | 1.0882 | 95.3 | 0.0124 | 5.6 | 0.002213 |
| 87.2 | 573.5 | 1.1417 | 0.8507 | 74.5 | 0.2375 | 5.6 | 0.042489 |
| 92.8 | 688.3 | 1.1417 | 0.6907 | 60.5 | 0.1600 | 5.6 | 0.028630 |
| 98.4 | 794.9 | 1.1417 | 0.6554 | 57.4 | 0.0354 | 5.6 | 0.006294 |
| 104.0 | 887.9 | 1.1417 | 0.6135 | 53.7 | 0.0419 | 5.6 | 0.007496 |
| 109.6 | 917.4 | 1.1417 | 0.6014 | 52.7 | 0.0120 | 5.6 | 0.002155 |
| 115.2 | 915.0 | 1.1417 | 0.5905 | 51.7 | 0.0110 | 5.6 | 0.001960 |
| 120.8 | 909.6 | 1.1417 | 0.5771 | 50.5 | 0.0134 | 5.7 | 0.002354 |
| 126.4 | 874.7 | 1.1417 | 0.5688 | 49.8 | 0.0083 | 5.6 | 0.001484 |
| 132.0 | 842.0 | 1.1417 | 0.5602 | 49.1 | 0.0086 | 5.6 | 0.001556 |
| 137.5 | 811.5 | 1.1417 | 0.5529 | 48.4 | 0.0073 | 5.6 | 0.001315 |
| 143.1 | 783.3 | 1.1417 | 0.5464 | 47.9 | 0.0065 | 5.6 | 0.001168 |
| 148.7 | 755.9 | 1.1417 | 0.5409 | 47.4 | 0.0055 | 5.6 | 0.000983 |
| 154.4 | 749.1 | 1.1417 | 0.5406 | 47.3 | 0.0003 | 5.6 | 0.000052 |
| 160.1 | 749.8 | 1.1417 | 0.5088 | 44.6 | 0.0318 | 5.7 | 0.005552 |
| 165.7 | 750.1 | 1.1417 | 0.4677 | 41.0 | 0.0410 | 5.6 | 0.007298 |
| 171.3 | 749.5 | 1.1417 | 0.4261 | 37.3 | 0.0416 | 5.6 | 0.007435 |
| 176.9 | 749.9 | 1.1417 | 0.3848 | 33.7 | 0.0413 | 5.6 | 0.007375 |
| 182.5 | 749.7 | 1.1417 | 0.3440 | 30.1 | 0.0408 | 5.6 | 0.007265 |
| 188.1 | 749.8 | 1.1417 | 0.3039 | 26.6 | 0.0401 | 5.6 | 0.007139 |
| 193.7 | 749.8 | 1.1417 | 0.2646 | 23.2 | 0.0393 | 5.6 | 0.007017 |
| 199.3 | 749.8 | 1.1417 | 0.2263 | 19.8 | 0.0383 | 5.6 | 0.006833 |
| 204.9 | 749.8 | 1.1417 | 0.1890 | 16.6 | 0.0373 | 5.6 | 0.006661 |
| 210.5 | 749.6 | 1.1417 | 0.1530 | 13.4 | 0.0360 | 5.6 | 0.006429 |
| 216.1 | 749.8 | 1.1417 | 0.1187 | 10.4 | 0.0343 | 5.6 | 0.006150 |
| 221.7 | 750.0 | 1.1417 | 0.0907 | 7.9 | 0.0280 | 5.6 | 0.005021 |
| 227.3 | 750.1 | 1.1417 | 0.0748 | 6.6 | 0.0159 | 5.6 | 0.002839 |
| 232.9 | 750.2 | 1.1417 | 0.0690 | 6.0 | 0.0058 | 5.6 | 0.001042 |
| 238.5 | 750.2 | 1.1417 | 0.0686 | 6.0 | 0.0004 | 5.6 | 0.000072 |

| Time (min) | Temperature (°C) | Original weight (g) | Final weight (g) | Weight (%) | Weight loss (g) | ΔT (min) | DTG (g/min) |
|-------------------|-------------------------|----------------------------|-------------------------|-------------------|------------------------|-----------------|--------------------|
| 244.1 | 750.0 | 1.1417 | 0.0683 | 6.0 | 0.0003 | 5.6 | 0.000060 |
| 249.7 | 749.8 | 1.1417 | 0.0680 | 6.0 | 0.0003 | 5.6 | 0.000048 |
| 255.3 | 749.9 | 1.1417 | 0.0678 | 5.9 | 0.0002 | 5.6 | 0.000036 |
| 260.9 | 750.0 | 1.1417 | 0.0676 | 5.9 | 0.0002 | 5.6 | 0.000035 |
| 266.5 | 750.0 | 1.1417 | 0.0674 | 5.9 | 0.0002 | 5.6 | 0.000042 |
| 272.1 | 750.0 | 1.1417 | 0.0672 | 5.9 | 0.0001 | 5.6 | 0.000024 |
| 277.7 | 750.0 | 1.1417 | 0.0671 | 5.9 | 0.0001 | 5.6 | 0.000018 |

Appendix 23: TG and DTG results for briquette B35

| Time (min) | Temperature (°C) | Original weight (g) | Final weight (g) | Weight loss (%) | Weight loss (g) | ΔT (min) | DTG (g/min) |
|-------------------|-------------------------|----------------------------|-------------------------|------------------------|------------------------|-----------------|--------------------|
| 0.0 | 24.1 | 1.2117 | 1.2117 | 100.0 | 0.0000 | 0.0000 | 0.000000 |
| 2.1 | 52.8 | 1.2117 | 1.2144 | 100.2 | -0.0027 | 2.1 | -0.001294 |
| 7.7 | 107.1 | 1.2117 | 1.2132 | 100.1 | 0.0012 | 5.6 | 0.000214 |
| 13.3 | 105.1 | 1.2117 | 1.2054 | 99.5 | 0.0078 | 5.6 | 0.001380 |
| 19.0 | 105.3 | 1.2117 | 1.1943 | 98.6 | 0.0111 | 5.6 | 0.001975 |
| 24.6 | 105.3 | 1.2117 | 1.1845 | 97.8 | 0.0098 | 5.6 | 0.001743 |
| 30.2 | 105.6 | 1.2117 | 1.1777 | 97.2 | 0.0068 | 5.6 | 0.001217 |
| 35.8 | 105.3 | 1.2117 | 1.1734 | 96.8 | 0.0043 | 5.6 | 0.000760 |
| 41.4 | 105.0 | 1.2117 | 1.1706 | 96.6 | 0.0028 | 5.6 | 0.000503 |
| 47.0 | 104.7 | 1.2117 | 1.1687 | 96.5 | 0.0019 | 5.6 | 0.000337 |
| 52.7 | 104.8 | 1.2117 | 1.1673 | 96.3 | 0.0014 | 5.6 | 0.000249 |
| 58.3 | 105.6 | 1.2117 | 1.1663 | 96.3 | 0.0010 | 5.6 | 0.000179 |
| 63.9 | 104.6 | 1.2117 | 1.1654 | 96.2 | 0.0009 | 5.6 | 0.000154 |
| 69.5 | 104.8 | 1.2117 | 1.1648 | 96.1 | 0.0006 | 5.6 | 0.000108 |
| 75.2 | 146.7 | 1.2117 | 1.1662 | 96.3 | -0.0014 | 5.7 | -0.000246 |
| 80.8 | 386.4 | 1.2117 | 1.1638 | 96.0 | 0.0025 | 5.6 | 0.000441 |
| 86.4 | 548.7 | 1.2117 | 1.0060 | 83.0 | 0.1577 | 5.6 | 0.028222 |
| 91.9 | 673.6 | 1.2117 | 0.6914 | 57.1 | 0.3146 | 5.6 | 0.056457 |
| 97.6 | 778.1 | 1.2117 | 0.6567 | 54.2 | 0.0347 | 5.6 | 0.006179 |
| 103.1 | 877.6 | 1.2117 | 0.6131 | 50.6 | 0.0436 | 5.6 | 0.007815 |
| 108.7 | 920.6 | 1.2117 | 0.6019 | 49.7 | 0.0112 | 5.6 | 0.001996 |
| 114.3 | 915.2 | 1.2117 | 0.5913 | 48.8 | 0.0106 | 5.6 | 0.001900 |
| 120.0 | 913.8 | 1.2117 | 0.5762 | 47.6 | 0.0151 | 5.7 | 0.002662 |
| 125.6 | 879.5 | 1.2117 | 0.5715 | 47.2 | 0.0047 | 5.6 | 0.000839 |
| 131.1 | 846.7 | 1.2117 | 0.5637 | 46.5 | 0.0078 | 5.5 | 0.001407 |
| 136.7 | 815.9 | 1.2117 | 0.5569 | 46.0 | 0.0068 | 5.6 | 0.001216 |
| 142.3 | 787.4 | 1.2117 | 0.5510 | 45.5 | 0.0059 | 5.6 | 0.001058 |
| 147.9 | 760.0 | 1.2117 | 0.5458 | 45.0 | 0.0053 | 5.6 | 0.000943 |
| 153.5 | 745.3 | 1.2117 | 0.5456 | 45.0 | 0.0001 | 5.6 | 0.000022 |
| 159.2 | 749.9 | 1.2117 | 0.5207 | 43.0 | 0.0249 | 5.7 | 0.004343 |
| 164.9 | 750.4 | 1.2117 | 0.4795 | 39.6 | 0.0412 | 5.6 | 0.007335 |
| 170.5 | 750.9 | 1.2117 | 0.4376 | 36.1 | 0.0420 | 5.6 | 0.007487 |
| 176.1 | 750.9 | 1.2117 | 0.3960 | 32.7 | 0.0415 | 5.6 | 0.007409 |
| 181.7 | 750.9 | 1.2117 | 0.3550 | 29.3 | 0.0411 | 5.6 | 0.007305 |
| 187.3 | 750.9 | 1.2117 | 0.3148 | 26.0 | 0.0402 | 5.6 | 0.007173 |

| Time (min) | Temperature (°C) | Original weight (g) | Final weight (g) | Weight loss (%) | Weight loss (g) | ΔT (min) | DTG (g/min) |
|-------------------|-------------------------|----------------------------|-------------------------|------------------------|------------------------|-----------------|--------------------|
| 192.9 | 750.9 | 1.2117 | 0.2755 | 22.7 | 0.0393 | 5.6 | 0.007017 |
| 198.5 | 750.9 | 1.2117 | 0.2372 | 19.6 | 0.0383 | 5.6 | 0.006834 |
| 204.1 | 750.9 | 1.2117 | 0.1998 | 16.5 | 0.0375 | 5.6 | 0.006684 |
| 209.7 | 751.2 | 1.2117 | 0.1636 | 13.5 | 0.0362 | 5.6 | 0.006470 |
| 215.3 | 750.7 | 1.2117 | 0.1293 | 10.7 | 0.0342 | 5.6 | 0.006126 |
| 220.9 | 750.7 | 1.2117 | 0.1009 | 8.3 | 0.0284 | 5.6 | 0.005082 |
| 226.5 | 750.6 | 1.2117 | 0.0817 | 6.7 | 0.0192 | 5.6 | 0.003422 |
| 232.0 | 750.3 | 1.2117 | 0.0719 | 5.9 | 0.0098 | 5.6 | 0.001760 |
| 237.6 | 750.2 | 1.2117 | 0.0685 | 5.7 | 0.0034 | 5.6 | 0.000610 |
| 243.2 | 750.2 | 1.2117 | 0.0683 | 5.6 | 0.0003 | 5.6 | 0.000047 |
| 248.8 | 750.1 | 1.2117 | 0.0680 | 5.6 | 0.0003 | 5.6 | 0.000053 |
| 254.4 | 749.9 | 1.2117 | 0.0678 | 5.6 | 0.0002 | 5.6 | 0.000036 |
| 260.0 | 749.9 | 1.2117 | 0.0675 | 5.6 | 0.0002 | 5.6 | 0.000042 |
| 265.6 | 749.9 | 1.2117 | 0.0674 | 5.6 | 0.0001 | 5.6 | 0.000018 |
| 271.2 | 750.0 | 1.2117 | 0.0672 | 5.5 | 0.0002 | 5.6 | 0.000036 |
| 276.9 | 750.0 | 1.2117 | 0.0672 | 5.5 | 0.0001 | 5.6 | 0.000012 |

Appendix 24: TG and DTG results for briquette B40

| Time (min) | Temperature (°C) | Original weight (g) | Final weight (g) | Weight loss (%) | Weight loss (g) | ΔT (min) | DTG (g/min) |
|-------------------|-------------------------|----------------------------|-------------------------|------------------------|------------------------|-----------------|--------------------|
| 0.0 | 24.11 | 1.2456 | 1.24560 | 100.0 | 0 | 0 | 0.000000 |
| 0.7 | 33.34 | 1.2456 | 1.24768 | 100.2 | -0.00208 | 0.7 | -0.002858 |
| 5.0 | 106.41 | 1.2456 | 1.24876 | 100.3 | -0.00108 | 4.3 | -0.000254 |
| 10.6 | 104.14 | 1.2456 | 1.24226 | 99.7 | 0.00650 | 5.6 | 0.001157 |
| 16.2 | 105.24 | 1.2456 | 1.23230 | 98.9 | 0.00997 | 5.6 | 0.001769 |
| 21.8 | 104.91 | 1.2456 | 1.22270 | 98.2 | 0.00960 | 5.6 | 0.001716 |
| 27.5 | 105.11 | 1.2456 | 1.21579 | 97.6 | 0.00690 | 5.6 | 0.001229 |
| 33.1 | 104.95 | 1.2456 | 1.21123 | 97.2 | 0.00457 | 5.6 | 0.000812 |
| 38.7 | 104.57 | 1.2456 | 1.20819 | 97.0 | 0.00303 | 5.6 | 0.000540 |
| 44.3 | 104.54 | 1.2456 | 1.20606 | 96.8 | 0.00213 | 5.6 | 0.000379 |
| 49.9 | 105.29 | 1.2456 | 1.20456 | 96.7 | 0.00150 | 5.6 | 0.000267 |
| 55.6 | 105.66 | 1.2456 | 1.20339 | 96.6 | 0.00117 | 5.6 | 0.000207 |
| 61.2 | 104.60 | 1.2456 | 1.20243 | 96.5 | 0.00096 | 5.6 | 0.000171 |
| 66.8 | 105.09 | 1.2456 | 1.20173 | 96.5 | 0.00070 | 5.6 | 0.000126 |
| 72.4 | 110.25 | 1.2456 | 1.18215 | 94.9 | 0.01958 | 5.6 | 0.003469 |
| 78.1 | 359.56 | 1.2456 | 1.20332 | 96.6 | -0.02117 | 5.6 | -0.003759 |
| 83.7 | 521.30 | 1.2456 | 1.11720 | 89.7 | 0.08612 | 5.6 | 0.015409 |
| 89.2 | 659.15 | 1.2456 | 0.67727 | 54.4 | 0.43994 | 5.6 | 0.078795 |
| 94.8 | 761.35 | 1.2456 | 0.64206 | 51.5 | 0.03520 | 5.6 | 0.006293 |
| 100.4 | 866.21 | 1.2456 | 0.59860 | 48.1 | 0.04347 | 5.6 | 0.007754 |
| 106.0 | 920.66 | 1.2456 | 0.58893 | 47.3 | 0.00967 | 5.6 | 0.001724 |
| 111.6 | 914.99 | 1.2456 | 0.57916 | 46.5 | 0.00977 | 5.6 | 0.001750 |
| 117.2 | 915.34 | 1.2456 | 0.57129 | 45.9 | 0.00787 | 5.6 | 0.001408 |
| 122.9 | 884.34 | 1.2456 | 0.56192 | 45.1 | 0.00937 | 5.6 | 0.001660 |
| 128.5 | 851.41 | 1.2456 | 0.55520 | 44.6 | 0.00672 | 5.6 | 0.001203 |
| 134.0 | 820.20 | 1.2456 | 0.54918 | 44.1 | 0.00602 | 5.6 | 0.001083 |
| 139.6 | 791.48 | 1.2456 | 0.54424 | 43.7 | 0.00494 | 5.6 | 0.000886 |
| 145.2 | 763.94 | 1.2456 | 0.53997 | 43.4 | 0.00427 | 5.6 | 0.000765 |
| 150.8 | 740.84 | 1.2456 | 0.53920 | 43.3 | 0.00077 | 5.6 | 0.000138 |
| 156.5 | 750.14 | 1.2456 | 0.52193 | 41.9 | 0.01727 | 5.7 | 0.003033 |
| 162.1 | 750.41 | 1.2456 | 0.48196 | 38.7 | 0.03997 | 5.6 | 0.007074 |
| 167.8 | 750.98 | 1.2456 | 0.44019 | 35.3 | 0.04177 | 5.6 | 0.007429 |
| 173.4 | 750.83 | 1.2456 | 0.39873 | 32.0 | 0.04146 | 5.6 | 0.007404 |
| 179.0 | 751.24 | 1.2456 | 0.35756 | 28.7 | 0.04116 | 5.6 | 0.007343 |
| 184.6 | 751.13 | 1.2456 | 0.31719 | 25.5 | 0.04037 | 5.6 | 0.007202 |
| 190.2 | 751.16 | 1.2456 | 0.27743 | 22.3 | 0.03976 | 5.6 | 0.007094 |

| Time (min) | Temperature (°C) | Original weight (g) | Final weight (g) | Weight loss (%) | Weight loss (g) | ΔT (min) | DTG (g/min) |
|-------------------|-------------------------|----------------------------|-------------------------|------------------------|------------------------|-----------------|--------------------|
| 195.8 | 751.02 | 1.2456 | 0.23853 | 19.1 | 0.03890 | 5.6 | 0.006940 |
| 201.4 | 751.07 | 1.2456 | 0.20049 | 16.1 | 0.03804 | 5.6 | 0.006779 |
| 207.0 | 751.01 | 1.2456 | 0.16359 | 13.1 | 0.03690 | 5.6 | 0.006589 |
| 212.6 | 750.85 | 1.2456 | 0.12836 | 10.3 | 0.03523 | 5.6 | 0.006298 |
| 218.2 | 750.64 | 1.2456 | 0.09836 | 7.9 | 0.03000 | 5.6 | 0.005373 |
| 223.8 | 750.31 | 1.2456 | 0.07780 | 6.2 | 0.02057 | 5.6 | 0.003684 |
| 229.3 | 750.12 | 1.2456 | 0.06856 | 5.5 | 0.00924 | 5.6 | 0.001654 |
| 234.9 | 750.13 | 1.2456 | 0.06746 | 5.4 | 0.00110 | 5.6 | 0.000197 |
| 240.5 | 750.09 | 1.2456 | 0.06713 | 5.4 | 0.00033 | 5.6 | 0.000059 |
| 246.1 | 750.18 | 1.2456 | 0.06689 | 5.4 | 0.00024 | 5.6 | 0.000042 |
| 251.7 | 750.12 | 1.2456 | 0.06670 | 5.4 | 0.00020 | 5.6 | 0.000035 |
| 257.3 | 750.05 | 1.2456 | 0.06653 | 5.3 | 0.00017 | 5.6 | 0.000030 |
| 262.9 | 750.01 | 1.2456 | 0.06639 | 5.3 | 0.00013 | 5.6 | 0.000024 |
| 268.5 | 749.94 | 1.2456 | 0.06629 | 5.3 | 0.00010 | 5.6 | 0.000018 |
| 274.1 | 749.97 | 1.2456 | 0.06623 | 5.3 | 0.00007 | 5.6 | 0.000012 |

Appendix 25: Proximate analysis of briquettes

| Sample | Weight (g) | Highly volatile matter (%) | Medium volatile matter (%) | Ash (%) | Fixed carbon (%) |
|---------------|-------------------|-----------------------------------|-----------------------------------|----------------|-------------------------|
| Briquettes | | | | | |
| B25 | 1.1384 | 4.45 | 40.39 | 5.69 | 49.46 |
| B25 | 1.1558 | 4.50 | 40.02 | 5.74 | 49.75 |
| B25 | 1.1078 | 5.08 | 40.99 | 5.02 | 48.91 |
| AVG | | 4.68 | 40.46 | 5.48 | 49.38 |
| STD | | 0.35 | 0.49 | 0.40 | 0.42 |
| B30 | 1.1405 | 4.24 | 43.86 | 5.59 | 46.31 |
| B30 | 1.1204 | 4.28 | 44.82 | 5.52 | 45.38 |
| B30 | 1.1641 | 4.19 | 44.87 | 5.31 | 45.63 |
| AVG | | 4.24 | 44.52 | 5.47 | 45.77 |
| STD | | 0.05 | 0.57 | 0.14 | 0.48 |
| B35 | 1.134 | 4.01 | 47.97 | 5.11 | 42.91 |
| B35 | 1.3147 | 3.90 | 47.62 | 5.19 | 43.29 |
| B35 | 1.1863 | 3.91 | 47.99 | 5.17 | 42.93 |
| AVG | | 3.94 | 47.86 | 5.15 | 43.04 |
| STD | | 0.06 | 0.20 | 0.04 | 0.21 |
| B40 | 1.1821 | 3.55 | 50.89 | 4.93 | 40.63 |
| B40 | 1.2341 | 3.57 | 50.49 | 4.97 | 40.97 |
| B40 | 1.3206 | 3.65 | 50.45 | 4.92 | 40.98 |
| AVG | | 3.59 | 50.61 | 4.94 | 40.86 |
| STD | | 0.05 | 0.24 | 0.02 | 0.20 |

Appendix 26: Ultimate analysis of briquettes

| Sample | Weight (mg) | Nitrogen (N) | Carbon (C) | Hydrogen (H) | Oxygen (O) |
|---------------|--------------------|---------------------|-------------------|---------------------|-------------------|
| B25 | 2.7 | 2.74 | 73.43 | 4.18 | 7.36 |
| B25 | 2.2 | 2.14 | 75.64 | 4.63 | 7.46 |
| B25 | 2.8 | 1.64 | 74.79 | 4.40 | 7.30 |
| AVG | | 2.17 | 74.62 | 4.40 | 7.37 |
| STD | | 0.55 | 1.11 | 0.23 | 0.08 |
| B30 | 2.1 | 1.95 | 75.55 | 5.40 | 7.32 |
| B30 | 2.6 | 1.78 | 76.13 | 4.69 | 7.44 |
| B30 | 2.6 | 2.10 | 73.70 | 4.51 | 7.26 |
| AVG | | 1.94 | 75.13 | 4.87 | 7.34 |
| STD | | 0.16 | 1.27 | 0.47 | 0.09 |
| B35 | 2.6 | 1.69 | 77.18 | 5.19 | 7.35 |
| B35 | 2.5 | 2.81 | 76.23 | 5.40 | 7.28 |
| B35 | 3 | 2.61 | 78.69 | 5.22 | 7.59 |
| AVG | | 2.37 | 77.37 | 5.27 | 7.41 |
| STD | | 0.60 | 1.24 | 0.11 | 0.16 |
| B40 | 2.6 | 1.72 | 78.14 | 5.98 | 5.90 |
| B40 | 2.8 | 1.67 | 79.36 | 5.73 | 5.10 |
| B40 | 2.5 | 1.72 | 81.52 | 6.29 | 6.18 |
| AVG | | 1.70 | 79.67 | 6.00 | 5.73 |
| STD | | 0.03 | 1.71 | 0.28 | 0.56 |

Appendix 27: Higher heating value of briquettes

| Sample | m±0.0001 g | HHV (MJ/kg) |
|---------------|-------------------|--------------------|
| B25 | 0.8932 | 30.5 |
| B25 | 0.6524 | 29.4 |
| B25 | 0.5783 | 29.0 |
| AVG | | 29.7 |
| STD | | 0.7 |
| B30 | 0.7972 | 32.0 |
| B30 | 0.6428 | 31.5 |
| B30 | 0.8791 | 31.2 |
| AVG | | 31.6 |
| STD | | 0.4 |
| B35 | 0.5327 | 31.5 |
| B35 | 0.7328 | 31.6 |
| B35 | 0.9794 | 30.9 |
| AVG | | 31.3 |
| STD | | 0.4 |
| B40 | 0.5922 | 31.3 |
| B40 | 0.5528 | 30.9 |
| B40 | 0.5794 | 30.5 |
| AVG | | 30.9 |
| STD | | 0.4 |

Appendix 28: Higher heating value (HHV), density and energy density of briquettes

| Briquette | HHV (MJ/kg) | Density (g/cm³) | Density (kg/m³) | Energy density (MJ/m³) | Energy density (GJ/m³) |
|------------------|------------------------|---------------------------------------|---------------------------------------|--|--|
| B25 | 29.7 | 0.770 | 770 | 22832 | 22.83 |
| B30 | 31.6 | 0.877 | 877 | 27678 | 27.68 |
| B35 | 31.3 | 0.951 | 951 | 29791 | 29.79 |
| B40 | 30.9 | 1.036 | 1036 | 32050 | 32.05 |

Appendix 29: Statistical analysis- ANOVA

| Property | Briquette | N Analysis | N missing | *Mean | Standard deviation | SE of Mean |
|------------------|-----------|------------|-----------|----------|--------------------|------------|
| Highly VM | B25 | 3 | 0 | 4.67823 | 0.35049 | 0.20236 |
| | B30 | 3 | 0 | 4.24003 | 0.04617 | 0.02665 |
| | B35 | 3 | 0 | 3.94187 | 0.06117 | 0.03532 |
| | B40 | 3 | 0 | 3.59213 | 0.05107 | 0.02948 |
| medium VM | B25 | 3 | 0 | 40.46407 | 0.48883 | 0.28222 |
| | B30 | 3 | 0 | 44.51513 | 0.56838 | 0.32815 |
| | B35 | 3 | 0 | 47.85963 | 0.20423 | 0.11791 |
| | B40 | 3 | 0 | 50.60663 | 0.24340 | 0.14053 |
| Ash | B25 | 3 | 0 | 5.48250 | 0.40201 | 0.23210 |
| | B30 | 3 | 0 | 5.47000 | 0.14385 | 0.08305 |
| | B35 | 3 | 0 | 5.15353 | 0.04255 | 0.02457 |
| | B40 | 3 | 0 | 4.94037 | 0.02376 | 0.01372 |
| FC | B25 | 3 | 0 | 49.37517 | 0.42451 | 0.24509 |
| | B30 | 3 | 0 | 45.77487 | 0.48157 | 0.27804 |
| | B35 | 3 | 0 | 43.04497 | 0.20931 | 0.12085 |
| | B40 | 3 | 0 | 40.86087 | 0.20138 | 0.11627 |
| C | B25 | 3 | 0 | 74.62000 | 1.11476 | 0.64361 |
| | B30 | 3 | 0 | 75.12667 | 1.26911 | 0.73272 |
| | B35 | 3 | 0 | 77.36667 | 1.24058 | 0.71625 |
| | B40 | 3 | 0 | 79.67333 | 1.71165 | 0.98822 |
| H | B25 | 3 | 0 | 4.40333 | 0.22502 | 0.12991 |
| | B30 | 3 | 0 | 4.86667 | 0.47057 | 0.27168 |
| | B35 | 3 | 0 | 5.27000 | 0.11358 | 0.06557 |
| | B40 | 3 | 0 | 6.00000 | 0.28054 | 0.16197 |
| N | B25 | 3 | 0 | 2.17333 | 0.55076 | 0.31798 |
| | B30 | 3 | 0 | 1.94333 | 0.16010 | 0.09244 |
| | B35 | 3 | 0 | 2.37000 | 0.59733 | 0.34487 |
| | B40 | 3 | 0 | 1.70333 | 0.02887 | 0.01667 |
| O | B25 | 3 | 0 | 7.37333 | 0.08083 | 0.04667 |
| | B30 | 3 | 0 | 7.34000 | 0.09165 | 0.05292 |
| | B35 | 3 | 0 | 7.40667 | 0.16258 | 0.09387 |
| | B40 | 3 | 0 | 5.72667 | 0.56048 | 0.32359 |
| HHV | B25 | 3 | 0 | 29.65600 | 0.79673 | 0.45999 |
| | B30 | 3 | 0 | 31.56333 | 0.43054 | 0.24857 |
| | B35 | 3 | 0 | 31.32467 | 0.40915 | 0.23622 |
| | B40 | 3 | 0 | 30.92433 | 0.38501 | 0.22228 |

*Null Hypothesis: The means of all levels are equal

*Alternative Hypothesis: The means of one or more levels are different

*At the 0.05 level, the population means are significantly different.

Appendix 30: Statistical analysis-Fisher's LSD

| Property | Briquette | Mean Diff | SEM | t Value | Prob | Alpha | Sign | LCL | UCL |
|------------------|-----------|-----------|---------|-----------|---------|-------|------|----------|----------|
| Highly VM | B30- B25 | -0.4382 | 0.14795 | -2.96189 | 0.01809 | 0.05 | 1 | -0.77936 | -0.09704 |
| | B35- B25 | -0.73637 | 0.14795 | -4.97727 | 0.00108 | 0.05 | 1 | -1.07753 | -0.3952 |
| | B35- B30 | -0.29817 | 0.14795 | -2.01538 | 0.07862 | 0.05 | 0 | -0.63933 | 0.043 |
| | B40-B25 | -1.0861 | 0.14795 | -7.3412 | 0.00008 | 0.05 | 1 | -1.42726 | -0.74494 |
| | B40-B30 | -0.6479 | 0.14795 | -4.37931 | 0.00235 | 0.05 | 1 | -0.98906 | -0.30674 |
| | B40-B35 | -0.34973 | 0.14795 | -2.36393 | 0.04568 | 0.05 | 1 | -0.6909 | -0.00857 |
| medium VM | B30-B25 | 4.05107 | 0.3324 | 12.18716 | 0.00000 | 0.05 | 1 | 3.28454 | 4.81759 |
| | B35-B25 | 7.39557 | 0.3324 | 22.2487 | 0.00000 | 0.05 | 1 | 6.62904 | 8.16209 |
| | B35-B30 | 3.3445 | 0.3324 | 10.06154 | 0.00001 | 0.05 | 1 | 2.57797 | 4.11103 |
| | B40-B25 | 10.14257 | 0.3324 | 30.51273 | 0.00000 | 0.05 | 1 | 9.37604 | 10.9091 |
| | B40-B30 | 6.0915 | 0.3324 | 18.32557 | 0.00000 | 0.05 | 1 | 5.32497 | 6.85803 |
| | B40-B35 | 2.747 | 0.3324 | 8.26403 | 0.00003 | 0.05 | 1 | 1.98047 | 3.51353 |
| Ash | B30-B25 | -0.0125 | 0.17544 | -0.07125 | 0.94495 | 0.05 | 0 | -0.41707 | 0.39207 |
| | B35-B25 | -0.32897 | 0.17544 | -1.87508 | 0.09764 | 0.05 | 0 | -0.73354 | 0.0756 |
| | B35-B30 | -0.31647 | 0.17544 | -1.80383 | 0.10891 | 0.05 | 0 | -0.72104 | 0.0881 |
| | B40-B25 | -0.54213 | 0.17544 | -3.0901 | 0.01489 | 0.05 | 1 | -0.9467 | -0.13756 |
| | B40-B30 | -0.52963 | 0.17544 | -3.01885 | 0.01659 | 0.05 | 1 | -0.9342 | -0.12506 |
| | B40-B35 | -0.21317 | 0.17544 | -1.21503 | 0.25899 | 0.05 | 0 | -0.61774 | 0.1914 |
| FC | B30-B25 | -3.6003 | 0.28766 | -12.51585 | 0.00000 | 0.05 | 1 | -4.26364 | -2.93696 |
| | B35-B25 | -6.3302 | 0.28766 | -22.0059 | 0.00000 | 0.05 | 1 | -6.99354 | -5.66686 |
| | B35-B30 | -2.7299 | 0.28766 | -9.49005 | 0.00001 | 0.05 | 1 | -3.39324 | -2.06656 |
| | B40-B25 | -8.5143 | 0.28766 | -29.59857 | 0.00000 | 0.05 | 1 | -9.17764 | -7.85096 |
| | B40-B30 | -4.914 | 0.28766 | -17.08272 | 0.00000 | 0.05 | 1 | -5.57734 | -4.25066 |
| | B40-B35 | -2.1841 | 0.28766 | -7.59267 | 0.00006 | 0.05 | 1 | -2.84744 | -1.52076 |
| C | B30-B25 | 0.50667 | 1.10469 | 0.45865 | 0.65869 | 0.05 | 0 | -2.04076 | 3.0541 |
| | B35-B25 | 2.74667 | 1.10469 | 2.48636 | 0.03774 | 0.05 | 1 | 0.19924 | 5.2941 |
| | B35-B30 | 2.24 | 1.10469 | 2.02771 | 0.07713 | 0.05 | 0 | -0.30743 | 4.78743 |
| | B40-B25 | 5.05333 | 1.10469 | 4.57442 | 0.00182 | 0.05 | 1 | 2.5059 | 7.60076 |
| | B40-B30 | 4.54667 | 1.10469 | 4.11577 | 0.00336 | 0.05 | 1 | 1.99924 | 7.0941 |
| | B40-B35 | 2.30667 | 1.10469 | 2.08806 | 0.07023 | 0.05 | 0 | -0.24076 | 4.8541 |
| H | B30-B25 | 0.46333 | 0.24619 | 1.88199 | 0.09661 | 0.05 | 0 | -0.10439 | 1.03106 |
| | B35-B25 | 0.86667 | 0.24619 | 3.52027 | 0.00784 | 0.05 | 1 | 0.29894 | 1.43439 |
| | B35-B30 | 0.40333 | 0.24619 | 1.63828 | 0.14000 | 0.05 | 0 | -0.16439 | 0.97106 |
| | B40-B25 | 1.59667 | 0.24619 | 6.48542 | 0.00019 | 0.05 | 1 | 1.02894 | 2.16439 |
| | B40-B30 | 1.13333 | 0.24619 | 4.60343 | 0.00175 | 0.05 | 1 | 0.56561 | 1.70106 |
| | B40-B35 | 0.73 | 0.24619 | 2.96515 | 0.01800 | 0.05 | 1 | 0.16228 | 1.29772 |
| N | B30-B25 | -0.23 | 0.33828 | -0.67991 | 0.51575 | 0.05 | 0 | -1.01007 | 0.55007 |
| | B35-B25 | 0.19667 | 0.33828 | 0.58137 | 0.57700 | 0.05 | 0 | -0.58341 | 0.97674 |
| | B35-B30 | 0.42667 | 0.33828 | 1.26128 | 0.24274 | 0.05 | 0 | -0.35341 | 1.20674 |
| | B40-B25 | -0.47 | 0.33828 | -1.38938 | 0.20216 | 0.05 | 0 | -1.25007 | 0.31007 |
| | B40-B30 | -0.24 | 0.33828 | -0.70947 | 0.49818 | 0.05 | 0 | -1.02007 | 0.54007 |
| | B40-B35 | -0.66667 | 0.33828 | -1.97075 | 0.08424 | 0.05 | 0 | -1.44674 | 0.11341 |
| O | B30-B25 | -0.03333 | 0.24341 | -0.13694 | 0.89446 | 0.05 | 0 | -0.59464 | 0.52798 |
| | B35-B25 | 0.03333 | 0.24341 | 0.13694 | 0.89446 | 0.05 | 0 | -0.52798 | 0.59464 |
| | B35-B30 | 0.06667 | 0.24341 | 0.27388 | 0.79111 | 0.05 | 0 | -0.49464 | 0.62798 |
| | B40-B25 | -1.64667 | 0.24341 | -6.7649 | 0.00014 | 0.05 | 1 | -2.20798 | -1.08536 |

| Property | Briquette | Mean Diff | SEM | t Value | Prob | Alpha | Sign | LCL | UCL |
|----------|-----------|-----------|---------|----------|---------|-------|------|----------|----------|
| HHV | B40-B30 | -1.61333 | 0.24341 | -6.62796 | 0.00016 | 0.05 | 1 | -2.17464 | -1.05202 |
| | B40-B35 | -1.68 | 0.24341 | -6.90184 | 0.00012 | 0.05 | 1 | -2.24131 | -1.11869 |
| | B30-B25 | 1.90733 | 0.43508 | 4.38386 | 0.00234 | 0.05 | 1 | 0.90404 | 2.91063 |
| | B35-B25 | 1.66867 | 0.43508 | 3.83531 | 0.00498 | 0.05 | 1 | 0.66537 | 2.67196 |
| | B35-B30 | -0.23867 | 0.43508 | -0.54856 | 0.59828 | 0.05 | 0 | -1.24196 | 0.76463 |
| | B40-B25 | 1.26833 | 0.43508 | 2.91517 | 0.01943 | 0.05 | 1 | 0.26504 | 2.27163 |
| | B40-B30 | -0.639 | 0.43508 | -1.46869 | 0.18010 | 0.05 | 0 | -1.6423 | 0.3643 |
| | B40-B35 | -0.40033 | 0.43508 | -0.92014 | 0.38441 | 0.05 | 0 | -1.40363 | 0.60296 |

*Sign equals 1 indicates that the difference of the means is significant at the 0.05 level.

*Sign equals 0 indicates that the difference of the means is not significant at the 0.05 level.

Appendix 31: Experimental (Exp), predicted (pred) and deviation (dev) values of the responses

| Run | Exp | Pred | Dev | Exp | Pred | Dev | Exp | Pred | Dev | Exp | Pred | Dev | Exp | Pred | Dev |
|-----|---------|-------|--------|--------|-------|---------|-------|-------|--------|-------|-------|--------|-------|-------|--------|
| | Density | | | IRI | | | F | | | T | | | WRI | | |
| 1 | 0.788 | 0.792 | -0.004 | 3.33 | -4.25 | 7.582 | 1.97 | 1.73 | 0.234 | 0.090 | 0.091 | -0.001 | 99.32 | 99.25 | 0.071 |
| 2 | 0.767 | 0.784 | -0.017 | 3.13 | 2.48 | 0.642 | 2.53 | 2.08 | 0.448 | 0.082 | 0.092 | -0.010 | 99.14 | 99.25 | -0.111 |
| 3 | 0.826 | 0.789 | 0.037 | 2.50 | -2.00 | 4.505 | 2.25 | 1.85 | 0.399 | 0.084 | 0.091 | -0.007 | 99.24 | 99.25 | -0.015 |
| 4 | 0.858 | 0.877 | -0.019 | 25.00 | 24.16 | 0.836 | 3.91 | 4.72 | -0.809 | 0.192 | 0.203 | -0.010 | 99.30 | 99.25 | 0.043 |
| 5 | 0.879 | 0.879 | 0.000 | 11.11 | 21.92 | -10.809 | 3.80 | 4.61 | -0.807 | 0.224 | 0.202 | 0.022 | 99.18 | 99.25 | -0.069 |
| 6 | 0.885 | 0.879 | 0.005 | 16.67 | 21.92 | -5.254 | 4.09 | 4.61 | -0.520 | 0.216 | 0.202 | 0.013 | 99.18 | 99.25 | -0.070 |
| 7 | 0.954 | 0.951 | 0.003 | 50.00 | 61.55 | -11.553 | 8.38 | 8.17 | 0.207 | 0.311 | 0.316 | -0.005 | 99.30 | 99.25 | 0.049 |
| 8 | 0.933 | 0.961 | -0.028 | 50.00 | 52.58 | -2.578 | 7.42 | 7.71 | -0.292 | 0.353 | 0.314 | 0.039 | 99.31 | 99.25 | 0.062 |
| 9 | 0.974 | 0.972 | 0.002 | 50.00 | 43.60 | 6.398 | 8.37 | 7.25 | 1.117 | 0.282 | 0.312 | -0.031 | 99.27 | 99.25 | 0.015 |
| 10 | 1.025 | 1.038 | -0.013 | 100.00 | 87.72 | 12.278 | 9.67 | 11.05 | -1.375 | 0.424 | 0.428 | -0.004 | 99.32 | 99.25 | 0.064 |
| 11 | 1.063 | 1.041 | 0.022 | 100.00 | 85.48 | 14.521 | 14.23 | 10.93 | 3.294 | 0.417 | 0.427 | -0.010 | 99.02 | 99.25 | -0.231 |
| 12 | 1.053 | 1.043 | 0.010 | 66.67 | 83.23 | -16.568 | 8.92 | 10.82 | -1.895 | 0.431 | 0.427 | 0.004 | 99.45 | 99.25 | 0.192 |

Appendix 32: Ignition time of the briquettes

| Sample | B25 | B30 | B35 | B40 |
|---------------|------------|------------|------------|------------|
| 1 | 7.12 | 6.32 | 6.75 | 6.2 |
| 2 | 7.22 | 6.67 | 6.15 | 6.76 |
| 3 | 6.68 | 6.43 | 7.08 | 6.53 |
| AVG | 7.01 | 6.47 | 6.66 | 6.50 |
| STD | 0.29 | 0.18 | 0.47 | 0.28 |

Appendix 33: Temperature profiles and gaseous emissions during the WBT (B25)

| Time (min) | T_{ambient} (°C) | T_{gas} (°C) | T_{water} (°C) | CO (ppm) | SO₂ (ppm) | C_xH_y (ppm) | CO₂ (ppm) | NO_x (ppm) |
|-------------------|---------------------------------|-----------------------------|-------------------------------|-----------------|-----------------------------|---|-----------------------------|-----------------------------|
| 0 | 24.5 | 23.0 | 19.20 | 0.00 | 0.0000 | 0.00 | 0.00 | 0.0000 |
| 1 | 24.6 | 23.0 | 19.20 | 0.37 | 0.0000 | 22.51 | 83.89 | 0.0000 |
| 2 | 24.7 | 23.0 | 19.20 | 2.22 | 0.0000 | 40.93 | 113.89 | 0.0000 |
| 3 | 24.8 | 23.0 | 19.20 | 6.17 | 0.0000 | 66.67 | 139.44 | 0.0000 |
| 4 | 24.8 | 24.0 | 19.20 | 10.62 | 0.0000 | 96.42 | 182.22 | 0.0000 |
| 5 | 24.9 | 24.3 | 19.20 | 17.02 | 0.0000 | 137.04 | 224.44 | 0.0000 |
| 6 | 25.0 | 26.0 | 19.20 | 21.77 | 0.0000 | 172.51 | 253.33 | 0.0000 |
| 7 | 25.0 | 25.3 | 19.36 | 26.48 | 0.0000 | 212.67 | 215.56 | 0.0000 |
| 8 | 25.1 | 25.0 | 20.30 | 26.67 | 0.0000 | 199.63 | 166.67 | 0.0000 |
| 9 | 25.1 | 24.0 | 21.08 | 26.63 | 0.0000 | 185.09 | 162.78 | 0.0000 |
| 10 | 25.2 | 24.0 | 21.94 | 29.78 | 0.0000 | 192.06 | 172.22 | 0.0000 |
| 11 | 25.3 | 24.0 | 22.99 | 32.96 | 0.0000 | 201.08 | 186.11 | 0.0000 |
| 12 | 25.4 | 24.0 | 23.94 | 37.10 | 0.0000 | 210.46 | 196.67 | 0.0000 |
| 13 | 25.4 | 24.0 | 24.93 | 41.30 | 0.0000 | 219.61 | 205.56 | 0.0000 |
| 14 | 25.5 | 24.0 | 25.97 | 47.08 | 0.0000 | 232.20 | 228.33 | 0.0000 |
| 15 | 25.5 | 24.0 | 27.14 | 53.02 | 0.0000 | 243.18 | 243.33 | 0.0000 |
| 16 | 25.6 | 24.0 | 28.40 | 58.97 | 0.0000 | 250.05 | 263.89 | 0.0000 |
| 17 | 25.6 | 24.0 | 29.80 | 64.44 | 0.0000 | 256.11 | 273.33 | 0.0000 |
| 18 | 25.8 | 24.0 | 31.32 | 70.66 | 0.0000 | 261.61 | 289.44 | 0.0000 |
| 19 | 25.8 | 24.0 | 32.68 | 77.39 | 0.0000 | 266.41 | 308.33 | 0.0000 |
| 20 | 25.9 | 24.0 | 34.17 | 84.58 | 0.0000 | 271.79 | 333.33 | 0.0000 |
| 21 | 25.9 | 24.0 | 35.80 | 92.79 | 0.0000 | 278.88 | 338.89 | 0.0000 |
| 22 | 25.9 | 24.0 | 37.65 | 100.25 | 0.0000 | 283.57 | 363.33 | 0.0000 |
| 23 | 26.0 | 24.0 | 39.50 | 107.94 | 0.0000 | 289.87 | 383.89 | 0.0000 |
| 24 | 26.1 | 24.8 | 41.49 | 117.01 | 0.0000 | 295.59 | 383.33 | 0.0000 |
| 25 | 26.2 | 25.3 | 43.55 | 127.28 | 0.0000 | 305.31 | 402.78 | 0.0000 |
| 26 | 26.2 | 26.0 | 45.61 | 133.96 | 0.0000 | 303.94 | 415.56 | 0.0000 |
| 27 | 26.2 | 26.0 | 47.86 | 142.68 | 0.0000 | 311.49 | 437.22 | 0.0000 |
| 28 | 26.3 | 26.0 | 50.00 | 152.62 | 0.0000 | 316.98 | 445.56 | 0.0000 |
| 29 | 26.4 | 26.0 | 52.96 | 161.46 | 0.0000 | 320.30 | 466.67 | 0.0000 |
| 30 | 26.4 | 26.0 | 57.19 | 129.16 | 0.0018 | 201.99 | 638.33 | 0.0000 |
| 31 | 26.5 | 26.0 | 61.86 | 105.54 | 0.0266 | 156.91 | 712.22 | 0.0000 |
| 32 | 26.5 | 26.0 | 66.74 | 91.88 | 0.1007 | 133.23 | 765.56 | 0.0000 |
| 33 | 26.6 | 26.0 | 70.70 | 81.43 | 0.1964 | 120.76 | 781.11 | 0.0422 |
| 34 | 26.6 | 26.0 | 74.27 | 73.92 | 0.2916 | 116.87 | 778.33 | 0.1267 |
| 35 | 26.7 | 27.0 | 77.79 | 70.11 | 0.2993 | 117.67 | 773.89 | 0.1267 |

| Time (min) | T_{ambient} (°C) | T_{gas} (°C) | T_{water} (°C) | CO (ppm) | SO₂ (ppm) | C_xH_y (ppm) | CO₂ (ppm) | NO_x (ppm) |
|-------------------|---------------------------------|-----------------------------|-------------------------------|-----------------|-----------------------------|---|-----------------------------|-----------------------------|
| 36 | 26.7 | 27.0 | 79.90 | 66.83 | 0.3081 | 122.71 | 745.56 | 0.1267 |
| 37 | 26.8 | 27.0 | 83.98 | 64.02 | 0.3221 | 123.39 | 713.33 | 0.1267 |
| 38 | 26.8 | 27.0 | 87.39 | 61.18 | 0.2777 | 122.02 | 673.89 | 0.1267 |
| 39 | 26.9 | 27.0 | 91.22 | 63.31 | 0.2496 | 132.09 | 645.00 | 0.1056 |
| 40 | 26.9 | 27.0 | 94.11 | 65.21 | 0.2081 | 137.35 | 625.00 | 0.0000 |
| 41 | 27.0 | 27.2 | 94.89 | 67.07 | 0.1398 | 141.01 | 611.11 | 0.0000 |
| 42 | 27.1 | 28.3 | 25.75 | 81.58 | 0.0853 | 166.99 | 630.00 | 0.0000 |
| 43 | 27.0 | 29.0 | 24.57 | 58.96 | 0.0791 | 114.81 | 427.78 | 0.0000 |
| 44 | 26.9 | 28.8 | 19.20 | 54.33 | 0.0648 | 111.72 | 381.67 | 0.0000 |
| 45 | 26.9 | 27.5 | 26.28 | 66.84 | 0.0429 | 139.41 | 405.56 | 0.0000 |
| 46 | 27.0 | 27.0 | 30.50 | 86.48 | 0.0356 | 170.87 | 436.11 | 0.0000 |
| 47 | 27.1 | 27.0 | 33.91 | 111.76 | 0.0293 | 216.18 | 445.56 | 0.0000 |
| 48 | 27.2 | 27.3 | 37.63 | 110.50 | 0.0000 | 203.37 | 435.56 | 0.0000 |
| 49 | 27.3 | 27.0 | 41.40 | 102.30 | 0.0000 | 185.98 | 401.11 | 0.0000 |
| 50 | 27.4 | 27.0 | 45.16 | 105.91 | 0.0000 | 190.32 | 397.78 | 0.0000 |
| 51 | 27.4 | 27.0 | 48.82 | 108.20 | 0.0000 | 192.96 | 388.89 | 0.0000 |
| 52 | 27.5 | 27.0 | 52.41 | 110.31 | 0.0000 | 194.67 | 389.44 | 0.0000 |
| 53 | 27.6 | 27.0 | 56.01 | 111.35 | 0.0000 | 195.82 | 370.56 | 0.0000 |
| 54 | 27.6 | 27.0 | 59.24 | 112.30 | 0.0000 | 199.02 | 372.22 | 0.0000 |
| 55 | 27.6 | 27.0 | 62.71 | 115.48 | 0.0000 | 204.17 | 375.00 | 0.0000 |
| 56 | 27.7 | 27.0 | 65.93 | 117.52 | 0.0000 | 206.23 | 380.00 | 0.0000 |
| 57 | 27.7 | 27.0 | 68.91 | 116.17 | 0.0000 | 203.60 | 369.44 | 0.0000 |
| 58 | 27.8 | 27.0 | 71.83 | 117.91 | 0.0000 | 208.63 | 368.33 | 0.0000 |
| 59 | 27.8 | 27.0 | 74.61 | 117.60 | 0.0000 | 208.29 | 363.89 | 0.0000 |
| 60 | 27.9 | 27.0 | 77.43 | 117.61 | 0.0000 | 210.23 | 361.11 | 0.0000 |
| 61 | 27.9 | 27.0 | 80.09 | 118.39 | 0.0000 | 210.35 | 346.67 | 0.0000 |
| 62 | 27.9 | 27.0 | 82.58 | 119.13 | 0.0000 | 212.86 | 351.67 | 0.0000 |
| 63 | 28.0 | 27.0 | 84.75 | 118.94 | 0.0000 | 214.35 | 338.33 | 0.0000 |
| 64 | 28.0 | 27.0 | 86.96 | 120.52 | 0.0000 | 219.04 | 335.56 | 0.0000 |
| 65 | 28.1 | 27.0 | 89.09 | 123.47 | 0.0000 | 222.59 | 331.67 | 0.0000 |
| 66 | 28.1 | 27.0 | 91.08 | 122.43 | 0.0000 | 221.67 | 322.78 | 0.0000 |
| 67 | 28.1 | 27.0 | 92.75 | 124.08 | 0.0000 | 225.22 | 334.44 | 0.0000 |
| 68 | 28.2 | 27.0 | 94.22 | 124.75 | 0.0000 | 227.28 | 334.44 | 0.0000 |
| 69 | 28.2 | 27.0 | 94.98 | 127.18 | 0.0000 | 231.40 | 326.67 | 0.0000 |
| 70 | 28.2 | 27.0 | 92.54 | 128.16 | 0.0000 | 233.91 | 355.00 | 0.0000 |
| 71 | 28.3 | 27.0 | 94.36 | 125.74 | 0.0000 | 233.77 | 342.22 | 0.0000 |
| 72 | 28.3 | 27.0 | 95.02 | 125.58 | 0.0000 | 233.65 | 351.67 | 0.0000 |

| Time (min) | T_{ambient} (°C) | T_{gas} (°C) | T_{water} (°C) | CO (ppm) | SO₂ (ppm) | C_xH_y (ppm) | CO₂ (ppm) | NO_x (ppm) |
|-------------------|---------------------------------|-----------------------------|-------------------------------|-----------------|-----------------------------|---|-----------------------------|-----------------------------|
| 73 | 28.3 | 27.0 | 95.01 | 123.65 | 0.0000 | 232.62 | 333.33 | 0.0000 |
| 74 | 28.4 | 27.0 | 95.00 | 126.37 | 0.0000 | 237.77 | 323.89 | 0.0000 |
| 75 | 28.4 | 27.0 | 95.00 | 122.10 | 0.0000 | 231.48 | 308.33 | 0.0000 |
| 76 | 28.5 | 27.0 | 95.00 | 120.36 | 0.0000 | 231.14 | 296.11 | 0.0000 |
| 77 | 28.5 | 27.0 | 95.02 | 119.93 | 0.0000 | 233.42 | 299.44 | 0.0000 |
| 78 | 28.5 | 27.5 | 95.01 | 119.56 | 0.0000 | 235.14 | 301.11 | 0.0000 |
| 79 | 28.6 | 27.0 | 95.02 | 118.14 | 0.0000 | 235.14 | 293.89 | 0.0000 |
| 80 | 28.6 | 27.0 | 95.03 | 118.02 | 0.0000 | 236.28 | 291.11 | 0.0000 |
| 81 | 28.6 | 27.0 | 95.06 | 115.61 | 0.0000 | 235.25 | 289.44 | 0.0000 |
| 82 | 28.7 | 27.0 | 95.03 | 114.68 | 0.0000 | 237.08 | 293.33 | 0.0000 |
| 83 | 28.7 | 27.0 | 95.03 | 112.86 | 0.0000 | 237.54 | 282.22 | 0.0000 |
| 84 | 28.7 | 27.0 | 95.01 | 112.05 | 0.0000 | 240.17 | 278.89 | 0.0000 |
| 85 | 28.8 | 27.0 | 95.01 | 109.70 | 0.0000 | 236.74 | 276.11 | 0.0000 |
| 86 | 28.8 | 27.0 | 95.01 | 108.22 | 0.0000 | 236.74 | 275.00 | 0.0000 |
| 87 | 28.8 | 27.0 | 95.01 | 105.37 | 0.0000 | 235.94 | 272.78 | 0.0000 |
| 88 | 28.8 | 27.0 | 95.01 | 103.99 | 0.0000 | 235.48 | 270.56 | 0.0000 |
| 89 | 28.8 | 27.0 | 95.00 | 103.08 | 0.0000 | 236.97 | 285.00 | 0.0000 |
| 90 | 28.8 | 27.0 | 95.00 | 101.01 | 0.0000 | 235.03 | 282.78 | 0.0000 |
| 91 | 28.8 | 27.0 | 95.05 | 99.07 | 0.0000 | 234.80 | 281.11 | 0.0000 |
| 92 | 28.8 | 27.0 | 95.01 | 96.92 | 0.0000 | 233.54 | 279.44 | 0.0000 |
| 93 | 28.8 | 27.0 | 95.00 | 94.45 | 0.0000 | 232.39 | 277.78 | 0.0000 |
| 94 | 28.8 | 27.0 | 95.00 | 92.17 | 0.0000 | 231.94 | 271.67 | 0.0000 |
| 95 | 28.8 | 27.0 | 95.00 | 91.09 | 0.0000 | 232.62 | 273.89 | 0.0000 |
| 96 | 28.8 | 27.0 | 95.01 | 88.67 | 0.0000 | 230.91 | 269.44 | 0.0000 |
| 97 | 28.8 | 27.0 | 95.00 | 87.11 | 0.0000 | 230.11 | 269.44 | 0.0000 |
| 98 | 28.8 | 27.0 | 95.00 | 84.61 | 0.0000 | 227.82 | 267.22 | 0.0000 |
| 99 | 28.8 | 27.0 | 95.00 | 82.61 | 0.0000 | 226.90 | 265.00 | 0.0000 |
| 100 | 28.8 | 27.0 | 95.00 | 81.29 | 0.0000 | 227.47 | 271.11 | 0.0000 |
| 101 | 28.8 | 27.0 | 95.00 | 79.86 | 0.0000 | 227.47 | 266.11 | 0.0000 |
| 102 | 28.8 | 27.0 | 95.00 | 77.98 | 0.0000 | 225.19 | 265.56 | 0.0000 |
| 103 | 28.8 | 27.0 | 95.00 | 75.96 | 0.0000 | 223.36 | 263.33 | 0.0000 |
| 104 | 28.8 | 27.0 | 95.00 | 73.20 | 0.0000 | 222.10 | 262.22 | 0.0000 |
| 105 | 28.8 | 27.0 | 95.01 | 72.12 | 0.0000 | 222.33 | 262.78 | 0.0000 |
| 106 | 28.8 | 27.0 | 95.00 | 69.66 | 0.0000 | 221.18 | 267.78 | 0.0000 |
| 107 | 28.8 | 27.0 | 95.00 | 67.99 | 0.0000 | 219.81 | 257.78 | 0.0000 |
| 108 | 28.8 | 27.0 | 95.00 | 65.27 | 0.0000 | 217.06 | 257.78 | 0.0000 |
| 109 | 28.8 | 27.0 | 94.98 | 63.22 | 0.0000 | 215.23 | 252.78 | 0.0000 |

| Time (min) | T_{ambient} (°C) | T_{gas} (°C) | T_{water} (°C) | CO (ppm) | SO₂ (ppm) | C_xH_y (ppm) | CO₂ (ppm) | NO_x (ppm) |
|-----------------------|---------------------------------|-----------------------------|-------------------------------|-----------------|-----------------------------|---|-----------------------------|-----------------------------|
| 110 | 28.8 | 27.0 | 94.98 | 60.82 | 0.0000 | 214.09 | 251.67 | 0.0000 |
| 111 | 28.8 | 27.0 | 94.90 | 59.70 | 0.0000 | 214.20 | 253.89 | 0.0000 |
| 112 | 28.8 | 27.0 | 94.91 | 57.49 | 0.0000 | 211.69 | 247.22 | 0.0000 |
| 113 | 28.8 | 27.0 | 94.86 | 55.91 | 0.0000 | 210.54 | 246.11 | 0.0000 |
| 114 | 28.8 | 27.0 | 94.76 | 53.54 | 0.0000 | 207.68 | 245.56 | 0.0000 |
| 114.2 | 28.8 | 27.0 | 94.75 | 51.25 | 0.0000 | 205.85 | 242.22 | 0.0000 |

Appendix 34: Temperature profiles and gaseous emissions during the WBT (B30)

| Time (min) | T_{ambient} (°C) | T_{gas} (°C) | T_{water} (°C) | CO (ppm) | SO₂ (ppm) | C_xH_y (ppm) | CO₂ (ppm) | NO_x (ppm) |
|-------------------|---------------------------------|-----------------------------|-------------------------------|-----------------|-----------------------------|---|-----------------------------|-----------------------------|
| 0 | 30.2 | 27.0 | 22.4 | 0.00 | 0.0000 | 0.00 | 0.00 | 0.0000 |
| 1 | 30.3 | 27.0 | 22.4 | 2.53 | 0.0000 | 13.04 | 0.00 | 0.0000 |
| 2 | 30.4 | 27.0 | 22.4 | 8.04 | 0.0000 | 37.87 | 3.33 | 0.0000 |
| 3 | 30.4 | 28.0 | 22.4 | 14.41 | 0.0000 | 69.68 | 10.00 | 0.0000 |
| 4 | 30.5 | 28.8 | 22.4 | 20.28 | 0.0000 | 93.59 | 37.22 | 0.0000 |
| 5 | 30.6 | 29.3 | 22.4 | 22.85 | 0.0000 | 94.05 | 113.33 | 0.0000 |
| 6 | 30.6 | 30.0 | 22.4 | 22.19 | 0.0000 | 94.51 | 143.89 | 0.0000 |
| 7 | 30.6 | 30.0 | 22.8 | 18.93 | 0.0000 | 85.58 | 136.67 | 0.0000 |
| 8 | 30.6 | 29.0 | 26.4 | 34.13 | 0.0000 | 113.39 | 135.00 | 0.0000 |
| 9 | 30.7 | 29.0 | 31.6 | 44.94 | 0.0160 | 134.44 | 194.44 | 0.1911 |
| 10 | 30.7 | 29.0 | 37.4 | 60.42 | 0.1717 | 162.24 | 253.33 | 0.3822 |
| 11 | 30.8 | 29.0 | 43.8 | 68.86 | 0.3234 | 173.57 | 281.67 | 0.3822 |
| 12 | 30.7 | 29.0 | 50.3 | 79.51 | 0.4626 | 183.75 | 298.89 | 0.3822 |
| 13 | 30.7 | 29.0 | 57.1 | 102.62 | 0.6693 | 220.25 | 337.22 | 0.4459 |
| 14 | 30.8 | 29.0 | 63.4 | 119.39 | 1.0287 | 236.61 | 332.22 | 0.9555 |
| 15 | 30.8 | 29.0 | 69.9 | 126.73 | 1.2727 | 235.24 | 344.44 | 1.4651 |
| 16 | 30.9 | 29.8 | 76.0 | 133.30 | 1.4222 | 235.46 | 332.22 | 1.5288 |
| 17 | 30.9 | 30.0 | 81.6 | 136.67 | 1.6876 | 240.27 | 338.33 | 1.6562 |
| 18 | 30.9 | 30.0 | 87.0 | 139.21 | 2.0096 | 243.13 | 346.11 | 1.9110 |
| 19 | 30.9 | 30.0 | 91.7 | 141.86 | 2.2768 | 240.84 | 351.11 | 2.5480 |
| 20 | 31.0 | 30.0 | 94.4 | 142.08 | 2.5217 | 234.09 | 353.89 | 3.1213 |
| 21 | 31.0 | 30.0 | 94.7 | 138.88 | 2.6376 | 222.08 | 386.11 | 3.4398 |
| 22 | 31.1 | 30.0 | 71.3 | 132.20 | 2.6929 | 202.74 | 411.11 | 3.6946 |
| 23 | 31.1 | 33.3 | 29.7 | 99.39 | 2.6797 | 115.33 | 685.00 | 4.5864 |
| 24 | 31.2 | 36.3 | 22.4 | 44.14 | 1.8969 | 26.09 | 948.33 | 6.1152 |
| 25 | 31.2 | 34.3 | 29.7 | 55.18 | 1.4654 | 65.33 | 556.11 | 5.1597 |
| 26 | 31.2 | 32.5 | 36.8 | 51.68 | 1.4177 | 59.61 | 401.67 | 4.5864 |
| 27 | 31.2 | 31.2 | 43.0 | 40.49 | 1.2369 | 53.89 | 348.89 | 3.8857 |
| 28 | 31.2 | 31.0 | 48.8 | 39.55 | 1.0212 | 61.67 | 297.78 | 3.5672 |
| 29 | 31.3 | 30.3 | 53.0 | 43.96 | 0.8888 | 80.21 | 273.33 | 3.3761 |
| 30 | 31.4 | 30.0 | 58.2 | 48.56 | 0.6880 | 93.71 | 249.44 | 2.9302 |
| 31 | 31.4 | 30.0 | 63.0 | 51.73 | 0.6266 | 99.09 | 231.67 | 2.6754 |
| 32 | 31.3 | 30.0 | 67.7 | 55.41 | 0.5509 | 102.63 | 223.89 | 2.4843 |
| 33 | 31.3 | 30.7 | 72.2 | 60.23 | 0.4723 | 108.47 | 232.22 | 2.2932 |
| 34 | 31.4 | 31.0 | 76.4 | 66.28 | 0.4187 | 117.16 | 227.22 | 2.2932 |
| 35 | 31.4 | 30.0 | 80.4 | 73.66 | 0.3077 | 129.98 | 226.11 | 2.2932 |

| Time (min) | T_{ambient} (°C) | T_{gas} (°C) | T_{water} (°C) | CO (ppm) | SO₂ (ppm) | C_xH_y (ppm) | CO₂ (ppm) | NO_x (ppm) |
|-------------------|---------------------------------|-----------------------------|-------------------------------|-----------------|-----------------------------|---|-----------------------------|-----------------------------|
| 36 | 31.4 | 30.0 | 84.4 | 78.85 | 0.2421 | 132.15 | 204.44 | 2.2932 |
| 37 | 31.4 | 30.0 | 88.0 | 83.88 | 0.2313 | 136.50 | 209.44 | 2.2932 |
| 38 | 31.5 | 30.0 | 91.3 | 90.44 | 0.2172 | 148.63 | 201.11 | 2.2932 |
| 39 | 31.5 | 30.0 | 93.9 | 97.67 | 0.2019 | 154.92 | 198.89 | 1.9110 |
| 40 | 31.5 | 30.0 | 94.8 | 104.41 | 0.1889 | 159.84 | 174.44 | 1.1466 |
| 41 | 31.6 | 30.8 | 81.0 | 113.50 | 0.1749 | 164.76 | 203.89 | 1.1466 |
| 42 | 31.6 | 30.5 | 94.9 | 109.90 | 0.1756 | 155.83 | 228.33 | 1.1466 |
| 43 | 31.6 | 30.0 | 95.0 | 106.52 | 0.1149 | 146.22 | 188.33 | 1.1466 |
| 44 | 31.6 | 30.0 | 95.0 | 109.04 | 0.0959 | 146.22 | 177.78 | 1.1466 |
| 45 | 31.6 | 30.0 | 95.0 | 110.46 | 0.0929 | 145.77 | 167.78 | 1.1466 |
| 46 | 31.5 | 30.0 | 95.0 | 113.66 | 0.0346 | 149.66 | 160.00 | 1.1466 |
| 47 | 31.6 | 30.0 | 95.0 | 115.12 | 0.0052 | 150.00 | 159.44 | 1.1466 |
| 48 | 31.7 | 30.0 | 95.0 | 118.15 | 0.0007 | 155.49 | 157.22 | 1.1466 |
| 49 | 31.8 | 30.0 | 95.0 | 120.21 | 0.0006 | 157.09 | 159.44 | 1.1466 |
| 50 | 31.8 | 30.0 | 95.0 | 120.98 | 0.0002 | 157.55 | 158.33 | 1.1466 |
| 51 | 31.7 | 30.0 | 95.0 | 122.39 | 0.0012 | 157.32 | 155.00 | 1.1466 |
| 52 | 31.8 | 30.0 | 95.0 | 121.52 | 0.0015 | 155.72 | 152.22 | 1.1466 |
| 53 | 31.8 | 30.0 | 95.0 | 122.16 | 0.0008 | 157.09 | 157.78 | 1.1466 |
| 54 | 31.8 | 30.0 | 95.0 | 122.44 | 0.0014 | 157.67 | 165.00 | 1.1466 |
| 55 | 31.8 | 30.0 | 95.0 | 122.65 | 0.0012 | 157.32 | 157.78 | 1.1466 |
| 56 | 31.8 | 30.0 | 95.0 | 122.51 | 0.0016 | 157.44 | 148.89 | 1.1466 |
| 57 | 31.8 | 30.0 | 95.0 | 122.89 | 0.0011 | 158.92 | 145.00 | 1.1466 |
| 58 | 31.9 | 30.0 | 95.0 | 123.81 | 0.0006 | 160.18 | 141.11 | 1.1466 |
| 59 | 31.9 | 30.0 | 95.0 | 125.69 | 0.0007 | 162.47 | 141.67 | 1.1466 |
| 60 | 31.8 | 30.0 | 95.0 | 126.06 | 0.0009 | 162.59 | 135.56 | 1.1466 |
| 61 | 31.8 | 30.0 | 95.0 | 128.36 | 0.0000 | 166.13 | 131.11 | 1.1466 |
| 62 | 31.8 | 30.0 | 95.0 | 128.41 | 0.0006 | 166.70 | 131.67 | 1.1466 |
| 63 | 31.8 | 30.0 | 95.0 | 130.58 | 0.0000 | 168.08 | 126.11 | 1.1466 |
| 64 | 31.8 | 30.0 | 95.0 | 131.44 | 0.0000 | 169.68 | 123.89 | 1.1466 |
| 65 | 31.8 | 30.0 | 95.0 | 132.97 | 0.0000 | 171.85 | 125.00 | 1.1466 |
| 66 | 31.9 | 30.0 | 95.0 | 134.34 | 0.0000 | 175.06 | 122.78 | 1.1466 |
| 67 | 31.9 | 30.0 | 95.0 | 135.35 | 0.0000 | 176.20 | 123.33 | 1.1466 |
| 68 | 31.9 | 30.0 | 95.0 | 135.29 | 0.0000 | 175.74 | 127.78 | 1.1466 |
| 69 | 31.9 | 30.0 | 95.0 | 136.63 | 0.0000 | 177.35 | 122.78 | 1.1466 |
| 70 | 31.9 | 30.0 | 95.0 | 134.96 | 0.0000 | 175.29 | 121.11 | 1.0829 |
| 71 | 32.0 | 30.0 | 95.0 | 134.79 | 0.0000 | 175.40 | 128.89 | 0.7644 |
| 72 | 32.0 | 30.0 | 95.0 | 131.24 | 0.0000 | 171.05 | 117.78 | 0.7007 |

| Time (min) | T_{ambient} (°C) | T_{gas} (°C) | T_{water} (°C) | CO (ppm) | SO₂ (ppm) | C_xH_y (ppm) | CO₂ (ppm) | NO_x (ppm) |
|-------------------|---------------------------------|-----------------------------|-------------------------------|-----------------|-----------------------------|---|-----------------------------|-----------------------------|
| 73 | 32.0 | 30.0 | 95.0 | 130.62 | 0.0000 | 169.68 | 117.22 | 0.3822 |
| 74 | 32.0 | 29.2 | 95.0 | 130.36 | 0.0000 | 168.54 | 115.56 | 0.3822 |
| 75 | 32.0 | 29.0 | 95.0 | 127.71 | 0.0000 | 165.68 | 111.67 | 0.3822 |
| 76 | 32.0 | 29.0 | 94.9 | 125.35 | 0.0000 | 161.79 | 110.00 | 0.3822 |
| 77 | 32.0 | 29.0 | 94.9 | 123.91 | 0.0000 | 161.21 | 106.11 | 0.3822 |
| 78 | 32.0 | 30.0 | 94.9 | 123.23 | 0.0000 | 159.73 | 107.22 | 0.3822 |
| 79 | 32.1 | 30.0 | 94.9 | 121.44 | 0.0000 | 157.41 | 107.22 | 0.3822 |
| 80 | 32.0 | 29.8 | 94.9 | 119.51 | 0.0000 | 155.23 | 115.56 | 0.3822 |
| 81 | 32.1 | 29.0 | 94.9 | 117.35 | 0.0002 | 153.17 | 115.00 | 0.3822 |
| 82 | 32.0 | 29.0 | 94.9 | 116.08 | 0.0001 | 151.79 | 110.00 | 0.3822 |
| 83 | 32.1 | 29.0 | 94.9 | 114.96 | 0.0006 | 150.42 | 106.11 | 0.3822 |
| 84 | 32.1 | 29.0 | 94.9 | 112.39 | 0.0024 | 148.36 | 108.33 | 0.3822 |
| 84.5 | 32.2 | 29.0 | 94.9 | 110.61 | 0.0021 | 148.13 | 118.33 | 0.3822 |

Appendix 35: Temperature profiles and gaseous emissions during the WBT (B35)

| Time (min) | T_{ambient} (°C) | T_{gas} (°C) | T_{water} (°C) | CO (ppm) | SO₂ (ppm) | C_xH_y (ppm) | CO₂ (ppm) | NO_x (ppm) |
|-------------------|---------------------------------|-----------------------------|-------------------------------|-----------------|-----------------------------|---|-----------------------------|-----------------------------|
| 0 | 26.9 | 25.0 | 20.3 | 0.00 | 0.0000 | 0.00 | 0.00 | 0.0000 |
| 1 | 26.9 | 25.8 | 20.3 | 0.81 | 0.0000 | 12.67 | 206.11 | 0.0000 |
| 2 | 27.1 | 26.0 | 20.3 | 5.49 | 0.0000 | 45.85 | 296.67 | 0.0000 |
| 3 | 27.1 | 27.0 | 20.3 | 10.92 | 0.0000 | 68.28 | 417.22 | 0.0000 |
| 4 | 27.2 | 28.3 | 20.3 | 10.20 | 0.0000 | 52.72 | 581.11 | 0.0000 |
| 5 | 27.3 | 30.5 | 20.3 | 6.98 | 0.0000 | 30.75 | 798.33 | 0.0000 |
| 6 | 27.3 | 33.2 | 20.3 | 7.02 | 0.0000 | 25.60 | 1022.22 | 0.0000 |
| 7 | 27.4 | 34.0 | 20.8 | 13.41 | 0.0000 | 45.28 | 1132.22 | 0.0000 |
| 8 | 27.4 | 31.3 | 24.8 | 38.11 | 0.0163 | 130.64 | 975.56 | 0.0000 |
| 9 | 27.5 | 30.2 | 31.1 | 60.37 | 0.2650 | 163.23 | 931.11 | 0.0000 |
| 10 | 27.6 | 29.0 | 37.4 | 74.70 | 0.3960 | 179.01 | 943.89 | 0.0000 |
| 11 | 27.7 | 29.0 | 43.6 | 82.00 | 0.4664 | 183.59 | 955.56 | 0.0000 |
| 12 | 27.8 | 29.0 | 50.2 | 89.38 | 0.6553 | 189.31 | 956.11 | 0.0000 |
| 13 | 27.8 | 29.0 | 56.6 | 98.46 | 0.8542 | 200.06 | 962.78 | 0.0000 |
| 14 | 27.9 | 29.0 | 62.9 | 105.29 | 1.0719 | 208.19 | 977.78 | 0.0000 |
| 15 | 27.9 | 28.0 | 69.0 | 111.87 | 1.2216 | 209.33 | 988.89 | 0.0000 |
| 16 | 27.9 | 28.0 | 74.6 | 116.05 | 1.2264 | 213.11 | 991.11 | 0.0000 |
| 17 | 28.0 | 28.0 | 79.8 | 122.83 | 1.4982 | 222.95 | 1017.78 | 0.0000 |
| 18 | 28.0 | 28.0 | 85.5 | 128.97 | 1.7446 | 233.24 | 1031.67 | 0.0000 |
| 19 | 28.1 | 28.0 | 90.6 | 130.31 | 1.9324 | 235.99 | 1060.56 | 0.0634 |
| 20 | 28.2 | 28.2 | 93.9 | 131.07 | 2.1082 | 234.50 | 1066.67 | 0.3801 |
| 21 | 28.3 | 29.0 | 94.7 | 130.15 | 2.3147 | 226.15 | 1095.00 | 0.3801 |
| 22 | 28.3 | 29.2 | 79.9 | 123.07 | 2.4389 | 208.99 | 1121.67 | 0.6986 |
| 23 | 28.3 | 33.0 | 35.0 | 89.05 | 2.3056 | 114.71 | 1526.67 | 1.7805 |
| 24 | 28.4 | 34.5 | 20.3 | 59.13 | 1.8108 | 63.22 | 1642.78 | 2.4164 |
| 25 | 28.5 | 31.5 | 29.6 | 65.82 | 1.5911 | 97.17 | 1354.44 | 1.8431 |
| 26 | 28.5 | 30.3 | 37.8 | 52.19 | 1.6067 | 70.40 | 1217.22 | 1.5246 |
| 27 | 28.6 | 29.2 | 43.9 | 46.80 | 1.5909 | 65.72 | 1145.56 | 1.0171 |
| 28 | 28.6 | 29.0 | 49.1 | 37.91 | 1.2962 | 53.93 | 1091.11 | 0.7623 |
| 29 | 28.7 | 28.2 | 53.3 | 32.95 | 1.0884 | 51.87 | 1058.33 | 0.6986 |
| 30 | 28.7 | 28.0 | 58.6 | 33.18 | 1.0198 | 65.84 | 1001.11 | 0.3801 |
| 31 | 28.8 | 28.0 | 63.3 | 37.62 | 0.8604 | 79.10 | 990.00 | 0.3801 |
| 32 | 28.8 | 28.0 | 68.0 | 42.43 | 0.7273 | 90.98 | 981.11 | 0.3801 |
| 33 | 28.8 | 28.0 | 72.5 | 46.72 | 0.7184 | 98.76 | 972.22 | 0.1267 |
| 34 | 28.8 | 28.0 | 76.6 | 52.27 | 0.6384 | 108.38 | 963.33 | 0.0000 |
| 35 | 28.9 | 28.0 | 80.8 | 57.22 | 0.5459 | 115.70 | 963.89 | 0.0000 |

| Time (min) | T_{ambient} (°C) | T_{gas} (°C) | T_{water} (°C) | CO (ppm) | SO₂ (ppm) | C_xH_y (ppm) | CO₂ (ppm) | NO_x (ppm) |
|-------------------|---------------------------------|-----------------------------|-------------------------------|-----------------|-----------------------------|---|-----------------------------|-----------------------------|
| 36 | 29.0 | 28.0 | 84.7 | 63.45 | 0.5192 | 127.71 | 973.33 | 0.0000 |
| 37 | 29.0 | 28.0 | 88.7 | 72.20 | 0.5006 | 144.07 | 964.44 | 0.0000 |
| 38 | 29.0 | 27.8 | 92.0 | 79.70 | 0.4301 | 157.92 | 958.33 | 0.0000 |
| 39 | 29.1 | 27.0 | 85.2 | 85.64 | 0.3902 | 163.75 | 958.33 | 0.0000 |
| 40 | 29.1 | 28.3 | 53.2 | 99.94 | 0.3604 | 184.81 | 1016.67 | 0.0000 |
| 41 | 29.1 | 28.0 | 93.8 | 92.50 | 0.3755 | 168.67 | 981.11 | 0.0000 |
| 42 | 29.2 | 28.0 | 95.0 | 93.38 | 0.3736 | 167.76 | 969.44 | 0.0000 |
| 43 | 29.2 | 28.0 | 95.1 | 94.75 | 0.3162 | 167.30 | 951.67 | 0.0000 |
| 44 | 29.2 | 28.0 | 95.1 | 96.63 | 0.2851 | 168.67 | 943.33 | 0.0000 |
| 45 | 29.2 | 28.0 | 95.1 | 101.64 | 0.2743 | 177.94 | 945.56 | 0.0000 |
| 46 | 29.2 | 28.0 | 95.1 | 101.35 | 0.2746 | 176.00 | 931.11 | 0.0000 |
| 47 | 29.3 | 27.2 | 95.1 | 100.02 | 0.2095 | 173.37 | 918.33 | 0.0000 |
| 48 | 29.4 | 27.5 | 95.1 | 100.40 | 0.1951 | 173.02 | 910.00 | 0.0000 |
| 49 | 29.4 | 28.0 | 95.1 | 100.44 | 0.1947 | 174.40 | 903.33 | 0.0000 |
| 50 | 29.4 | 28.0 | 95.1 | 100.27 | 0.1951 | 175.20 | 901.67 | 0.0000 |
| 51 | 29.4 | 28.0 | 95.1 | 100.43 | 0.1951 | 177.60 | 897.22 | 0.0000 |
| 52 | 29.4 | 28.0 | 95.1 | 103.79 | 0.1881 | 185.15 | 904.44 | 0.0000 |
| 53 | 29.5 | 28.0 | 95.1 | 104.50 | 0.1872 | 187.10 | 898.89 | 0.0000 |
| 54 | 29.5 | 28.0 | 95.1 | 104.90 | 0.1873 | 188.13 | 908.89 | 0.0000 |
| 55 | 29.5 | 28.0 | 95.1 | 106.24 | 0.1858 | 191.21 | 892.22 | 0.0000 |
| 56 | 29.5 | 28.0 | 95.1 | 106.64 | 0.1856 | 193.85 | 918.89 | 0.0000 |
| 57 | 29.5 | 28.0 | 95.1 | 107.43 | 0.1843 | 196.36 | 906.67 | 0.0000 |
| 58 | 29.6 | 28.0 | 95.1 | 107.72 | 0.1838 | 198.08 | 901.11 | 0.0000 |
| 59 | 29.6 | 28.0 | 95.1 | 107.82 | 0.1817 | 200.25 | 906.67 | 0.0000 |
| 60 | 29.6 | 28.0 | 95.0 | 108.13 | 0.1812 | 202.89 | 905.00 | 0.0000 |
| 61 | 29.6 | 28.0 | 95.1 | 108.75 | 0.1803 | 205.06 | 894.44 | 0.0000 |
| 62 | 29.7 | 28.0 | 95.1 | 110.42 | 0.1783 | 208.72 | 874.44 | 0.0000 |
| 63 | 29.7 | 28.0 | 95.1 | 112.01 | 0.1764 | 211.70 | 877.78 | 0.0000 |
| 64 | 29.7 | 28.0 | 95.1 | 112.69 | 0.1761 | 213.98 | 878.89 | 0.0000 |
| 65 | 29.7 | 28.0 | 95.1 | 113.99 | 0.1193 | 216.84 | 870.56 | 0.0000 |
| 66 | 29.7 | 28.0 | 95.1 | 115.25 | 0.0894 | 221.19 | 868.89 | 0.0000 |
| 67 | 29.7 | 28.0 | 95.1 | 116.84 | 0.0851 | 224.74 | 881.11 | 0.0000 |
| 68 | 29.7 | 28.0 | 95.1 | 117.89 | 0.0827 | 227.94 | 874.44 | 0.0000 |
| 69 | 29.7 | 28.0 | 95.1 | 117.93 | 0.0809 | 228.40 | 871.11 | 0.0000 |
| 70 | 29.8 | 28.0 | 95.1 | 117.76 | 0.0803 | 230.00 | 867.22 | 0.0000 |
| 71 | 29.8 | 28.0 | 95.1 | 116.93 | 0.0803 | 230.35 | 860.56 | 0.0000 |
| 72 | 29.9 | 28.0 | 95.1 | 115.52 | 0.0828 | 230.09 | 871.67 | 0.0000 |

| Time (min) | T_{ambient} (°C) | T_{gas} (°C) | T_{water} (°C) | CO (ppm) | SO₂ (ppm) | C_xH_y (ppm) | CO₂ (ppm) | NO_x (ppm) |
|-------------------|---------------------------------|-----------------------------|-------------------------------|-----------------|-----------------------------|---|-----------------------------|-----------------------------|
| 73 | 29.8 | 28.0 | 95.1 | 114.20 | 0.0846 | 228.71 | 871.67 | 0.0000 |
| 74 | 29.8 | 28.0 | 95.1 | 112.88 | 0.0859 | 226.99 | 867.78 | 0.0000 |
| 75 | 29.8 | 28.0 | 95.1 | 112.05 | 0.0874 | 227.79 | 868.33 | 0.0000 |
| 76 | 29.9 | 28.0 | 95.1 | 110.36 | 0.0893 | 226.31 | 866.67 | 0.0000 |
| 77 | 29.9 | 28.0 | 95.1 | 108.53 | 0.0921 | 225.16 | 870.00 | 0.0000 |
| 78 | 29.9 | 28.0 | 95.1 | 107.07 | 0.0942 | 223.90 | 868.89 | 0.0000 |
| 79 | 30.0 | 28.0 | 95.1 | 106.06 | 0.0947 | 223.68 | 872.22 | 0.0000 |
| 80 | 30.0 | 28.0 | 95.1 | 103.17 | 0.0990 | 221.73 | 872.78 | 0.0000 |
| 81 | 30.0 | 28.0 | 95.1 | 102.29 | 0.0999 | 222.74 | 874.44 | 0.0000 |
| 82 | 30.0 | 28.0 | 95.1 | 100.74 | 0.1029 | 221.58 | 875.56 | 0.0000 |
| 83 | 30.0 | 28.0 | 95.1 | 99.13 | 0.1041 | 220.67 | 872.78 | 0.0000 |
| 84 | 30.0 | 28.0 | 95.1 | 97.62 | 0.1069 | 219.87 | 880.00 | 0.0000 |
| 84.5 | 30.0 | 28.0 | 95.1 | 97.20 | 0.1079 | 220.89 | 885.56 | 0.0000 |

Appendix 36: Temperature profiles and gaseous emissions during the WBT (B40)

| Time (min) | T_{ambient} (°C) | T_{gas} (°C) | T_{water} (°C) | CO (ppm) | SO₂ (ppm) | C_xH_y (ppm) | CO₂ (ppm) | NO_x (ppm) |
|-------------------|---------------------------------|-----------------------------|-------------------------------|-----------------|-----------------------------|---|-----------------------------|-----------------------------|
| 0 | 26.1 | 23.7 | 20.5 | 0.00 | 0.0000 | 0.00 | 0.00 | 0.0000 |
| 1 | 26.1 | 23.9 | 13.8 | 0.87 | 0.0000 | 3.32 | 133.33 | 0.0000 |
| 2 | 26.2 | 24.4 | 20.5 | 4.40 | 0.0000 | 23.00 | 196.67 | 0.1275 |
| 3 | 26.3 | 25.0 | 20.5 | 9.92 | 0.0000 | 50.69 | 260.00 | 0.0425 |
| 4 | 26.4 | 26.9 | 20.5 | 15.98 | 0.0000 | 65.22 | 493.89 | 0.0000 |
| 5 | 26.4 | 29.7 | 20.6 | 15.12 | 0.0000 | 46.91 | 823.33 | 0.0000 |
| 6 | 26.5 | 33.3 | 20.6 | 18.84 | 0.0000 | 36.96 | 1205.00 | 0.0212 |
| 7 | 26.5 | 35.2 | 22.5 | 52.02 | 0.0658 | 112.02 | 1523.89 | 0.1274 |
| 8 | 26.6 | 31.3 | 28.4 | 120.65 | 0.6716 | 295.90 | 866.67 | 0.1699 |
| 9 | 26.6 | 29.0 | 35.2 | 148.02 | 1.4458 | 310.77 | 736.67 | 0.2548 |
| 10 | 26.6 | 28.0 | 42.4 | 154.80 | 1.8266 | 289.37 | 748.89 | 0.2548 |
| 11 | 26.7 | 27.6 | 49.5 | 154.30 | 2.1006 | 266.83 | 750.56 | 0.4884 |
| 12 | 26.7 | 27.6 | 58.6 | 151.98 | 2.2692 | 250.93 | 772.78 | 0.5096 |
| 13 | 26.8 | 27.3 | 65.1 | 156.89 | 2.3818 | 246.46 | 773.33 | 0.5096 |
| 14 | 26.8 | 27.3 | 71.5 | 159.34 | 2.4446 | 244.63 | 784.44 | 0.5521 |
| 15 | 26.9 | 27.3 | 77.3 | 165.00 | 2.5282 | 255.85 | 797.78 | 0.6370 |
| 16 | 26.9 | 27.7 | 83.0 | 166.39 | 2.6889 | 252.99 | 829.44 | 0.7007 |
| 17 | 26.9 | 28.9 | 88.3 | 178.04 | 2.8556 | 233.19 | 1104.44 | 0.8918 |
| 18 | 27.0 | 28.4 | 80.7 | 169.14 | 3.0507 | 251.96 | 870.00 | 0.8918 |
| 19 | 27.0 | 28.2 | 73.6 | 154.36 | 3.1773 | 231.25 | 813.33 | 0.8918 |
| 20 | 27.1 | 29.1 | 67.7 | 124.34 | 3.0366 | 160.76 | 942.22 | 0.9555 |
| 21 | 27.1 | 30.8 | 53.0 | 98.19 | 2.7506 | 108.13 | 1122.78 | 1.0617 |
| 22 | 27.2 | 30.4 | 50.9 | 93.28 | 2.5168 | 109.16 | 1060.56 | 1.3589 |
| 23 | 27.2 | 29.8 | 36.9 | 89.42 | 2.4558 | 104.35 | 990.00 | 1.3377 |
| 24 | 27.3 | 30.3 | 39.7 | 54.73 | 2.0933 | 36.62 | 1066.67 | 1.4014 |
| 25 | 27.3 | 29.2 | 43.9 | 44.60 | 1.7197 | 26.66 | 837.22 | 1.1891 |
| 26 | 27.3 | 28.2 | 48.5 | 36.40 | 1.4093 | 21.51 | 735.56 | 0.9980 |
| 27 | 27.4 | 27.5 | 54.2 | 36.25 | 1.2056 | 42.91 | 686.11 | 0.7644 |
| 28 | 27.4 | 27.3 | 59.4 | 38.19 | 1.1193 | 55.61 | 654.44 | 0.5945 |
| 29 | 27.5 | 27.3 | 64.0 | 40.48 | 0.8555 | 64.08 | 626.67 | 0.5096 |
| 30 | 27.5 | 27.3 | 69.1 | 45.64 | 0.7898 | 76.55 | 625.56 | 0.5096 |
| 31 | 27.5 | 27.0 | 73.3 | 51.14 | 0.6692 | 89.71 | 598.89 | 0.5096 |
| 32 | 27.6 | 27.0 | 77.3 | 58.46 | 0.5310 | 104.12 | 592.78 | 0.5096 |
| 33 | 27.6 | 27.0 | 81.3 | 66.02 | 0.4737 | 116.37 | 587.22 | 0.4247 |
| 34 | 27.6 | 26.9 | 81.1 | 72.76 | 0.4182 | 127.01 | 579.44 | 0.3822 |
| 35 | 27.7 | 26.7 | 68.6 | 78.07 | 0.4072 | 132.39 | 571.67 | 0.2973 |

| Time (min) | T_{ambient} (°C) | T_{gas} (°C) | T_{water} (°C) | CO (ppm) | SO₂ (ppm) | C_xH_y (ppm) | CO₂ (ppm) | NO_x (ppm) |
|-------------------|---------------------------------|-----------------------------|-------------------------------|-----------------|-----------------------------|---|-----------------------------|-----------------------------|
| 36 | 27.7 | 26.6 | 88.7 | 87.01 | 0.3882 | 144.17 | 591.11 | 0.2548 |
| 37 | 27.7 | 26.7 | 87.9 | 82.40 | 0.3987 | 135.02 | 568.33 | 0.1274 |
| 38 | 27.8 | 27.3 | 73.3 | 98.27 | 0.3656 | 159.14 | 605.56 | 0.1274 |
| 39 | 27.8 | 27.4 | 93.2 | 99.87 | 0.3614 | 154.89 | 608.33 | 0.1274 |
| 40 | 27.8 | 27.3 | 85.9 | 97.80 | 0.3652 | 149.40 | 578.89 | 0.1274 |
| 41 | 27.9 | 27.7 | 86.0 | 107.32 | 0.3177 | 160.15 | 602.78 | 0.1274 |
| 42 | 27.9 | 27.4 | 94.1 | 98.19 | 0.2659 | 143.45 | 565.56 | 0.1274 |
| 43 | 27.9 | 27.0 | 95.1 | 100.96 | 0.1797 | 145.62 | 569.44 | 0.1274 |
| 44 | 27.9 | 27.0 | 95.0 | 102.88 | 0.1786 | 146.42 | 556.67 | 0.1274 |
| 45 | 28.0 | 27.0 | 95.0 | 103.80 | 0.1782 | 147.34 | 548.33 | 0.1274 |
| 46 | 28.0 | 27.0 | 95.0 | 104.63 | 0.1766 | 147.34 | 536.11 | 0.1274 |
| 47 | 28.0 | 27.0 | 95.0 | 105.85 | 0.1735 | 147.80 | 544.44 | 0.1274 |
| 48 | 28.0 | 27.0 | 95.0 | 106.08 | 0.1732 | 147.80 | 542.78 | 0.0849 |
| 49 | 28.1 | 27.0 | 95.0 | 106.31 | 0.1731 | 148.83 | 527.78 | 0.0000 |
| 50 | 28.1 | 27.0 | 95.0 | 107.09 | 0.1735 | 151.23 | 528.33 | 0.0000 |
| 51 | 28.1 | 27.0 | 95.0 | 108.42 | 0.1188 | 151.69 | 528.89 | 0.0000 |
| 52 | 28.1 | 26.9 | 95.0 | 104.12 | 0.0903 | 145.85 | 521.67 | 0.0000 |
| 53 | 28.2 | 26.7 | 95.0 | 109.84 | 0.0202 | 155.46 | 506.11 | 0.0000 |
| 54 | 28.2 | 26.7 | 95.0 | 109.81 | 0.0068 | 156.15 | 507.78 | 0.0000 |
| 55 | 28.2 | 26.7 | 95.0 | 111.31 | 0.0062 | 157.29 | 507.78 | 0.0000 |
| 56 | 28.2 | 26.7 | 95.0 | 111.84 | 0.0050 | 158.09 | 505.56 | 0.0000 |
| 57 | 28.3 | 26.7 | 95.0 | 112.02 | 0.0057 | 158.67 | 498.89 | 0.0000 |
| 58 | 28.3 | 26.6 | 95.0 | 112.88 | 0.0054 | 161.30 | 492.78 | 0.0000 |
| 59 | 28.3 | 26.3 | 95.0 | 113.74 | 0.0033 | 162.90 | 480.56 | 0.0000 |
| 60 | 28.3 | 26.3 | 95.0 | 114.45 | 0.0035 | 163.81 | 472.78 | 0.0000 |
| 61 | 28.4 | 26.3 | 95.0 | 114.37 | 0.0039 | 163.81 | 470.00 | 0.0000 |
| 62 | 28.4 | 26.3 | 95.0 | 114.25 | 0.0049 | 163.47 | 471.67 | 0.0000 |
| 63 | 28.4 | 26.1 | 95.0 | 114.49 | 0.0058 | 163.36 | 477.22 | 0.0000 |
| 64 | 28.4 | 26.0 | 95.0 | 114.55 | 0.0049 | 163.13 | 468.89 | 0.0000 |
| 65 | 28.4 | 26.0 | 95.0 | 115.94 | 0.0044 | 165.53 | 468.33 | 0.0000 |
| 66 | 28.4 | 26.0 | 94.9 | 116.70 | 0.0032 | 166.79 | 470.00 | 0.0000 |
| 67 | 28.4 | 26.0 | 94.9 | 116.98 | 0.0027 | 167.46 | 484.44 | 0.0000 |
| 68 | 28.5 | 26.0 | 94.9 | 116.18 | 0.0030 | 166.75 | 471.11 | 0.0000 |
| 69 | 28.5 | 26.0 | 94.9 | 116.78 | 0.0023 | 169.50 | 472.22 | 0.0000 |
| 70 | 28.5 | 26.0 | 94.9 | 119.12 | 0.0006 | 171.44 | 467.78 | 0.0000 |
| 71 | 28.5 | 26.0 | 94.9 | 118.77 | 0.0004 | 169.95 | 456.11 | 0.0000 |
| 72 | 28.5 | 26.0 | 94.9 | 117.31 | 0.0016 | 167.89 | 463.89 | 0.0000 |

| Time (min) | T_{ambient} (°C) | T_{gas} (°C) | T_{water} (°C) | CO (ppm) | SO₂ (ppm) | C_xH_y (ppm) | CO₂ (ppm) | NO_x (ppm) |
|-------------------|---------------------------------|-----------------------------|-------------------------------|-----------------|-----------------------------|---|-----------------------------|-----------------------------|
| 73 | 28.6 | 26.0 | 94.9 | 116.40 | 0.0016 | 167.55 | 461.67 | 0.0000 |
| 74 | 28.6 | 26.0 | 94.9 | 115.34 | 0.0023 | 167.09 | 462.22 | 0.0000 |
| 75 | 28.6 | 26.1 | 94.9 | 113.92 | 0.0037 | 163.55 | 472.22 | 0.0000 |
| 76 | 28.6 | 26.3 | 94.9 | 113.22 | 0.0022 | 162.40 | 463.89 | 0.0000 |
| 77 | 28.7 | 26.4 | 94.9 | 111.97 | 0.0021 | 162.63 | 458.33 | 0.0000 |
| 78 | 28.7 | 26.7 | 94.9 | 110.15 | 0.0032 | 160.91 | 464.44 | 0.0000 |
| 79 | 28.7 | 26.7 | 94.9 | 109.01 | 0.0038 | 159.54 | 468.33 | 0.0000 |
| 80 | 28.7 | 26.7 | 94.9 | 107.97 | 0.0053 | 158.28 | 465.56 | 0.0000 |
| 81 | 28.7 | 26.7 | 94.9 | 105.89 | 0.0053 | 155.77 | 464.44 | 0.0000 |
| 82 | 28.8 | 26.7 | 94.9 | 104.73 | 0.0053 | 154.39 | 464.44 | 0.0000 |
| 83 | 28.8 | 26.7 | 94.9 | 103.72 | 0.0053 | 153.94 | 472.78 | 0.0000 |
| 84 | 28.8 | 26.7 | 94.9 | 102.62 | 0.0053 | 151.99 | 474.44 | 0.0000 |
| 84.5 | 28.8 | 26.7 | 94.9 | 102.51 | 0.0053 | 151.86 | 479.26 | 0.0000 |

Appendix 37: Water Boiling Test performance metrics

| Basic Operation | units | B25 | B30 | B35 | B40 |
|-------------------------------------|--------------|--------|--------|--------|--------|
| COLD START HIGH POWER PHASE | | | | | |
| Time to boil | min | 41.9 | 21.9 | 21.7 | 20.3 |
| Burning rate | g/min | 3.7 | 5.7 | 6.6 | 8.2 |
| Thermal efficiency | % | 22.52 | 28.50 | 30.86 | 21.79 |
| Specific fuel consumption | g/L | 65.4 | 53.2 | 60.5 | 70.1 |
| Temp-corrected specific consumption | g/L | 66.7 | 54.4 | 60.6 | 70.7 |
| Firepower | W | 1775.0 | 2900.1 | 3305.8 | 4123.2 |
| Equivalent Dry Fuel Consumed | g | 156.6 | 125.5 | 142.9 | 165.8 |
| HOT START HIGH POWER PHASE | | | | | |
| Time to boil | min | 25.2 | 15.8 | 17.0 | 14.7 |
| Burning rate | g/min | 2.1 | 3.6 | 3.8 | 4.2 |
| Thermal efficiency | % | 54.61 | 49.63 | 44.62 | 47.72 |
| Specific fuel consumption | g/L | 21.7 | 23.3 | 26.1 | 24.5 |
| Temp-corrected specific consumption | g/L | 22.1 | 23.8 | 26.2 | 24.7 |
| Firepower | W | 1011.5 | 1833.2 | 1908.8 | 2091.8 |
| Equivalent Dry Fuel Consumed | g | 53.6 | 57.2 | 64.5 | 60.5 |
| SIMMER PHASE | | | | | |
| Burning rate | g/min | 1.1 | 1.7 | 1.7 | 1.7 |
| Thermal efficiency | % | 39.14 | 47.96 | 50.34 | 46.87 |
| Specific fuel consumption 45 min | g/L | 22.8 | 39.4 | 39.3 | 39.3 |
| Firepower | W | 535.9 | 870.1 | 857.3 | 867.8 |
| Turn down ratio | | 2.6 | 2.7 | 3.0 | 3.6 |
| Equivalent Dry Fuel Consumed | g | 50.8 | 77.3 | 76.9 | 77.8 |
| Energy Consumption | | | | | |
| Net Calorific Value (dry) | kJ/kg | 28500. | 30400. | 30100. | 30100. |
| | | 0 | 0 | 0 | 0 |
| Moisture Content | % | 4.68 | 4.24 | 3.94 | 3.59 |
| COLD START HIGH POWER PHASE | | | | | |
| Temp-Corrected Time to Boil | min | 42.8 | 22.4 | 21.7 | 20.4 |
| Energy Consumption Rate | kJ/min | 106.5 | 174.0 | 198.3 | 247.4 |
| Temp-Corrected Specific Energy | kJ/L | 1901.8 | 1655.0 | 1825.2 | 2128.1 |
| Consumption | | | | | |
| Specific Energy Consumption Rate | MJ/min/ L | 0.0 | 0.1 | 0.1 | 0.1 |
| Dry Fuel Consumed | g | 157.3 | 125.9 | 143.4 | 166.3 |

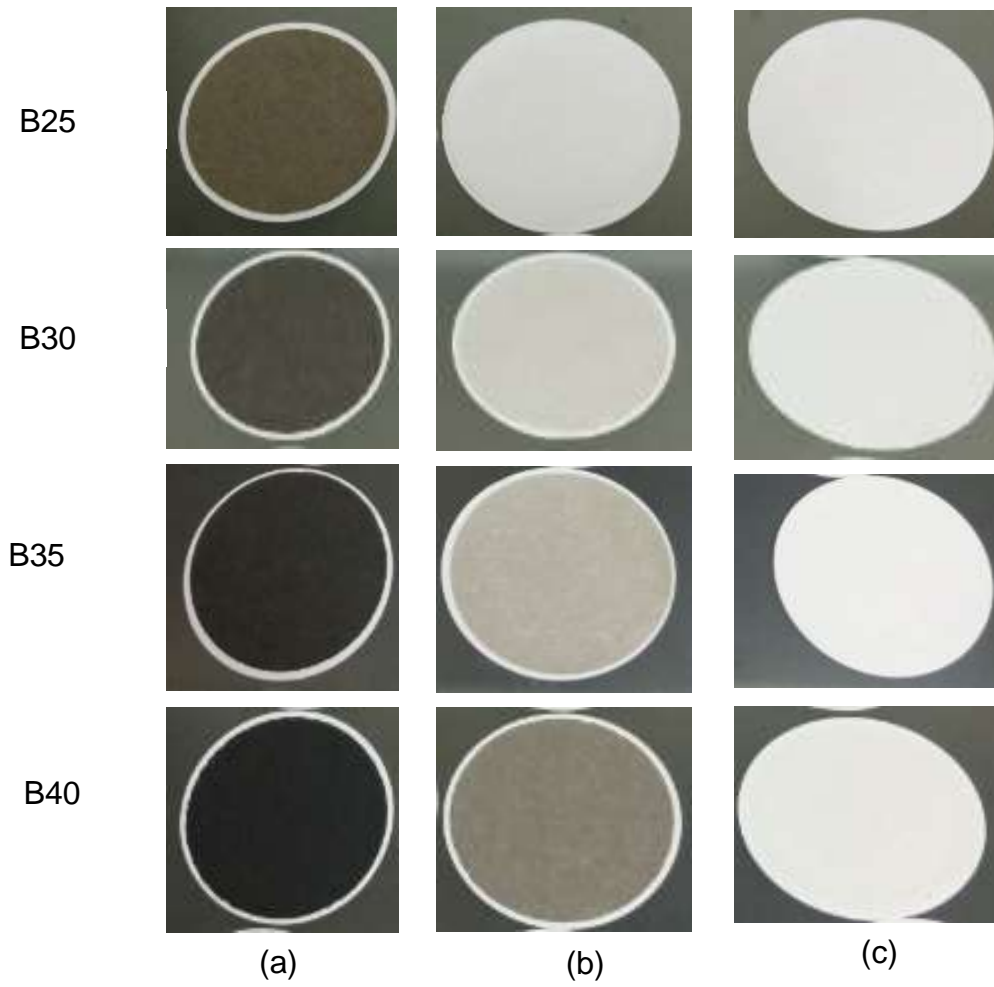
| Basic Operation | units | B25 | B30 | B35 | B40 |
|---|--------------|------------|------------|------------|------------|
| Total Energy Consumed | kJ | 4482.4 | 3828.1 | 4317.8 | 5005.8 |
| | units | B25 | B30 | B35 | B40 |
| Energy Delivered to the Cooking Pot | MJ | 1.0 | 1.1 | 1.3 | 1.1 |
| Average Cooking Power | kW | 0.4 | 0.8 | 1.0 | 0.9 |
| HOT START HIGH POWER PHASE | | | | | |
| Temp-Corrected Time to Boil | min | 25.7 | 16.2 | 17.1 | 14.8 |
| Energy Consumption Rate | kJ/min | 60.7 | 110.0 | 114.5 | 125.5 |
| Temp-Corrected Specific Energy Consumption | kJ/L | 628.4 | 723.8 | 787.6 | 744.2 |
| Consumption | | | | | |
| Specific Energy Consumption Rate | MJ/min/ L | 0.0 | 0.0 | 0.0 | 0.1 |
| Dry Fuel Consumed | g | 53.9 | 57.5 | 64.7 | 60.7 |
| Total Energy Consumed | kJ | 1534.9 | 1746.7 | 1946.9 | 1828.2 |
| Energy Delivered to the Cooking Pot | MJ | 0.8 | 0.9 | 0.9 | 0.9 |
| Average Cooking Power | kW | 0.5 | 0.9 | 0.9 | 1.0 |
| SIMMER PHASE | | | | | |
| Energy Consumption Rate | kJ/min | 32.2 | 52.2 | 51.4 | 52.1 |
| Time-Corrected Specific Energy Consumption | kJ/L | 650.9 | 1198.6 | 1182.7 | 1183.8 |
| Specific Energy Consumption Rate | MJ/min/ L | 0.0 | 0.0 | 0.0 | 0.0 |
| Dry Fuel Consumed | g | 51.0 | 77.6 | 77.2 | 78.1 |
| Total Energy Consumed | kJ | 1453.4 | 2358.0 | 2322.8 | 2350.6 |
| Energy Delivered to the Cooking Pot | MJ | 0.6 | 1.1 | 1.2 | 1.1 |
| Average Cooking Power | kW | 0.2 | 0.4 | 0.4 | 0.4 |
| Total Emissions | | | | | |
| COLD START HIGH POWER PHASE | | | | | |
| CO | g | 28.9 | 21.4 | 21.0 | 28.0 |
| CO₂ | g | 114.6 | 104.2 | 129.1 | 172.4 |
| PM_{2.5} | mg | 14.3 | 10.5 | 17.1 | 25.5 |
| HOT START HIGH POWER PHASE | | | | | |
| CO | g | 28.9 | 11.6 | 11.4 | 9.3 |
| CO₂ | g | 108.2 | 92.4 | 110.1 | 101.0 |
| PM_{2.5} | mg | 0.5 | 0.8 | 1.4 | 1.9 |
| SIMMER PHASE | | | | | |
| CO | g | 44.5 | 58.0 | 49.0 | 49.2 |
| CO₂ | g | 123.5 | 136.3 | 166.4 | 173.2 |

| Basic Operation | units | B25 | B30 | B35 | B40 |
|---|-------------------|------------|------------|------------|------------|
| PM _{2.5} | mg | 0.3 | 0.4 | 0.3 | 0.8 |
| Emissions per MJ Delivered to the Cooking Pot | | | | | |
| COLD START HIGH POWER PHASE | | | | | |
| | units | B25 | B30 | B35 | B40 |
| CO | g/MJ | 28.8 | 19.7 | 16.8 | 25.7 |
| CO ₂ | g/MJ | 115.8 | 95.5 | 99.7 | 160.4 |
| PM _{2.5} | mg/MJ | 14.2 | 9.6 | 14.1 | 23.6 |
| HOT START HIGH POWER PHASE | | | | | |
| CO | g/MJ | 34.7 | 13.4 | 13.4 | 10.7 |
| CO ₂ | g/MJ | 129.3 | 107.0 | 129.5 | 116.2 |
| PM _{2.5} | mg/MJ | 0.7 | 0.9 | 1.7 | 2.2 |
| SIMMER PHASE | | | | | |
| CO | g/MJ | 78.6 | 51.5 | 42.4 | 44.8 |
| CO ₂ | g/MJ | 218.4 | 121.2 | 141.4 | 157.7 |
| PM _{2.5} | mg/MJ | 0.6 | 0.4 | 0.3 | 0.7 |
| Specific Emissions | | | | | |
| COLD START HIGH POWER PHASE | | | | | |
| CO | g/L | 12.0 | 9.1 | 8.9 | 11.8 |
| CO ₂ | g/L | 47.7 | 44.3 | 54.7 | 72.8 |
| PM _{2.5} | µg/m ³ | 19904. | 28337. | 47265. | 76692. |
| | | 9 | 9 | 8 | 9 |
| Log (PM _{2.5}) | µg/m ³ | 4.3 | 4.4 | 4.7 | 4.9 |
| HOT START HIGH POWER PHASE | | | | | |
| CO | g/L | 11.7 | 4.7 | 4.6 | 3.8 |
| CO ₂ | g/L | 43.7 | 37.5 | 44.5 | 40.9 |
| PM _{2.5} | µg/m ³ | 1288.3 | 3050.1 | 5071.4 | 7857.4 |
| Log (PM _{2.5}) | µg/m ³ | 3.1 | 3.5 | 3.7 | 3.9 |
| SIMMER PHASE | | | | | |
| CO | g/L | 20.0 | 29.6 | 25.1 | 24.8 |
| CO ₂ | g/L | 55.6 | 69.5 | 85.4 | 87.6 |
| PM _{2.5} | µg/m ³ | 422.1 | 570.6 | 404.8 | 1034.9 |
| Log (PM _{2.5}) | µg/m ³ | 2.6 | 2.8 | 2.6 | 3.0 |
| Specific Emissions Rate | | | | | |
| COLD START HIGH POWER PHASE | | | | | |
| CO | g/min/L | 0.287 | 0.415 | 0.409 | 0.584 |
| CO ₂ | g/min/L | 1.145 | 2.021 | 2.518 | 3.639 |

| Basic Operation | units | B25 | B30 | B35 | B40 |
|---|--------------|------------|------------|------------|------------|
| PM _{2.5} | mg/min/ L | 0.143 | 0.202 | 0.334 | 0.530 |
| HOT START HIGH POWER PHASE | | | | | |
| CO | g/min/L | 0.464 | 0.298 | 0.269 | 0.257 |
| CO ₂ | g/min/L | 1.736 | 2.372 | 2.577 | 2.810 |
| | units | B25 | B30 | B35 | B40 |
| PM _{2.5} | mg/min/ L | 0.009 | 0.021 | 0.034 | 0.055 |
| SIMMER PHASE | | | | | |
| CO | g/min/L | 0.445 | 0.658 | 0.557 | 0.552 |
| CO ₂ | g/min/L | 1.235 | 1.545 | 1.897 | 1.946 |
| PM _{2.5} | mg/min/ L | 0.003 | 0.005 | 0.003 | 0.009 |
| Emissions Rate | | | | | |
| COLD START HIGH POWER PHASE | | | | | |
| CO | g/min | 0.7 | 1.0 | 1.0 | 1.4 |
| CO ₂ | g/min | 2.8 | 4.8 | 5.9 | 8.6 |
| PM _{2.5} | mg/min | 0.34 | 0.48 | 0.79 | 1.26 |
| HOT START HIGH POWER PHASE | | | | | |
| CO | g/min | 1.1 | 0.7 | 0.7 | 0.6 |
| CO ₂ | g/min | 4.3 | 5.8 | 6.4 | 6.9 |
| PM _{2.5} | mg/min | 0.02 | 0.05 | 0.09 | 0.14 |
| SIMMER PHASE | | | | | |
| CO | g/min | 1.0 | 1.3 | 1.1 | 1.1 |
| CO ₂ | g/min | 2.7 | 3.0 | 3.7 | 3.8 |
| PM _{2.5} | mg/min | 0.01 | 0.010 | 0.01 | 0.02 |
| Emission per kg Fuel | | | | | |
| COLD START HIGH POWER PHASE | | | | | |
| g CO/kg dry fuel consumed | g/kg | 183.5 | 170.6 | 146.4 | 167.9 |
| g CO ₂ /kg dry fuel consumed | g/kg | 730.9 | 833.0 | 903.7 | 1038.8 |
| g PM _{2.5} /kg dry fuel consumed | g/kg | 0.09 | 0.083 | 0.1 | 0.154 |
| HOT START HIGH POWER PHASE | | | | | |
| g CO/kg dry fuel consumed | g/kg | 538.2 | 202.0 | 175.3 | 152.9 |
| g CO ₂ /kg dry fuel consumed | g/kg | 1999.6 | 1607.0 | 1675.0 | 1663.9 |
| g PM _{2.5} /kg dry fuel consumed | g/kg | 0.010 | 0.014 | 0.022 | 0.031 |
| SIMMER PHASE | | | | | |
| g CO/kg dry fuel consumed | g/kg | 872.1 | 748.3 | 636.5 | 629.9 |

| Basic Operation | units | B25 | B30 | B35 | B40 |
|--|--------------|------------|------------|------------|------------|
| g CO₂/kg dry fuel consumed | g/kg | 2417.3 | 1756.7 | 2170.1 | 2214.8 |
| g PM_{2.5}/kg dry fuel consumed | g/kg | 0.006 | 0.006 | 0.004 | 0.010 |

Appendix 38: Images of the filter paper for briquettes B25, B30, B35, B40; (a) CSHP phase (b) HSHP phase, (c) Simmer phase



RESEARCH OUTPUTS

(i) Publication

Kivumbi, B., Jande, Y. A. C., Kirabira, J. B., & Kivevele, T. T. (2021a). Production of carbonized briquettes from charcoal fines using African Elemi (*Canarium schweinfurthii*) resin as an organic binder. *Energy Sources, Part A: Recovery, Utilization, and Environmental Effects*, 2021, 1–17. <https://doi.org/10.1080/15567036.2021.1977870>

Kivumbi, B., Jande, Y. A. C., Kirabira, J. B., & Kivevele, T. T. (2021b). Water Boiling Test of carbonized briquettes produced from charcoal fines using African Elemi (*Canarium schweinfurthii*) resin as an organic binder. *Biomass Conversion and Biorefinery*, 2021, 1-16. <https://doi.org/10.1007/s13399-021-02000-z>

(ii) Poster Presentation